

School of Molecular and Life Sciences

**Covalently linked molecule–electrode contacts toward robust
molecular-electronics circuits**

Malwattage Chandramalika Rukmali Peiris

This thesis is presented for the Degree of

Doctor of Philosophy

of

Curtin University

October 2020

Declaration

To the best of my knowledge I declare that this thesis is my own account of my research and this thesis contains no materials previously published by any other person except where due acknowledgement has been made.

This thesis contains as its main content work which has not previously been submitted for a degree or diploma at any university.

M. C. R. Peiris

Date: 22 October 2020

Abstract

The use of molecules as active components in electronic devices is a trend in current electronics and a potential alternative to semiconductor-based nanoelectronics. The first aim of this thesis is to develop mechanically stable molecule-electrode contacts on Si surfaces, on the macro and nano scales, to avoid the disadvantages of using Au substrates specifically in molecular electronics. The second aim is to develop insulating zones to separate molecular arrays using SiO_x formed via conductive atomic force microscope (AFM) tip induced oxidation. Furthermore, this project aims to examine the as yet unrevealed properties of these oxide films.

The combination of self-assembled monolayers with scanning tunnelling junction approaches allowed studying of electron transfer at the single-molecule level by fabricating single-molecule circuitry. After modification of the surface by different molecules, single molecular contacts are formed by bridging a molecule, which connects to a scanning tunnelling microscope (STM) tip made of Au or Si. The scanning tunnelling microscope-break junction approach (STM-BJ) was used to measure the current versus distance (tapping) and the STM-blinking method was used to measure the current versus time. It was employed as a measure of the stability and the conductance of single molecular contacts.

The study on the single-molecule level was complemented by characterisation using electrochemical techniques such as cyclic voltammetry (CV), X-ray reflectometry (XRR), X-ray photoelectron spectroscopy (XPS) and atomic force microscopy (AFM). These systems were further examined by theoretical calculations.

To mitigate the drawbacks of using Au in molecular electronics, this thesis presents a significant advancement in terms of stable molecular junctions on a non-gold substrate material at ambient conditions. Molecules terminated by diazonium salts from both ends were used to engineer a Si-C top-to-bottom single-molecule device with a stability of 1.1 s. This is a significant leap forward in both terms of stability and substrate material. The high stability and lifetime enabled the measurement of current-voltage properties during the lifetime of the molecular junction.

The properties of this Au–Si junction were found to change, from being a Schottky contact in the absence of a molecular bridge to an ohmic contact when a single molecule was covalently bridged to both Si and Au electrodes. This showed that the electrical properties can be controlled when a single-molecule bridges the gap in the junction. In addition to these STM studies, this work shows that the kinetics of film grafting is crystal-facet dependent, being more favourable on Si(111) than on Si(100), a finding that adds control over surface chemistry during the device fabrication.

After forming stable single-molecule contacts using diazonium salts, thiols such as 1,6-hexanedithiol were found to covalently link to Si under mild conditions in the presence of dissolved oxygen. The molecular coverage was determined by cyclic voltammetry on Si(111)–H to be 75% of a full monolayer. Density functional theory calculations were used to probe the reaction mechanisms. The impact of this Si–S chemistry in single-molecule electronics was demonstrated using STM-junction approaches by forming Si–1,6-hexanedithiol–Si junctions. These Si–S contacts developed from 1,6-hexanedithiol showed a record lifetime of 2.7 s which is higher than that reported for conventional molecular junctions formed between gold electrodes. This finding brings the field of single-molecule electronics into a workable timescale.

After developing stable molecular contacts with diazonium salts and thiols, an AFM tip induced oxidation method was used to develop SiO_x layers with the aim of forming insulating zones between molecular contacts. A range of positive and negative biases was examined to explore the mechanism, rate of the oxidation and the thickness of the oxide films formed. It was revealed that the thin oxide layers can form a tunable Schottky diode with different rectification ratios.

To date, the mechanism of AFM induced oxidation was not clearly understood. In particular, it was yet to be determined whether electron tunnelling or the electric field induces the desorption of H and the subsequent oxidation. Pt–Si Schottky junctions were used with both n–type and p–type Si to separate the effects of the electric field from electron tunnelling. The junctions enabled blocking the current at the reverse bias and allowed disentangling electric current and electric-field-induced effects. It was demonstrated that the oxidation is dependent mainly on the electric field and not the tunnelling current. In addition to Si doping and bias, the oxidation rate was also found to be reduced by substituting the hydrogen with deuterium. These electrical properties of Schottky diodes and the underlying mechanisms of oxidation were examined in detail using I–V measurements and current maps. Importantly, SiO_x structures were discovered to have behaviours other than simply insulating and showed that the oxide layer can break down with applying a high bias such as ± 6 V. With the high applied bias, the properties of the oxide changed from insulating to highly conductive ohmic contacts by forming conducting channels that extend deep into the bulk silicon. These channels can be reversed back to the insulating state by applying ± 2 V. This switching between Schottky and ohmic contacts can potentially be used for future write-erase memory devices. This thesis provides a step forward in terms of potential chemistries for molecular electronics on silicon. Monolayers derived from thiols and diazonium salts have high stabilities and facile syntheses. This work explores the potential of silicon oxide as a material in molecular electronics, as both a component and as a storage medium.

Acknowledgement

First I would like to acknowledge many individuals at Curtin University and the School of Molecular and Life Sciences (MLS) for their support and supervision during my PhD. The following people I'd like to acknowledge in particular due to their unconditional support and guidance:

Dr Nadim Darwish, my primary supervisor, for his guidance, support and for showing me the correct path to be a better scientist and for his thorough review of this thesis and all the papers I have published up to date. Dr Nadim was not only a great scientist but also provided me with support and encouragement throughout my candidature to the final talk. His knowledge, excitement and curiosity with the new findings led me to do more research and ultimately ended up as publications in high impact factor journals for which I would like to give him the full credit and my gratitude. It has been an honour to work under his kind mentorship where he always kept me on the right track and motivated me even during the hard times in my PhD journey.

In the same way as Nadim, another person behind my success is my co-supervisor Dr Simone Ciampi. His guidance and wealth of knowledge in silicon chemistry helped me to understand the basics and get to do advanced research with the knowledge I gained. I would also like to give my gratitude for believing in me and recommending me as a PhD student for Dr Darwish. I would like to mention that Dr Nadim and Dr Simone are the two pillars behind my success.

I would also like to give my special thanks to Curtin University, for offering me a PhD scholarship (Curtin International Postgraduate Research Scholarship (CIPRS) and Research Stipend Scholarship) for the financial assistance throughout my PhD. Also, I acknowledge the John de Laeter Centre, Curtin University for the equipments, facilities and technical assistance, special thanks goes to Ms Elaine Miller, Dr William D. A Rickard and Dr Xiao Sun for the transmission electron microscopy (TEM), focussed ion beam milling-scanning electron microscopy (FIB-SEM) assistance. Dr Jean-Pierre Veder of Curtin University for helping me out with the X-ray photoelectron emission spectroscopic analysis (XPS) in the John de Laeter Centre, Curtin University.

Dr Anton P. Le Brun from the Australian Centre for Neutron Scattering, Australian Nuclear Science and Technology Organization (ANSTO) for helping me out with X-ray reflectometry (XRR) analysis and being a co-author for two of my publications. Dr Peter J. Canfield (International Centre for Quantum and Molecular Structures and School of Physics, Shanghai University, Shanghai, China), Dr Daniel S. Kosov (College of Science and Engineering, James Cook University, Townsville, QLD, Australia) and Prof. Jeffrey R. Reimers (School of Mathematical and Physical Sciences, University of Technology Sydney, Australia) for their assistance as being collaborators for one of my projects by doing the computational calculations of my publications.

Dr Albert C. Aragoes of the Department of Chemistry, Faculty of Natural & Mathematical Sciences, King's College London, Dr Michelle L. Coote of ARC Centre of Excellence for Electromaterials Science, Research School of Chemistry, Australian National University, Canberra, Australia, Dr Ismael Díez-Perez of Department of Chemistry, Faculty of Natural & Mathematical Sciences, King's College London, United Kingdom for their unconditional support with the publication of my first paper by contributing their knowledge, time and proofreading the paper which ultimately published in a high impact factor journal.

Prof. Paul Low from the University of Western Australia for providing me with the molecules synthesised by his group to continue my research and his guidance and knowledge led me to do successful research.

Dr Thomas Becker of Curtin University for allowing me to use the atomic force microscope (AFM) facility by myself and for his helpful advice on this part of my research work.

Dr Kristy Noakes and Mr Robert Herman who were always concerned about our safety, showing us how to conduct research safely and allowing me to get access to the lab and building when I wanted to work on holidays and weekends.

From the School of Molecular and Life Sciences at Curtin, I would like to acknowledge all past and present members of the Molecular Electronics group that I have interacted with. In particular, Dr Yan Boris Vogel, a former colleague in our group for the help and advice which was helpful in my research and for teaching me how to be a better person beyond science.

Mr Stuart Paul Ferrie who is a very close colleague I met during my PhD and was always happy to give me free counselling sessions during the coffee breaks to cheer me up in my difficult times and correcting my English and proof-reading to fix the science and grammar in my thesis.

I would also like to thank all the members of the academic and the administrative staff for their support over the years. Especially Mr Peter Chapman who has always been helpful to me at times when I needed his technical support.

From outside my department, I would like to sincerely thank my friends, Shamika Gorokgahagedara, Dr Buddhika Dorakubura, Dr Kuldeep Moore, Darren Cheah, Asanka Maduranga, Waruni Iresha Ekanayake, Shaline Herath Marapana, Kanishka Gunesekara, Andrew Bonds, Heinz Teichmann, Shaghrif javaid, Wei Chen and Jossi Bakre for their friendship and for being by my side for 3 years who filled my life with their unconditional friendship, love, delicious food and kind words.

All of my lab mates Dr Long Zhang, Dr Ruth B. Domínguez-Espíndola, Song Zhang, Soraya Rahpeima, Mattia Belotti, Jinyang Zhang and Essam Mohomad Dief for being wonderful colleagues and friends who made my lab time stress free and helped me to do successful research.

Finally, I would like to thank my family for their continuous encouragement, support and love that they always provided. My Dad (Mr Positive) and my deceased Mom who always wanted me to achieve the best in my life and whose last wish was to see the “Dr” added to my name. Even though we were not nearby during the last 3 years, I always felt her love. Special thanks go to my dad who always had time to listen to me and encourage me to achieve the best. Last but not least, my gratitude goes to my sister, Sulani Peiris Perks, niece Marly, nephew Nathan and brother-in-law, Andrew Perks for looking after me and supporting me financially. Also, I would like to acknowledge my little brother Gayan Peiris for his encouraging words and love.

I would like to dedicate this thesis to my Dad and Mom who always dreamt of this day.

Malwattage Chandramalika Rukmali Peiris 2020

Table of Contents

Declaration	i
Abstract	ii
Acknowledgement	v
Table of Contents	viii
List of Figures	xiii
List of Tables	xli
List of Abbreviations	xlii
Dedication	xliv
List of awards, publications and presentations	xl v
1. Awards	xl v
2. As a first/ co-first author.....	xl v
3. As a co-author	xl v
4. Oral presentations	xlvi
Chapter 1 Thesis Overview.....	1
Chapter 2 General Introduction.....	4
2.1 Overview.....	4
2.2 Basics of SAMs	7
2.3 Self-assembled monolayers on Si and Au	10
2.3.1 Grafting of SAMs on Au surfaces.....	11
2.4 Grafting of SAM on the Si surface	18
2.4.1 SAMs on native Si oxide	18
2.4.2 Preparation of Si-H surfaces.....	23
2.4.3 SAMs directly on Si-X surface (where X= Cl, Br or I)	23
2.4.4 Spontaneous Grafting of SAMs on Si Surfaces.....	24
2.4.5 Electrografting of SAM on Si Surface	25
2.4.6 Thermal induced monolayer formation on Si.....	27
2.4.7 Ultraviolet photochemical hydrosilylation	28
2.4.8 Visible light photochemical hydrosilylation	30
2.4.9 Other methods of surface modification	31

2.5 Characterization of SAMs	33
2.5.1 Conductivity measurements of SAMs.....	33
2.6 Applications of single-molecular contacts for future electronics	39
2.7 References	43
Chapter 3 Experimental details.....	59
3.1 Experimental set up.....	59
3.1.1 Preparation of Au polycrystalline electrodes	59
3.1.2 Preparation of Au (111) single crystal electrode	59
3.1.3 Preparation of Si single crystal electrodes.....	60
3.2 Cyclic voltammetry	60
3.3 Atomic Force Microscope.....	62
3.3.2. AFM ICON head.....	62
3.3.2 AFM Fast scan head	63
3.4. X-ray photoelectrone spectroscopy (XPS).....	64
3.5 X-ray refractometer (XRR)	65
3.6 Scanning tunnelling microscope (STM)	66
3.7 Transmission electron microscopy (TEM)	70
3.8 Scanning electron microscope (SEM).....	71
Chapter 4 Metal–single-molecule–semiconductor junctions formed by a radical reaction bridging gold and silicon electrodes.....	72
4.1 Summary of this chapter	73
4.2 Abstract	74
4.3 Introduction.....	74
4.4 Experimental Methods	76
4.4.1 Chemicals and Materials	76
4.4.2 Surface Modification	77
4.4.3 Electrochemical measurements.....	79
4.4.4 Atomic Force Microscopy (AFM).....	79
4.4.5 Scanning electron microscopy (SEM).....	79
4.4.6 STM break junction	79
4.4.7 X-ray reflectometry (XRR)	80
4.5 Results and Discussion	81

4.5.1 Electro- versus spontaneous-grafting of bis-diazo on gold.....	81
4.5.2 Electro-versus spontaneous-grafting of bis-diazo on silicon	85
4.5.3 Single-molecule STMBJ studies.....	88
4.6 Conclusion	93
4.7 Acknowledgement.....	93
4.8 References	94
Chapter 5 Spontaneous S–Si bonding of alkanethiols to Si(111)–H: towards Si– molecule–Si circuits	100
5.1 Summary of this chapter	101
5.2 Abstract	102
5.3 Introduction.....	102
5.4 Experimental methods	105
5.4.1 General chemicals and materials.....	105
5.4.2 Thiol–functionalized silicon (100) and (111) surfaces.	106
5.4.3 Electrochemical Measurements.	106
5.4.4 AFM Measurements.....	106
5.4.5 X-ray photoelectron spectroscopy (XPS) measurements.	107
5.4.6 STM break junction.	108
5.4.7 DFT Calculations.....	108
5.4.8 STM tip preparation.	109
5.5 Results and discussion.....	110
5.5.1 Synthesis.	110
5.5.2 SAM characterization by cyclic voltammetry.	112
5.5.3 SAM characterization by AFM and C-AFM.....	113
5.5.4 SAM characterization by XPS and XRR.....	115
5.5.5 DFT understanding of the SAM formation process.	116
5.5.6 SAM completion at high coverage for the binding of 2 to Si(111)–H	118
5.5.7 Control experiments using S–CH ₃ contacts.	119
5.5.8 Single molecule STM-junction studies	119
5.6 Conclusions.....	121
5.7 Acknowledgement.....	122

5.8 References	123
Chapter 6 Silicon oxide nanostructures formation using atomic force microscope tip induced oxidation. Revealing the mechanism and more.....	133
6.1 Overview of this chapter	133
6.2 Introduction.....	136
6.3 Experimental methods	138
6.3.1 Chemicals and materials	138
6.3.2 Si(111)–H surface modification.....	139
6.3.3 Si(111)–D surface modification.....	139
6.3.4 Formation of Si oxide squares on Si(111)	140
6.3.5 Conducting oxide tunnels formation on SiO _x	141
6.4 Results and discussion	141
6.4.1 Conductivity change of the oxide hillocks on Si(111)–H formed by different positive bias voltages.....	141
6.4.2 Conductivity of the oxide hillocks formed on Si(111)–H by negative bias voltages	143
6.4.3 Si–D versus Si–H	148
6.4.4 Advanced oxide architecture using different writing bias voltages	151
6.4.5 Tunable Schottky diodes	154
6.4.6 Possible mechanisms of oxide formation	155
6.4.7 Forming conducting oxide channels/ memory devices	159
6.5 Conclusion	165
6.6 Acknowledgement.....	167
6.7 References	168
Chapter 7 Conclusions and future outlook	173
7.1 Conclusions.....	173
7.2 Future outlook.....	177

Appendix A179
Appendix B205
Appendix C210
Appendix D223
Appendix E228

List of Figures

- Figure 2. 1** Self-assembly of molecules on a solid surface8
- Figure 2. 2** Current trends in molecular electronics.¹⁵ Figure 2.2 adapted from ref. 15 with permission from, Royal society of chemistry Copyright © 2010.9
- Figure 2. 3** Schematic diagram of typical self-assembling molecules with three major components (head, backbone and terminal group) which are highlighted on the left and examples for the head, backbone and terminal groups are shown on the right.11
- Figure 2. 4** Schematic presentation of the proposed DNA sensor showing the AuNPs–GO/GCE surface with the hybridization of target DNA.⁴ Figure 2.4 adapted from ref. 4 with permission from, Elsevier Copyright © 2017.....13
- Figure 2. 5** Scheme of the functionalization method of combining diazonium salt and click chemistries for obtaining AuNPs assemblies on Au electrodes and AFM images A) diazonium salt modified Au B, C are the AuNP attachment to Au with 30 minutes and overnight, respectively. Unpublished results-Curtin University, molecular electronics group.....14
- Figure 2. 6** Proposed binding mechanisms of the alkynes to an Au and Au nanoparticle.⁷⁸ Figure 2.6 adapted from ref. 78 with permission from, American Chemical Society Copyright © 2013.15
- Figure 2. 7** Cyclic voltammograms at 100 mV/s of $\text{Fe}(\text{CN})_6^{3-/4-}$ at the bare Au bead and SAM modified Au electrodes with compounds.⁷⁹ Figure 2.7 adapted from ref. 79 with permission from, American Chemical Society Copyright © 2007.....15
- Figure 2. 8** Molecules studied on the Au surface by. Zhang .S et al.⁷⁹ Figure 2.8 adapted from ref. 79 with permission from, American Chemical Society Copyright © 2007.16

- Figure 2. 9** Schematic of the CuAAC reaction of a DEB modified surface with a redox-active ferrocene moiety and the formation of junctions examined by STM via a single DEB molecule.⁶² Figure 2.9 adapted from ref. 62 with permission from, IOP Publishing Ltd © 2015.. **16**
- Figure 2. 10** Electrochemical grafting of diazonium salt on mono- and polycrystalline Au surfaces: a) solid line Au (gold(1 1 1) epitaxied on mica), dotted line Au (polycrystalline gold evaporated on glass), dashed line Au (gold deposited on bronze by galvanoplasty). (b) diazonium salt (0.005 M) cyclic voltammetry in acetonitrile (TEAP 0.05 M) on Au. The solid line and dashed line represent experiments that were conducted successively on the same substrate (Au).⁸⁰ Figure 2.10 adapted from ref. 80 with permission from, Elsevier Copyright © 2008. **17**
- Figure 2. 11** A schematic diagram of Si-substrate with different doping type, where doping with phosphorus gives n-type and doping with boron forms p-type semiconducting Si. **18**
- Figure 2. 12** Process of the SAM formation on a native oxide surface of Si. ... **21**
- Figure 2. 13** Model of a growing monolayer crystallite resulting from the reaction of alkyl trichlorosilane with a Si oxide surface⁹⁴. Figure 2.13 adapted from ref. 94 with permission from, WILEY-VCH Verlag GmbH & Co. KGaA, Weinheim Copyright © 2005..... **22**
- Figure 2. 14** The process of conversion of SiO_x into Si-H technique..... **23**
- Figure 2. 15** The process of conversion of SiO₂ into Si-X technique. **24**
- Figure 2. 16** Possible reaction mechanisms. (a) Electrochemical reduction of NR₄⁺ followed by radical pathways, leading to Si-C bonds. (b) The alkyl radical is reduced to the anion, which attacks the Si-Si bond in a nucleophilic fashion. (c) Silyl anion attack on NR₄⁺ cations to form Si-C bonds.¹⁰⁴ Figure 2.16 adapted from ref. 104 with permission from Elsevier B.V. © 2005..... **26**

- Figure 2. 17** Hydrosilylation of 1,8-nonadiyne 1 onto a Si(100)–H electrode (S-1) and covalent attachment of 4-Azido–TEMPO 2 via a CuAAC reaction to yield the redox-active radical film (S-2).⁸⁸ Figure 2.17 adapted from ref. 88 with permission from, American Chemical Society Copyright © 2016.**28**
- Figure 2. 18** Mechanism for UV-initiated grafting of alkenes to H–terminated Si surfaces: (a) photoemission to an acceptor level followed by nucleophilic attack by the C=C group of a second alkene; (b) overall result of the grafting reaction.¹²⁰ Figure 2.18 adapted from ref. 120 with permission from, American Chemical Society Copyright © 2010.**29**
- Figure 2. 19** Esterification changes the reactivity of the Si surface. Organomethoxysilanes react specifically with the esterified region of a photopatterned porous Si sample. This demonstrates a versatile two-step synthetic procedure for patterning Si surfaces with a variety of molecular species.¹²³ Figure 2.19 adapted from ref. 123 with permission from, American Chemical Society Copyright © 1996.**30**
- Figure 2. 20** Representation of the proposed (a) Radical chain mechanism under thermal and UV conditions and (b) electron/hole pair mechanism for visible-light initiated hydrosilylation on porous Si.¹²⁴ Figure 2.20 adapted from ref. 124 with permission from, American Chemical Society Copyright © 2005.**31**
- Figure 2. 21** Grafting mechanism of alkyl on Si substrates.¹¹⁶ Figure 2.21 adapted from ref. 116 with permission from, American Chemical Society Copyright © 2004**32**
- Figure 2. 22** Lewis acid-mediated hydrosilylation in the presence of the Lewis acid EtAlCl₂, resulting in alkenyl– or alkyl–terminated surfaces, respectively¹³¹. Figure 2.22 adapted from ref. 131 with permission from, American Chemical Society Copyright © 1999.**33**

- Figure 2. 23** Molecular structures of conjugated molecules used in the study.¹³⁴
 Figure 2.23 adapted from ref. 134 with permission from, American Chemical Society Copyright © 2002.....**34**
- Figure 2. 24** I–V curves of the SAMs. (a) BM; (b) BP1; (c) TP1. The load was applied to minimize the damage to the SAM surface (1 nN).¹³⁴
 Figure 2.24 adapted from ref. 134 with permission from, American Chemical Society Copyright © 2002.....**34**
- Figure 2. 25** (A) Conductance of a Au contact formed between a Au STM tip and a Au substrate (B) A histogram constructed from conductance curves (C) contact shown in (A) is completely broken, corresponding to the collapse of the last quantum step, a new series of conductance steps appears due to molecules such as 4,4'-bipyridine present in the solution. These steps are due to the formation of the stable molecular junction between the tip and the substrate (D) A histogram obtained from 1000 measurements as shown in (C) shows peaks near 0.01, 0.02, and 0.03 G_0 that are ascribed to one, two, and three molecules, respectively. (E and F) in the absence of molecules, no such steps or peaks are observed in the same conductance range.¹⁴⁵ Figure 2.25 adapted from ref. 145 with permission from, American Association for the Advancement of Science Copyright © 2003**37**
- Figure 2. 26** Single-molecular scanning tunnelling microscopy–blinking method (a) schematic of the STM junction experiment describing the formation and breakdown of the Au–nonadiyne–Si junction.⁶¹ (b) captured ‘blink’ when a 1,8-nonadiyne molecule bridges the two electrodes. Current jumps (blinks) appear when the molecule bridges the gap between the Au and the Si electrodes. (c) current response during a voltage bias ramp of an Au–nonadiyne–Si.⁶¹ Figure. 2.26 adapted from ref. 61 with permission from, Springer Nature Copyright © 2017.....**38**

Figure 2.27 (a, b, c, d and e) a) conducting molecule wire developed¹⁶³ by using M(II)-5,15-diphenylporphyrin single-molecule junctions (M=Co, Ni, Cu, or Zn), which investigate the current flows perpendicular to the plane of the porphyrin and also the influence of the metal ion to the conductivity. Figure 2.27a adapted from ref. 163 with permission from, Springer nature Copyright © 2016 b) transistor developed¹⁵⁴ using anthraquinone/hydroanthraquinone redox reaction. Here single norbornyl anthraquinone unit can be switched between a low-conducting and a high-conducting form using electrochemical gating. Figure 2.27b adapted from ref. 154 with permission from, WILEY-VCH Verlag GmbH & Co. KGaA, Weinheim Copyright © 2012 c) molecule resistor developed⁶⁴ using 1,4-diaminobenzene and 2,7-diaminofluorene junctions where conductance for the series decreases with increasing twist angle. Figure. 2.27c adapted from ref. 64 with permission from, Springer Nature Copyright © 2006 d) diode developed⁸ using trimethylstannyl lithium which demonstrate a new method of achieving rectification in single-molecule devices using the high-bias properties of gold-carbon bonds Figure. 2.27d adapted from ref. 8 with permission from, American Chemical Society Copyright © 2013. e) molecule switch developed.³ by using spiropyran derivatives where consequently, switch the electrical conductivity of the single-molecular device in the presence of light pointer or chemical signal. Figure. 2.27e adapted from ref. 3 with permission from, American Chemical Society Copyright © 2014.....42

Figure 3. 1 (a, b) Electrochemical cell setup used to characterize monolayers on silicon and gold single crystal. b) photo image of AFM and (c) Ag/AgCl reference electrode (1M KCl), d) Pt counter electrode, e) leakless Ag/ AgCl reference electrode, f) gold polycrystalline working electrode g) silicon working electrode (1mm ²) h) gold single crystal electrode i) electrochemical workstation and enclosure for electrochemical experiments.....	61
Figure 3. 2 (a) Schematic diagram of the AFM PF–TUNA setup use for this tip induced local oxidation b) photo image of AFM and (c) photograph of TUNA module which controls current sensitivity of the TUNA output and feedback.....	63
Figure 3. 3 The set up of the Bruker AFM fast scan head a) use for experiments b) silicon cantilevers (TESPA-V2), c) FastScan head and d) Pt tips used for the conductivity measurements.	64
Figure 3. 4 a) Kratos Axis Ultra DLD spectrometer XPS (John de Laeter research centre, Curtin University of Technology, Department of Physics), b) scheme of the XPS instrument.....	65
Scheme 3. 1 Schematic diagram of X-ray reflectometer	66
Figure 3. 5 a) Scheme of STM of PicoSPM 1, b) PicoSPM 1 microscope head controlled by a “Picoscan 2,500 electronics c) NI-DAQmx/BNC-2,110 national instruments (LabVIEW data collection system) d) STM instrument in SPM facilities, Curtin University of Technology, School of Molecular and Life Sciences.....	68
Figure 3. 6 a) Scheme of STM blinking method and b) break junction technique.	69
Figure 3. 7 Photo images of the FEI Talos, TEM a) load lock, b) inside view of the load lock c) control panel and the turbo-pump available at John de Laeter research centre Curtin University, Australia	70
Figure 3. 8 Photo images of the Tescan Mira3 FESEM at John de Laeter research centre Curtin University, Australia	71

Figure 4. 1 Structure of the molecule (bis-diazo) studied and a schematic describing its reaction with surface and tip electrodes or with ferrocene. The surface and tip electrodes can be gold or silicon.76

Figure 4. 2 Electrochemical grafting of bis-diazo on mono- and poly-crystalline gold surfaces. Cyclic voltammograms showing the oxidation and reduction waves of a) 100 % single crystal Au (111). The Inset in (a) shows an AFM topography image of the single crystal surface. b) 70% Au (111) and c) polycrystalline gold (0.5 M H₂SO₄ as the electrolyte) at scan rate 100 mV s⁻¹. The potential is expressed in mV against aq. Ag/AgCl electrode (1 M KCl). The inset in (c) shows an AFM topography image of the polycrystalline Au surface. The gold oxidation wave is a single peak at around +1300 mV for 100% Au (111). (b–c) Multiple oxidation waves between +1000 mV and +1400 mV appear for 70% Au (111)/30% polycrystalline in (b) and for a 100% polycrystalline surfaces in (c). (d–f) Electrochemical reduction waves for the grafting of bis-diazo (1 mM) with Bu₄NPF₆ (0.1 M) in a 1:49 (v/v) dimethyl sulfoxide/acetonitrile (DMSO/ACN) solvent mixture on the different gold surfaces shown in panels a–c. The scan rates in panels d–f are 50 mV s⁻¹ and the potential is expressed in mV against Fc/Fc⁺ (1 mM in ACN). The more polycrystalline the Au surface is the broader and the more split are the reduction waves.82

Figure 4. 3 Electrochemical and spontaneous grafting of bis-diazo on Au(111) followed by a reaction with ferrocene. a) Schematics describing the formation of a diazonium film on an Au surface and the reduction of the distal diazonium moiety by ferrocene molecules. b) Cyclic voltammogram for an Au(111) surface that was first modified with bis-diazo then exposed to a solution of ferrocene. The electrochemical reduction was first performed via 1 potential cycle (0 to -1 V vs Fc/Fc⁺) in a solution of bis-diazo (1mM) with Bu₄NPF₆ (0.1 M) in a 1:49 (v/v) DMSO/ACN solvent mixture. The surface was then exposed to a solution of ferrocene (1 mM in ACN) for 30 min at open circuit. Note that the schematic in (a) does not take into account the polymerization of the film, see Appendix C, Figure C-4-3 for details. c) Cyclic voltammogram for the spontaneous reduction of bis-diazo, by means of resting an Au(111) sample in a solution of bis-diazo for 2 h at open circuit, followed by the spontaneous reaction with ferrocene (30 min) to indirectly probe the presence of an intact unreacted diazo group at the distal end of the monolayer. The potential scan rate is 50 mVs⁻¹. d) Stability of the interface tested by means of 30 repetitive cyclic voltammograms scans for a surface that is prepared in a similar way to that described in (c), see Appendix C, Figure C-4-4 for details. The voltammograms in (b-d) were recorded in 1 M HClO₄ and the potential is expressed in mV against Ag/AgCl electrode (1 M KCl). **84**

Figure 4. 4 Electrochemical and spontaneous grafting of bis-diazo on silicon. a) Reductive grafting of bis-diazo (1 mM bis-diazo with 0.1 M Bu₄NPF₆ in a 1:49 (v/v) DMSO/ACN solvent mixture) on Si(111) (red line) and on Si(100) (black line) using one potential cycle (+0.4 V to -1.8 V for Si(111) and +0.5 V to -2.1 V for Si(100)) at scan rate of 50 mV s⁻¹. The second potential cycle is shown in Appendix C, Figure C-4-5. b) Reduction of bis-diazo on Si(111) using one potential cycle at different scan rates (10, 25 and 200 mV s⁻¹). c) XRR profiles for samples prepared by grafting bis-diazo on Si(111)-H electrochemically (black trace) or spontaneously (blue trace). The inset in (c) shows an AFM topography image of the Si(111)-H surface. The symbols with error bars are the collected data and the red solid lines are the fits to each data set. The data is vertically offset for clarity and the parameters used in the interpretation of the XRR data are listed in Appendix C, Table C-4-1. d) Cyclic voltammogram at a scan rate of 200 mV s⁻¹ of a film of bis-diazo spontaneously prepared by resting a hydrogen-terminated Si(111)-H surface in a solution of bis-diazo for 8 h and then exposing it to a solution of ferrocene for 30 min. The potential in (a-b) is expressed in mV against Fc/Fc⁺ (1 mM in ACN). The voltammogram in (d) was recorded in 1M HClO₄ and the potential is expressed in mV against Ag/AgCl electrode (1 M KCl)..... **86**

Figure 4. 5 Electrochemical grafting of bis-diazo on crystalline silicon: Si(100) vs Si(111). a) AFM image of Si(111) pyramids grown on Si(100) by anisotropic etching of the surface in a solution of KOH solution. b) SEM image for the same surface. c) A zoom-in AFM image of a single pyramid. d) The electrochemical reduction wave of bis-diazo (1 mM bis-diazo with 0.1 M Bu₄NPF₆ in a 1:49 v/v DMSO/ACN mixture) on the sample presented in (a) and (b). The potential scan rate in (d) is 50 mV s⁻¹ and the potential is expressed in mV against Fc/Fc⁺ (1 mM in ACN)..... **87**

Figure 4. 6 Single-molecule junction measurements of a Si(111) surface pre-modified electrochemically (one potential cycle from +0.4 V to -1.8 V Fc/Fc⁺) by a bis-diazo film with a gold tip forming the top contact. a) Schematic depicting the molecular junction formed. b) Conductance histogram built from ca. 200 blinks averaging $90 \pm 35 \mu G_0$. (inset). Representative Au-bis-diazo-Si blink, measured at a bias of 0.5 V. c) Histogram of blink lifetimes with the average being 1.1 ± 0.2 s d) Blinking color maps obtained by accumulating ca. 200 blinks and normalized to a common time origin. (e) Representative data for a voltage sweep applied during a blink of a single-molecule Au-bis-diazo-Si junction. Current is monitored before and after the voltage sweep to ensure the voltage is ramped while the molecular junction is still intact. (inset) shows the corresponding current-voltage curve. The STM experiments were performed at room temperature in mesitylene.90

Figure 4. 7 STM-current-voltage measurements. a) Schematic and current-voltage measurements of Au-Si tunneling junctions in the absence of bis-diazo molecules. b) Schematic and current-voltage measurements Au-bis-diazo-Si junctions in the absence of a "blink" and therefore absence of covalent bonding to both electrodes. c) Schematic and current-voltage measurements of Au-bis-diazo-Si junctions in which the bis-diazo molecule is covalently bonded to both electrodes. The data for each set is the accumulation of 30 different voltage sweeps and the bias is applied to the silicon surface. The characteristics of the current-voltage curves changes from rectifying in (a) to ohmic in the presence of a top contact with the molecule in (c) where the path of charge transfer is restricted to within the molecule. If the electrons can tunnel in the gaps between the molecules the rectification characteristic is intermediate. The STM experiments were performed at room temperature in mesitylene.91

Figure 5. 1 (a) Molecular and SAM structures: 1 enables electrochemical studies while 2 enables STM-junction studies (a) molecules are reacted with H-terminated silicon surfaces (b) via a thiyl free-radical polymerization (c), as illustrated for propanethiol, to form covalently bonded SAMs (d). (e) Si-molecule-Si junction formed from 2 using single-molecule STM-junction technology (e). S- yellow, Si- fawn, C- cyan, H- white..... **105**

Figure 5. 2 Cyclic voltammetry. (a) Cyclic voltammetry at different scan rates for a SAM of 1 on p-type Si(111)-H of resistivity 0.001 Ω cm. The estimated surface coverage is 2.53×10^{14} molecules cm^{-2} . (b) Current versus scan rate for the SAM formed of 1. The current increases linearly with scan rate, indicating a surface redox reaction. (c) Cyclic voltammetry for a SAM of 1 on Si(111)-H at 50 mV s^{-1} on n-type phosphorus doped of resistivity 0.001 Ω cm. Coverage is dopant independent, the results leading to coverages of 2.50×10^{14} molecules cm^{-2} and is comparable to that obtained on p-type boron doped silicon shown in (a). (d) Cyclic voltammetry at 50 mV s^{-1} for SAMs of 1 on Au(111), showing very similar appearances to those reported for Si in (a) at a similar scan rate. The deduced coverages are 2.20×10^{14} molecules cm^{-2} , slightly less than that for the corresponding monolayers on Si(111)-H. (e) Cyclic voltammetry at 50 mV s^{-1} for SAMs of 1 on Si(100)-H showing a similar appearances to those reported for Si(111)-H; however the surface coverage is lower and estimated at 9.3×10^{13} molecules cm^{-2} . (f) Cyclic voltammetry for SAMs of 1 on Si(111)-H prepared from fresh solid of 1 dissolved in deoxygenated DCM. Oxygen was removed by bubbling Ar for 60 min in the DCM solution containing 1 using a septum sealed vessel and a needle as a vent. The SAM reaction flask was kept under a positive pressure of Ar during the 24 h reaction time. The surface coverage is estimated to be 2.10×10^{13} molecules cm^{-2} and is about 10% of that produced under ambient conditions..... **111**

Figure 5. 3 Surface characterization. (a) $10 \times 10 \mu\text{m}^2$ of a p-type Si(111)-H surface covered by dithiol 2 on Si(111). (b) XRR measurements of 2 on Si(111)-H for various silicon dopant levels: high p-doped (green), low n-doped (red), low p-doped (yellow) and high n-doped (blue). The symbols with error bars are the collected data and the solid lines are the fits to each data set. The data is offset for clarity (c) XPS spectra showing the absence of Si-O_x at 102–104 eV for SAMs of 2 on high p-doped (green), low p-doped (yellow), low n-doped (red) and high n-doped (blue). The data is offset for clarity. (d) S2p narrow XPS scan of monolayers of 2 on Si (p-type, 0.001 Ω cm). Two sets of spin-orbit-split S2p peaks (2p_{1/2} and 2p_{3/2}, high and low binding energy, respectively), held 1.16 eV apart, are evident between 162 and 165 eV. The intensity ratio between the 3/2 and 1/2 emission is set to two, and values of full width at half maximum are 1.3 eV. The S2p emission centred at 164.7 eV is ascribed to thiols in a R-SH configurations, and the emission 163.3 eV is associated to thiols bound to Si (RS-Si) .. **114**

Figure 5. 4 Proposed reaction scheme for the consumption of ambient oxygen as an initiator leading to surface free-radical polymerization. (a) Known solution reactions of thiols (RSH). (b) DFT mechanism for surface SAM formation starting at low coverage. Calculations indicate that thiyl radicals (RS^\bullet , with here $R = C_3H_7$) react with Si(111)-H to abstract hydrogen to form thiol physisorbed to a silicon surface radical (black dot). Reaction over a barrier then leads to chemisorption and radical regeneration. This provides initiation for a free-radical polymerization reaction that then covers the surface with adsorbate. Some critical bond lengths are shown, in Å; only one copy of the used 3×3 supercell is shown. These results show Gibbs free energy changes for surface reactions, while Appendix E, Figure E-5-4 provides analogous electronic energy changes, with detailed internal reaction coordinate descriptions provided in Appendix E, Figure E-5-7. Also, Figures. E-5-5 and E-5-6 provide analogous energies for a model compound. **117**

Figure 5. 5 DFT calculated SAM structures for 2 on Si(111)-H as a function of coverage, showing each four copies of the 3×3 supercell used in the calculations. **118**

Figure 5. 6 (a) Cartoons of the junctions studied. (b) Representative blinks for single molecules of 2 bonded to two Au(111) electrodes (blue), one Au(111) and one Si(111)-H electrode (yellow), and two Si(111)-H electrodes (red). (c) Blinking histograms for the Au-2-Au, Au-2-Si and Si-2-Si junctions. The blinking histograms were constructed by the accumulation of 300 blinks for each system. The blinking histogram was normalised to the total number of blinks (d) Representative current-distance traces for the Si-2-Si junctions. (e) Representative current-distance traces for the Si-2-Si junctions. (f) Current-distance traces histograms constructed from the accumulation of 3000 curves for each system. The blinking histogram was normalised to the total number of traces. **120**

Scheme 6. 1 a) schematic diagram of preparation Si(111)-H surface, b) Si(111)-D surface using Si wafers after piranha treatment..... **140**

Figure 6. 2 AFM height topography of the oxide hillocks obtained on n-type Si-H with the AFM-tip induced oxidation at an applied positive bias voltage of 0 V (a), +0.5 V (c), +2 V (e), +3 V (g) and +5 V (i). The corresponding forward and reverse I-V characteristics recorded on the oxide hillocks are presented at current sensitivity 100 nA/V, at 0 V (b) and after oxidation of Si(111)-H surface with +0.5 V (d), +2 V (f), +3 V (h), +5 V (j). **142**

Figure 6. 3 Heights of the oxide hillocks on Si(111)-H surface as a function of applied positive bias voltage under a relative humidity ~55 % at 25 °C, scan rate 1 Hz, and peak force 554 nN for 8 minutes..... **143**

Figure 6. 4 AFM height topography of the oxide hillocks obtained for the n-type Si-H with the AFM-tip induced oxidation at an applied negative bias voltage of 0 V (a), -0.5 V (c), -1 V (e), -3 V (g) and -5 V (i). The corresponding forward and reverse I-V characteristics on the oxide hillocks are presented (current sensitivity 100 nA/V) at 0 V (b), after oxidation of Si(111)-H surface at -0.5 V (d), -1 V (f), -3 V (h) and -5 V (j)..... **144**

- Figure 6. 5** Height topography of the oxide hillocks for the n-type Si-H formed by different bias +0.5 V, -0.5 V, +3 V and -3 V (a, b, c, d) for 8 minutes, TUNA current was measured by AFM-PF TUNA mode by applying +1 V bias (e, f, g, h) and -1 V (i, j, k, l) at scan rate 1 Hz and peak force 554 nN for 4 minutes. **145**
- Figure 6. 6** AFM height topography (p-type) of the oxide hillocks obtained for the p-type Si-H with the AFM-tip induced oxidation at an applied positive bias voltage of 0 V (a), +0.5 V (c), +2 V (e), +3 V (g) and +5 V (i). The corresponding forward and reverse I-V characteristics recorded on the oxide hillocks are presented at current sensitivity 100 nA/ V, 0 V (b) and after oxidation of p-type Si(111)-H surface at +0.5 V (d), +2 V (f), +3 V (h), +5 V (j), respectively. **146**
- Figure 6. 7** AFM height topography of the oxide hillocks obtained for the p-type Si-H with the AFM-tip induced oxidation at an applied negative bias voltage of 0 V (a), -0.5 V (c), -1 V (e), -2 V (g) and -3 V (i). The corresponding forward and reverse I-V characteristics on the oxide hillocks are presented (current sensitivity 100 nA/ V) at 0 V (b), after oxidation of p-type Si(111)-H surface at 0 (b), -0.5 V (d), -1 V (f), -2 V (h) and -3 V (j), respectively. **147**
- Figure 6. 8** The height topography of the oxide hillocks formed on p-type Si by different bias +0.5 V, -0.5 V, +3 V and -3 V (a, c, e, g) for 8 minutes and TUNA current was read by AFM-PF TUNA mode by applying +1 V bias (b, d, f, h) at scan rate 1 Hz and peak force 554 nN for 4 minutes (one scan) **148**
- Figure 6. 9** AFM height topography of the oxide hillocks obtain for the n-type Si-D with positive applied bias voltage at 0 V (a), +0.5 V (c), +2 V (e), +3 V (g) and +5 V (i). The corresponding forward and reverse I-V characteristics are presented on the oxide hillocks at 0 V (b), after oxidation of Si(111)-D surface at +0.5 V (d), +2 V (f), +3 V (h) and +5 V (j), respectively with current sensitivity 100 nA/V..... **149**

Figure 6. 10 The height topography of the oxide hillocks formed on the n-type Si-D by different bias +0.5 V, +2 V, +3 V, +4 V and +5 V (a, c, e, g, i) for 8 minutes (two scans) and TUNA current was measured by AFM-PF TUNA mode by applying +1 V bias (b, d, f, h, j) at scan rate 1 Hz and peak force 554 nN for 4 minutes (one scan) **150**

Figure 6. 11 Oxide hillocks heights for n-type Si(111)-D surface as a function of applied positive bias voltage. The oxide thickness is smaller to that of Si(111)-H at the same bias range (see Figure 6.3) **151**

Figure 6. 12 (a) height topography for the area of 10 $\mu\text{m} \times 10 \mu\text{m}$ Si(111)-H surface oxidised first with +3 V (2 $\mu\text{m} \times 2 \mu\text{m}$, 8 minutes), then read with -1 V (5 $\mu\text{m} \times 5 \mu\text{m}$, 4 minutes) and finally read again with applying -1 V (10 $\mu\text{m} \times 10 \mu\text{m}$, 4 minutes). (b), (d) and (f) are the corresponding I-V curves for the area of A, B and C. Differences of the forward current shows that oxide growth can be controlled to a degree that current-voltage can be predicted in nanodevices. **152**

Figure 6. 13 TUNA image for the area of 10 \times 10 μm Si(111)-H surface oxidised first with -1 V (2 \times 2 μm , 8 minutes), then enlarge the area and read with applying -1 V (5 \times 5 μm , 4 minutes) and finally reading the whole image (10 \times 10 μm , 4 minutes) with -1 V. **153**

Figure 6. 14 Shows the accumulation of 20 I-V curves of a) Pt-Si (n-type) and Pt-oxide-Si (n-type) junctions (b, c), formed with the applied voltages of (b) +0.5 V and (c) +3 V. The I-V curves averaged from 20 I-Vs of Pt-oxide-Si (n-type) junctions showing a change in the slope beyond an applied forward bias of ca. ± 0.5 V which behave as a tunable Schottky diode. Analogue behaviour was observed with the Pt-oxide-Si (p-type) junctions as shown in Figure 6.6, 6.7. **155**

Scheme 6. 2. A possible mechanism for the oxidation of silicon surface by molecular oxygen **157**

Scheme 6. 3 Schematic diagram of tip induced oxidation on Si(111)–H surface with a conductive Pt tip keeps in and out contact (tapping) with the sample surface. The surface under the tip is locally oxidized to produce oxide hillocks simultaneously when the tip is moving across the Si(111)–H surface with applied bias voltage. a) illustrate the mechanism of oxidation with the applied electric field and b) represent the electric field-assisted OH⁻ migration and electrochemical oxidation of Si..... **158**

Figure 6.15 a) Schematic representation of the Schottky junction between Pt and Si. b) height topography of the area of 5 μm × 5 μm Si(111)–H surface before the oxidation. c) corresponding I–V curves for the area representing in “X” marks in Figure 6.15b. d) Schematic representation of the dense oxide layer formation on Si. e) height topography of the area of 5 μm × 5 μm Si(111)–H surface oxidised by applying +3 V f) corresponding I–V curves for the area marked in “X”. g) Schematic representation of the formation of electric field-induced defects (conductive tunnels) on oxide by the AFM tip. h) corresponding height image for the area of 5 μm × 5 μm Si(111)–H surface oxidised with +3 V and defects formed by 20, – 6 to +6 to –6 V ramps i) TUNA current image at an applied bias of +1 V, for the area of 5 μm × 5 μm Si(111)–H surface of the oxide tunnels). j) corresponding I–V curves for the creation of oxide defects in h). k) enlarged TUNA current image of one oxide tunnel as seen in i). l) schematic diagram representing the movement of electrons through the low-density oxide with oxygen vacancies. **161**

Figure 6.16 After the creation of these conducting tunnels on to the oxidised surface, the site of interest was cut out by a focused ion beam (FIB) and the cross-section of one single conductive channel was examined by transmission electron microscopy (TEM) as shown in Figure 6.16. The dark hemisphere appeared around the oxide channel (Figure 6.16e) implies the structural changes of the bulk Si ³³ after forming conductive oxide channels, which was not observed in the silicon oxide structure without the formation of these channels. Figure 6.16 d and 6.16 e show the TEM cross-section of oxide channels formed after applying ± 6 V. The white spots in the SEM represent the edge of the oxide holes (blue circle in Figure 6.16c) and larger white regions are the oxide produced by the applied electric field (green circle in Figure 6.16c) instead of forming conductive channels. The nanometer-scale hemisphere appeared under the oxide channel inhomogeneity is evident as contrast variation of the silicon where the size of one oxide channel is ~ 50 nm and depth of the oxide channel is 2–3 nm which is sufficient to reach the bulk silicon to change the properties of the Si–Pt contact from insulating to ohmic. **162**

Figure 6.17 a) height image for Si(111)–H surface oxidised with 3 V b) and c) are the adhesion and TUNA current images of a. d) is the corresponding I–V curves for the area marked in “X”. e) corresponding height image for the formation of electric field-induced defects (conductive tunnels) on oxides by AFM tip where the defects formed by ramped with +6 V– (–6 V). f) and g) are the corresponding Adhesion and TUNA current images of e and h) is the corresponding I–V curves for the area conductive channels formed. i) disappearance of the conductive channels in the height topography (5 μm \times 5 μm) after oxidising the conductive channels by applying $\pm 2\text{V}$, where electric field-induced defects (conducting tunnels) formed with applying +6 V– (–6 V). j) and k) are the corresponding Adhesion and TUNA current images of i and d) is the corresponding I–V curves for the area marked in ramps after oxidising the channels with $\pm 2\text{V}$ **164**

Figure 6.18 a) corresponding height image for the area of 2 μm \times 2 μm Si(111)–H surface oxidised by 20, –6 to +6 to –6 V ramps b) TUNA current image at an applied bias of +1 V, for the area of 2 μm \times 2 μm Si(111)–H surface of the oxides showing that without holes there is no conducting channels. **165**

Figure C–4–1 a) An image of the 70% Au (111) single crystal. The melted edge is circled in red. b) Cyclic voltammogram for the 70% Au (111) oxidation/reduction showing two waves between +1150 mV and +1350 mV..... **210**

Figure C–4–2 Schematic describing the formation of Si(111)–H and Si(100)–H surfaces via surface oxidation of Si(111) and Si(100) surfaces for 30 min in a 3:1 H₂SO₄: H₂O₂ piranha mixture followed by oxide etching with ammonium fluoride. **210**

Figure C-4-3 a) Schematics diagram describing the possible polymerization outcome during one cycle of electro-reduction of the bis-diazo compound. This mechanism describes the formation of a covalent bond between the free bis-diazo radicals in solution with the bis-diazo grafted on the surface. A companion reaction is that between the radicals of bis-diazo attached to the electrode surface with excess bis-diazo in solution. This results in 3 polymerized units which has a thickness of ca. 2.43 nm comparable to the thickness of the film obtained via XRR measurements. b) Theoretical 3D Structure of the bis-diazo molecules with 3 polymerized units (Si-purple, C- grey, N-blue).
 **211**

Figure C-4-4 Testing the stability of the interface. The red curve shows a cyclic voltammogram of the spontaneous reduction of bis-diazo by means of resting an Au(111) sample in a solution of bis-diazo for 2 h at open circuit, followed by the reaction with ferrocene (30 min). The blue curve shows a cyclic voltammogram of a spontaneously reduced diazo-film that was held at +1 V vs Ag/AgCl for 300 s before being exposed to a solution of ferrocene (30 min). The efficiency of ferrocene reaction with the pre-biased bis-diazo film (blue trace) is comparable to that on the fresh unbiased diazonium film (red trace) both being $1.08 (\pm 0.17) \times 10^{14}$ molecule cm^{-2} , testifying for the stability of the interface. The potential scan rate is 50 mVs^{-1} and the potential is expressed in mV against an aqueous Ag/AgCl (1.0 M KCl) reference electrode. **212**

Figure C-4-5 Cyclic voltammograms for the 1st and 2nd reduction cycles at a scan rate of 50 mV s^{-1} of bis-diazo ((1 mM) and Bu_4NPF_6 (0.1 M) in a 1:49 (v/v) mixture of DMSO and ACN) on a) Si(111) and b) Si(100). **213**

Figure C-4-6 Cyclic voltammograms of 1 mM bis-diazo salt in 0.1 M ACN/Bu₄NPF₆ at polycrystalline gold electrodes (0.13 cm²). Experimental (solid lines) and simulated (empty symbols) curves for an E_{C_{irrev}} mechanism. The best-fit kinetics parameters for the heterogeneous E step (the one electron process for the bis-diazo⁺/bis-diazo couple) are $k_{et} = 4.0 \times 10^{-3} \text{ cm s}^{-1}$ on Au(111) facets, and $k_{et} = 1.0 \times 10^{-5} \text{ cm s}^{-1}$ on Au(100) facets. For the C_{irrev} step, that is the bis-diazo → bis-diazo[•] + N₂ homogeneous chemical reaction, the k_f is $5 \times 10^3 \text{ s}^{-1}$. The apparent formal potential is 0 mV. The optimized diffusivity (D) for bis-diazo, bis-diazo⁺ and bis-diazo[•] is $3.0 \times 10^{-6} \text{ cm}^2 \text{ s}^{-1}$ and $2.5 \times 10^{-4} \text{ cm}^2 \text{ s}^{-1}$ for nitrogen. The voltage sweep rate is changed between 10 mV s⁻¹ (black traces), 50 mV s⁻¹ (red traces) and 100 mV s⁻¹ (blue traces). The experimental reduction peak is at -37 mV at 10 mV s⁻¹, -70 mV at 50 mV s⁻¹ and -105 mV at 100 mV s⁻¹. **214**

Figure C-4-7 Cyclic voltammograms of 1 mM bis-diazo salt in 0.1 M ACN/Bu₄NPF₆ at Si(111). Experimental (solid lines) and simulated (empty symbols) curves for an E_{C_{irrev}} mechanism. The best-fit kinetics parameters for the heterogeneous E step (the one electron redox process for the bis-diazo⁺/bis-diazo couple) are $k_{et} = 2.0 \times 10^{-7} \text{ cm s}^{-1}$ for Si(111). The k_f for the C_{irrev} step, that is the bis-diazo → bis-diazo[•] + N₂ homogeneous chemical reaction, is $5.0 \times 10^3 \text{ s}^{-1}$ and the apparent formal potential is 0 mV. The optimized diffusivity (D) for bis-diazo, bis-diazo⁺ and bis-diazo[•] is $3.0 \times 10^{-6} \text{ cm}^2 \text{ s}^{-1}$ and D for nitrogen is set to $2.5 \times 10^{-4} \text{ cm}^2 \text{ s}^{-1}$. The electrode area is 0.35 cm². The voltage sweep rate is changed between 10 mV s⁻¹ (red traces), 50 mV s⁻¹ (black traces) and 100 mV s⁻¹ (green traces). The experimental reduction peak is at -564 mV at 10 mV s⁻¹, -650 mV at 50 mV s⁻¹ and -671 mV at 100 mV s⁻¹. **215**

Figure C-4-8 Cyclic voltammograms of 1 mM bis-diazo salt in 0.1 M ACN/ Bu_4NPF_6 at Si(111) or Si(100) electrodes (blue and red trace, respectively). Experimental (solid lines) and simulated (empty symbols) curves for an EC_{irrev} mechanism. The best-fit kinetics parameters for the heterogeneous E step (the one electron redox process for the bis-diazo⁺/bis-diazo couple) are $k_{\text{et}} = 2.0 \times 10^{-7} \text{ cm s}^{-1}$ for Si(111) and $k_{\text{et}} = 5.0 \times 10^{-9} \text{ cm s}^{-1}$ for Si(100). The k_{f} for the C_{irrev} step, that is the bis-diazo \rightarrow bis-diazo[•] + N_2 homogeneous chemical reaction, is $5.0 \times 10^3 \text{ s}^{-1}$ and the apparent formal potential is 0 mV. The optimized diffusivity (D) for bis-diazo, bis-diazo⁺ and bis-diazo[•] is $3.0 \times 10^{-6} \text{ cm}^2 \text{ s}^{-1}$ and D for nitrogen is set to $2.5 \times 10^{-4} \text{ cm}^2 \text{ s}^{-1}$. The electrode area is 0.35 cm^2 and the voltage sweep rate is 50 mV s^{-1} **216**

Figure C-4-9 Cyclic voltammogram of a film of bis-diazo electrochemically reduced on Si(111) and then exposed to a solution of ferrocene for 30 min at a scan rate of 100 mV s^{-1} . b) Cyclic voltammograms at different scan rates for the surface in (a). **217**

Figure C-4-10 Cyclic voltammogram of a film of bis-diazo spontaneously grafted on Si(111) by resting a Si(111)-H surface in a solution of bis-diazo and then exposed to a solution of ferrocene at a scan rate of 50 mV s^{-1} . The surfaces were rested in a bis-diazo compound for a) 2 h, b) 5 h and c) 8h. d) Cyclic voltammograms at different scan rates for the surface in (c). Due to the low coverage in (a) and (b) of $7.67 (\pm 1.15) \times 10^{11} \text{ molecule cm}^{-2}$, the current increases significantly at anodic potentials (more anodic than +100 mV) which is attributed to the oxidation of silicon. The current-increase at anodic potentials is relatively lower in (c) and (d) which is attributed to the surface having a relatively higher molecular coverage of $3.89 (\pm 0.58) \times 10^{12} \text{ molecule cm}^{-2}$ **218**

Figure C-4-11 Repetitive cyclic voltammograms at a scan rate 50 mV s^{-1} of a film of bis-diazo spontaneously reduced (resting a Si(111)-H surface in a solution of bis-diazo for 8 h and then exposed to a solution of ferrocene for 30 min)..... **219**

Figure C-4-12 Cyclic voltammogram of a film of bis-diazo spontaneously reduced on Si(100)-H surface (resting in a solution of bis-diazo for 2 h and then exposed to a solution of ferrocene for 30 min at a scan rate 50 mV s^{-1}). Due to the very low coverage of the bis-diazo on Si(100), no clear ferrocene signals are detected and the current increases significantly at anodic potentials (more anodic than +100 mV) which is attributed to the oxidation of the silicon substrate. The absence of ferrocene signals is attributed to the rate of reduction of bis-diazo being slower on Si(100) than it is on Si(111) **219**

Figure C-4-13 a) AFM (height) image showing the Si(111) pyramids on Si(100) surface obtained by anisotropic etching of a Si(100) surface in 20% KOH solution. b) AFM (amplitude error) image for the same surface. c) The electrochemical reduction wave of 4-bromobenzene diazonium on separate Si(111) and Si(100) surfaces are at -540 and -808 mV, respectively. d) The electrochemical reduction wave of 4-bromobenzene diazonium on the mixed Si(111)/Si(100) surfaces showing two waves at -570 and -805 mV corresponding to the reduction of 4-bromobenzene diazonium on Si(111) and Si(100), respectively..... **220**

Figure C-4-14 2D conductance histograms of blinking experiments between a gold STM tip and a gold electrode using either (a) neat mesitylene, with an accumulation time of 2 h, (b) 1,4-phenylenediamine (Au-molecule-Au) (c) benzene-1,4-dithiol (Au-molecule-Au) (d) bis-diazo (Au-C-Si). The 2D maps in (b-d) are obtained from the accumulations of ca. 250 blinks and an accumulation time of 2-3 h. Insets in (b-d) show the corresponding 1D linear histograms obtained from the same data used to accumulate the 2D maps. The average blinking lifetime was 0.20, 0.50 and 0.75 s for 1,4-phenylenediamine, benzene-1,4-dithiol and bis-diazo, respectively..... **221**

Figure C-4-15 (a) A representative Au-bis-diazo-Au blink measured at a bias of 0.2 V, with a bias sweep (-1 to +1 V) applied during the lifetime of the blink. (b) Current-voltage data acquired during a blink of the Au-bis-diazo-Au systems shown in panel (a). (c) Current-voltage measurements of Au-bis-diazo-Au junctions in which the bis-diazo molecule is covalently bound to both electrodes. (d) Current-voltage measurements of Au-Au tunneling junctions in the absence of bis-diazo molecules. Each data set is the accumulation of 30 different voltage sweeps..... **222**

Figure E-5-1 (a-c) SEM images of mechanically cut gold STM tips at different scales. The radius of these conventional gold tips is comparable to that formed with silicon (111) tips shown in (d-f). SEM images of typical silicon (111) tips prepared by etching in 3.50 M KOH solution for 48 h at 65 °C. The tip preparation procedure consistently led to tip radii less than 1 μm and is comparable to that of gold STM tips..... **228**

Figure E-5-2 AFM characterisation of $20 \times 20 \mu\text{m}$ of a p-type Si(111)-H surface covered by dithiol 2. The topography shows flat terraces separated by atomic steps. The peak-to-peak roughness measured within one Si(111) terrace is ca. 1.7 \AA , consistent with an atomically smooth alkyl monolayer on Si(111). The high-quality topography confirms that the SAMs are homogeneous monolayers at the nanoscale, free of any contaminants or oxidative damage. AFM images of the same surfaces kept for 7 days under ambient condition did not show any sign of deterioration..... **229**

Figure E-5-3 (a) and (d) show the topography images ($5 \times 5 \mu\text{m}$) of the Si-H and the Si-S(CH₂)₆SH after a squared ($2 \times 2 \mu\text{m}$) area in the center of the Si surface was held at +2 V for a period of 8 min with constant peak force of 554 nN . The “x” labels indicate the location where a bias sweep was applied. (b) and (e) show the current-voltage (I-V) sweeps applied on the bias-treated areas at the center of the surfaces. The I-V curves of the Si-S(CH₂)₆SH surface are almost all rectifying (e) as expected for a platinum-n-type Si Schottky junction indicating that the hexanethiol monolayer prevent the surface from oxidation; however, after oxidation of the Si-H surface (b) a clearly AFM-visible oxide layer forms ($3.0 \pm 0.6 \text{ nm}$) which significantly blocks the current passing through the surface in more than 75% of the collected current-voltage curves meaning that the thin layer of oxide acts as dielectric film. Since the first step of oxidation of the Si surface requires the desorption of the -H or the -S(CH₂)₆SH, we conclude that the high density Si-S(CH₂)₆SH monolayers are exceptional in preventing silicon oxidation. (c) and (f) are schematic diagrams of the studied surfaces. **230**

Figure E-5-4 DFT mechanism for SAM formation starting at low coverage.

Calculations indicate that thiyl radicals (RS^\bullet , with here $R = C_3H_7$) produced by attack of solution O_2 on the thiol reactants (RSH) react with Si(111)-H to abstract hydrogen and for thiol physisorbed to a silicon surface radical (black dot). Reaction over a barrier then leads to chemisorption and radical regeneration. This provides initiation for a free-radical polymerization reaction that then covers the surface with adsorbate. Some critical bond lengths are shown, in Å; only one copy of the used 3×3 supercell is shown. These results show the electronic energy changes coming from the VASP calculations that are analogous to the Gibbs free energy changes shown in Figure 5.4. **233**

Figure E-5-5 DFT mechanism for SAM formation based on the properties of a model compound.

Calculations indicate that thiyl radicals (RS^\bullet , with here $R = C_3H_7$) produced by attack of solution O_2 on the thiol reactants (RSH) react with Si(111)-H to abstract hydrogen and for thiol physisorbed to a silicon surface radical (black dot). Reaction over a barrier then leads to chemisorption and radical regeneration. This provides initiation for a free-radical polymerization reaction that then covers the surface with adsorbate. Some critical bond lengths are shown, in Å. **234**

Figure E-5-6 A chemisorbed intermediate found on the 2D surface, showing

the covalent-bond lengths to sulfur, in Å. **235**

Figure E-5-7 The top frame shows the energy calculated for the indicated model cluster system as a function of a continuous reaction coordinate, going from the physisorbed intermediate over the transition state to form products. The lower frame shows the critical Si-S, S-H, H-H, and H-Si bond lengths (see Figure 5.4) along this reaction coordinate. While at the transition state, the H-H and Si-S bonds are largely formed whilst the S-H and Si-H are largely unbroken, critical changes to all 4 bond lengths do occur at this structure. The reaction coordinate follows the eigenvector of the hessian matrix with imaginary eigenvalue away from the transition state (green region), but afterwards becomes the results of unconstrained geometry optimization. The reaction profile for the model compound is similar. **236**

Scheme E-5-1 Synthesis of compound 3..... **240**

Figure E-5-8 ¹H NMR 400 MHz (CDCl₃) spectrum of 3 **241**

Figure E-5-9 ¹³C NMR (CDCl₃, 101 MHz) spectrum of 3 **242**

Figure E-5-10 ¹³C NMR spectra for 3 (blue) and 1 (red) with the methyl signal in 3 at δ=15.7. **243**

Figure E-5-11 a) XPS High-resolution Si 2p emission and b) S 2p emission for a Si(111)-H surface incubated in 4 mM solution of 3 for 24 h. ... **244**

Figure E-5-12 a) XPS high resolution Si 2p emission and b) S 2p emission for untreated Si(111)-H electrode stored in DCM for 24 h. **244**

Figure E-5-13 Cyclic voltammograms of Si(111)-H surface incubated in 4 mM solution of 3 for 24 h. The voltammograms show absence of ferrocene signals and an increase in current beyond + 400 mV, indicating surface oxidation in the absence of a monolayer, suggesting that 3 does not form a monolayer on Si(111)-H surfaces. **245**

Figure E-5-14 Plateau length histogram for (a) Au-2-Au with average plateau length of 0.25 nm and (b) Si-2-Si junctions with average plateau length of 0.70 nm. This suggests that due to the enhanced mechanical stability, the Si-2-Si junctions are resistant to breakage during the entire pulling cycle while the typical Au-2-Au junctions break before a full molecular stretch **246**

List of Tables

Table 2.1 List of abbreviations, structures and names of the used self-assembly molecules. ⁹¹ Table 2.1 adapted from ref. 91 with permission from, Royal Society of Chemistry Copyright © 2010	20
Table 6.1 TUNA currents recorded for the areas A, B and C of the oxide hillocks formed by negative bias (−1 V).	154
Table C–4–1. Fitted SAM thickness and surface roughness (in Å), and fitted SLD (in 10 ^{−6} Å ^{−2}) for bis-diazo on Si(111)–H for the electrochemical and spontaneous grafting as determined from XRR data (see XRR curves in Figure 4.4 in the main text).	211
Table E–5–1 Theoretical parameters used in the modelling.....	231
Table E–5–2 Fitted SAM thickness and surface roughness (in Å), and fitted SLD (in 10 ^{−6} Å ^{−2}) for 2 on Si(111)–H as determined from XRR data (see XRR curves in Figure. 5.2c).....	232

List of Abbreviations

List of abbreviations commonly used in this thesis

Abbreviation	Definition
ACN	Acetonitrile
AFM	Atomic force microscopy
c-AFM	Conductive atomic force microscopy
CV	Cyclic voltammetry
DCM	Dichloromethane
DFT	Density functional theory
DMSO	Dimethyl sulfoxide
ET	Electron transfer
Fc	Ferrocene
Fc ⁺	Ferrocenium
I-V	Current-Voltage
NMR	Nuclear magnetic resonance
PF-TUNA	PeakForce tunnelling current atomic force microscopy

ppm	Parts per million
SAM	Self-assembled monolayer
SEM	Scanning electron microscope
STM	Scanning tunnelling microscopy
TEM	Transmission electron microscopy
UV	Ultraviolet
XPS	X-ray photoelectron spectroscopy
XRR	X-ray reflectometry

Dedication

I would like to dedicate this thesis to my dear mother and father.

List of awards, publications and presentations

1. Awards

Kagi-Alexander HDR Publication Prize 2019

(Awarded by the Curtin University in recognition of truly outstanding academic performance in 2019)

2. As a first/ co-first author

- C. R. Peiris, S. Ciampi, E. M. Dief, J. Zhang, P. Canfield, A. P. Le Brun, D. Kosov, J. R. Reimers and N. Darwish, Spontaneous S–Si bonding of alkanethiols to Si(111)–H: towards Si–molecule–Si circuits, *Chem. Sci*, 2020, 11, 5246–5256.

DOI: 10.1039/D0SC01073A.

- C. R. Peiris, Y. B. Vogel, A. P. Le Brun, A. C. Aragonès, M. L. Coote, I. Díez-Pérez, S. Ciampi and N. Darwish, Metal–Single-Molecule–Semiconductor Junctions Formed by a Radical Reaction Bridging Gold and Silicon Electrodes, *J. Am. Chem. Soc*, 2019, 141, 14788–14797.

<https://doi.org/10.1021/jacs.9b07125>

- M. C. Walkey, C. R. Peiris, S. Ciampi, A. C. Aragonès, R. B. Domínguez-Espíndola, D. Jago, T. Pulbrook, B. W. Skelton, A. N. Sobolev, I. Díez Pérez, M. J. Piggott, G. A. Koutsantoni and N. Darwish, Chemically and Mechanically Controlled Single-Molecule Switches Using Spiropyran, *ACS Appl. Mater. Interfaces*, 2019, 11, 36886–36894.

<https://doi.org/10.1021/acsami.9b11044>

3. As a co-author

S. Rahpeima, E. M. Dief, C. R. Peiris, S. Ferrie, X. Duan, C. L. Raston and N. Darwish, Reduced graphene oxide–silicon interface involving direct Si–O bonding as a conductive and mechanical stable ohmic contact, *Chem. Commun*, 2020, 56, 6209–6212.

DOI: 10.1039/D0CC02310H.

• K. Vimalanathan, I. Suarez-Martinez, M. C. R. Peiris, J. Antonio, C. de Tomas, Y. Zou, J. Zou, X. Duan, R. N. Lamb, D. P. Harvey, T. M. D. Alharbi, C. T. Gibson, N. A. Mark, N. Darwish and C. L. Raston, Vortex fluidic mediated transformation of graphite into highly conducting graphene scrolls, *Nanoscale Adv*, 2019, 1, 2495-2501.

<https://doi.org/10.1021/jacs.9b00297>

• J. Zhang, S. Ferrie, S. Zhang, Y. B. Vogel, C. R. Peiris, N. Darwish and S. Ciampi, Single-Electrode Electrochemistry: Chemically Engineering Surface Adhesion and Hardness To Maximize Redox Work Extracted from Tribocharged Silicon, *ACS Appl. Nano Mater*, 2019, 2, 7230-7236.

<https://doi.org/10.1021/acsnm.9b01726>

• J. Zhang, F. J. Rogers, N. Darwish, V. R. Gonçalves, Y. B. Vogel, F. Wang, J. J. Gooding, M. C. R. Peiris, G. Jia, J. P. Veder, M. L. Coote and S. Ciampi, Electrochemistry on Tribocharged Polymers Is Governed by the Stability of Surface Charges Rather than Charging Magnitude, *J. Am. Chem. Soc*, 2019, 141, 5863-5870.

<https://doi.org/10.1021/jacs.9b00297>

• E.M. Dief, Y.B. Vogel, C.R. Peiris, A.P. Le Brun, V.R. Gonçalves, S. Ciampi, J.R. Reimers and N. Darwish, Covalent linkages of molecules and proteins to Si-H surfaces formed by disulfide reduction, *Langmuir*, 2020, 36, 49, 14999–15009.

<https://doi.org/10.1021/acs.langmuir.0c02391>

4. Oral presentations

• Peiris, M. C. R.; Ciampi, S and Darwish, N. Spontaneous Formation of Diazonium Salts Thin Films on Silicon Electrodes, *Electrochemical Society (236th ECS Meeting)*, Atlanta, USA (2019).

• Peiris, M. C. R.; Ciampi, S and Darwish, N. Towards Single-Molecule Diodes via diazonium salts on Silicon, *Meeting Abstracts, The 20th International Union of Materials Research Societies–International Conference in Asia (IUMRS-ICA)*, 22-26 September, Perth, Australia (2019).

Chapter 1

Thesis Overview

This thesis consists of seven chapters, where Chapter 1 is an overview of this thesis. Chapter 2 discusses in detail the background of self-assembled monolayers and their application in molecular electronics to develop single-molecular circuitry. Three main results and discussion chapters are presented where two chapters are already published in peer-reviewed articles which are presented in Chapter 4, 5 and 6 respectively. Chapter 7 presents the overall picture of my PhD and future work to be done. It should be noted here that Chapter 4 and 5 are content of already published articles where reformatted according to the thesis format with the consent of all authors contributed to this work. Supporting information of these articles are sequentially presented in Appendix C and E with slight modifications.

As mentioned above, Chapter 2 discusses self-assembled monolayer formation methods on Au and Si and the importance of the SAMs on Si for future molecular electronics. This chapter also discusses in details about the molecules which can be used to develop monolayers on Si and the methods which can be applied to have complete coverage.

Chapter 3 presents the specific information regarding the instruments used for the characterization and basic details about preparing the electrodes for the monolayer formation.

Chapter 4, already published in *Journal of American Society of Chemistry (JACS)* describes the molecular films formed from diazonium salts with diazonium moieties at both ends which enables the facile synthesis of single-molecular contacts between gold and silicon electrodes at open circuit potential via a radical reaction. Here this Chapter also demonstrates that the kinetics of film grafting is crystal-facet dependent, being more favourable on (111) than on (100), a finding that adds control over surface chemistry during the device fabrication.

Chapter 5, already published in *Chemical Science* describes the synthesis of covalently linked self-assembled monolayers (SAMs) on silicon surfaces, using mild conditions, in a way that is compatible with silicon-electronics fabrication technologies. To date, alkanethiols on metal surfaces, mainly Au, are the most common due to the well-established Au–thiol contact. Here we report the self-assembly of 1,6-hexanedithiol on Si–H electrodes. The monolayer formation is spontaneous and requires no heating, UV irradiation, or external catalysis, but is dependent on having ambient levels of dissolved O₂ in solution. DFT calculations are used to confirm the mechanism of the thiol reaction with H–terminated silicon surfaces. The impact of the Si–S chemistry in single-molecule electronics is demonstrated using a scanning tunnelling microscope (STM–junction) approaches by forming Si–1,6-hexanedithiol–Si junctions.

Chapter 6 demonstrates how silicon oxidation can be used as a technique to separate molecular arrays for future molecular electronic circuits. Oxide on silicon can be used as an insulator to separate molecular components from each other or as a resistor depending on the thickness of the oxide layer. Chapter 6, aims to determine first, the threshold voltage needed to oxidise the Si surface to form a uniform and insulating layer of oxide on Si(111)–H compared to the isotope substituted Si(111)–D surfaces. Secondly, the current-voltage (I–V) properties of the thin oxide layers are explored by using conducting atomic force microscope (AFM), peak force tunnelling current (PF–TUNA) mode. Importantly, this chapter demonstrates that topography is deceptive in visually assessing the oxide formation as minimal changes in the oxide thickness lead to a large change in the electrical measurement. To determine the mechanism of the oxidation and separate the effects of the electric field from electron tunnelling, Pt–Si Schottky junctions with both n–type and p–type Si were examined. This work also illustrated that SiO_x structures have other behaviours than simply insulating and showed that oxide layer breakdown with applying a high bias such as ±6 V can develop conducting oxide channels and by applying a lower voltage above these conducting channels can reverse this process, a concept that where this can be used for future memory devices.

Chapter 7 discusses the conclusions derived from all of the results and discussion chapters (4, 5 and 6) along with the future outlook of this work. The permission to use the articles and signed author contribution letters for Chapter 4, published in *Journal of American Society of Chemistry (JACS)* and Chapter 5 published in *Chemical Science* are provided in Appendix B and D respectively.

Chapter 2

General Introduction

2.1 Overview

Covalently linked single-molecule electronic circuits can be described as chemically modified surfaces where single organic molecules are exploited as the switching,¹⁻³ sensing⁴⁻⁷ or current rectifying components.⁸⁻¹⁰ In molecular electronics devices, organic molecules serve as the medium of transporting electrical current, and/or they can be chosen to engineer the charge-transport properties of the substrates onto which they are grafted.¹¹ The field of molecular electronics has been constantly expanding over the past decade. This expansion has been prompted mainly by the expectation that electronics incorporating molecules will replace complementary metal-oxide-semiconductor (CMOS) technologies.¹²

The biggest challenge interposed between this concept and its practical implementation, is, at ambient conditions, the lack of sufficiently robust contacts between an electrode surface and a molecule. Up-to-date, the most widely reported and used single-molecule contacts have been thiols (RSH), typically chemisorbed to gold surfaces. Such contacts are easy to form under ambient conditions from dilute solutions. For example, forming a self-assembled monolayer (SAM) of a thiol molecule on gold (Au) surfaces requires merely to rest a clean gold surface in a dilute solution of the monolayer-forming molecule.¹³⁻¹⁵ Although extensively used in the laboratory, molecular electronics based on gold platforms suffer from major drawbacks, such as the high mobility of the S–Au bonds and also the wide range of bonding structural motifs of relatively similar energies. The central issue is that the Au–S bonds are governed by dispersion forces and they are relatively weak, poorly directional, and can contain a broad range of coordination numbers.¹⁴

Metal–S junctions suffer from a limitation associated with the use of metal: the properties of the metal are fixed and so only the molecules are available to orchestrate control of the device properties. While alloys offer some prospects, the electronic properties and reactivity of alloys are generally complex and hard to

predict. On the other hand, the use of a semiconductor as the substrate would open up many forms of device design and control, effectively allowing the technology of molecular electronics to develop further.

Therefore, an increasing interest in expanding the field of single-molecule electronics from using conducting materials such as gold towards semiconducting materials (GaAs and Si)¹⁶ as these materials are freely available and are manufactured by the electronics industry to develop electronic devices. Merging the tunable electrical properties of these semiconducting materials with the large pool of organic molecules is expected to lead to a range of new technologies. Si provides an attractive alternative for a bottom substrate for molecular electronics because Si is compatible with solid-state electronic devices which are normally made of semiconducting materials, also Si is commercially available as atomically flat substrates, which can be readily modified by standard etching procedures. Obviously, the electronic properties of the Si wafer can be controlled via doping level and type.

From previous work carried out on SAMs on Au and Si, it is apparent that extensive research is required to fill the gaps left by the problems encountered. In this PhD, the main focus is the development of SAM-modified Au and Si substrates, using covalent bonding via diazonium and thiol chemistries. Both electrochemical, and non-electrochemical techniques will be explored in the context of surface functionalization and a strong emphasis will go towards testing these contact chemistries in molecular electronics devices. Characterization of the SAM-modified Au and Si surfaces are carried out by using X-ray reflectivity (XRR), X-ray photoelectron spectroscopy (XPS), atomic force microscopy (AFM), scanning tunnelling microscopy (STM), and electrochemical methods. The results of this doctorate contribute to developing stable covalent single-molecule circuits to contribute towards the prospects of molecular electronics.

For diazonium salts such as Fast Blue B salt, the application scope is very broad due to the presence of two diazo group in the same molecule where it can make a connection with two electrode at once. Molecules such as Fast Blue B salt can be used in numerous applications such as sensors, Au nanoparticle attachment and as chemical resistors. These applications indicate the importance of carrying out the work related to diazonium salts. Therefore, discovering new conductive and stable

single-molecular circuit components will bring us closer to the ultimate target of molecular electronics as the active components in our everyday devices and open many possibilities in electronics. In this thesis, it is discovered that thiols (at certain conditions) can be grafted onto Si surfaces spontaneously, similarly to Au. Considering the application scope of thiols, this is a giant step towards future molecular and other applications which have so far used Au as the substrate.

Even though oxide formation on Si is considered a disadvantage in some cases, especially uncontrolled oxide growth, forming oxide of the right thickness in the right place is very important in molecular electronics and nanolithography. In Chapter 6, it is discussed in detail how lithography conducted by AFM to form SiO_x can be used in applications for isolating molecular arrays, resistors and diodes. Si oxide growth on Si has been studied by different methods. Here, this aims to determine firstly, the threshold voltage of the oxidation of Si surface which forms an insulating layer of oxide and secondly, the current-voltage (I-V) properties of the thin oxide layers by using conductive AFM (c-AFM) peak force tunnelling current (PF-TUNA) mode. The AFM PF-TUNA method is capable of recording current which is passing through the oxide. The topography is deceptive in visually assessing the oxide formation as minimal changes in the oxide thickness lead to large changes in the electrical measurements. Hence, the study of the I-V response on different oxide thicknesses will help to understand that at what bias voltage the oxide layer will function as a complete insulator and in which potential window or as an ohmic resistor in series with a Schottky diode. This work also illustrated that SiO_x structures have other behaviours than simply insulating and showed that oxide layer breakdown with applying a high bias. By applying high bias, the properties of the oxide can be changed from insulating to highly conducting and ohmic by forming conducting oxide channels. These switching Schottky/ohmic properties can be potentially used as nanoscale memory devices also in the perspective of molecular electronics devices. This introduction surveys the current landscape of work on the SAMs of organic monolayers primarily on Au, Si and SiO_x substrates reported with a view towards molecular electronic circuits. A range of strategies employed for the grafting of SAMs are discussed in detail mainly for diazonium salts, thiols, alkenes and alkynes on bare Au, Si and SiO_x surfaces. These techniques are handy for the grafting of SAMs and the

study of electron transfer mechanisms using scanning probe techniques. Characterization and applications as molecular electronic devices are discussed in the latter part of this chapter.

2.2 Basics of SAMs

Self-assembled monolayers can be formed by the spontaneous adsorption of molecular, ionic and radical adsorbates on the surfaces of a variety of substrates. Self-assembly is initially driven by the adsorption of molecules that come in contact with an interface. Stable monolayers are derived from a chemical interaction between an adsorbate and a substrate through a stable covalent bond. Self-assembled monolayers delivered a convenient and facile method for altering the interfacial properties of substrates (Figure 2.1). Although the majority of SAMs are on solid crystalline surfaces, SAMs also can form on liquid surfaces.¹⁷ When SAMs form on liquid surfaces,¹⁸⁻¹⁹ a weakly physisorbed bond is formed with properties such as bond strength is in between the chemisorbed bond with the solids and Langmuir films.²⁰ Organic molecules can form monolayers with carbon,²¹⁻²² metals (Au,²²⁻²⁴ Ni,²⁵⁻²⁷ Cu,²⁷⁻²⁹ Co²⁷), semiconductors (Si,³⁰ InAs,³¹ GaAs³²⁻³³), hydroxylated surfaces (SiO₂ / Si,³⁴⁻³⁵ Al₂O₃ / Al,³⁶ TiO₂ /Ti,³⁷ mica,³⁸⁻³⁹ glass^{5, 40}) and metal oxides (AgO).⁴¹ Among SAMs, the most popular are those of thiols and dithiols on Au^{13-15, 42-44} because of their applications in several fields of nanotechnology. Au has attracted considerable interest,⁴⁵⁻⁵² owing to their ease of preparation from gas or solution phases. Another reason is the order and stability of SAMs dependent on the Van der Waals forces between the alkyl chains. Therefore, flat surfaces produce more ordered SAMs compared to rougher surfaces. Au surfaces which are atomically flat can be easily obtained by the flame-annealing of Au single crystals, or template stripping from mica.

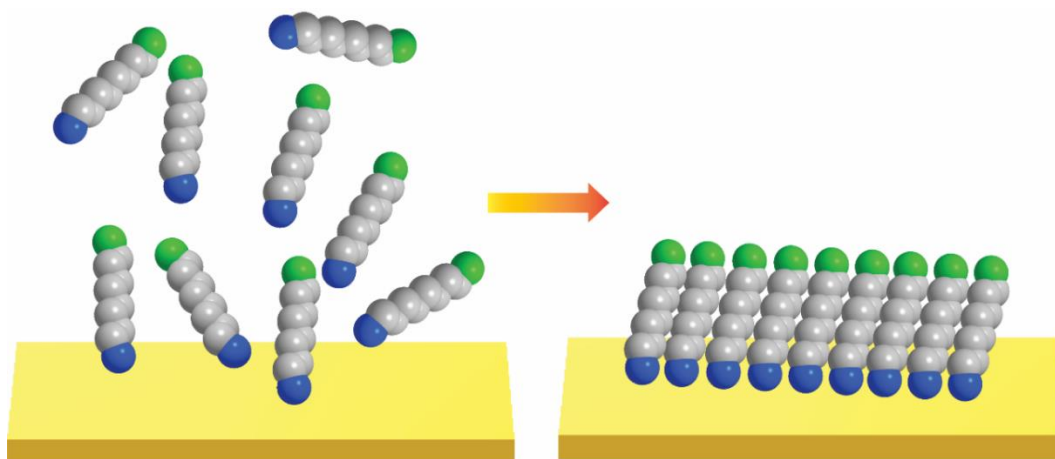


Figure 2. 1 Self-assembly of molecules on a solid surface

SAMs provide a straight forward approach to construct materials with various physical and chemical properties from readily accessible building blocks. The self-assembly process can entail different methods of construction, such as protein folding.⁵³ Specifically, a top-down approach is the method where the sample is a blank canvas and an external stimulus is used to write patterns. In contrast, a bottom-up approach is where the final structure is determined by the substrate itself and the molecules self-assemble into the anticipated arrangement. In recent years, top-down control is used to guide bottom-up methods which are extensively used in modern nanotechnology.^{6, 54}

The applications of SAMs in nanotechnology are countless. Among them is the functionalization and stabilization of nanomaterials such as nanoparticles,⁵⁵ nanorods and nanowires; surface protection of materials from corrosion; anti-stiction coatings and friction reduction. In device fabrication, SAMs can be used as building blocks in sensors. They can further be utilized as active or passive elements in electronic devices,⁵⁵⁻⁵⁷ such as transistors, diodes, resistors, switches; and function as molecular wires in single-molecule circuits, also as inks in microcontact printing and dip pen lithography⁵⁸⁻⁵⁹ as shown in Figure 2.2. Among the other possible applications of SAMs, here this chapter mainly focuses on discussing the potential application of self-assembled monolayers for the molecular electronic industry to develop robust single-molecule circuits.

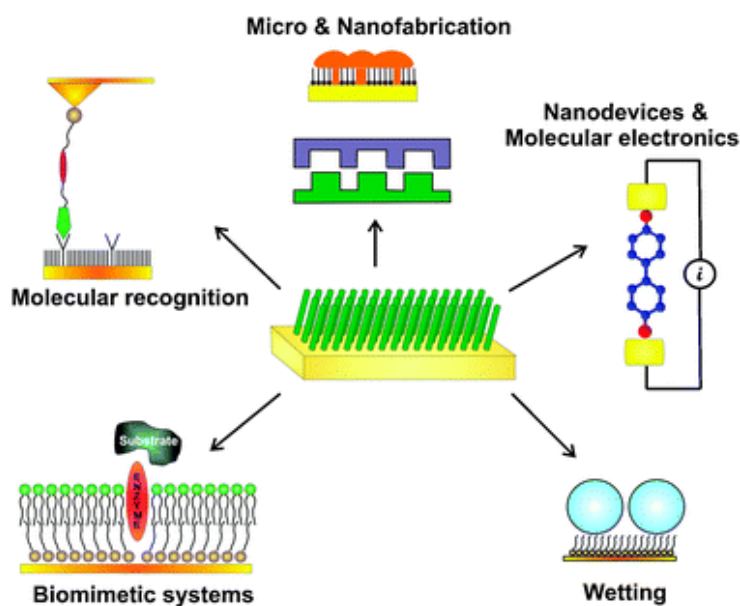


Figure 2. 2 Current trends in molecular electronics.¹⁵ Figure 2.2 adapted from ref. 15 with permission from, Royal society of chemistry Copyright © 2010.

Microelectronics is a fast-growing field related to nanotechnology aiming at the utilization of electrical properties of molecules. The discovery of these electrical properties of single-molecules will help substitute traditional micro or semi-micro-scale materials which are used to make the components inside an electronic device, further miniaturizing electronic devices. The main advantage that comes with molecules as the building block of electronic devices is the tunability. The chemical and physical properties can be easily modified by using different molecules attached to a single substrate in a few angstroms distance. In 1965, G. E. Moore described Moore's law which is that the number of transistors in an integrated circuit will double approximately every two years.⁶⁰ With the size of electronic devices getting smaller, we are already in the position of moving from a submicron to the nanoscale. The fact with current device components such as transistors which are made of Si has already reached the nanoscale (7 nm and with up to 39 billion transistors fitted on a single chip). The use of molecules at this point is the only way forward because we can't make transistors with Si much smaller than 7 nm. Therefore, in the past few years, scientists were trying to develop these electronic devices by using organic molecules which are connected to another conductive layer on top. At present, molecular electronics devices have taken a step further by developing single-

molecular contacts which can function as a single electronic component. This will allow the printing of hundred billion transistors in a single Si chip. Due to this innovation, this will bring the computing power of devices to the next level with a very smaller size with higher capacities and functions.

At present, molecular electronics are in the experimental level, exploring anchoring new organic molecules with different functional groups on Si surfaces. The functionality of the molecular electronic device is measured by its electrical properties. The current methods employed to quantify the electrical properties are the scanning tunnelling microscopy break-junction method (STM-BJ), STM-“blinking” method,^{1-2, 61-64} conductive probe atomic force microscopy and tunnelling current atomic force microscopy.^{38, 65-66}

This chapter covers the various aspects of developing SAMs on Au and Si surfaces. Section 2.3 and 2.4 of this chapter describes the methods that can be used to anchor SAMs on Au and Si in detail and characterization methods of SAMs are covered in section 2.5. Finally, section 2.6 will outline the application and importance of SAMs on Si surfaces.

2.3 Self-assembled monolayers on Si and Au

The molecules used for SAMs are schematically composed of three main parts: (i) the head group, which is the end of the molecule that binds to the substrate, (ii) a backbone made of an aliphatic chain or an aromatic oligomer, which is also accountable for the molecular arranging, and (iii) the terminal group, which defines the surface energy, and chemistry of the outer interface as shown in Figure 2.3.

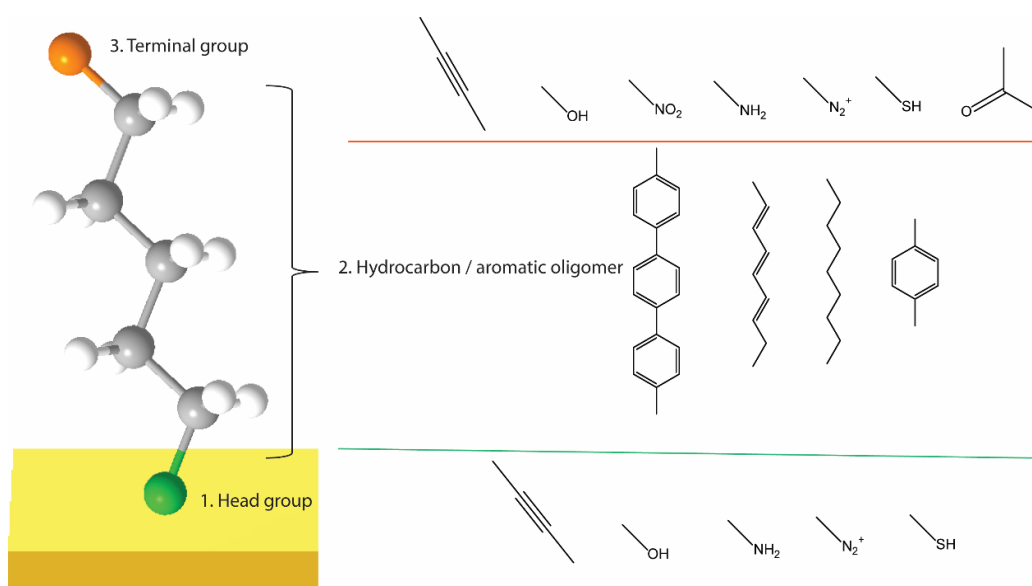


Figure 2. 3 Schematic diagram of typical self-assembling molecules with three major components (head, backbone and terminal group) which are highlighted on the left and examples for the head, backbone and terminal groups are shown on the right.

Self-assembly on a substrate results from the interactions of the head group with the surface, which constructs a chemical bond with the substrate atoms of the substrate which help molecules to bind to a surface. The hydrocarbon chain backbone and the head group will impart the orientation of the layer and the non-covalent Van der Waals lateral interactions between the chains stabilize the structure and yield molecular order. The terminal group can comprise a range of functional groups which will determine the chemical and physical properties of the surface. The combination of these three parts can be used to construct molecular electronic devices or other applications such as chemical or biosensors. The intramolecular interactions of the backbone will define the fine specifics of the superlattice structure such as tilt-angle. When there is a higher coverage with the chemisorbed molecules, interchain Van der Waals forces become valuable and it leads to close-packed and more ordered structures. When the surface coverage is poor it forms more disordered structures.

2.3.1 Grafting of SAMs on Au surfaces

Thiols form highly organized monolayers under mild conditions and the formed monolayers can be used to create interfaces with a diversity of functional groups.

These thiol altered surfaces have been used for applications such as biosensors^{4, 7, 67-69} and surface patterning.⁷⁰ Thiolate–Au complexes have been suggested as the bonding motif of SAMs not only for planar surfaces but also for thiol–capped Au nanoparticles as shown in Figure 2.4.⁴ The understanding of the S–Au interface structure and determine the nature of the S–Au bond is important in molecular electronics and device construction.¹³ The structure of alkanethiol SAMs on Au(111) and other single-crystal faces were addressed using electron diffraction studies.⁷¹ Even though the thiol modified surfaces have many advantages such as the preparation being easy to achieve and can be done both in the gas phase and in liquid environments, it has some drawbacks such as the instability of the thiol–SAM under certain conditions e.g. sonication or high temperature and the ability of the Au–S interaction permitting self-organization, which is the root of some of the limitations of this adsorbate–substrate arrangement. As a result, the potential of a Au–C covalent bond provides the impetus for the examination of SAMs derived from diazonium salts as an alternative to thiol-based SAMs for applications where exceedingly stable surface chemistry is required.²³ Thus, significant attention has been directed towards nitriles,⁷² amides,⁷³ alkynes⁷⁴ and diazonium salts^{22, 24, 73} as alternative organic molecules for SAMs on Au.

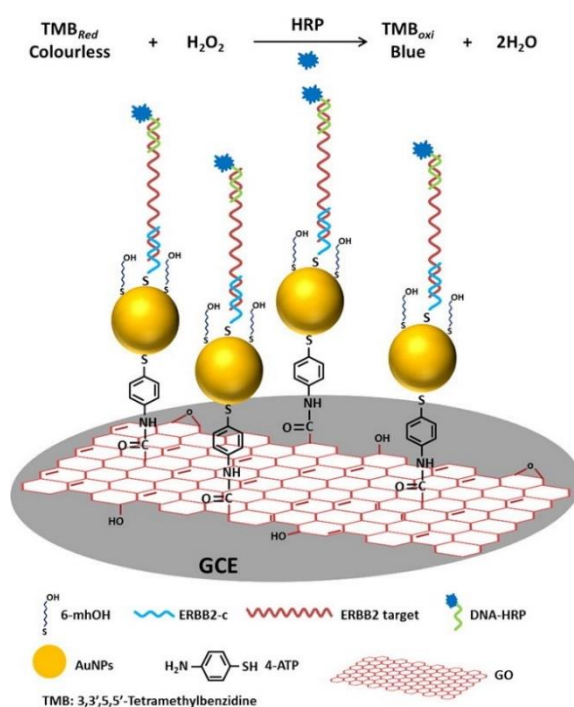


Figure 2. 4 Schematic presentation of the proposed DNA sensor showing the AuNPs–GO/GCE surface with the hybridization of target DNA.⁴ Figure 2.4 adapted from ref. 4 with permission from, Elsevier Copyright © 2017.

Among these organic molecules, SAMs of diazonium salts on Au surfaces are readily formed due to the high reactivity of diazonium salts. Diazonium salts can be easily reduced spontaneously which allows making the anchoring process more convenient forming a covalent bond via a radical reaction.^{23, 75} Since the radical formed from the decomposition of diazonium salts is very reactive, it tends to form monolayers and multilayers.²³ The advantage of the diazonium grafting is the stability of the diazonium derived aryl groups that form covalent bonds with Au surfaces.⁷⁶ The surface is stable even under ultrasonication, boiling in various solvents or exposing to ambient environments for a long time. In the same way, most diazonium salts reduce rapidly facilitating the process more readily²³ than with other organic molecules as shown in Figure 2.5. In 2009, Shewchuk et al.⁷⁵ compared and investigated the stability of monolayers on Au derived from 4-nitrobenzenediazonium tetrafluoroborate, a diazonium salt, and 4-nitrobenzenethiol, a thiol. Here, immersion in octadecanethiol solution results in the extensive displacement of the thiol derived monolayer, while the diazonium derived

films are comparatively stable to displacement. This shows that under these conditions, aryl films formed from the reduction of diazonium salts are more strongly bonded to Au surfaces than thiols.

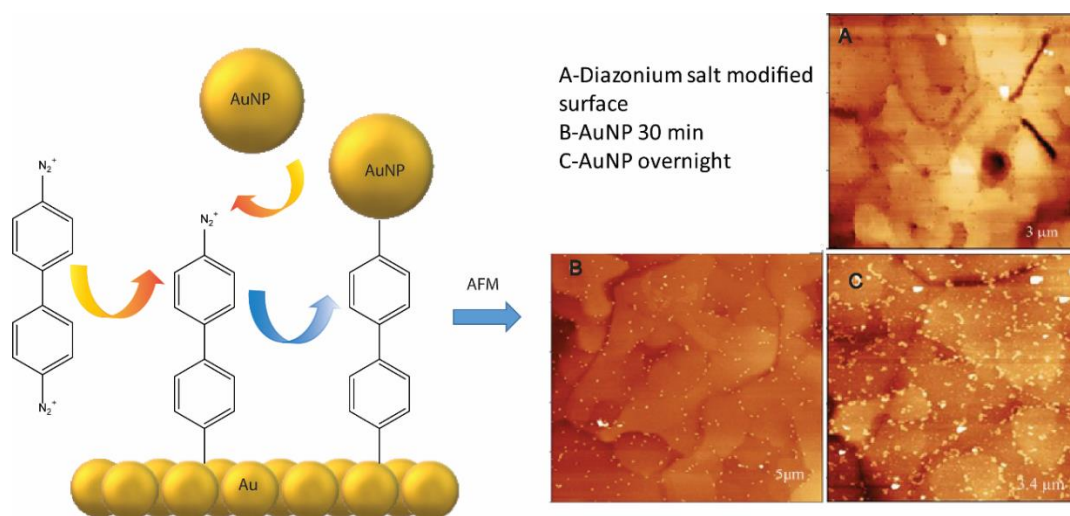


Figure 2. 5 Scheme of the functionalization method of combining diazonium salt and click chemistries for obtaining AuNPs assemblies on Au electrodes and AFM images A) diazonium salt modified Au B, C are the AuNP attachment to Au with 30 minutes and overnight, respectively. Unpublished results-Curtin University, molecular electronics group.

The study of alkynes and alkenes adsorbed on Au surfaces is also of significant interest. Patterson and Weaver in 1985 studied alkenes and alkynes on Au surfaces⁷⁷ to examine interactions in the aqueous phase. This study revealed that alkynes form a stable bond with Au, unlike other transition metals. The mechanism of attachment of alkynes on Au was proposed by Maity et al.⁷⁸ in 2013. In their survey, the bonding motif of these alkynes on Au clusters was investigated revealing that the terminal hydrogen is lost through the ligand exchange and that the $C\equiv C$ bond of the alkynyl group is weakened upon attachment to the Au clusters⁷⁸ as shown in Figure 2.6.

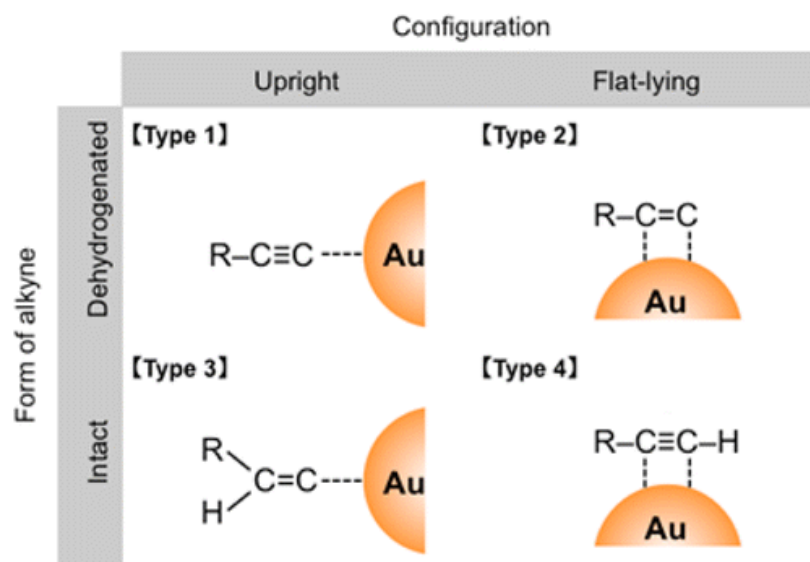


Figure 2. 6 Proposed binding mechanisms of the alkynes to an Au and Au nanoparticle.⁷⁸ Figure 2.6 adapted from ref. 78 with permission from, American Chemical Society Copyright © 2013.

Zhang et al.⁷⁹ reported a range of alkynes that can be spontaneously assembled on Au for nanoparticle attachment.⁷⁹ Here, as shown in Figures 2.7 and 2.8 show that terminal alkynes form comparatively organized and stable SAMs on Au which can also be used to stabilize Au nanoparticles. It was proposed that a Au–alkylate interaction was the mechanism of bonding.

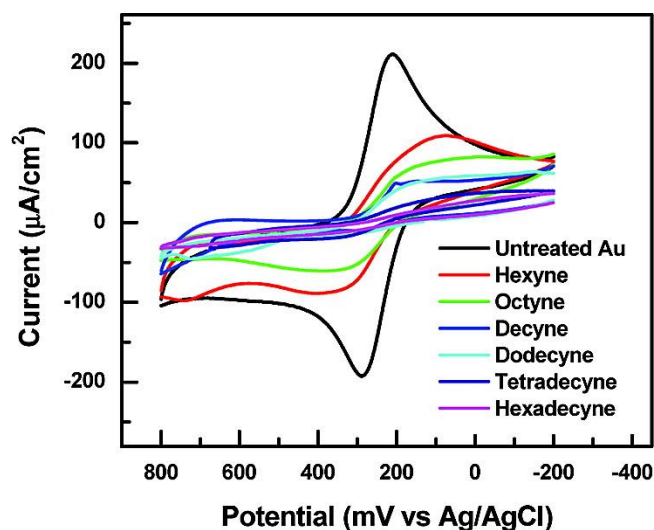


Figure 2. 7 Cyclic voltammograms at 100 mV/s of Fe(CN)₆^{3- / 4-} at the bare Au bead and SAM modified Au electrodes with compounds.⁷⁹ Figure 2.7 adapted from ref. 79 with permission from, American Chemical Society Copyright © 2007.

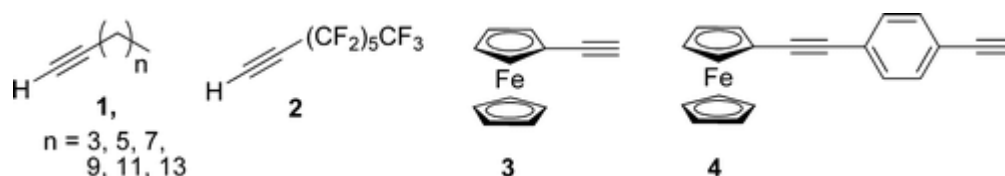


Figure 2. 8 Molecules studied on the Au surface by. Zhang .S et al.⁷⁹ Figure 2.8 adapted from ref. 79 with permission from, American Chemical Society Copyright © 2007.

One of the promising application of these alkynes on Au was reported by Pla-Vilanova et al.⁶² in 2015 by developing single molecular junctions using 1,4-diethynylbenzene (DEB). Here, the SAM was characterized by attaching ferrocene azide on the distal end of the alkyne by copper-catalyzed azide-alkyne cycloaddition as shown in Figure 2.9 The alkyne contact showed an elevated conductance comparable to amine and thiol groups. Here, the important point is the alkyne produced single-molecular junctions spontaneously with terminal alkynes and required no electrochemical control or chemical deprotonation.

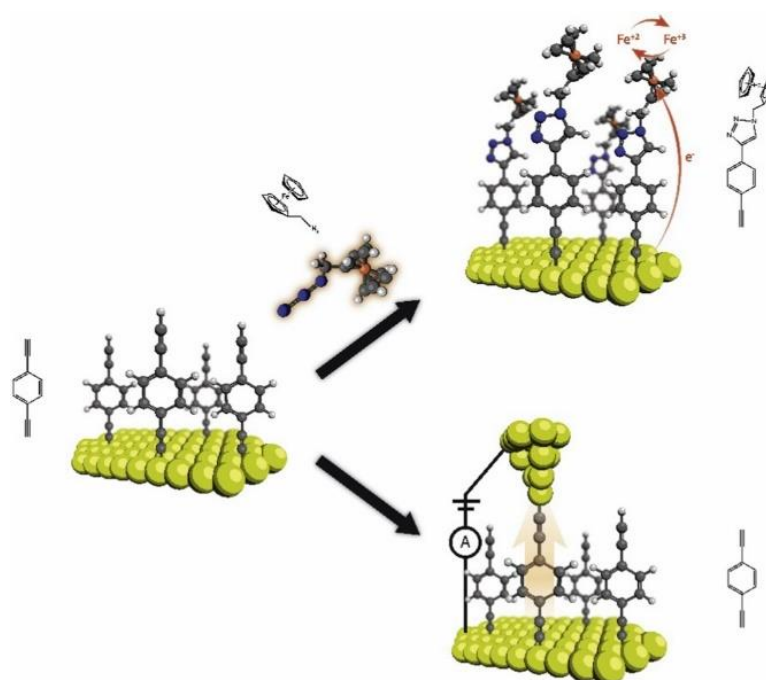


Figure 2. 9 Schematic of the CuAAC reaction of a DEB modified surface with a redox-active ferrocene moiety and the formation of junctions examined by STM via a single DEB molecule.⁶² Figure 2.9 adapted from ref. 62 with permission from, IOP Publishing Ltd © 2015.

Electrografting is one of the best methods to obtain an evenly distributed monolayer on Au surfaces. This method involves either an electron transfer between the electrode and the adsorbate or also by when a reducing or oxidizing reagent is added to generate the reactive species. Electroreductions on Au are reported for diazonium salts^{23, 75, 80-83} and diquinone⁸⁴. Electrografting provides higher surface coverage and overcomes disadvantages like multilayer formation where it can control the polymerization of the species.²³ Electrografting is also an important technique to determine the behaviour and redox potentials of molecules which are reduced on different crystalline phases. Benedetto et al.⁸⁰ showed that by using the electrochemical properties of diazonium salts that exhibit a strongly passivating behaviour on various microcrystalline Au electrodes which is shown in Figure 2.10, that each sub-peak observed in cyclic voltammetry corresponds to the reduction of the diazonium salts on a distinct crystallographic face.^{23, 80}

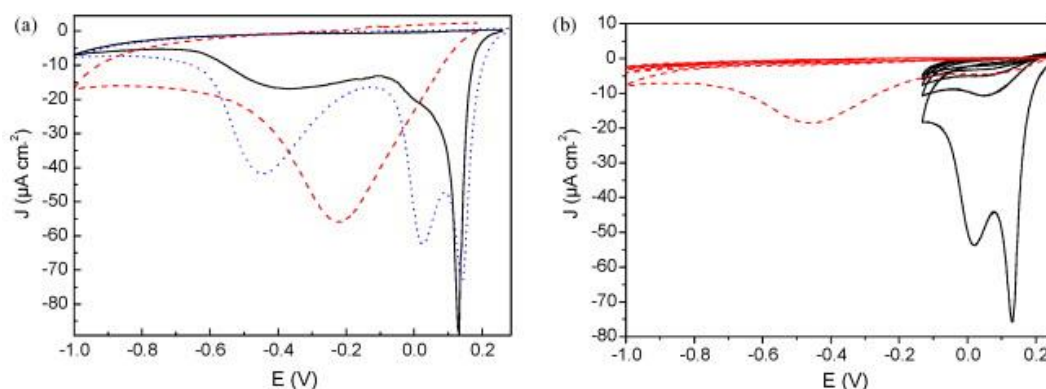


Figure 2. 10 Electrochemical grafting of diazonium salt on mono- and polycrystalline Au surfaces: a) solid line Au (gold(1 1 1) epitaxied on mica), dotted line Au (polycrystalline gold evaporated on glass), dashed line Au (gold deposited on bronze by galvanoplasty). (b) diazonium salt (0.005 M) cyclic voltammetry in acetonitrile (TEAP 0.05 M) on Au. The solid line and dashed line represent experiments that were conducted successively on the same substrate (Au).⁸⁰ Figure 2.10 adapted from ref. 80 with permission from, Elsevier Copyright © 2008.

Although these molecules form chemical bonds with Au, for most modern-day applications, such as electronic devices, Si is the most suitable substrate due to its low cost, highly tailorable properties, and readily available atomically flat surfaces. There are comparatively few reported Si surfaces modifications with molecules such

as diazonium salts⁸⁵⁻⁸⁶ and alkynes⁸⁷⁻⁸⁸ when compared to Au. Therefore, Si is ripe to be explored for modification with different SAMs.

2.4 Grafting of SAM on the Si surface

2.4.1 SAMs on native Si oxide

Commercially available Si materials always come with a thin layer of SiO₂ on the surface. Unoxidized Si readily reacts with oxygen and water to form an oxide layer. The most common technique is to remove this native SiO₂ layer, and to replace it with reactive Si–H, Si–Cl or Si–OH bonds, before the grafting of the SAM for molecular electronics applications. This is to overcome disadvantages such as uneven surface due to the thick oxide layer, high resistivity and oxide weakening the SAM which induces degradation of the monolayer.

The properties of Si can be changed by doping. In doping, a tiny amount of an impurity is added into the Si. Si can be doped to be either n-type or p-type. By doping small quantities of elements with extra electrons such as phosphorus or arsenic into the Si, one forms n-type Si. This places electrons into the conduction band, increasing the conductivity of the Si. By doping with elements with fewer valence electrons than Si, typically boron, p-type Si is formed. This forms holes, leading to an incompletely filled valence band, similarly increasing the conductivity of the Si. This doping converts Si into from an intrinsic semiconductor to a doped semiconductor as shown in Figure 2.11.

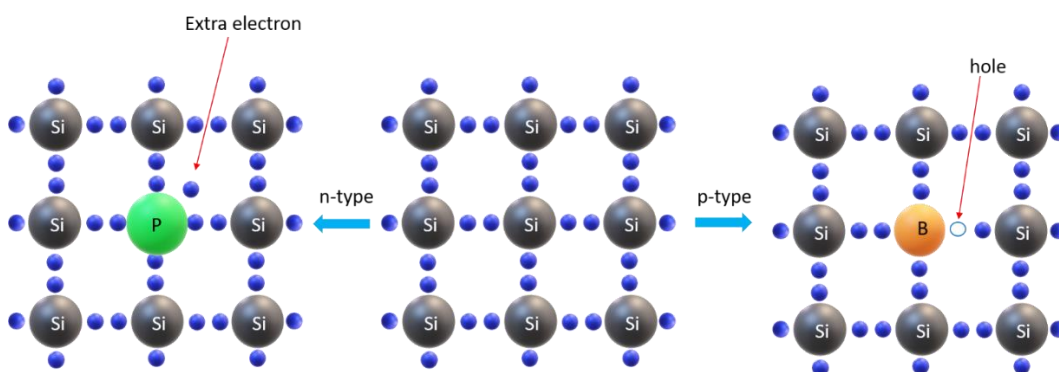


Figure 2. 11 A schematic diagram of Si-substrate with different doping type, where doping with phosphorus gives n-type and doping with boron forms p-type semiconducting Si.

In 1980, Sagiv et al.⁸⁹ published the first article demonstrating the formation of well-defined organosilane monolayers on SiO₂ by self-assembly from solution. Here, on the native oxide layer of Si, three types of molecules: silanes (RSiX₃, where X= Cl, OMe, OEt), organometallics (RLi, RMgX) and alcohols, are commonly used for the formation of self-assembled monolayers. An oxide layer with a high density of silanol groups is one of the prerequisites for obtaining a monolayer on SiO_x. These silanol groups provide anchoring sites for silanization reactions or converted into reactive functions such as Si–Cl or Si–NEt₂ groups.⁹⁰ A range of molecules which can be used for various applications after assembly onto Si oxide are shown in Table 2.1.

Table 2.1 List of abbreviations, structures and names of the used self-assembly molecules.⁹¹

Table 2.1 adapted from ref. 91 with permission from, Royal Society of Chemistry Copyright

© 2010

Abbreviation	Structure	Name
OTS		<i>n</i> -Octadecyltrichlorosilane
BTS		11-Bromoundecyltrichlorosilane
PFDTs		1 <i>H</i> ,1 <i>H</i> ,2 <i>H</i> ,2 <i>H</i> -Perfluoro-decyltrichlorosilane
EDATMS		<i>N</i> -[3-(Trimethoxysilyl)propyl]-ethylenediamine
APTMS		(3-Aminopropyl)trimethoxy-silane
APTES		(3-Aminopropyl)triethoxysilane
MPTMS		(3-Mercaptopropyl)trimethoxysilane
PEG silanes	$R-O-(CH_2CH_2O)_n-CH_3$ <p>R1 = SiCl₃ R2 = Si(OMe)₃ R3 = Si(OEt)₃</p>	Poly(ethylene glycol)
		R1 = trichlorosilane
		R2 = trimethoxysiloxane
		R3 = triethoxysiloxane
AHAPS		<i>N</i> -(6-Aminohexyl)-3-aminopropyltrimethoxysilane
PTCS		Phenyltrichlorosilane
BTCS		Benzyltrichlorosilane
ODS		<i>n</i> -Octadecyltrimethoxysilane
FAS17		Heptadecafluoro-1,1,2,2-tetrahydro-decyl-1-trimethoxy-silane
FAS3		3,3,3-Trifluoropropyltrimethoxysilane
CMPS		(4-Chloromethyl)phenyltrimethoxysilane
NTS		18-Nonadecenyltrichlorosilane
TFEE		2,2,2-Trifluoroethyl undec-10-enoate

Harsh treatment of the substrate is a requirement for obtaining a reactive oxide layer with a high density of silanol groups on the surface. There are two procedures to form these silanol groups as shown in Figure 2.12.

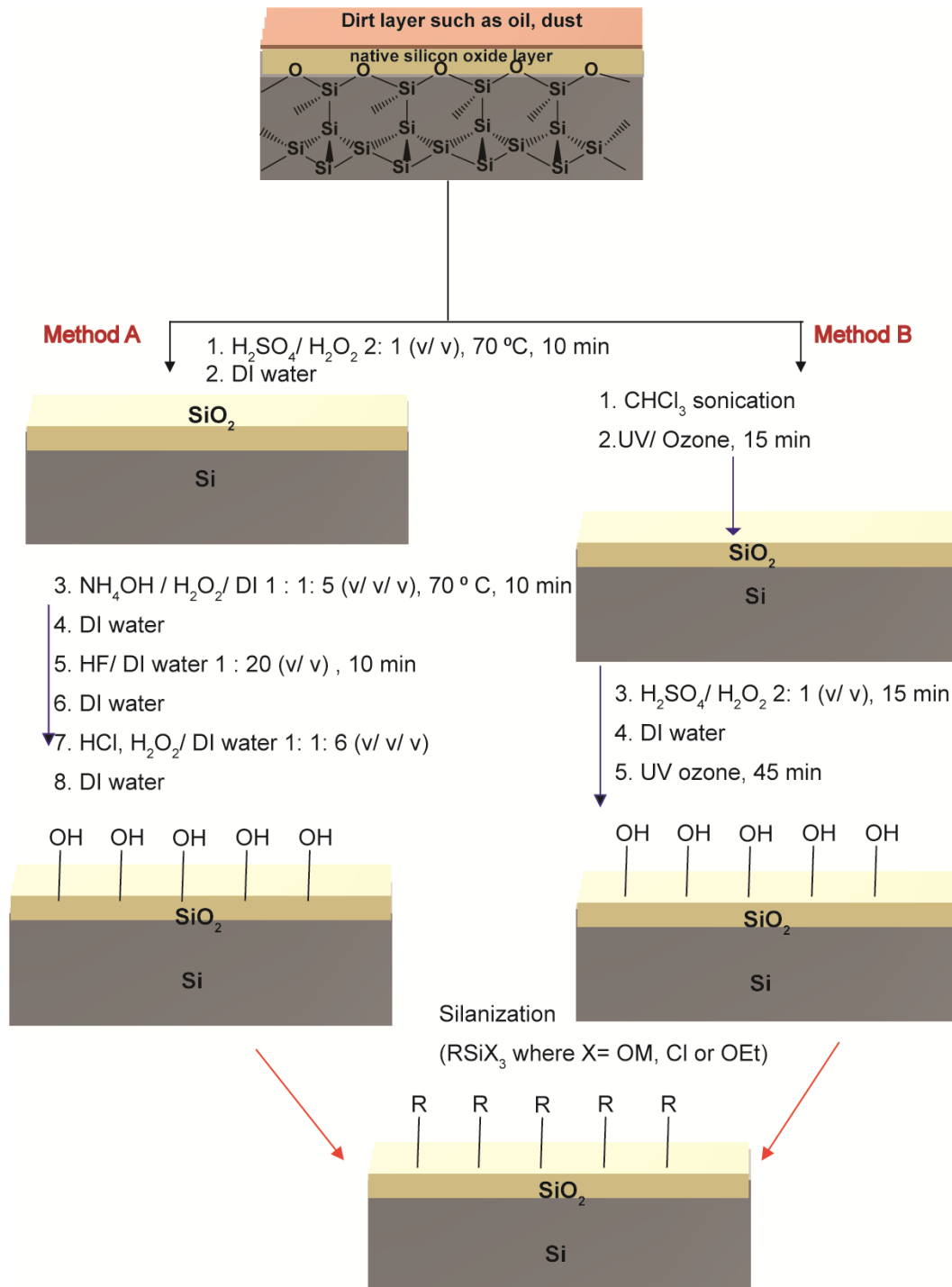


Figure 2. 12 Process of the SAM formation on a native oxide surface of Si.

Usually, the chemisorption of silane molecules on the hydroxylated Si surface as shown in Figure 2.13 is achieved by dipping the freshly hydroxylated surface into a silane solution.⁹²⁻⁹⁴

One issue with the usage of silanization is the Si–O bond is more sensitive to solvolysis than Si–C bond especially in solvents like water and alcohols due to their high nucleophilicity. As a solution, the Si oxide is converted into Si–H before forming the Si–C monolayer. The issue arises that Si–H is only stable on the order of tens of minutes in a normal atmosphere. To overcome this issue, it needs to have a complete or at least high surface coverage with Si–C bonded molecules. The next sections of this chapter discuss the preparation of Si surfaces for SAMs and common molecules which are used to form SAMs.

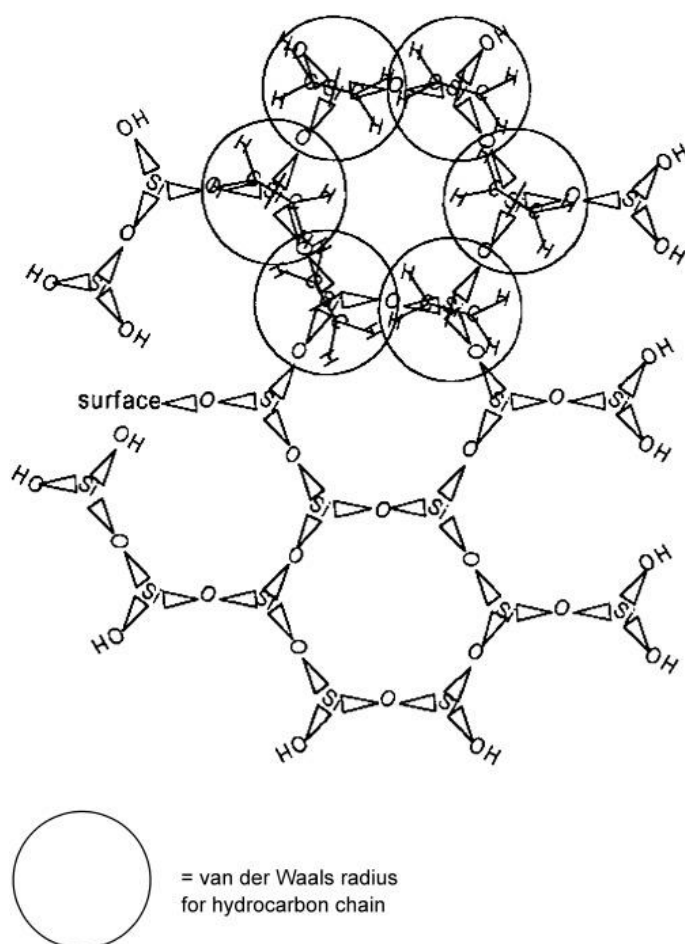


Figure 2. 13 Model of a growing monolayer crystallite resulting from the reaction of alkyl trichlorosilane with a Si oxide surface⁹⁴. Figure 2.13 adapted from ref. 94 with permission from, WILEY-VCH Verlag GmbH & Co. KGaA, Weinheim Copyright © 2005.

2.4.2 Preparation of Si–H surfaces

To prepare surfaces for hydrosilylation, Si wafers are first cleaned using Piranha solution (con. sulfuric acid: 30% hydrogen peroxide, 3:1) and rinsed in deionised water. To remove the SiO₂ and replace it with Si–H, the Si wafer is etched with hydrofluoric acid or a solution of ammonium fluoride. The summary of the process is as described in Figure 2.14.

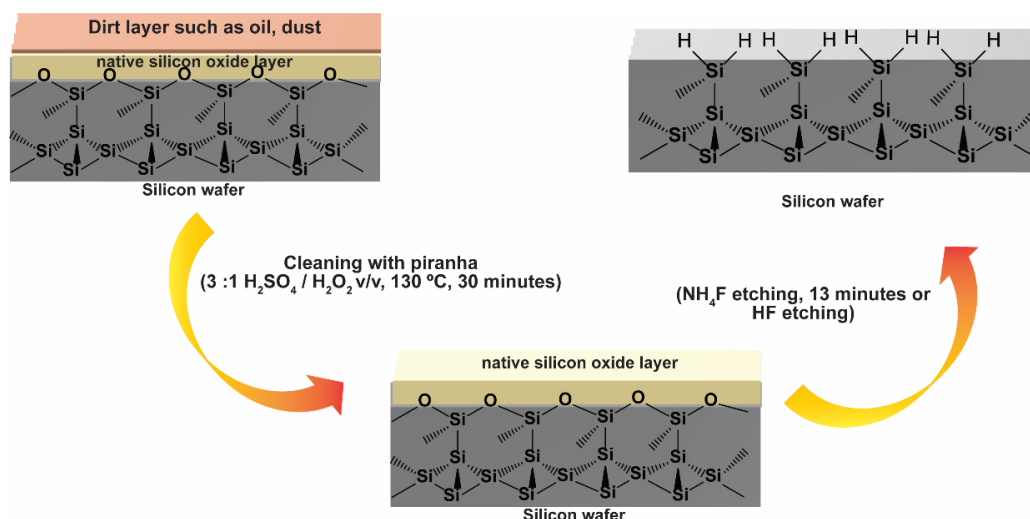


Figure 2. 14 The process of conversion of SiO_x into Si–H technique.

The monolayer formation on this Si–H surface involves a series of free radical reactions in the presence of molecules such as alkynes and alkenes.⁹⁵ This radical formation can also be induced by UV radiation^{87, 95} (photochemical hydrosilylation) or temperatures beyond 150 °C (thermally induced hydrosilylation), as the Si–H bond undergoes a homolytic cleavage and produces a Si radical at the surface.⁹⁶

2.4.3 SAMs directly on Si–X surface (where X= Cl, Br or I)

The second method used for attaching molecules directly on the Si surface is to convert Si–H into Si–X where the X is Cl, Br or I. There are a few methods that can be used for this technique by the way of converting Si–H into Si–X as shown in Figure 2.15. This Si–X reacts with organomagnesium, organolithium or alcohols to form monolayers (Figure 2.15).

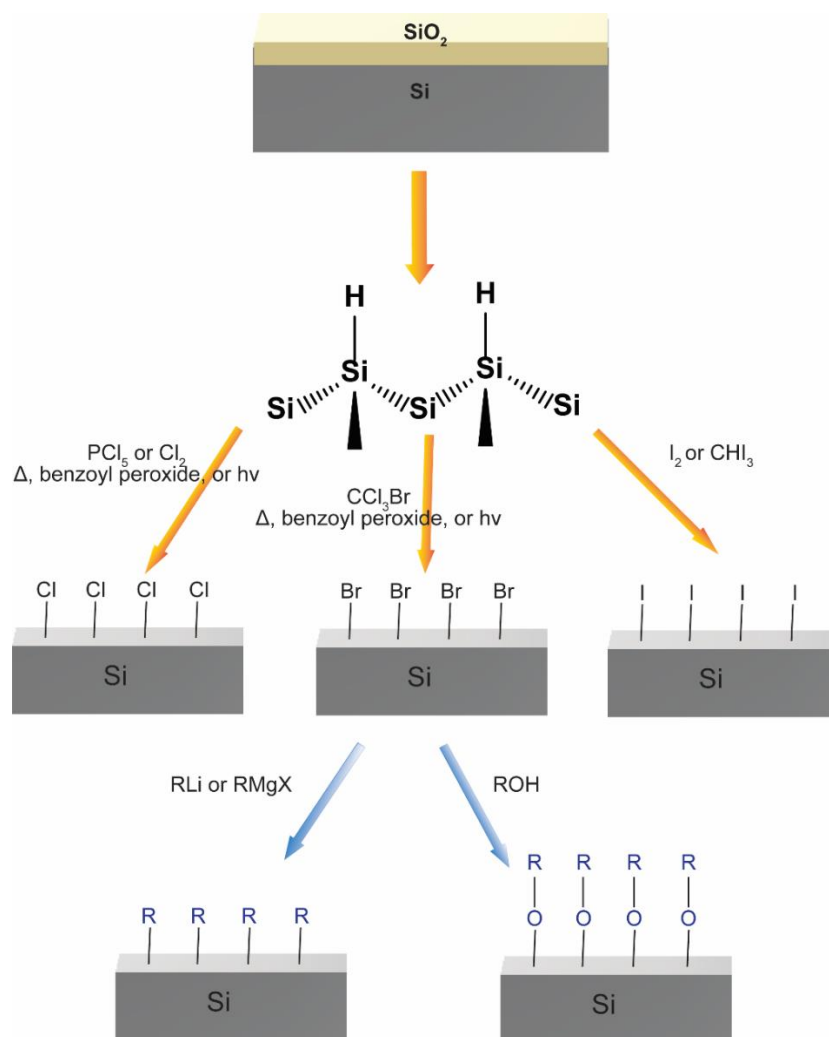


Figure 2. 15 The process of conversion of SiO₂ into Si-X technique.

2.4.4 Spontaneous Grafting of SAMs on Si Surfaces

Organic SAMs can be readily formed on reactive Si surfaces.^{2, 16, 97} With time scientists have discovered that spontaneous grafting of SAM on the Si surface is the most economical and easiest way to anchor molecules to Si. The freshly prepared hydrogen-terminated Si surface, which is commonly used for molecular electronics, is reacted with the targeted organic molecules for the formation of SAMs. This spontaneous grafting technique has been used with highly reactive species such as diazonium salts,^{23, 98} alkynes,⁹⁹ and recently thiols⁹⁷ to form monolayers with high surface coverage for molecular electronic applications. For the desired molecular electronic applications such as developing molecular wires, diodes and transistors, the formation of the rigid monolayer is very important but, most of the time,

spontaneous grafting will end up forming multilayers, especially with the highly reactive species such as diazonium salts²³ and does not yield complete coverage due to the random formation of diazonium derived radicals which attach to the surface. Some of the diazonium salts used to contain two diazo groups which will spontaneously react with another diazonium salt when the surface is completely covered. Lu et al.¹⁰⁰ formed porphyrin derived monolayers on Si to use with electronic applications. Here, two methods have been established for covalently grafting these porphyrins and metalloporphyrins with Zn, Cu, and Co on Si(100) surfaces. They discovered that the thickness can be controlled by the grafting conditions similarly to diazonium salts on Si.

Thiols are the most common molecules used with spontaneous grafting on Au but have not been previously studied extensively on Si without using any harsh conditions. Therefore, spontaneous grafting of thiols is worthy of further study and, in Chapter 5 examine in detail how thiols can be spontaneously grafted on Si which is the first work on the usage of thiols on Si for the formation of stable SAMs under mild conditions.

2.4.5 Electrografting of SAM on Si Surface

Electrografting has now become a widely used technique due to several benefits. Electrografting will easily form complete coverage of organic molecules on Si substrates. Depending on the functional groups attached to the molecule, the reduction potential can be tuned to higher or lower potentials.¹⁰¹ de Villeneuve et al.¹⁰² in 1997 showed a close-packed monolayer can be formed on a Si(111) surface using electrochemical reduction. Here, 4-nitro and 4-bromobenzene diazonium salts were electrochemically reduced on H-Si(111). Electrochemical measurements showed that these reactions formed robust monolayers with covalent $\equiv\text{Si}-\text{Ar}$ bonds with no oxide at the interface. Further work used electrochemical reductions to graft different diazonium salts on different semiconducting surfaces. Here reduction potentials varied depending on the crystalline phase of Si and the diazonium salt.²³ Hurley et al.¹⁰³ reported that electrochemical grafting terminal alkynes to porous Si gave two distinct types of surface derivatizations, depending on the polarity of the surface bias. Here, cathodic electrografting attached alkynes to the surface and

anodic electrografting yields an alkyl surface as a result of grafting. Wang and Buriak¹⁰⁴ also reported that alkylammonium and alkyl phosphonium cations can act as sources of organic moieties which can bind to hydrogen-terminated flat and porous Si with the proposed mechanism shown in Figure 2.16.

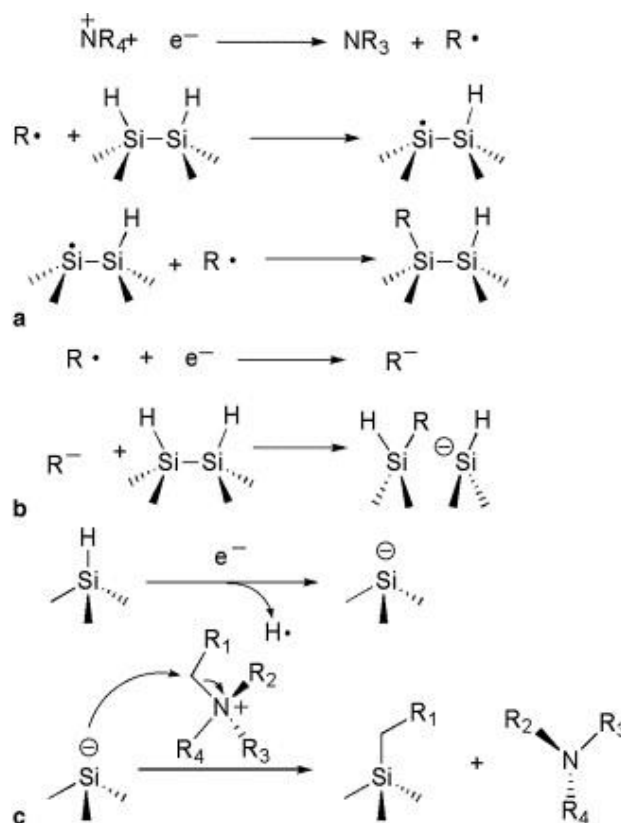


Figure 2. 16 Possible reaction mechanisms. (a) Electrochemical reduction of NR_4^+ followed by radical pathways, leading to Si–C bonds. (b) The alkyl radical is reduced to the anion, which attacks the Si–Si bond in a nucleophilic fashion. (c) Silyl anion attack on NR_4^+ cations to form Si–C bonds.¹⁰⁴ Figure 2.16 adapted from ref. 104 with permission from Elsevier B.V. © 2005.

Alkynes reduced by cyclic voltammetry to modify Si surfaces have applications such as modifying electrochemiluminescence¹⁰⁵ and the usage in nanoelectronics.^{16, 106} Ngunjiri et al.¹⁰⁷ used polystyrene microspheres which self-assembled on a Si(100) surface to serve as a dielectric mask to which cathodic potentials were applied in liquid hexynoic acid or phenylacetylene to produce nanoscale islands of bound hexynoic acid or phenylacetylene monolayers. Some porphyrins such as 5-(4-undecenyloxyphenyl)-10,15,20-triphenylporphyrin can be grafted to the Si surface by

electrografting for use in nanoelectronic devices.¹⁰⁸ Alkenyl pyrenes have also been reported to be electrografted on to Si in 2014 by Chattopadhyay et al.¹⁰⁹ Here, hybrid nanoelectronic devices showed the maximum rectification ratio of this respective alkenyl pyrene monolayers is 2.5×10^5 at ± 2.5 V.¹¹⁰ Not only monomers, but polymers such as poly-N-succinimidyl acrylate (PNSA) have been electrografted on to Si for sensors.¹¹¹ Autonomous growth of molecular lines on Si(100) surfaces using vinyl ferrocene have been reported and were proposed as a potential catalyst which can be used to induce nanotube growth.¹¹² Electrografting showed alkoxy monolayers formation such as those derived from 1-decanol are capable of forming stable Si–O–C bonds which can be used for the molecular electronic applications.¹¹³

2.4.6 Thermal induced monolayer formation on Si.

There are few reported examples of self-assembly of molecules on Si using high temperatures. In pioneering work, Linford and Chidsey⁹⁶ carried out a control experiment when examining diacylperoxide initiated olefin hydrosilylation on Si(111) surfaces, which showed the reaction could occur in the absence of diacylperoxide initiator at elevated temperatures (>150 °C).^{30, 114} This has become a widely used method to graft olefins on to Si. In 2015, Khung et al.¹¹⁵ reported the thermal and UV hydrosilylation of bifunctional hydroxyalkynes on Si(111) surfaces: and how surface radicals influence surface bond formation. In 2000, Fellah et al.¹¹⁶ reported the formation mechanisms of Si–OR monolayers from the thermal reactions of alcohols and aldehydes with Si(111)–H. Bateman et al.¹¹⁷ reported that refluxing porous Si for 18-20 hours at 110-180 °C in an aliphatic alkyne or alkene yields alkyl monolayers. At higher temperatures around 150 °C, the Si–H bond will undergo homolytic cleavage and the silyl radical can then react with alkynes to form a Si–C bond. In 2016, Zhang et al.⁸⁸ probed the effect of electrostatic interactions on the electroactivity of a persistent organic free radical. This was achieved by attachment of 4-azido-2,2,6,6-tetramethyl-1-piperdinyloxy (4-azido-TEMPO) onto monolayer-modified Si(100) using a two-step chemical procedure as shown in Figure 2.17.

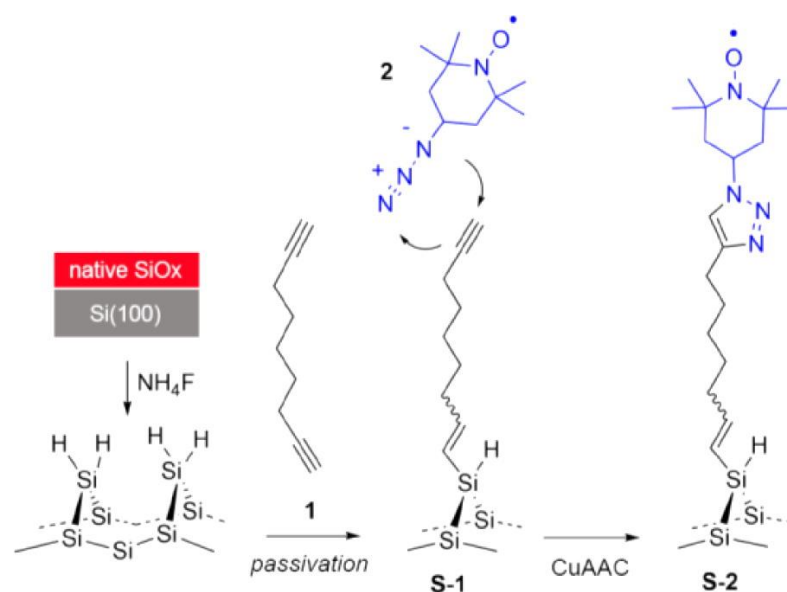


Figure 2. 17 Hydrosilylation of 1,8-nonadiyne 1 onto a Si(100)–H electrode (S-1) and covalent attachment of 4-Azido–TEMPO 2 via a CuAAC reaction to yield the redox-active radical film (S-2).⁸⁸ Figure 2.17 adapted from ref. 88 with permission from, American Chemical Society Copyright © 2016.

Recent reports by Hua et al.¹¹⁸ and by Cohen et al.¹¹⁹ also report densely packed but chemically unstable Si(111) monolayers of undecylenic acid 2-bromoethyl ester¹¹⁸ and 11-bromo-1-undecene¹¹⁹ by thermally induced monolayer formation.

2.4.7 Ultraviolet photochemical hydrosilylation

It is well known according to the literature that UV irradiation can initiate hydrosilylation of unsaturated molecules such as alkynes and alkenes due to homolytic cleavage of Si–H bonds, comparable to thermal initiation.¹¹⁵ Using UV instead of thermal energy is preferable in many studies, especially in molecular electronics because it will protect the delicate or small features of modified Si. Therefore, the minimum use of thermal energy would be preferable in applications of SAMs. Wang et al.¹²⁰ proposed a mechanism for UV-initiated grafting of alkenes on to H-terminated Si surfaces in which photo-emission to an acceptor level is followed by nucleophilic attack by the C=C group of a second alkene as shown in Figure 2.18. UV irradiation gives higher coverage and less time required to have a complete monolayer on Si than thermal methods. Vogel et al.⁸⁷ reported reproducible flaws to reveal the electrostatic aspects of semiconductor

electrochemistry by using 1,8-nonadiyne modified Si.⁸⁷ Here 1,8-nonadiyne was grafted on to the Si(100) surface using UV irradiation for 2 hours and achieved a 80% complete monolayer on Si surface.

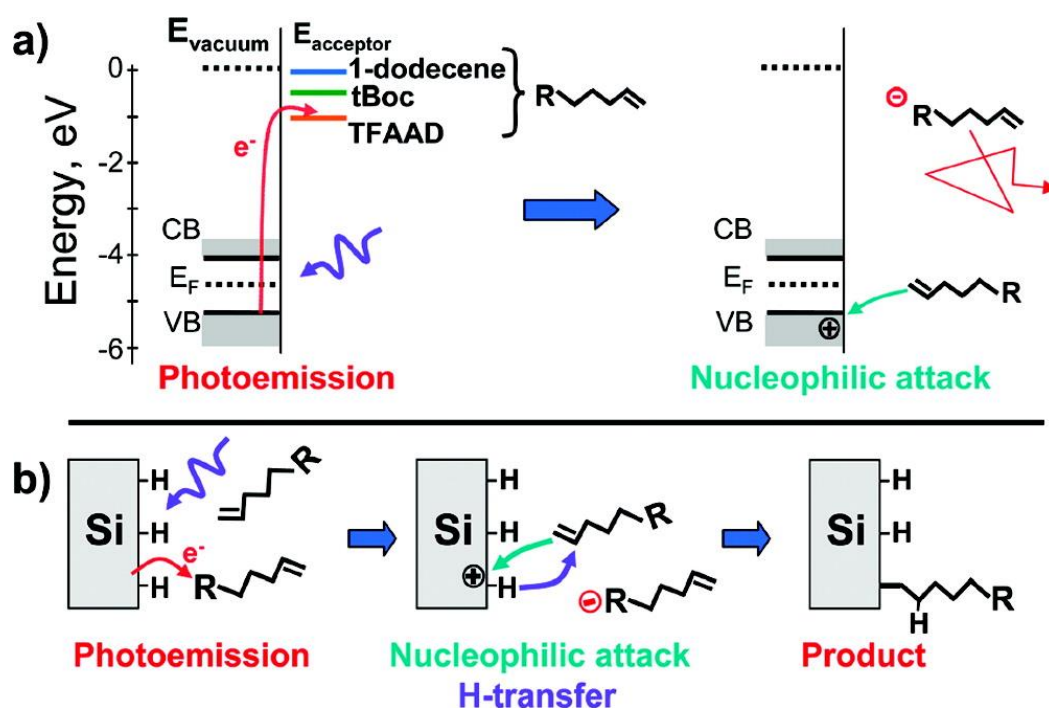


Figure 2. 18 Mechanism for UV-initiated grafting of alkenes to H-terminated Si surfaces: (a) photoemission to an acceptor level followed by nucleophilic attack by the C=C group of a second alkene; (b) overall result of the grafting reaction.¹²⁰ Figure 2.18 adapted from ref. 120 with permission from, American Chemical Society Copyright © 2010.

In 2004, Jin et al.¹¹⁸ reported the preparation of SAMs of undecylenic acid methyl ester and undec-10-enoic acid 2-bromoethyl ester grown on Si(111)-H. These SAMs were grown by immersion of Si(111)-H substrates in neat esters and irradiated by UV irradiation. XRR data reveals that the molecules have area densities of ~ 50% and 57% and layer thicknesses of 12.2 and 13.2 Å.¹¹⁸ In the following year, Xu et al.¹²¹ reported UV-induced coupling of 4-vinylbenzyl chloride (VBC) on Si(100)-H surfaces for the preparation of polymer-Si hybrids via surface-initiated atom transfer radical polymerization. To give a dense and flat surface the chain ends were used as the macroinitiator for the synthesis of diblock copolymer brushes.

2.4.8 Visible light photochemical hydrosilylation

Not only UV radiation but white light from tungsten light sources can induce hydrosilylation. As reported by Stewart and Buric,¹²² illumination of photoluminescent Si samples with white light at room temperature for 30-60 minutes, with the illumination of the white light of moderate-intensity ($22\text{-}44\text{ mW cm}^{-2}$) in the presence of an alkene or alkyne induces hydrosilylation, by yielding alkyl and alkenyl termination, respectively. Lee et al.¹²³ in 1996 demonstrated that carboxylic acids can be attached to the Si surfaces using visible light. Light-induced reactions of Si surfaces with carboxylic acids generates Si ester-modified surfaces as shown in Figure 2.19, where photoelectrochemical oxidation of porous or Si (100) oriented single-crystal n-type Si can be modified by formic, acetic or trifluoroacetic acids.¹²³

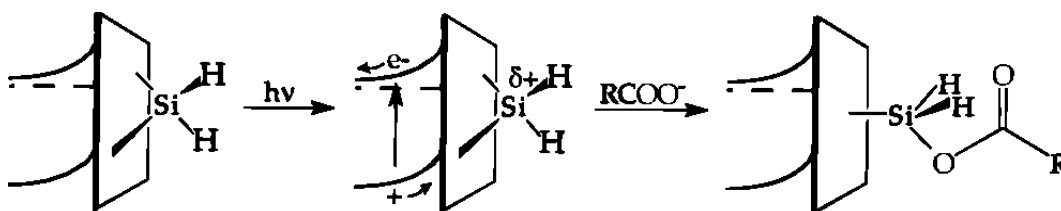


Figure 2. 19 Esterification changes the reactivity of the Si surface. Organomethoxysilanes react specifically with the esterified region of a photopatterned porous Si sample. This demonstrates a versatile two-step synthetic procedure for patterning Si surfaces with a variety of molecular species.¹²³ Figure 2.19 adapted from ref. 123 with permission from, American Chemical Society Copyright © 1996.

In 2005, Sun et al.¹²⁴ discovered that mild irradiation by visible light can covalently attach monolayers on Si(100)-H: in which they used 5 hours of irradiation for Si(100)-H with low doped (p- or n-type) and 10 hours of irradiation for highly doped p-type Si(100)-H. The proposed mechanism requires a wavelength of 447 nm. Furthered this work by attachment of organic monolayers on crystalline Si surfaces by using visible light sources (447 to 658 nm) for a variety of alkenes and alkynes on Si(100)-H and Si(111)-H at room temperature. Mechanisms proposed by Sun et al. under visible light are shown in Figure 2.20.

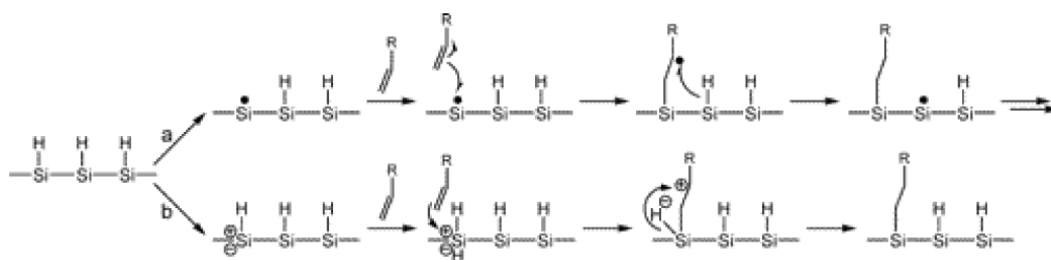


Figure 2. 20 Representation of the proposed (a) Radical chain mechanism under thermal and UV conditions and (b) electron/hole pair mechanism for visible-light initiated hydrosilylation on porous Si.¹²⁴ Figure 2.20 adapted from ref. 124 with permission from, American Chemical Society Copyright © 2005.

2.4.9 Other methods of surface modification

Apart from these well-known methods of hydrosilylation, other methods such as Lewis acid-catalyzed hydrosilylation and the usage of alkyl Grignard on Si-H have been shown to attach organic molecules on to Si. In 1996, Bansal et al.¹²⁵ demonstrated the alkylation of Si surfaces using a two-step halogenation/Grignard reaction. Vegunta et al.¹²⁶ reported passivation of Si(100) using alkyl Grignard reagents via electrochemical and thermal grafting methods. Here, methyl or ethyl Grignard reagents in tetrahydrofuran were investigated using cyclic voltammetry. In 2006, Yamada et al.¹²⁷ showed grafting of unsaturated hydrocarbons ($-\text{CH}_2-\text{CH}=\text{CH}_2$, $-\text{CH}=\text{CH}_2$, $-\text{CH}_2-\text{CH}=\text{CH}-\text{CH}_3$, and $-\text{C}\equiv\text{CH}$) by a stable C-Si covalent bond to hydrogen-terminated Si(111) with Grignard reagents which have nanofabrication and biological applications.

According to Fellah et al.¹¹⁶ covalent graftings of alkyl chains on Si can be obtained by thermal treatment with Grignard reagents with the alkyl halide impurity present in the Grignard solution appearing to play a key role in the grafting process. They proposed the mechanism of the unrevealed electrochemistry in the thermal grafting of Si surfaces with the presence of Grignard reagents. Grafting efficiency is increased on n-type compared to p-type substrates and by increased alkyl halide concentration and reactivity. Here, alkyl halide reduction is the rate-determining step as shown in Figure 2.21. Results reveal that the negative charging of the Si surface can lower the energetic barrier, allowing for more efficient grafting on n-type Si than p-type Si.

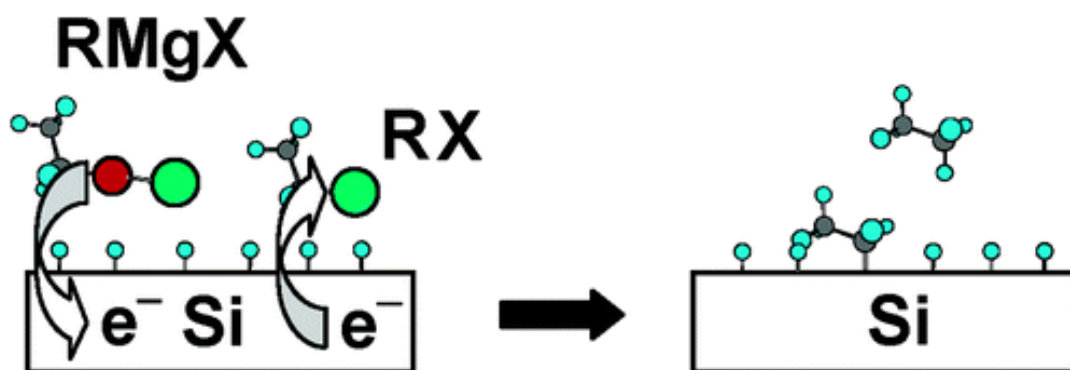


Figure 2. 21 Grafting mechanism of alkyl on Si substrates.¹¹⁶ Figure 2.21 adapted from ref. 116 with permission from, American Chemical Society Copyright © 2004

Lewis acid-catalyzed hydrosilylation is of interest for the attachment of alkynes to Si-H. In 1996, Asao et al.¹²⁸ demonstrated the hydrosilylation of alkynes with trialkyl silanes being catalyzed by Lewis acids such as AlCl_3 and EtAlCl_2 , leading to cis-alkenyl silanes with a very high ratio and stereo selectivities. Similar work reported by Sudo et al.¹²⁹ in 1999 examining Lewis acids such as AlCl_3 or EtAlCl_2 dramatic catalysis of the hydrosilylation of alkynes with trialkyl silanes to produce the corresponding cis-vinylsilanes in a high ratio and trans-stereoselective manner.

As a method for modifying Si-H surfaces, Lewis acid-mediated (e.g. AlEtCl_2) attachment of olefins and acetylenes for the derivatization of hydride-terminated porous Si was reported by Buriak and Allan.¹³⁰ In 1999, Buriak demonstrated Lewis acid-mediated hydrosilylation of alkynes and alkenes on non-oxidized porous Si-H as shown in Figure 2.22, respectively.¹³¹

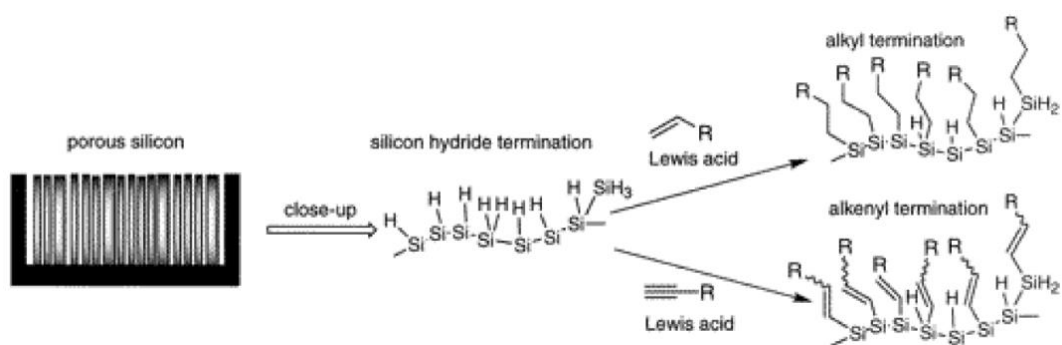


Figure 2. 22 Lewis acid-mediated hydrosilylation in the presence of the Lewis acid EtAlCl_2 , resulting in alkenyl- or alkyl-terminated surfaces, respectively¹³¹. Figure 2.22 adapted from ref. 131 with permission from, American Chemical Society Copyright © 1999.

2.5 Characterization of SAMs

2.5.1 Conductivity measurements of SAMs

To measure the conductivity of the monolayer, c-AFM is one of the techniques that can be used.^{65-66, 132-133} Here, the AFM tip is in contact with the SAMs and the conductivity of the SAM is measured.^{66, 134} The total current is then divided by the number of head groups under the AFM tip contact area to determine the conductivity of a single-molecule. This method was used for a long time to determine the conductivity of proteins, DNA^{65, 135} and polymers.¹³⁶⁻¹³⁸ In 2002, Ishida et al.¹³⁴ using conductive AFM reported electrical conduction through SAMs made from conjugated molecules with a focus on the molecular structural effect on the electrical conduction. In this work, they used phenylene oligomer SAMs and the results obtained are shown in Figure 2.23 and 2.24. Results revealed that the phenylene oligomer SAMs, resistances through the monolayers increased with increases in molecular length.

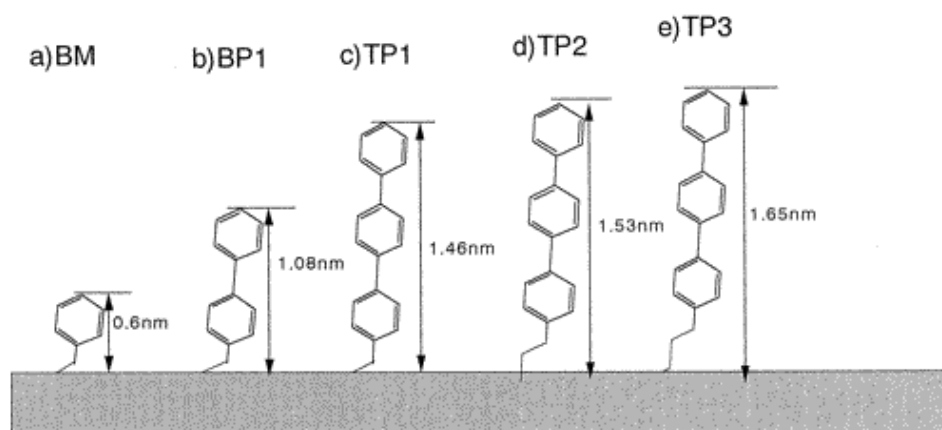


Figure 2. 23 Molecular structures of conjugated molecules used in the study.¹³⁴ Figure 2.23 adapted from ref. 134 with permission from, American Chemical Society Copyright © 2002.

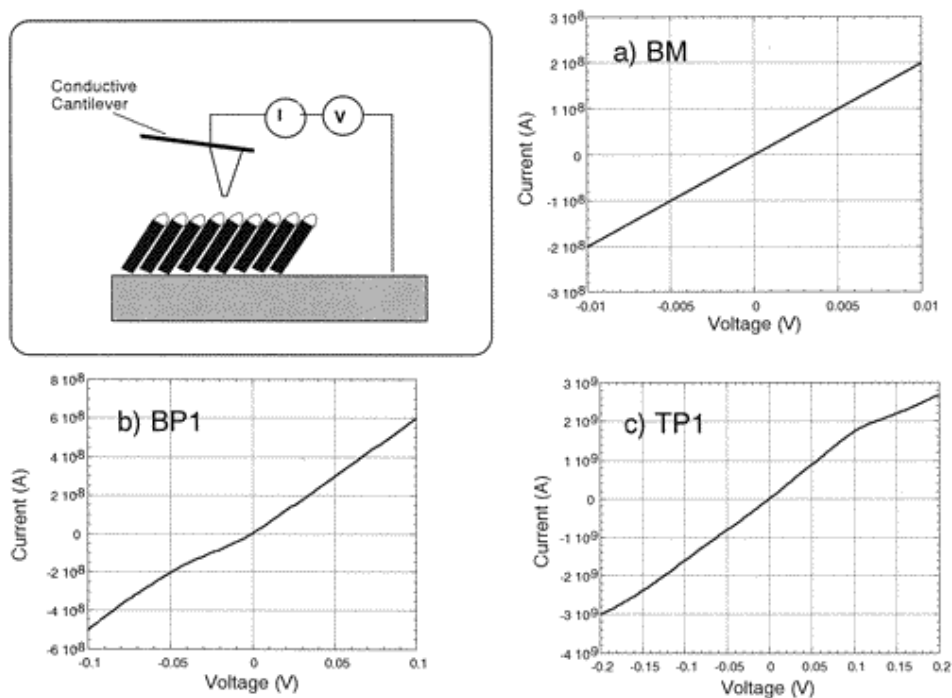


Figure 2. 24 I–V curves of the SAMs. (a) BM; (b) BP1; (c) TP1. The load was applied to minimize the damage to the SAM surface (1 nN).¹³⁴ Figure 2.24 adapted from ref. 134 with permission from, American Chemical Society Copyright © 2002

Not only for the conductive measurements, but AFM is also a commonly used technique for grafting and patterning molecules on conducting and semiconducting electrodes,^{136, 139-141} where the molecule grafting pattern can be controlled by the tip movement. Recently, AFM nanolithography has shown itself to be a practical tool for

patterning different oxides,^{12, 142-144} where these oxides can be generated easily by using an AFM tip on a conducting or semiconducting surface. These patterns can be used to separate molecular arrays¹² to separate different molecules on a substrate where they can be used with potential applications in future molecular electronics. Supplementary to the AFM, scanning tunnelling microscopy (STM) with single molecular contacts has been used in recent studies. To determine the single-molecular contacts, first, it should be able to isolate and identify them separately. Until 1981, it was an impossible task until Gerd Binnig and Heinrich Rohrer invented STM and won the Nobel Prize in 1980 for this invention. This invention changed the field of microelectronics drastically. STM uses the theory of quantum tunnelling. Here electrons will flow through a small nanogap and allow current to flow between the substrate and the STM tip. The current observed from this process decreases exponentially with increasing distance between the substrate and the tip. The piezo attached to the tip will change the height of the tip by a feedback system to maintain a constant current or height. AFM works differently than STM, in which a sharp tip will contact the surface and tap (tapping mode) or be dragged along the surface (contact mode). The force that is applied to the tip will vary depending on the surface and this difference of the deflection caused by force will be recorded used and plot the image of the surface. In the STM the tip is constructed from Au or Pt which have good conductivity and for the AFM the cantilevers are commonly made out of Si or Si₃N₄ and for conductive AFM with Pt or Si₃N₄ tips with doped diamond or metallic coating.

An ideal STM tip comes to a single atom point that will contact with one molecule in the SAM. This allows measuring the conductivity of one molecule of the SAM. One single-molecule can act as a diode, a transistor, a molecular wire or a molecular switch depending on the type and properties of the molecule used. In STM, the two techniques which are widely used for measuring conductivity are break junction (current versus distance) and blinking methods (current versus time). In STM break junction method (STMBJ), a Au / Si or other conducting tips is driven in and out from a gold surface containing the molecule of interest in a solution. When the tip is crushed into the surface, gold nanowires form. For the case of Au, as the tip is retracted from the surface, these Au–Au contact break sequentially and this is

reflected as plateaus in the current-versus distance plots. The same thing happens for the molecular junctions as the bond break, but this happens at a lower current level as shown in Figure 2.25C. Hence, Au–Au plateaus appear at multiple integers of G_0 (quantum point contact conductance) where $1 G_0$ is 77.5 micro siemens. The plateaus for molecular junctions, however, appear at a much lower conductivity as molecules are usually less conducting than a Au–Au metallic wire. The current will drop sequentially until the bridge between the last molecule breaks as shown in Figure 2.25E. The data for this process is plotted with respect to the pulling portion of the cycles and detect the current versus distance curves attributed to the current passing through a single-molecule. Plateaus from thousands of curves are combined to form statistical histograms of single-molecular events which are represented as in Figure 2.25B, 2.25D and 2.25F for each stage. The last step of the current drop represents the conductivity of the last molecule or in other words, the conductivity of a single-molecule represents the area of the rectangle highlighted red in Figure 2.25A.

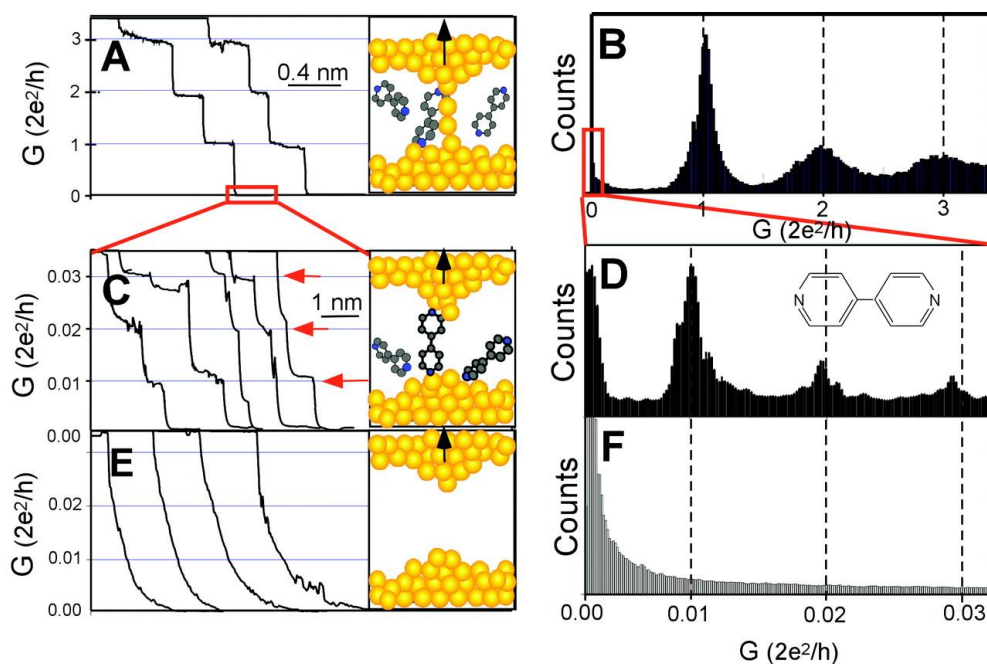


Figure 2. 25 (A) Conductance of a Au contact formed between a Au STM tip and a Au substrate (B) A histogram constructed from conductance curves (C) contact shown in (A) is completely broken, corresponding to the collapse of the last quantum step, a new series of conductance steps appears due to molecules such as 4,4'-bipyridine present in the solution. These steps are due to the formation of the stable molecular junction between the tip and the substrate (D) A histogram obtained from 1000 measurements as shown in (C) shows peaks near 0.01, 0.02, and 0.03 G_0 that are ascribed to one, two, and three molecules, respectively. (E and F) in the absence of molecules, no such steps or peaks are observed in the same conductance range.¹⁴⁵ Figure 2.25 adapted from ref. 145 with permission from, American Association for the Advancement of Science Copyright © 2003

Even though this mechanically controlled break junction method is suitable to determine the conductivity, this method is not the best at studying the stability and surface properties. Therefore, the scanning probe break junction method is mostly used to study only the conductivity of a single-molecular contact.

To determine the stability and conductivity of a single-molecular contact, the blinking method (current versus time) is used. In the blinking approach, under a fixed electrode gap separation, the STM tunnelling current feedback is turned off. Once

the system is stabilized, the current transients are captured. While the tip is moving across the surface, the molecules will make contacts with the tip as shown in Figure 2.26a. When a molecule is attached between both electrodes, a sudden jump or ‘blink’ above the tunnelling current is obtained in the form of telegraphic blinks shown in Figure 2.26b. These conductance histograms are built by the collection of hundreds of individual blinks. As the tip moves further, the bond will break and current will drop. In the blinking experiments, the current is plotted against time and gives a solid idea about the stability of the single-molecular junction (Figure 2.26c).

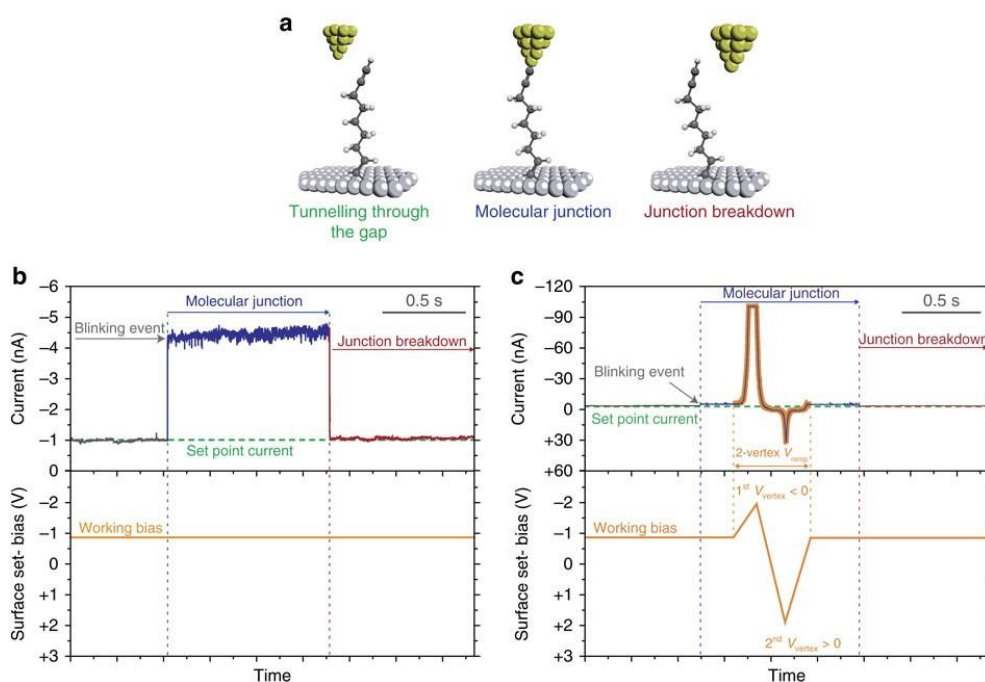


Figure 2. 26 Single-molecular scanning tunnelling microscopy–blinking method (a) schematic of the STM junction experiment describing the formation and breakdown of the Au–nonadiyne–Si junction.⁶¹ (b) captured ‘blink’ when a 1,8-nonadiyne molecule bridges the two electrodes. Current jumps (blinks) appear when the molecule bridges the gap between the Au and the Si electrodes. (c) current response during a voltage bias ramp of an Au–nonadiyne–Si.⁶¹ Figure. 2.26 adapted from ref. 61 with permission from, Springer Nature Copyright © 2017

2.6 Applications of single-molecular contacts for future electronics

Prior work has reported molecules acting as diodes,^{8, 23, 63, 97, 146-148} wires,^{1, 149-152} field-effect transistors,¹⁵³⁻¹⁵⁴ resistors^{64, 145, 155-156} and molecular switches.^{1, 3, 157-158} Single-molecular contacts can be controlled by changing the length, conjugation, substitution and anchoring chemical groups.¹⁵⁹⁻¹⁶⁰ One of the issues associated with the molecules is the formation of stable covalent contacts with the conducting or semiconducting interfaces, which is an important factor that should be considered when developing molecular electronic devices.

Frequently used molecular wires are made out of conjugated hydrocarbons,¹⁶¹ porphyrins,¹⁶²⁻¹⁶³ phthalocyanines,¹⁶⁴ fullerenes¹⁶⁵ and carbon nanotubes.¹⁶⁶ In 2014, Aragonès et al.¹⁶² developed a porphyrin-based molecular wire which is structurally unique. This work demonstrates single-molecular wires with metalloporphyrins linked via their central metal ion by modifying STM tip and surface electrodes. The work showed that the flat configuration of the metalloporphyrins resulted in single-molecular junctions of a high lifetime and conductance than similar porphyrin molecules but wired from either end of the porphyrin ring, suggesting that the orientation of the molecular wire govern the conductivity output.

Similar to that in 2016, Noori et al.¹⁶³ developed a supermolecular wire of M(II)-5,15-diphenylporphyrin (M-DPP) single-molecular junctions (M=Co, Ni, Cu, or Zn divalent metal ions), where the current flows perpendicular to the plane of the porphyrin. STM measurements demonstrate that current perpendicular to the plane higher electrical conductances than their current in-plane (Figure 2.27a). There are plenty of studies reporting multi molecular contacts with metal–molecule–metal structures⁹⁻¹⁰ but few reported with semiconductor–molecule–metal and semiconductor–molecule–semiconductors structures. Therefore, there is still more to investigate about single-molecular contacts as molecular wires on the semiconducting platform.

Transistors are another hot topic in molecular electronics, but so far only a few are developed by using single–molecule contacts. Halik et al.¹⁶⁷ demonstrated a manufacturing process for thin-film transistors with a SAM gate dielectric and a high–mobility organic semiconductor (pentacene) which operate with a supply voltage of

>2 V and have gate currents lower than advanced Si field-effect transistors with SiO₂ dielectrics. In 2012, Darwish et al.¹⁵⁴ developed a single-molecule transistor by using a single norbornyl anthraquinone unit which can be switched between a low- and high-conducting form using an electrochemical gating which is shown in Figure 2.27b.

In 2006, Venkataraman et al.⁶⁴ developed molecule resistors by using seven different biphenyl molecules with different ring substitution that can modify the twist angle of the molecules. Results show that the conductance decreases with increasing twist angle which is shown in Figure 2.27c. Similarly, in 2008, Lee et al.¹⁶⁸ described the anchoring group effect on current rectifying behaviour. Results demonstrated that the rectifying effect of a single-molecule is affected by the anchoring groups due to the bond dipoles at the interface and the internal polarization inside the molecules, suggesting that the molecule–electrode interface is a crucial element in designing these circuits a central concept that this thesis address.

Developing the molecular switches and molecular diodes^{63, 146-148} is also of interest In 2013, Batra et al.⁸ demonstrated a method of achieving rectification in single-molecular devices using Au–C bonds. This uses an asymmetric, conjugated molecular backbone with a single methylsulfide group linking one end to an Au substrate and formed a covalent Au–C bond at the other end. The diode properties of a molecule were demonstrated through single–molecule current-voltage measurements where the rectification ratio can be efficiently tuned as shown in Figure 2.27d. The properties of these molecule diodes can be easily altered by protonation or by changing the orientation of the molecules.^{63, 148}

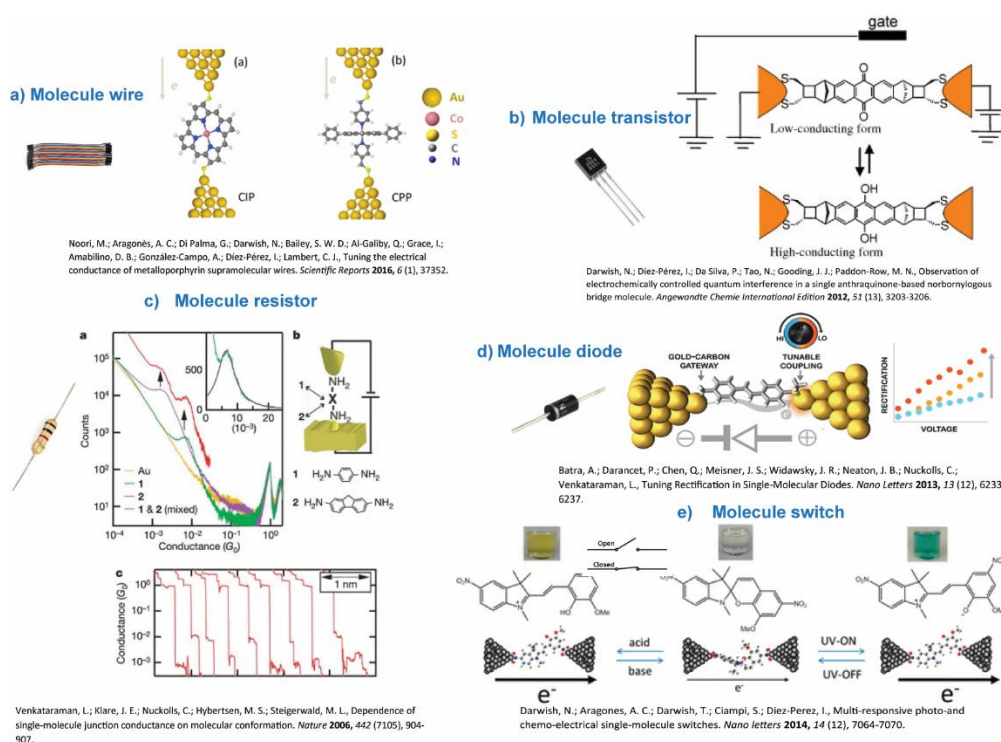


Figure 2.27 (a, b, c, d and e) a) conducting molecule wire¹⁶³ developed by using M(II)-5,15-diphenylporphyrin single-molecule junctions (M=Co, Ni, Cu, or Zn), which investigate the current flows perpendicular to the plane of the porphyrin and also the influence of the metal ion to the conductivity. Figure 2.27a adapted from ref. 163 with permission from, Springer nature Copyright © 2016 b) transistor¹⁵⁴ developed by using anthraquinone/hydroanthraquinone redox reaction. Here single norbornyl anthraquinone unit can be switched between a low-conducting and a high-conducting form using electrochemical gating. Figure 2.27b adapted from ref. 154 with permission from, WILEY-VCH Verlag GmbH & Co. KGaA, Weinheim Copyright © 2012 c) molecule resistor⁶⁴ developed by using 1,4-diaminobenzene and 2,7-diaminofluorene junctions where conductance for the series decreases with increasing twist angle. Figure. 2.27c adapted from ref. 64 with permission from, Springer Nature Copyright © 2006 d) diode⁸ developed by using trimethylstannyl lithium which demonstrate a new method of achieving rectification in single-molecule devices using the high-bias properties of gold-carbon bonds Figure. 2.27d adapted from ref. 8 with permission from, American Chemical Society Copyright © 2013.

e) molecule switch³ developed by using spiropyran derivatives where consequently, switch the electrical conductivity of the single-molecular device in the presence of light pointer or chemical signal. Figure. 2.27e adapted from ref. 3 with permission from, American Chemical Society Copyright © 2014

For a molecular switch, previously studied avenues include molecules which are either redox-active or UV or visible light active.^{1, 3, 158} In 2012 Paddon-Row.¹⁵⁴ and co-workers reported the electrochemical gating of a single anthraquinone molecule bridged between two gold electrodes using the STM break-junction technique. The results showed that the conductance increases with the conversion from the oxidized anthraquinone form to the reduced hydroanthraquinone form, which can be used as an ON and OFF switch. Similar to the anthraquinone study, Darwish et al.³ reported a single-molecule switching device that responds electrically to light and chemical stimuli. A light or a chemical signal can rapidly and reversibly induce the isomerization of the spiropyran, which can switch the electrical conductivity of the single-molecule between a low and a high level which is shown in Figure 2.27e.

The field of single molecular electronics is on a steep rise with many, gaps yet to be filled. For example, the anchoring of different types of organic molecules to a metal or Si surface is the key factor that affects both charge transport and stability in future electronics where Si is easily available and is a low-cost material. This thesis will describe the methods that can be used to develop stable covalent monolayers and single-molecular contacts on Au and Si surfaces by using diazonium salts, thiols and study the conductivity of individual molecules by STM using Au and Si tips.

The second part of this thesis will discuss developing oxide patterns on Si to separate these molecular arrays on a circuit and study I-V characteristics of these oxides. Not only that, this thesis also discusses the possibility of substituting molecular arrays with SiO_x for electronic applications by investigating the dynamic properties of oxides which can be used for future electronic devices.

2.7 References

1. Darwish, N.; Paddon-Row, M. N.; Gooding, J. J., Surface-bound norbornylogous bridges as molecular rulers for investigating interfacial electrochemistry and as single molecule switches. *Acc. Chem. Res.* **2014**, *47* (2), 385-395.
2. Walkey, M. C.; Peiris, C. R.; Ciampi, S.; C Aragonès, A.; Domínguez-Espíndola, R. B.; Jago, D.; Pulbrook, T.; Skelton, B. W.; Sobolev, A. N.; Díez Pérez, I.; Piggott, M. J.; Koutsantonis, G. A.; Darwish, N., Chemically and mechanically controlled single-molecule switches using spiropyrans. *ACS Appl Mater Interfaces* **2019**, *11* (40), 36886-36894.
3. Darwish, N.; Aragonès, A. C.; Darwish, T.; Ciampi, S.; Díez-Perez, I., Multi-responsive photo-and chemo-electrical single-molecule switches. *Nano Lett.* **2014**, *14* (12), 7064-7070.
4. Saeed, A. A.; Sánchez, J. L. A.; O'Sullivan, C. K.; Abbas, M. N., DNA biosensors based on gold nanoparticles-modified graphene oxide for the detection of breast cancer biomarkers for early diagnosis. *Bioelectrochemistry* **2017**, *118*, 91-99.
5. Crego-Calama, M.; Reinhoudt, D. N., New materials for metal ion sensing by self-assembled monolayers on glass. *Adv. Mater.* **2001**, *13* (15), 1171-1174.
6. Frasconi, M.; Mazzei, F.; Ferri, T., Protein immobilization at gold-thiol surfaces and potential for biosensing. *Anal. Bioanal. Chem.* **2010**, *398* (4), 1545-1564.
7. Dong, S.; Li, J., Self-assembled monolayers of thiols on gold electrodes for bioelectrochemistry and biosensors. *Bioelectrochem. Bioenerg.* **1997**, *42* (1), 7-13.
8. Batra, A.; Darancet, P.; Chen, Q.; Meisner, J. S.; Widawsky, J. R.; Neaton, J. B.; Nuckolls, C.; Venkataraman, L., Tuning rectification in single-molecular diodes. *Nano Lett.* **2013**, *13* (12), 6233-6237.
9. Nijhuis, C. A.; Reus, W. F.; Barber, J. R.; Dickey, M. D.; Whitesides, G. M., Charge transport and rectification in arrays of SAM-based tunneling junctions. *Nano Lett.* **2010**, *10* (9), 3611-3619.
10. Chen, X.; Roemer, M.; Yuan, L.; Du, W.; Thompson, D.; del Barco, E.; Nijhuis, C. A., Molecular diodes with rectification ratios exceeding 10⁵ driven by electrostatic interactions. *Nat. Nanotechnol.* **2017**, *12* (8), 797-803.

11. Creager, S.; Yu, C. J.; Bamdad, C.; O'Connor, S.; MacLean, T.; Lam, E.; Chong, Y.; Olsen, G. T.; Luo, J.; Gozin, M.; Kayyem, J. F., Electron transfer at electrodes through conjugated "Molecular Wire" bridges. *J. Am. Chem. Soc.* **1999**, *121* (5), 1059-1064.
12. Loeffler, F. F.; Cheng, Y.-C.; Muenster, B.; Striffler, J.; Liu, F. C.; Bischoff, F. R.; Doersam, E.; Breitling, F.; Nesterov-Mueller, A., Printing peptide arrays with a complementary metal oxide semiconductor chip. In *Fundamentals and Application of New Bioproduction Systems*, Springer: 2013; pp 1-23.
13. Grönbeck, H.; Curioni, A.; Andreoni, W., Thiols and disulfides on the Au (111) surface: The headgroup– gold interaction. *J. Am. Chem. Soc.* **2000**, *122* (16), 3839-3842.
14. Häkkinen, H., The gold–sulfur interface at the nanoscale. *Nat. Chem.* **2012**, *4* (6), 443–455.
15. Vericat, C.; Vela, M.; Benitez, G.; Carro, P.; Salvarezza, R., Self-assembled monolayers of thiols and dithiols on gold: New challenges for a well-known system. *Chem. Soc. Rev.* **2010**, *39* (5), 1805-1834.
16. Aswal, D. K.; Koiry, S. P.; Jousseme, B.; Gupta, S. K.; Palacin, S.; Yakhmi, J. V., Hybrid molecule-on-silicon nanoelectronics: Electrochemical processes for grafting and printing of monolayers. *Phys. E* **2009**, *41* (3), 325-344.
17. Tran, E.; Duati, M.; Ferri, V.; Müllen, K.; Zharnikov, M.; Whitesides, G. M.; Rampi, M. A., Experimental approaches for controlling current flowing through metal–molecule–metal junctions. *Adv. Mater.* **2006**, *18* (10), 1323-1328.
18. Weinstein, R. D.; Yan, D.; Jennings, G. K., Self-assembled monolayer films from liquid and supercritical carbon dioxide. *Ind. Eng. Chem. Res.* **2001**, *40* (9), 2046-2053.
19. Kraack, H.; Tamam, L.; Sloutskin, E.; Deutsch, M.; Ocko, B. M., Alkyl-thiol langmuir films on the surface of liquid mercury. *Langmuir* **2007**, *23* (14), 7571-7582.
20. Schreiber, F., Structure and growth of self-assembling monolayers. *Prog. Surf. Sci.* **2000**, *65* (5-8), 151-257.
21. Alagta, A.; Felhösi, I.; Bertoti, I.; Kálmán, E., Corrosion protection properties of hydroxamic acid self-assembled monolayer on carbon steel. *Corros. Sci.* **2008**, *50* (6), 1644-1649.

22. Liu, G.; Liu, J.; Böcking, T.; Eggers, P. K.; Gooding, J. J., The modification of glassy carbon and gold electrodes with aryl diazonium salt: The impact of the electrode materials on the rate of heterogeneous electron transfer. *Chem. Phys.* **2005**, *319* (1-3), 136-146.
23. Peiris, C. R.; Vogel, Y. B.; Le Brun, A. P.; Aragonès, A. C.; Coote, M. L.; Díez-Pérez, I.; Ciampi, S.; Darwish, N., Metal–single-molecule–semiconductor junctions formed by a radical reaction bridging gold and silicon electrodes. *J. Am. Chem. Soc.* **2019**, *141* (37), 14788-14797.
24. Liu, G.; Böcking, T.; Gooding, J. J., Diazonium salts: Stable monolayers on gold electrodes for sensing applications. *J. Electroanal. Chem.* **2007**, *600* (2), 335-344.
25. Bengió, S.; Fonticelli, M.; Benítez, G.; Creus, A. H.; Carro, P.; Ascolani, H.; Zampieri, G.; Blum, B.; Salvarezza, R. C., Electrochemical self-assembly of alkanethiolate molecules on Ni (111) and polycrystalline Ni surfaces. *J. Phys. Chem. B* **2005**, *109* (49), 23450-23460.
26. Blobner, F.; Abufager, P. N.; Han, R.; Bauer, J.; Duncan, D.; Maurer, R.; Reuter, K.; Feulner, P.; Allegretti, F., Thiolate-bonded self-assembled monolayers on Ni (111): Bonding strength, structure, and stability. *J. Phys. Chem. C* **2015**, *119* (27), 15455-15468.
27. Agboola, B.; Nyokong, T., Comparative electrooxidation of sulphite by self-assembled monolayers (SAMs) of Co (II), Fe (II), Ni (II) and Mn (III) tetrakis benzylmercapto and dodecylmercapto metallophthalocyanines complexes on gold electrodes. *Talanta* **2007**, *72* (2), 691-698.
28. Whelan, C. M.; Kinsella, M.; Ho, H. M.; Maex, K., Corrosion inhibition by thiol-derived SAMs for enhanced wire bonding on Cu surfaces. *J. Electrochem. Soc.* **2004**, *151* (2), B33-B38.
29. Schmidt, C.; Götzen, J.; Witte, G., Temporal evolution of benzenethiolate SAMs on Cu (100). *Langmuir* **2011**, *27* (3), 1025-1032.
30. Buriak, J. M., Organometallic chemistry on Silicon and Germanium surfaces. *Chem. Rev.* **2002**, *102* (5), 1271-1308.
31. Petrovykh, D. Y.; Smith, J. C.; Clark, T. D.; Stine, R.; Baker, L. A.; Whitman, L. J., Self-assembled monolayers of alkanethiols on InAs. *Langmuir* **2009**, *25* (20), 12185-12194.

32. Zhou, C.; Walker, A. V., UV photooxidation and photopatterning of alkanethiolate self-assembled monolayers (SAMs) on GaAs (001). *Langmuir* **2007**, *23* (17), 8876-8881.
33. Ohno, H.; Motomatsu, M.; Mizutani, W.; Tokumoto, H., AFM observation of self-assembled monolayer films on GaAs (110). *Jpn. J. Appl. Phys.* **1995**, *34* (2S), 1381.
34. Maury, P.; Peter, M.; Mahalingam, V.; Reinhoudt, D. N.; Huskens, J., Patterned self-assembled monolayers on silicon oxide prepared by nanoimprint lithography and their applications in nanofabrication. *Adv. Funct. Mater.* **2005**, *15* (3), 451-457.
35. Komeda, T.; Namba, K.; Nishioka, Y., Self-assembled-monolayer film islands as a self-patterned-mask for SiO₂ thickness measurement with atomic force microscopy. *Annu. Rev. Phys. Chem.* **1997**, *70* (25), 3398-3400.
36. Mitchon, L. N.; White, J., Growth and analysis of octadecylsiloxane monolayers on Al₂O₃ (001). *Langmuir* **2006**, *22* (15), 6549-6554.
37. Marcinko, S.; Helmy, R.; Fadeev, A. Y., Adsorption properties of SAMs supported on TiO₂ and ZrO₂. *Langmuir* **2003**, *19* (7), 2752-2755.
38. Paszternák, A.; Pilbáth, A.; Keresztes, Z.; Felhósi, I.; Telegdi, J.; Kálmán, E. In *Atomic force microscopy studies of alkyl-phosphonate SAMs on mica*, Materials Science Forum, Trans Tech Publ: 2008; pp 257-262.
39. Benítez, J.; San-Miguel, M.; Domínguez-Meister, S.; Heredia-Guerrero, J.; Salmeron, M., Structure and chemical state of octadecylamine self-assembled monolayers on mica. *J. Phys. Chem. C* **2011**, *115* (40), 19716-19723.
40. Basabe-Desmonts, L.; Beld, J.; Zimmerman, R. S.; Hernando, J.; Mela, P.; García Parajó, M. F.; van Hulst, N. F.; van den Berg, A.; Reinhoudt, D. N.; Crego-Calama, M., A simple approach to sensor discovery and fabrication on self-assembled monolayers on glass. *J. Am. Chem. Soc.* **2004**, *126* (23), 7293-7299.
41. Ulman, A., Formation and structure of self-assembled monolayers. *Chem. Rev.* **1996**, *96* (4), 1533-1554.
42. Bain, C. D.; Whitesides, G. M., Formation of monolayers by the coadsorption of thiols on gold: Variation in the length of the alkyl chain. *J. Am. Chem. Soc.* **1989**, *111* (18), 7164-7175.
43. Weisbecker, C. S.; Merritt, M. V.; Whitesides, G. M., Molecular self-assembly of aliphatic thiols on gold colloids. *Langmuir* **1996**, *12* (16), 3763-3772.

44. Kohli, P.; Taylor, K.; Harris, J.; Blanchard, G., Assembly of covalently-coupled disulfide multilayers on gold. *J. Am. Chem. Soc.* **1998**, *120* (46), 11962-11968.
45. Rieley, H.; Kendall, G. K., X-ray Studies of Self-Assembled Monolayers on Coinage Metals. 3. Angularly Resolved Near Edge X-ray Absorption Fine Structure Determination of the Orientation in 1-Octanethiol SAMs on Ag(111) and Cu(111). *Langmuir*. **1999**, *15* (26), 8867-8875.
46. Love, J. C.; Estroff, L. A.; Kriebel, J. K.; Nuzzo, R. G.; Whitesides, G. M., Self-Assembled Monolayers of Thiolates on Metals as a Form of Nanotechnology. *Chem. Rev.* **2005**, *105* (4), 1103-1170.
47. Heimel, G.; Romaner, L.; Zojer, E.; Brédas, J. L., Toward Control of the Metal–Organic Interfacial Electronic Structure in Molecular Electronics: A First-Principles Study on Self-Assembled Monolayers of π -Conjugated Molecules on Noble Metals. *Nano Lett.* **2007**, *7* (4), 932-940.
48. Van Alsten, J. G., Self-Assembled Monolayers on Engineering Metals: Structure, Derivatization, and Utility. *Langmuir*. **1999**, *15* (22), 7605-7614.
49. Haick, H.; Paz, Y., Long-Range Effects of Noble Metals on the Photocatalytic Properties of Titanium Dioxide. *J. Phys. Chem. B.* **2003**, *107* (10), 2319-2326.
50. Vericat, C.; Vela, M. E.; Benitez, G.; Carro, P.; Salvarezza, R. C., Self-assembled Monolayers of Thiols and Dithiols on Gold: New Challenges for a Well-Known System. *Chem. Soc. Rev.* **2010**, *39* (5), 1805-1834.
51. Vilan, A.; Aswal, D.; Cahen, D., Large-Area, Ensemble Molecular Electronics: Motivation and Challenges. *Chem. Rev.* **2017**, *117* (5), 4248-4286.
52. Darwish, N.; Eggers, P. K.; Ciampi, S.; Tong, Y.; Ye, S.; Paddon-Row, M. N.; Gooding, J. J., Probing the Effect of the Solution Environment Around Redox-Active Moieties Using Rigid Anthraquinone Terminated Molecular Rulers. *J. Am. Chem. Soc.* **2012**, *134* (44), 18401-18409.
53. Lombardo, D.; Kiselev, M. A.; Magazù, S.; Calandra, P., Amphiphiles Self-Assembly: Basic Concepts and Future Perspectives of Supramolecular Approaches. *Adv. Condens. Matter Phys.* **2015**, *2015*, 151683.
54. Liu, G.-Y.; Amro, N. A., Positioning protein molecules on surfaces: A nanoengineering approach to supramolecular chemistry. *Proc. Natl. Acad. Sci.* **2002**, *99* (8), 5165-5170.

55. Akkerman, H. B.; Blom, P. W.; De Leeuw, D. M.; De Boer, B., Towards molecular electronics with large-area molecular junctions. *Nature* **2006**, *441* (7089), 69-72.
56. Reed, M. A., Molecular-scale electronics. *Proc. IEEE* **1999**, *87* (4), 652-658.
57. Haynie, B.; Walker, A.; Tighe, T. B.; Allara, D.; Winograd, N., Adventures in molecular electronics: How to attach wires to molecules. *Appl. Surf. Sci.* **2003**, *203*, 433-436.
58. Zhang, H.; Li, Z.; Mirkin, C. A., Dip-pen nanolithography-based methodology for preparing arrays of nanostructures functionalized with oligonucleotides. *Adv. Mater.* **2002**, *14* (20), 1472-1474.
59. Lim, J. H.; Mirkin, C. A., Electrostatically driven dip-pen nanolithography of conducting polymers. *Adv. Mater.* **2002**, *14* (20), 1474-1477.
60. Gustafson, J. L., Moore's Law. In *Encyclopedia of parallel computing*, Padua, D., Ed. Springer US: Boston, MA, 2011; pp 1177-1184.
61. Aragonès, A. C.; Darwish, N.; Ciampi, S.; Sanz, F.; Gooding, J. J.; Díez-Pérez, I., Single-molecule electrical contacts on silicon electrodes under ambient conditions. *Nat. Commun.* **2017**, *8* (1), 1-8.
62. Pla-Vilanova, P.; Aragonès, A. C.; Ciampi, S.; Sanz, F.; Darwish, N.; Díez-Pérez, I., The spontaneous formation of single-molecule junctions via terminal alkynes. *Nanotechnol.* **2015**, *26* (38), 381001.
63. Díez-Pérez, I.; Hihath, J.; Lee, Y.; Yu, L.; Adamska, L.; Kozhushner, M. A.; Oleynik, I. I.; Tao, N., Rectification and stability of a single molecular diode with controlled orientation. *Nat. Chem.* **2009**, *1* (8), 635-641.
64. Venkataraman, L.; Klare, J. E.; Nuckolls, C.; Hybertsen, M. S.; Steigerwald, M. L., Dependence of single-molecule junction conductance on molecular conformation. *Nature* **2006**, *442* (7105), 904-907.
65. Xu, D.; Watt, G. D.; Harb, J. N.; Davis, R. C., Electrical conductivity of ferritin proteins by conductive AFM. *Nano Lett.* **2005**, *5* (4), 571-577.
66. Ishida, T.; Mizutani, W.; Liang, T. T.; Azehara, H.; Miyake, K.; Sasaki, S.; Tokumoto, H., Conductive probe AFM measurements of conjugated molecular wires. *Annals of the New York Academy of Sciences* **2003**, *1006*, 164-86.

67. Frederix, F.; Bonroy, K.; Laureyn, W.; Reekmans, G.; Campitelli, A.; Dehaen, W.; Maes, G., Enhanced performance of an affinity biosensor interface based on mixed self-assembled monolayers of thiols on gold. *Langmuir* **2003**, *19* (10), 4351-4357.
68. Marie, R.; Jensenius, H.; Thaysen, J.; Christensen, C. B.; Boisen, A., Adsorption kinetics and mechanical properties of thiol-modified DNA-oligos on gold investigated by microcantilever sensors. *Ultramicroscopy* **2002**, *91* (1-4), 29-36.
69. Crespo, P.; Litrán, R.; Rojas, T.; Multigner, M.; De la Fuente, J.; Sánchez-López, J.; García, M.; Hernando, A.; Penadés, S.; Fernández, A., Permanent magnetism, magnetic anisotropy, and hysteresis of thiol-capped gold nanoparticles. *Phys. Rev. Lett.* **2004**, *93* (8), 087204.
70. Arnold, M.; Cavalcanti-Adam, E. A.; Glass, R.; Blümmel, J.; Eck, W.; Kantelehner, M.; Kessler, H.; Spatz, J. P., Activation of integrin function by nanopatterned adhesive interfaces. *ChemPhysChem* **2004**, *5* (3), 383-388.
71. Strong, L.; Whitesides, G. M., Structures of self-assembled monolayer films of organosulfur compounds adsorbed on gold single crystals: Electron diffraction studies. *Langmuir* **1988**, *4* (3), 546-558.
72. Mishchenko, A.; Zotti, L. A.; Vonlanthen, D.; Bürkle, M.; Pauly, F.; Cuevas, J. C.; Mayor, M.; Wandlowski, T., Single-molecule Junctions based on nitrile-terminated biphenyls: A promising new anchoring group. *J. Am. Chem. Soc.* **2011**, *133* (2), 184-187.
73. Liu, G.; Luais, E.; Gooding, J. J., The fabrication of stable gold nanoparticle-modified interfaces for electrochemistry. *Langmuir* **2011**, *27* (7), 4176-4183.
74. Herrero, L.; González-Orive, A.; Marqués-González, S.; Martín, S.; Nichols, R. J.; Serrano, J. L.; Low, P. J.; Cea, P., Electrically transmissive alkyne-anchored monolayers on gold. *Nanoscale* **2019**, *11* (16), 7976-7985.
75. Shewchuk, D. M.; McDermott, M. T., Comparison of diazonium salt derived and thiol derived nitrobenzene layers on gold. *Langmuir* **2009**, *25* (8), 4556-4563.
76. Lehr, J.; Williamson, B. E.; Flavel, B. S.; Downard, A. J., Reaction of gold substrates with diazonium salts in acidic solution at open-circuit potential. *Langmuir* **2009**, *25* (23), 13503-13509.

77. Patterson, M. L.; Weaver, M. J., Surface-enhanced Raman spectroscopy as a probe of adsorbate-surface bonding: Simple alkenes and alkynes adsorbed at gold electrodes. *J. Phys. Chem.* **1985**, *89* (23), 5046-5051.
78. Maity, P.; Takano, S.; Yamazoe, S.; Wakabayashi, T.; Tsukuda, T., Binding motif of terminal alkynes on gold clusters. *J. Am. Chem. Soc.* **2013**, *135* (25), 9450-9457.
79. Zhang, S.; Chandra, K. L.; Gorman, C. B., Self-assembled monolayers of terminal alkynes on gold. *J. Am. Chem. Soc.* **2007**, *129* (16), 4876-4877.
80. Benedetto, A.; Balog, M.; Viel, P.; Le Derf, F.; Sallé, M.; Palacin, S., Electro-reduction of diazonium salts on gold: Why do we observe multi-peaks? *Electrochim. Acta* **2008**, *53* (24), 7117-7122.
81. Paulik, M. G.; Brooksby, P. A.; Abell, A. D.; Downard, A. J., Grafting aryl diazonium cations to polycrystalline gold: Insights into film structure using gold oxide reduction, redox probe electrochemistry, and contact angle behavior. *J. Phys. Chem. C* **2007**, *111* (21), 7808-7815.
82. Belanger, D.; Pinson, J., Electrografting: A powerful method for surface modification. *Chem. Soc. Rev.* **2011**, *40* (7), 3995-4048.
83. Smida, H.; Lebègue, E.; Bergamini, J.-F.; Barrière, F.; Lagrost, C., Reductive electrografting of in situ produced diazopyridinium cations: Tailoring the interface between carbon electrodes and electroactive bacterial films. *Bioelectrochemistry* **2018**, *120*, 157-165.
84. Katz, E.; Schmidt, H.-L., Gold electrode modification with a monolayer of 1,4,5,8-naphthalenetetrone as a four-electron transfer mediator: electrochemical reduction of dioxygen. *J. Electroanal. Chem.* **1994**, *368* (1), 87-94.
85. Allongue, P.; de Villeneuve, C. H.; Cherouvrier, G.; Cortes, R.; Bernard, M.-C., Phenyl layers on H-Si (111) by electrochemical reduction of diazonium salts: monolayer versus multilayer formation. *J. Electroanal. Chem.* **2003**, *550*, 161-174.
86. Pandey, D.; Zemlyanov, D. Y.; Bevan, K.; Reifenberger, R. G.; Dirk, S. M.; Howell, S. W.; Wheeler, D., UHV STM I (V) and XPS studies of aryl diazonium molecules assembled on Si (111). *Langmuir* **2007**, *23* (9), 4700-4708.
87. Vogel, Y. B.; Zhang, L.; Darwish, N.; Gonçalves, V. R.; Le Brun, A.; Gooding, J. J.; Molina, A.; Wallace, G. G.; Coote, M. L.; Gonzalez, J., Reproducible flaws unveil

electrostatic aspects of semiconductor electrochemistry. *Nat. Commun.* **2017**, *8* (1), 2066 (1-8).

88. Zhang, L.; Vogel, Y. B.; Noble, B. B.; Gonçalves, V. R.; Darwish, N.; Brun, A. L.; Gooding, J. J.; Wallace, G. G.; Coote, M. L.; Ciampi, S., TEMPO monolayers on Si(100) electrodes: electrostatic effects by the electrolyte and semiconductor space-charge on the electroactivity of a persistent radical. *J. Am. Chem. Soc.* **2016**, *138* (30), 9611-9619.

89. Sagiv, J., Organized monolayers by adsorption. 1. Formation and structure of oleophobic mixed monolayers on solid surfaces. *J. Am. Chem. Soc.* **1980**, *102* (1), 92-98.

90. Peor, N.; Sfez, R.; Yitzchaik, S., Variable density effect of self-assembled polarizable monolayers on the electronic properties of silicon. *J. Am. Chem. Soc.* **2008**, *130* (12), 4158-4165.

91. Herzer, N.; Hoepfener, S.; Schubert, U. S., Fabrication of patterned silane based self-assembled monolayers by photolithography and surface reactions on silicon-oxide substrates. *Chem. Commun.* **2010**, *46* (31), 5634-5652.

92. Ulman, A., *An Introduction to ultrathin organic films: From Langmuir-Blodgett to self-assembly*. Academic press: 2013.

93. Vuillaume, D.; Boulas, C.; Collet, J.; Allan, G.; Delerue, C., Electronic structure of a heterostructure of an alkylsiloxane self-assembled monolayer on silicon. *Phys. Rev. B* **1998**, *58* (24), 16491-16498.

94. Onclin, S.; Ravoo, B. J.; Reinhoudt, D. N., Engineering silicon oxide surfaces using self-assembled monolayers. *Angew. Chem., Int. Ed.* **2005**, *44* (39), 6282-6304.

95. Buriak, J. M., Illuminating silicon surface hydrosilylation: An unexpected plurality of mechanisms. *Chem. Mater.* **2014**, *26* (1), 763-772.

96. Linford, M. R.; Chidsey, C. E. D., Alkyl monolayers covalently bonded to silicon surfaces. *J. Am. Chem. Soc.* **1993**, *115* (26), 12631-12632.

97. Peiris, C. R.; Ciampi, S.; Dief, E. M.; Zhang, J.; Canfield, P. J.; Le Brun, A. P.; Kosov, D. S.; Reimers, J. R.; Darwish, N., Spontaneous S-Si bonding of alkanethiols to Si(111)-H: Towards Si-molecule-Si circuits. *Chem. Sci.* **2020**, *11* (20), 5246-5256.

98. Wang, D.; Buriak, J. M., Trapping silicon surface-based radicals. *Langmuir* **2006**, *22* (14), 6214-6221.

99. Pujari, S. P.; Spruijt, E.; Cohen Stuart, M. A.; van Rijn, C. J. M.; Paulusse, J. M. J.; Zuilhof, H., Ultralow adhesion and friction of fluoro-hydro alkyne-derived self-assembled monolayers on H-terminated Si(111). *Langmuir* **2012**, *28* (51), 17690-17700.
100. Lu, M.; Chen, B.; He, T.; Li, Y.; Tour, J. M., Synthesis, grafting, and film formation of porphyrins on silicon surfaces using triazenes. *Chem. Mater.* **2007**, *19* (18), 4447-4453.
101. Menanteau, T.; Dias, M.; Levillain, E.; Downard, A. J.; Breton, T., Electrografting via diazonium chemistry: The key role of the aryl substituent in the layer growth mechanism. *J. Phys. Chem. C* **2016**, *120* (8), 4423-4429.
102. de Villeneuve, C. H.; Pinson, J.; Bernard, M. C.; Allongue, P., Electrochemical formation of close-packed phenyl layers on Si(111). *J. Phys. Chem. B* **1997**, *101* (14), 2415-2420.
103. Hurley, P. T.; Ribbe, A. E.; Buriak, J. M., Nanopatterning of alkynes on hydrogen-terminated silicon surfaces by scanning probe-induced cathodic electrografting. *J. Am. Chem. Soc.* **2003**, *125* (37), 11334-11339.
104. Wang, D.; Buriak, J. M., Electrochemically driven organic monolayer formation on silicon surfaces using alkylammonium and alkylphosphonium reagents. *Surf. Sci.* **2005**, *590* (2), 154-161.
105. Choi, H. C.; Buriak, J. M., Effects of organic monolayer formation on electrochemiluminescence behavior of porous silicon. *Chem. Mater.* **2000**, *12* (8), 2151-2156.
106. Veerbeek, J.; Huskens, J., Applications of monolayer-functionalized H-terminated silicon surfaces: A review. *Small Methods* **2017**, *1* (4), 1700072.
107. Ngunjiri, J. N.; Vegunta, S. S.; Flake, J. C., Cathodic electrografting of alkyl nanopatterns on silicon (100). *J. Electrochem. Soc.* **2009**, *156* (7), H516-H521.
108. Koiry, S. P.; Aswal, D. K.; Chauhan, A. K.; Saxena, V.; Nayak, S. K.; Gupta, S. K.; Yakhmi, J. V., Electrical bistability in electrografted 5-(4-undecenyloxyphenyl)-10,15,20-triphenylporphyrin monolayer on Si. *Chem. Phys. Lett.* **2008**, *453* (1), 68-72.
109. Garg, K.; Majumder, C.; Nayak, S. K.; Aswal, D. K.; Gupta, S. K.; Chattopadhyay, S., Silicon-pyrene/perylene hybrids as molecular rectifiers. *Phys. Chem. Chem. Phys.* **2015**, *17* (3), 1891-1899.

110. Garg, K.; Majumder, C.; Gupta, S. K.; Aswal, D. K.; Nayak, S. K.; Chattopadhyay, S., A novel design for porphyrin based D–s–A systems as molecular rectifiers. *Chem. Sci.* **2016**, *7* (2), 1548-1557.
111. Cuenot, S.; Gabriel, S.; Jérôme, R.; Jérôme, C.; Fustin, C.-A.; Jonas, A. M.; Duwez, A.-S., First insights into electrografted polymers by AFM-based force spectroscopy. *Macromol.* **2006**, *39* (24), 8428-8433.
112. Kruse, P.; Johnson, E. R.; DiLabio, G. A.; Wolkow, R. A., Patterning of Vinylferrocene on H–Si(100) via self-directed growth of molecular lines and STM-induced decomposition. *Nano Lett.* **2002**, *2* (8), 807-810.
113. Wallart, X.; Henry de Villeneuve, C.; Allongue, P., Truly quantitative XPS characterization of organic monolayers on silicon: Study of alkyl and alkoxy monolayers on H–Si(111). *J. Am. Chem. Soc.* **2005**, *127* (21), 7871-7878.
114. Ciampi, S.; Harper, J. B.; Gooding, J. J., Wet chemical routes to the assembly of organic monolayers on silicon surfaces via the formation of Si–C bonds: Surface preparation, passivation and functionalization. *Chem. Soc. Rev.* **2010**, *39* (6), 2158-2183.
115. Khung, Y. L.; Ngalim, S. H.; Scaccabarozzi, A.; Narducci, D., Thermal and UV hydrosilylation of alcohol-based bifunctional alkynes on Si (111) surfaces: How surface radicals influence surface bond formation. *Sci. Rep.* **2015**, *5* (1), 11299.
116. Fellah, S.; Boukherroub, R.; Ozanam, F.; Chazalviel, J.-N., Hidden electrochemistry in the thermal grafting of silicon surfaces from Grignard reagents. *Langmuir* **2004**, *20* (15), 6359-6364.
117. Bateman, J. E.; Eagling, R. D.; Worrall, D. R.; Horrocks, B. R.; Houlton, A., Alkylation of porous silicon by direct reaction with alkenes and alkynes. *Angew. Chem., Int. Ed.* **1998**, *37* (19), 2683-2685.
118. Jin, H.; Kinser, C. R.; Bertin, P. A.; Kramer, D. E.; Libera, J. A.; Hersam, M. C.; Nguyen, S. T.; Bedzyk, M. J., X-ray studies of self-assembled organic monolayers grown on hydrogen-terminated Si (111). *Langmuir* **2004**, *20* (15), 6252-6258.
119. Cohen, Y. S.; Vilan, A.; Ron, I.; Cahen, D., Hydrolysis improves packing density of bromine-terminated alkyl-chain, silicon– carbon monolayers linked to silicon. *J. Phys. Chem. C* **2009**, *113* (15), 6174-6181.

120. Wang, X.; Ruther, R. E.; Streifer, J. A.; Hamers, R. J., UV-induced grafting of alkenes to silicon surfaces: Photoemission versus excitons. *J. Am. Chem. Soc.* **2010**, *132* (12), 4048-4049.
121. Xu, F. J.; Kang, E. T.; Neoh, K. G., UV-induced coupling of 4-Vinylbenzyl chloride on hydrogen-terminated Si(100) surfaces for the preparation of well-defined polymer-Si hybrids via surface-initiated ATRP. *Macromol.* **2005**, *38* (5), 1573-1580.
122. Stewart, M. P.; Buriak, J. M., Photopatterned hydrosilylation on porous silicon. *Angew. Chem., Int. Ed.* **1998**, *37* (23), 3257-3260.
123. Lee, E. J.; Bitner, T. W.; Ha, J. S.; Shane, M. J.; Sailor, M. J., Light-induced reactions of porous and single-crystal Si surfaces with carboxylic Acids. *J. Am. Chem. Soc.* **1996**, *118* (23), 5375-5382.
124. Sun, Q.-Y.; de Smet, L. C. P. M.; van Lagen, B.; Giesbers, M.; Thüne, P. C.; van Engelenburg, J.; de Wolf, F. A.; Zuilhof, H.; Sudhölter, E. J. R., Covalently attached monolayers on crystalline hydrogen-terminated silicon: extremely mild attachment by visible light. *J. Am. Chem. Soc.* **2005**, *127* (8), 2514-2523.
125. Bansal, A.; Li, X.; Lauermann, I.; Lewis, N. S.; Yi, S. I.; Weinberg, W. H., Alkylation of Si surfaces using a two-step halogenation/Grignard route. *J. Am. Chem. Soc.* **1996**, *118* (30), 7225-7226.
126. Vegunta, S. S. S.; Ngunjiri, J. N.; Flake, J. C., Electrochemical and thermal grafting of alkyl Grignard reagents onto (100) silicon surfaces. *Langmuir* **2009**, *25* (21), 12750-12756.
127. Yamada, T.; Shirasaka, K.; Noto, M.; Kato, H. S.; Kawai, M., Adsorption of unsaturated hydrocarbon moieties on H:Si(111) by Grignard reaction. *J. Phys. Chem. B* **2006**, *110* (14), 7357-7366.
128. Asao, N.; Sudo, T.; Yamamoto, Y., Lewis acid-catalyzed trans-hydrosilylation of alkynes. *J. Org. Chem.* **1996**, *61* (22), 7654-7655.
129. Sudo, T.; Asao, N.; Gevorgyan, V.; Yamamoto, Y., Lewis acid catalyzed highly regio- and stereocontrolled trans-hydrosilylation of alkynes and alkenes. *J. Org. Chem.* **1999**, *64* (7), 2494-2499.
130. Buriak, J. M.; Allen, M. J., Lewis acid mediated functionalization of porous silicon with substituted alkenes and alkynes. *J. Am. Chem. Soc.* **1998**, *120* (6), 1339-1340.

131. Buriak, J. M.; Stewart, M. P.; Geders, T. W.; Allen, M. J.; Choi, H. C.; Smith, J.; Raftery, D.; Canham, L. T., Lewis acid mediated hydrosilylation on porous silicon surfaces. *J. Am. Chem. Soc.* **1999**, *121* (49), 11491-11502.
132. Musumeci, C.; Liscio, A.; Palermo, V.; Samorì, P., Electronic characterization of supramolecular materials at the nanoscale by conductive atomic force and Kelvin probe force microscopies. *Mater. Today* **2014**, *17* (10), 504-517.
133. Iwata, K.; Yamazaki, S.; Mutombo, P.; Hapala, P.; Ondráček, M.; Jelínek, P.; Sugimoto, Y., Chemical structure imaging of a single molecule by atomic force microscopy at room temperature. *Nat. Commun.* **2015**, *6* (1), 7766 (1-8).
134. Ishida, T.; Mizutani, W.; Aya, Y.; Ogiso, H.; Sasaki, S.; Tokumoto, H., Electrical conduction of conjugated molecular SAMs studied by conductive atomic force microscopy. *J. Phys. Chem. B* **2002**, *106* (23), 5886-5892.
135. Heim, T.; Deresmes, D.; Vuillaume, D., Conductivity of DNA probed by conducting-atomic force microscopy: Effects of contact electrode, DNA structure, and surface interactions. *J. Appl. Phys.* **2004**, *96* (5), 2927-2936.
136. Al-Maawali, S.; Bemis, J. E.; Akhremitchev, B. B.; Liu, H.; Walker, G. C., Single-molecule AFM study of polystyrene grafted at gold surfaces. *J. Adhes.* **2005**, *81* (10-11), 999-1016.
137. Sonnenberg, L.; Parvole, J.; Borisov, O.; Billon, L.; Gaub, H. E.; Seitz, M., AFM-based single molecule force spectroscopy of end-grafted poly (acrylic acid) monolayers. *Macromol.* **2006**, *39* (1), 281-288.
138. Goodman, D.; Kizhakkedathu, J. N.; Brooks, D. E., Molecular weight and polydispersity estimation of adsorbing polymer brushes by atomic force microscopy. *Langmuir* **2004**, *20* (8), 3297-3303.
139. Shivashankar, G.; Libchaber, A., Single DNA molecule grafting and manipulation using a combined atomic force microscope and an optical tweezer. *Annu. Rev. Phys. Chem.* **1997**, *71* (25), 3727-3729.
140. Liang, J.; Scoles, G., Nanografting of alkanethiols by tapping mode atomic force microscopy. *Langmuir* **2007**, *23* (11), 6142-6147.
141. Anne, A.; Cambril, E.; Chovin, A.; Demaille, C., Touching surface-attached molecules with a microelectrode: Mapping the distribution of redox-labeled

- macromolecules by electrochemical-atomic force microscopy. *Anal. Chem.* **2010**, *82* (15), 6353-6362.
142. Xie, X. N.; Chung, H. J.; Sow, C. H.; Wee, A. T. S., Nanoscale materials patterning and engineering by atomic force microscopy nanolithography. *Mater. Sci. Eng. R Rep.* **2006**, *54* (1), 1-48.
143. Marchi, F.; Bouchiat, V.; Dallaporta, H.; Safarov, V.; Tonneau, D.; Doppelt, P., Growth of silicon oxide on hydrogenated silicon during lithography with an atomic force microscope. *J. Vac. Sci. Technol., B: Microelectron. Nanometer Struct. Process., Meas., Phenom.* **1998**, *16* (6), 2952-2956.
144. Buyukkose, S.; Okur, S.; Aygun, G., Local oxidation nanolithography on HF thin films using atomic force microscopy (AFM). *J. Phys. D: Appl. Phys.* **2009**, *42* (10), 105302.
145. Xu, B.; Tao, N. J., Measurement of single-molecule resistance by repeated formation of molecular junctions. *Science* **2003**, *301* (5637), 1221-1223.
146. Siqueira, M. R. S.; Corrêa, S. M.; Gester, R. M.; Del Nero, J.; Neto, A. M. J. C., Single-molecular diodes based on opioid derivatives. *J. Mol. Model.* **2015**, *21* (12), 317.
147. Handayani, M.; Gohda, S.; Tanaka, D.; Ogawa, T., Design and synthesis of perpendicularly connected metal porphyrin-imide dyads for two-terminal wired single molecular diodes. *Chem. - Eur. J.* **2014**, *20* (25), 7655-7664.
148. Morales, G. M.; Jiang, P.; Yuan, S.; Lee, Y.; Sanchez, A.; You, W.; Yu, L., Inversion of the rectifying effect in diblock molecular diodes by protonation. *J. Am. Chem. Soc.* **2005**, *127* (30), 10456-10457.
149. Sakaguchi, H.; Matsumura, H.; Gong, H., Electrochemical epitaxial polymerization of single-molecular wires. *Nat. Mater.* **2004**, *3* (8), 551-557.
150. Ponce, J.; Arroyo, C. R.; Tatay, S.; Frisenda, R.; Gaviña, P.; Aravena, D.; Ruiz, E.; van der Zant, H. S. J.; Coronado, E., Effect of metal complexation on the conductance of single-molecular wires measured at room temperature. *J. Am. Chem. Soc.* **2014**, *136* (23), 8314-8322.
151. Lo, W.-Y.; Zhang, N.; Cai, Z.; Li, L.; Yu, L., Beyond molecular wires: Design molecular electronic functions based on dipolar effect. *Acc. Chem. Res.* **2016**, *49* (9), 1852-1863.

152. Liu, K.; Wang, X.; Wang, F., Probing charge transport of ruthenium-complex-based molecular wires at the single-molecule level. *ACS Nano* **2008**, *2* (11), 2315-2323.
153. Schön, J. H.; Meng, H.; Bao, Z., Self-assembled monolayer organic field-effect transistors. *Nature* **2001**, *413* (6857), 713-716.
154. Darwish, N.; Díez-Pérez, I.; Da Silva, P.; Tao, N.; Gooding, J. J.; Paddon-Row, M. N., Observation of electrochemically controlled quantum interference in a single anthraquinone-based norbornylogous bridge molecule. *Angew. Chem., Int. Ed.* **2012**, *51* (13), 3203-3206.
155. Venkataraman, L.; Klare, J. E.; Tam, I. W.; Nuckolls, C.; Hybertsen, M. S.; Steigerwald, M. L., Single-molecule circuits with well-defined molecular conductance. *Nano Lett.* **2006**, *6* (3), 458-462.
156. Quek, S. Y.; Kamenetska, M.; Steigerwald, M. L.; Choi, H. J.; Louie, S. G.; Hybertsen, M. S.; Neaton, J. B.; Venkataraman, L., Mechanically controlled binary conductance switching of a single-molecule junction. *Nat. Nanotechnol.* **2009**, *4* (4), 230-234.
157. Walkey, M. C.; Peiris, C. R.; Ciampi, S.; C. Aragonès, A.; Domínguez-Espíndola, R. B.; Jago, D.; Pulbrook, T.; Skelton, B. W.; Sobolev, A. N.; Díez Pérez, I., Chemically and Mechanically Controlled Single-Molecule Switches Using Spiropyrans. *ACS Appl Mater Interfaces* **2019**, *11* (40), 36886-36894.
158. Darwish, N.; Díez-Pérez, I.; Guo, S.; Tao, N.; Gooding, J. J.; Paddon-Row, M. N., Single molecular switches: Electrochemical gating of a single anthraquinone-based norbornylogous bridge molecule. *J. Phys. Chem. C* **2012**, *116* (39), 21093-21097.
159. Lafferentz, L.; Ample, F.; Yu, H.; Hecht, S.; Joachim, C.; Grill, L., Conductance of a single conjugated polymer as a continuous function of its length. *Science* **2009**, *323* (5918), 1193-1197.
160. Kushmerick, J. G.; Holt, D. B.; Pollack, S. K.; Ratner, M. A.; Yang, J. C.; Schull, T. L.; Naciri, J.; Moore, M. H.; Shashidhar, R., Effect of bond-length alternation in molecular wires. *J. Am. Chem. Soc.* **2002**, *124* (36), 10654-10655.
161. Walter, D.; Neuhauser, D.; Baer, R., Quantum interference in polycyclic hydrocarbon molecular wires. *Chem. Phys.* **2004**, *299* (1), 139-145.

162. Aragonès, A. C.; Darwish, N.; Saletta, W. J.; Pérez-García, L.; Sanz, F.; Puigmartí-Luis, J.; Amabilino, D. B.; Díez-Pérez, I., Highly Conductive Single-Molecule Wires with Controlled Orientation by Coordination of Metalloporphyrins. *Nano Lett.* **2014**, *14* (8), 4751-4756.
163. Noori, M.; Aragonès, A. C.; Di Palma, G.; Darwish, N.; Bailey, S. W. D.; Al-Galiby, Q.; Grace, I.; Amabilino, D. B.; González-Campo, A.; Díez-Pérez, I.; Lambert, C. J., Tuning the electrical conductance of metalloporphyrin supramolecular wires. *Sci. Rep.* **2016**, *6* (1), 37352.
164. van Nostrum, C. F.; Picken, S. J.; Schouten, A.-J.; Nolte, R. J., Synthesis and supramolecular chemistry of novel liquid crystalline crown ether-substituted phthalocyanines: toward molecular wires and molecular ionoelectronics. *J. Am. Chem. Soc.* **1995**, *117* (40), 9957-9965.
165. Vail, S. A.; Krawczuk, P. J.; Guldi, D. M.; Palkar, A.; Echegoyen, L.; Tomé, J. P.; Fazio, M. A.; Schuster, D. I., Energy and electron transfer in polyacetylene-linked zinc-porphyrin-[60] fullerene molecular wires. *Chem. - Eur. J.* **2005**, *11* (11), 3375-3388.
166. Seifert, G.; Köhler, T.; Frauenheim, T., Molecular wires, solenoids, and capacitors by sidewall functionalization of carbon nanotubes. *Annu. Rev. Phys. Chem.* **2000**, *77* (9), 1313-1315.
167. Halik, M.; Klauk, H.; Zschieschang, U.; Schmid, G.; Dehm, C.; Schütz, M.; Maisch, S.; Effenberger, F.; Brunnbauer, M.; Stellacci, F., Low-voltage organic transistors with an amorphous molecular gate dielectric. *Nature* **2004**, *431* (7011), 963-966.
168. Lee, Y.; Carsten, B.; Yu, L., Understanding the anchoring group effect of molecular diodes on rectification. *Langmuir* **2009**, *25* (3), 1495-1499.

Every reasonable effort has been made to acknowledge the owners of copyright material. I would like to apologize if any copyright owner who has been omitted or incorrectly acknowledged.

Chapter 3

Experimental details

This chapter summarises the experimental details used for the monolayer formation on Au and Si surfaces reported in this thesis. A brief description of each instrument used for the characterization of the monolayer and oxide formation are provided in this chapter and subsequent details for each molecule are provided in the respective Chapters 4, 5 and 6.

3.1 Experimental set up

3.1.1 Preparation of Au polycrystalline electrodes

Au polycrystalline electrodes were polished with 0.05 μm Al_2O_3 for 5-6 minutes on a micro cloth pad. The electrodes were then rinsed with Milli-Q water ($>18 \text{ M}\Omega \text{ cm}$), acetone and sonicated for 5 minutes in an ultrasonic bath. Finally, the electrodes were electrochemically cleaned using 0.5 M H_2SO_4 by cycling the electrode between the -0.3 V and $+1.6 \text{ V}$ versus aqueous Ag/AgCl reference electrode. The cyclic voltammetry was repeated until a reproducible voltammogram obtained (typically 25 cycles). Finally, the electrode was rinsed with water and stored in distilled acetone.

3.1.2 Preparation of Au (111) single crystal electrode

An Au (111) single crystal electrode was cleaned for 5-10 min in hot Piranha solution ($130 \text{ }^\circ\text{C}$, a 3:1 (v/v) mixture of concentrated sulfuric acid to 30% hydrogen peroxide), rinsed several times with Milli-Q water ($>18 \text{ M}\Omega \text{ cm}$) and then annealed with a butane torch for 5 minutes.

3.1.3 Preparation of Si single crystal electrodes

Silicon wafers were cut into pieces (approximately 10 × 10 mm), cleaned for 20–30 min in hot Piranha solution (130 °C, a 3:1 (v/v)) mixture of concentrated sulfuric acid to 30% hydrogen peroxide). Silicon wafers were rinsed with water. 40% aqueous ammonium fluoride solution was deoxygenated by sparging with Ar and a small amount of sodium sulphite was added. The silicon wafers were then placed in this solution for 13 min. The freshly etched Si–H surface was then treated with molecules or used for the AFM tip induced oxide formation.

3.2 Cyclic voltammetry

All electrochemical measurements of the reduction of molecules (diazonium and thiols) on Au and Si surfaces were performed with a CHI650 (CH Instruments, USA) electrochemical workstation. A conventional three-electrode system was used where, a platinum wire used as the auxiliary electrode (CH Instruments, USA). Ag/AgCl aqueous (3.0 M KCl, CH Instruments, USA) was used for the electrochemical cleaning of polycrystalline gold electrodes. Ag/AgCl non-aqueous reference electrode (Ag/AgCl “leakless” electrode, eDAQ, part ET072-1) was used as the organic reference at room temperature (25 °C). Voltammograms were normalized relative to the ferrocene potential when the non-aqueous Ag/AgCl electrode was used. All aqueous electrolyte solutions for electrochemical experiments contained 1.0 M of either NaClO₄ or HClO₄. The surface coverage, Γ , expressed in mol cm⁻². The coverage was calculated from the background-subtracted faradaic charge taken as the integrated current from the voltammograms (anodic scan). A special custom-built Teflon electrochemical cell was used for the experiments where Si and Au(111) used as the working electrodes (Figure 3.1).

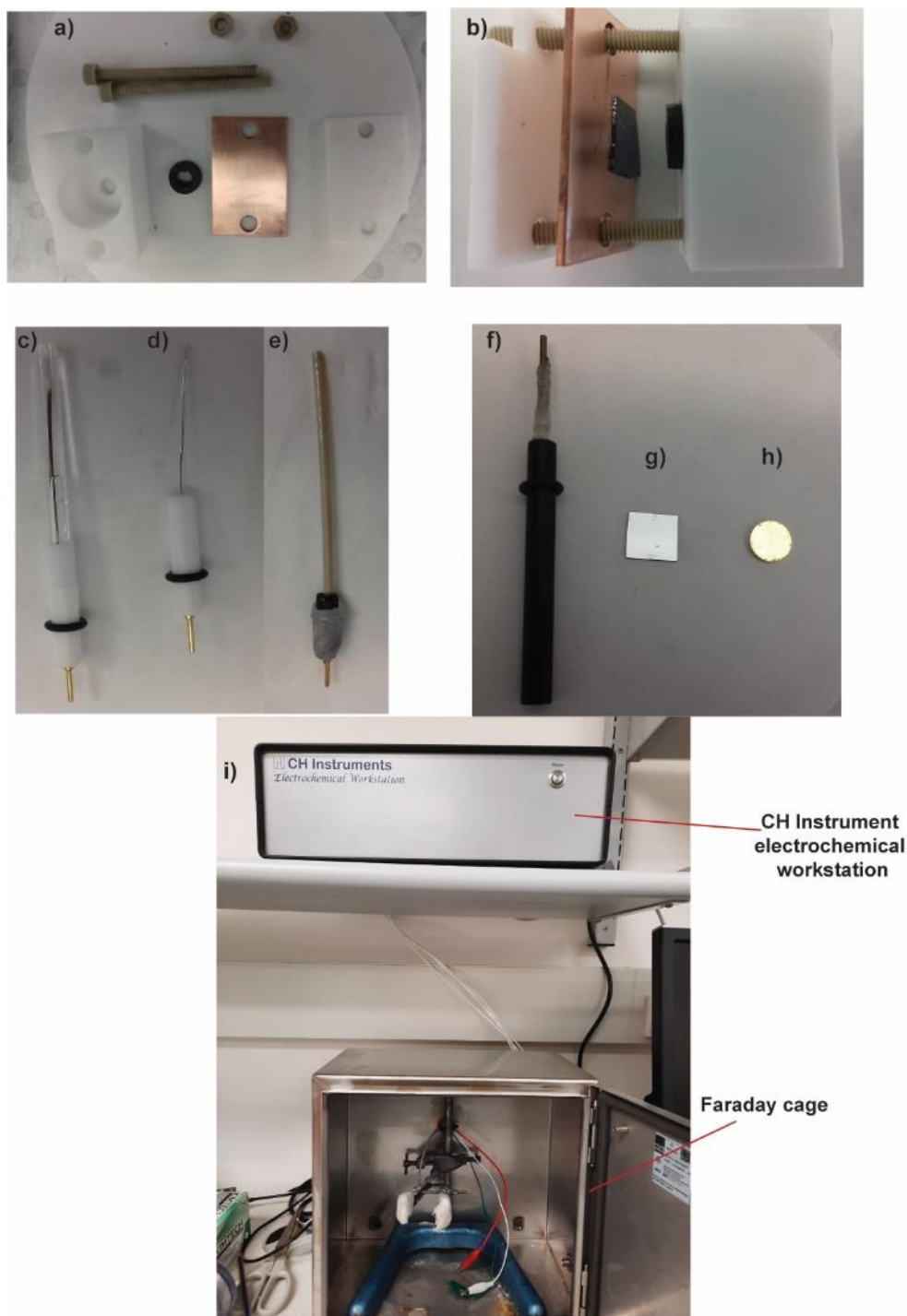
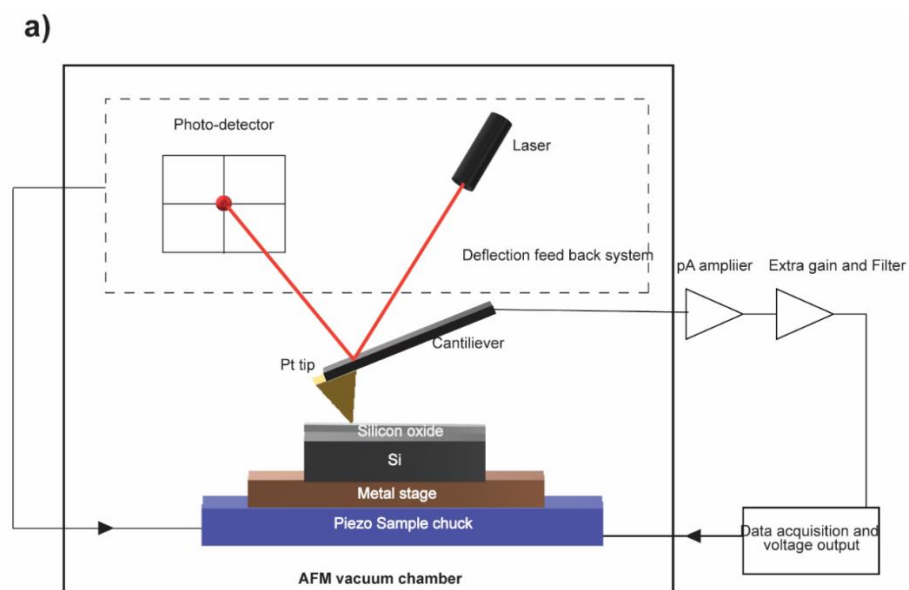


Figure 3. 1 (a, b) Electrochemical cell setup used to characterize monolayers on silicon and gold single crystal. b) photo image of AFM and (c) Ag/ AgCl reference electrode (1M KCl), d) Pt counter electrode, e) leakless Ag/ AgCl reference electrode, f) gold polycrystalline working electrode g) silicon working electrode (1mm²) h) gold single crystal electrode i) electrochemical workstation and enclosure for electrochemical experiments.

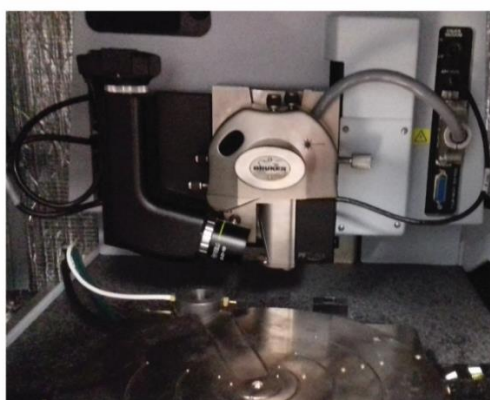
3.3 Atomic Force Microscope

3.3.2. AFM ICON head

All the current measurements of the different oxide heights developed by AFM tip induced oxidation were performed in the ambient conditions (room temperature 20 °C and humidity ~ 55 %) with Bruker Dimension Icon atomic force microscopy (AFM) fitted with a PF-TUNA module operating in peak force tunnelling current (PF-TUNA) mode (Figure 3.2). All images and I-V curves were obtained in air, at room temperature, and using solid Pt tips (RMN-25PT300B tip, nominal spring constant = 18 N/m, nominal resonant frequency = 20 kHz, tip radius < 20 nm) purchased from Rocky Mountain Nanotechnology. The Si sample was mounted on the base plate of the AFM with carbon tape which acts as a pathway to electrical ground via the metal stage. The AFM and control software (Nanoscope 9.4) was set up to allow the sample to be biased whilst maintaining the tip at the ground. Figure 3.2 shows a schematic of the conventional AFM-PF TUNA setup (a) use for this local oxidation experiments and the image of AFM (b) with the TUNA module (c) data were analysed by Nanoscope analysis 9.1 and Gwyddion 2.52 analysis software.



b)



c)



Figure 3. 2 (a) Schematic diagram of the AFM PF–TUNA setup use for this tip induced local oxidation b) photo image of AFM and (c) photograph of TUNA module which controls current sensitivity of the TUNA output and feedback.

3.3.2 AFM Fast scan head

Atomic force microscopy images of the Au and Si surface with and without molecules were obtained using a Bruker Dimension microscope Fast Scan head operating in tapping mode. All images were obtained in air, at room temperature, and using silicon cantilevers (TESPA-V2, Bruker, nominal spring constant = 37 N/m, nominal resonant frequency = 320 kHz, tip radius < 10 nm). Figure 3.3 shows the AFM fast scan head setup a) use for experiments b) silicon cantilevers (TESPA-V2), c) FastScan head scanner, and d) Pt tips used for the conductivity measurements.

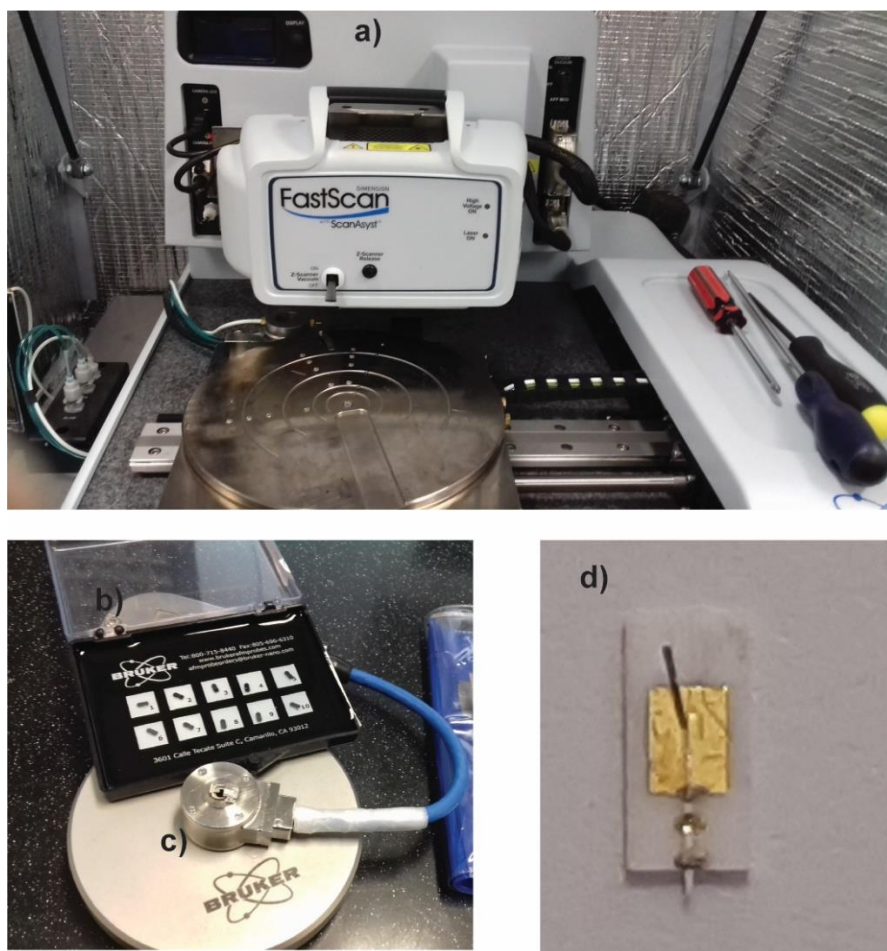
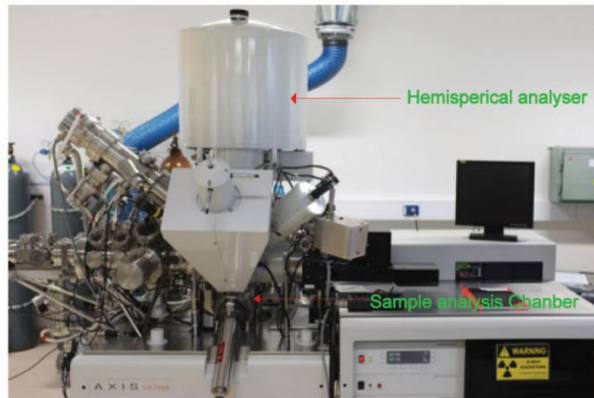


Figure 3. 3 The set up of the Bruker AFM fast scan head a) use for experiments b) silicon cantilevers (TESPA-V2), c) FastScan head and d) Pt tips used for the conductivity measurements.

3.4. X-ray photoelectron spectroscopy (XPS)

X-ray photoelectron spectroscopy was used for the quantitative measurements of elemental composition and the determination of the binding states of the elements of the self-assembled monolayers on Au and Si surfaces. The XPS measurements were achieved on a Kratos Axis Ultra DLD spectrometer where monochromatic Al-K α (1486.6 eV) irradiation source operating at 150 W. All the XPS data were processed using CasaXPS© software. The reported XPS energies are binding energies expressed in eV after background subtraction (Shirley), spectra were fitted with Voigt functions. Corrections for energy shifts caused by adventitious charging. All the peak energies were corrected with a rigid shift to bring the C 1s emission to 285.0 eV. The photograph of the instrument is shown in Figure 3.4.

a)



b)

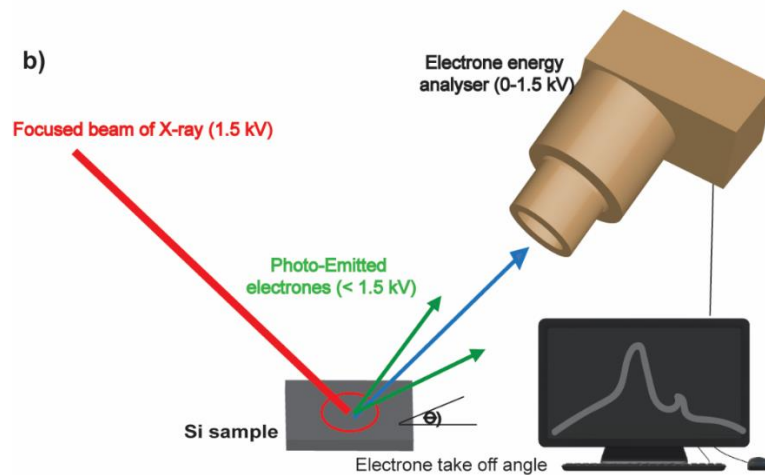
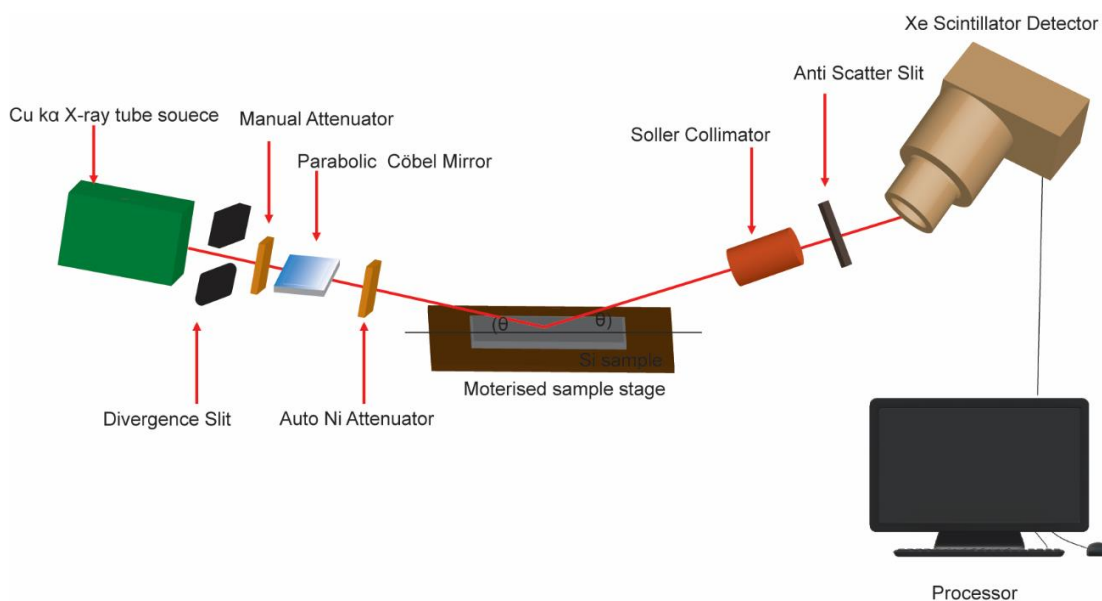


Figure 3. 4 a) Kratos Axis Ultra DLD spectrometer XPS (John de Laeter research centre, Curtin University of Technology, Department of Physics), b) scheme of the XPS instrument

3.5 X-ray refractometer (XRR)

X-ray refractivity (XRR) was used to obtain information about the surface roughness, thin-film thickness and density of the self-assembled monolayers or multilayers on the surface. The XRR Specular X-ray reflectometry at the solid-air interface was conducted on a Panalytical Ltd X'Pert Pro instrument with a rotating anode source (Cu K α radiation, $\lambda = 1.54 \text{ \AA}$). The X-ray beam was focused using a Göbel mirror and collimated using fixed slits of 0.1 mm. Samples were mounted onto a motorized stage to adjust the sample into the optimal position for measurements. Angles of incidence were measured from 0.05° to 5.00° in 0.01° steps for 20 seconds per step. The raw data was reduced so that the critical edge was normalized to a reflectivity of unity

and the data was presented as reflectivity versus momentum transfer, Q , which is equal to $4\pi \sin\theta/\lambda$, where θ is the angle of incidence and λ is the x-ray wavelength (1.54 Å). Structural parameters for the monolayer were refined in MOTOFIT reflectometry analysis software. Samples were analysed by Australian ANSTO, NSW. The scheme of the instrument is shown in Scheme 3.1.



Scheme 3. 1 Schematic diagram of X-ray reflectometer

3.6 Scanning tunnelling microscope (STM)

The scanning tunnelling microscope was used to measure the conductivity of single-molecules on Si and Au surfaces by using break junction (Current versus distance) and blinking methods. The STM experiments were carried out with PicoSPM 1 microscope where the head controlled by a “Picoscan 2,500 electronics, from Agilent” available at SPM facilities, Curtin University. The STM junction data were collected using an NI-DAQmx/BNC-2,110 national instruments (LabVIEW data collection system). The data were analysed with code based on LabVIEW software. An ideal STM tip comes to a single atom point. This allows measuring the conductivity of one single-molecule of the SAM.

In STM, the two techniques which are widely used for measuring conductivity are break junction (Current versus distance) and blinking methods (current versus time). In STM break junction method (STMBJ), a Au or Si tip is driven in and out from a surface containing the molecule of interest in a solution. When the tip is crushed into the surface, surface-tip contact will form. As the tip is retracted from the surface, these surface-tip contacts break sequentially and this is reflected as plateaus in the current-versus distance plots. The same thing happens for the molecular junctions as the bond break, but this happens at a lower current level. An example of these techniques is discussed in details in section 2.5.1.

In the blinking approach, the tunnelling current is first stabilized for 1 h. Current transients are then captured when the molecule connects between the STM tip and the surface in the presence of molecules. When a molecule is bridged between tip and surface, a sudden jump or 'blink' above the tunnelling current is obtained in the form of telegraphic blinks. These conductance histograms are built by the collection of hundreds of individual blinks. As the tip moves further, the bond will break and the current will drop. In the blinking experiments, the current is plotted against time. The photograph and the schematic diagram of the STM are shown in Figure 3.5. The schematic diagram of the STM-BJ and blinking method is described in Figure 3.6.

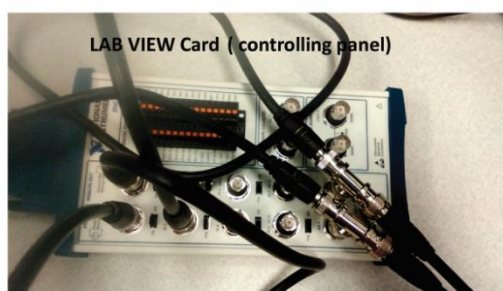
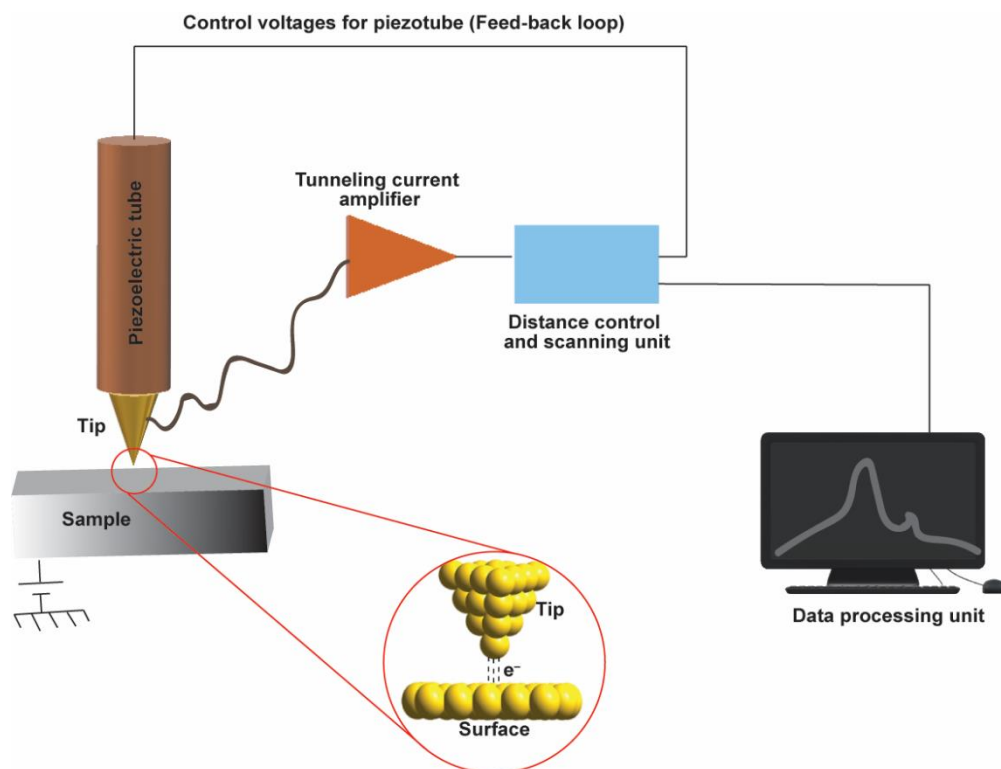


Figure 3. 5 a) Scheme of STM of PicoSPM 1, b) PicoSPM 1 microscope head controlled by a “Picoscan 2,500 electronics c) NI-DAQmx/BNC-2,110 national instruments (LabVIEW data collection system) d) STM instrument in SPM facilities, Curtin University of Technolgy, School of Molecular and Life Sciences.

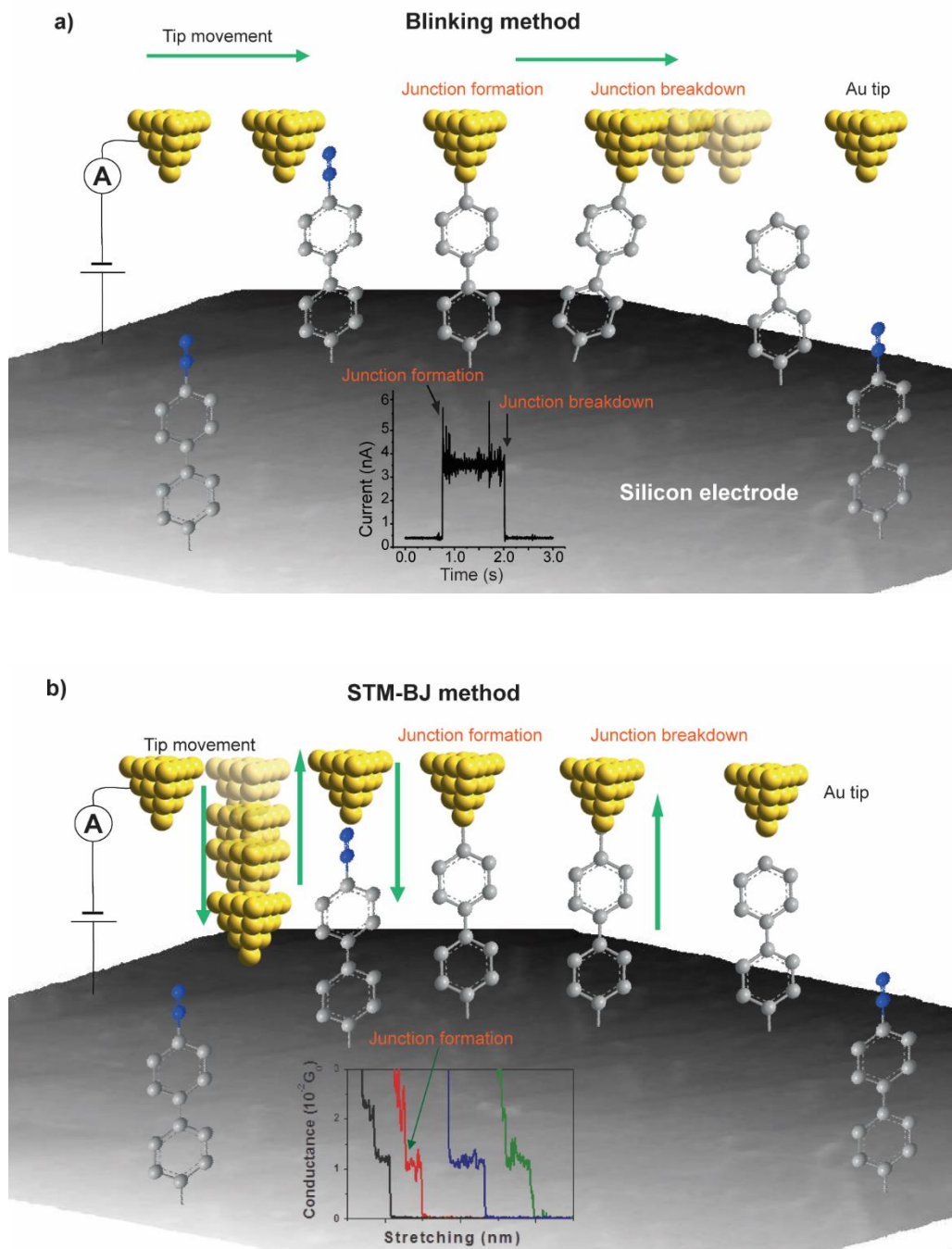


Figure 3. 6 a) Scheme of STM blinking method and b) break junction technique.

3.7 Transmission electron microscopy (TEM)

The transmission electron microscope was used to obtain high-resolution images of the cross-section of silicon oxide (SiO_x) and oxide tunnels formed on SiO_x by applied biases. TEM measurements were obtained using FEI Talos FS200X G2 FEG at the John de Laeter Centre, Curtin University. TEM used to characterize the cross-section of the conducting oxide channels produced by silicon oxides. In addition to the TEM images, scanning electron maps were also obtained from the same instrument along with energy-dispersive spectrum(EDS) and elemental maps. Samples were collected on a copper grid after coating the sample with Pt. Photograph of the instrument is provided in Figure 3.7.



Figure 3. 7 Photo images of the FEI Talos, TEM a) load lock, b)inside view of the load lock c) control panel and the turbo-pump available at John de Laeter research centre Curtin University, Australia

3.8 Scanning electron microscope (SEM)

The scanning electron microscope was used to obtain high-resolution images of the pyramids formed on Si (100) surfaces by different potassium hydroxide etching conditions. The SEM images were obtained using a Zeiss Neon 40EsB FESEM, with a Schottky field emission gun operating at 5 kV and a chamber pressure of approximately 4×10^{-6} mbar and a Tescan Mira3 FESEM, equipped with a Schottky field emission gun operating at 5 kV and a chamber pressure of 3×10^{-4} mbar. at the John de Laeter Centre, Curtin University. TEM used to characterize the cross-section of the conducting oxide channels produced by silicon oxides and characterize the silicon STM tips. A photograph of the instrument is provided in Figure 3.8.

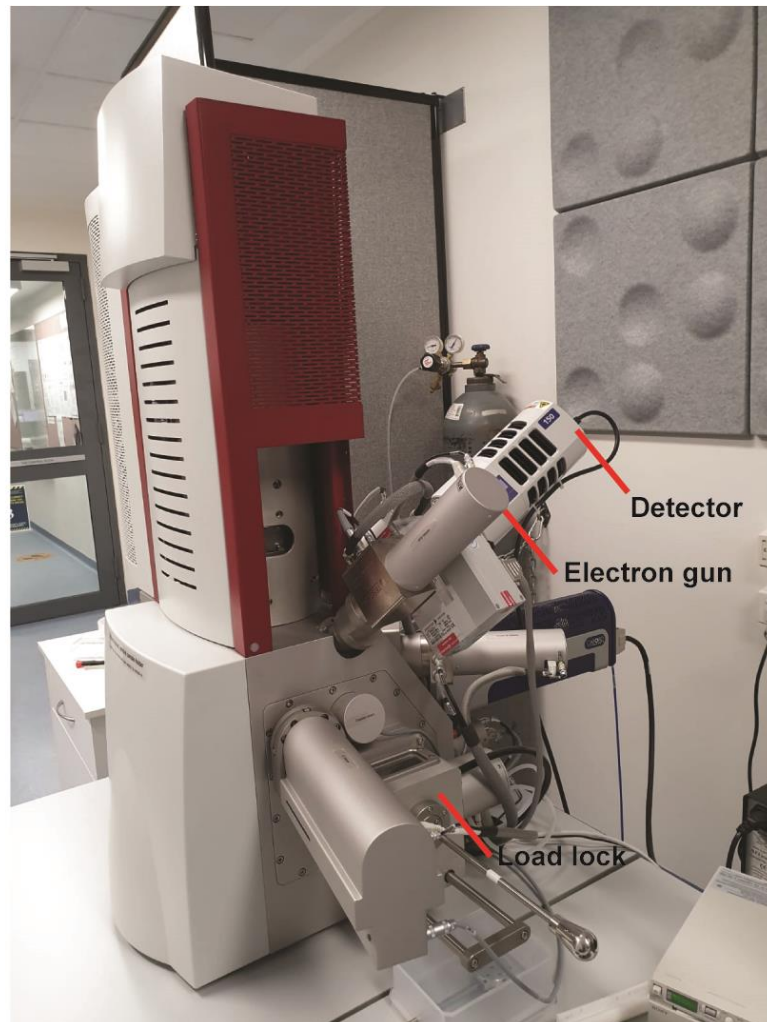


Figure 3. 8 Photo images of the Tescan Mira3 FESEM at John de Laeter research centre Curtin University, Australia

Chapter 4

Metal–single-molecule–semiconductor junctions formed by a radical reaction bridging gold and silicon electrodes

Chandramalika R. Peiris, Yan B. Vogel, Anton P. Le Brun, Albert C. Aragonès, Michelle L. Coote, Ismael Díez-Pérez, Simone Ciampi and Nadim Darwish

Journal of the American Chemical Society, Volume 141, Issue 37, 27th August 2019, Pages 14788–14797

DOI: <https://doi.org/10.1021/jacs.9b07125>

“Reproduced with permission from (Journal of the American Chemical Society, Volume 141, Issue 37, 27th August 2019, Pages 14788–14797.) Copyright (2019) American Chemical Society.”

4.1 Summary of this chapter

One of the major challenges in molecular electronics is to devise mechanically robust and reproducible molecular contacts for source and drain electrodes. Here, we first report the formation of diazonium salts films on gold and silicon electrodes either at an open circuit or and with aid of electrochemical potential. This work shows that the grafting of diazonium salts is crystal-facet dependent and being more favourable on silicon (111) than it is on (100) for both gold and silicon electrodes, a property that adds control over device fabrication. The prospect of this chemistry in single-molecule electronics is demonstrated by forming metal-molecule-semiconductor junctions between silicon and gold electrodes using STM-break junction approaches. Further details are provided in the form of the published manuscript in the Journal of the American Chemical Society, based on this work. I am the primary contributor to this work. The signed author contribution letter is provided in Appendix B (B-4-1).

4.2 Abstract

Here we report molecular films terminated with diazonium salts moieties at both ends which enables single-molecule contacts between gold and silicon electrodes at open circuit via a radical reaction. We show that the kinetics of film grafting is crystal-facet dependent, being more favourable on (111) than on (100), a finding that adds control over surface chemistry during the device fabrication. The impact of this spontaneous chemistry in single-molecule electronics is demonstrated using STM-break junction approaches by forming metal–single-molecule–semiconductor junctions between silicon and gold source and drain, electrodes. Au–C and Si–C molecule-electrode contacts result in single-molecule wires that are mechanically stable, with an average lifetime at room temperature of 1.1 s which is 30–400 % higher than that reported for conventional molecular junctions formed between gold electrodes using thiol and amine contact groups. The high stability enabled measuring current-voltage properties during the lifetime of the molecular junction. We show that current rectification, which is intrinsic to metal-semiconductor junctions, can be controlled when a single-molecule bridges the gap in the junction. The system changes from being a current-rectifier in the absence of a molecular bridge to an ohmic contact when a single-molecule is covalently bonded to both silicon and gold electrodes. This study paves the way for the merging of the fields of single-molecule and silicon electronics.

4.3 Introduction

One of the main goals of molecular electronics is to use molecular films, or even single molecules, as functional electronic components such as diodes, resistors or transistors.¹⁻³ The biggest challenge preventing this concept from becoming reality is the lack of mechanically robust contacts of an organic molecule with source and drain electrodes.⁴⁻⁵ To date, the most used electrode–molecule contacts have relied on the chemisorption of thiols on gold surfaces.⁶⁻¹¹ Such contacts are spontaneously formed from dilute solutions of thiols.¹²⁻¹⁴ Although widely used, molecular electronics on gold platforms suffer from major drawbacks, such as the lability of the S–Au bonds, electric field-induced structural changes and the lack of tunability of the electric properties of the gold substrate which limits the scope of these junctions.¹⁵⁻¹⁶ In the

last few years there has been an increasing interest in expanding the field of molecular electronics from gold towards semiconducting platforms, particularly GaAs¹⁷⁻¹⁸ and Si.¹⁹⁻²¹ It is anticipated that combining the vast and tunable range of the electrical properties of semiconductors with the chemical variety of molecules, new technological development can be achieved.

Among all the methods developed to modify semiconducting surfaces, the most common is the addition of an 1-alkene or 1-alkyne to a silicon radical to produce a covalent Si–C bond.²²⁻²³ This process, although successful in forming well packed monolayers, requires either a source of UV-light or heat, as well as a concentrated solution of the alkene or alkyne molecule. Such assembly requirements are not viable to form a stable contact in molecular electronics devices, and it is therefore essential to find new chemical strategies to form contacts on silicon electrodes that are of comparable ease to those for standard thiol-based contacts on gold. In this context, the cathodic electrochemical reduction of aryldiazonium salts is one of the most widely used methods for chemically modifying metal, carbon and silicon surfaces, which leads to strong covalent bonds.^{21, 23-33} Tao and co-workers³⁴ have reported the formation of single-molecule junctions in the presence of diazonium molecules in solution by means of electrochemically reducing, simultaneously, the two diazonium terminal groups. This allowed to form two Au–C covalent bonds, *in-situ*, using a bipotentiostatic “gated” control of two gold electrodes against a reference electrode. The Au–C contact is significantly more stable to what is achievable with thiol and amine molecules, which are typically used for molecular junction contacts.

In this study the diazonium radical reaction is demonstrated on semi-conducting electrodes, Si (111) and Si (100), and is utilized to form metal–molecule–semiconductor junctions at the single-molecule level. We use two axial diazonium terminal groups to form covalently bonded molecular junctions on gold and silicon electrodes. We show that molecular contacts on both silicon and gold can be made spontaneously by using a diazonium salt of high redox potential such that it can be reduced and consequently bridge both electrodes at open circuit. The role of surface energy was investigated by studying the effect of crystal orientation [(100) vs (111)] on the grafting process. Our findings remove the need of applying an electrochemical gate because the top and bottom contacts can be formed on the same molecule

spontaneously and yet sequentially. Further, our strategy does not require the continuous presence of molecules in the solution, which simplifies device fabrication for molecular junctions. The molecular films reported here are characterized by electrochemical methods, X-ray reflectometry and by atomic force microscopy. The scope of this chemistry in single-molecule electronics is demonstrated by means of single-molecule STM-break junction technique to electrically bridge silicon and gold electrodes via axial diazonium terminal groups. The mechanical stability of these covalently bonded single-molecule junctions were investigated using the “blinking approach” and compared to standard Au–molecule contacts. Current-voltage properties are reported for junctions made in the presence or absence of molecules; demonstrating the tunability of semiconductor junctions by the electronics of a single-molecule.



Figure 4. 1 Structure of the molecule (bis-diazo) studied and a schematic describing its reaction with surface and tip electrodes or with ferrocene. The surface and tip electrodes can be gold or silicon.

4.4 Experimental Methods

4.4.1 Chemicals and Materials

Unless stated otherwise all chemicals were of analytical grade and used as received. Hydrogen peroxide (30 wt% in water), sulfuric acid (Puranal™, 95–97%), ammonium fluoride (Puranal™, 40 wt% in water), ammonium sulfite monohydrate (Sigma-

Aldrich, $(\text{NH}_4)_2\text{SO}_3$, 92%) used for wafer cleaning plus etching, and silicon modification procedures were obtained from Sigma Aldrich. Acetonitrile (ACN) and dichloromethane (DCM) were distilled before use. *o*-Dianisidine bis(diazotized) zinc double salt (Sigma Aldrich, 98%), **bis-diazo** hereafter, 1,4-phenylenediamine (Sigma Aldrich $\geq 99\%$), benzene-1,4-dithiol (Sigma Aldrich, 99%), potassium hydroxide (VWR, 86%) and dimethyl sulfoxide (DMSO) were used as received. Tetrabutylammonium hexafluorophosphate (Bu_4NPF_6 , Sigma-Aldrich, $>99\%$), used as supporting electrolyte, was recrystallized twice from 2-propanol. Milli-Q™ water ($>18 \text{ M}\Omega \text{ cm}$) was used for surface cleaning procedures and to prepare electrolytic solutions. Gold polycrystalline (rod like) electrodes were purchased from CH Instruments, USA. Gold single crystal electrodes (99.999%) were purchased from Goodfellow. Prime-grade, single-side polished silicon wafers were obtained from Siltronix, S.A.S. (Archamps, France) and were n-type (phosphorous doped), $500 \pm 25 \mu\text{m}$ thick and either $(100) \pm 0.5^\circ$ (with resistivity of $0.003 \Omega \text{ cm}$), or $(111) \pm 0.5^\circ$ ($0.003 \Omega \text{ cm}$).

4.4.2 Surface Modification

4.4.2.1 Polycrystalline Au modification

Au polycrystalline electrodes were polished to a mirror-like finish by means of mechanical polishing (ca. 5 min) on a micro cloth pad, using a slurry of $0.05 \mu\text{m}$ Al_2O_3 . The electrodes were then rinsed with water, acetone, and then sonicated for 5 min in Milli-Q™ water. The electrodes were then electrochemically cleaned by cycling them between -300 mV and $+1600 \text{ mV}$ (versus an aqueous Ag/AgCl reference electrode) in $0.5 \text{ M H}_2\text{SO}_4$. The electrode cleaning by cyclic voltammetry was continued until a reproducible voltammogram was obtained (typically after 25 cycles), and the electrode was then rinsed with Milli-Q™ water and rested in distilled acetone prior to use.

4.4.2.2 Preparation of 100% Au(111) and 70% Au(111) single crystal

Single-crystal Au(111) disks were cleaned in a hot Piranha solution for 2-3 min (3:1 (v/v) mixture of concentrated sulfuric acid to 30 wt % hydrogen peroxide), rinsed with Milli-Q™ water and then annealed using a hydrogen flame. Annealed crystals were

cooled down to room temperature, washed with Milli-Q™ water, DCM and then blown dry under stream of argon gas. The crystals were then transferred to a deoxygenated solution of **bis-diazo** (1 mM) and Bu₄NPF₆ (0.1 M) in a 1:49 (v/v) mixture of DMSO and ACN and then either dynamically biased against a reference electrode or rested at open circuit.

For the preparation of surfaces exposing only ~70% of Au(111), a single-crystal Au(111) disk was melted on one of its edges (Appendix C, Figure C-4-1). The remaining intact surface area of Au(111) was estimated from the oxidation wave in cyclic voltammetry (Figure 4.2). The samples exposing ~70 % of Au(111) were modified with **bis-diazo** in a similar way to that described for the 100 % Au(111) crystals (section 4.4.2.2).

4.4.2.3. Si(111) and Si(100) modification

Silicon electrodes were cleaned and etched following literature procedures.¹⁹ In brief, silicon wafers were cut into pieces (approximately 10 × 10 mm), cleaned for 30 min in hot Piranha solution, rinsed with Milli-Q™ water and then etched with a deoxygenated 40 wt% aqueous ammonium fluoride solution for 13 min (Appendix C, Figure C-4-2). This process leads to a hydrogen-terminated silicon surface (Si-H). To the etching bath was added a small amount (ca. 5 mg) of ammonium sulfite. The etched samples were rinsed sequentially with Milli-Q™ water, DCM and blown dry in a stream of argon before modifying the silicon surface using the same procedure as described in section 4.4.2.2.

4.4.2.4 Formation of (111) pyramids on silicon (100)

Hydrogenated n-type silicon (100) substrates (generally 10 × 10 mm in size) were rinsed with DCM, 2-propanol and Milli-Q™ water, and then dried under the steam of argon. The samples were then etched for 90 min in a 20 % (w/v) aqueous solution of potassium hydroxide (10 mL) with 2-propanol (200 μL) and kept at 45 °C. The etched samples were then rinsed with copious amounts of water before a final etching step in deoxygenated 40% aqueous ammonium fluoride solution (13 min) followed by modification with the **bis-diazo** film as described in section 4.4.2.2.

4.4.3 Electrochemical measurements

All electrochemical measurements were performed using a CHI650 (CH Instruments, USA) electrochemical workstation and a conventional three-electrode system with a platinum wire as the auxiliary electrode. An Ag/AgCl aqueous electrode (1.0 M KCl, CH Instruments, USA) served as the reference in the electrochemical cleaning of gold surfaces, while a non-aqueous “leakless” Ag/AgCl electrode (eDAQ, part ET072-1) was used in the experiments for the **bis-diazo** reduction. The non-aqueous “leakless” reference electrode (3.4 M KCl) was calibrated before and after each experiment against the position, on an Au electrode, of the ferrocene/ferricenium couple Fc/Fc⁺ (1 mM ferrocene solutions in acetonitrile containing 0.1 M Bu₄NPF₆). All potentials are reported versus the apparent formal potential of the Fc/Fc⁺ couple unless otherwise specified.

4.4.4 Atomic Force Microscopy (AFM)

Atomic force microscopy images were obtained using Bruker dimension microscope operating in tapping mode. All images were obtained in air, at room temperature, and using silicon nitride cantilevers (TESPA from Bruker, with a spring constant of 20 N m⁻¹).

4.4.5 Scanning electron microscopy (SEM)

The SEM images were obtained using a Zeiss Neon 40EsB FESEM equipped with a Schottky field emission gun operating at 5 kV and a chamber pressure of 4×10^{-6} mbar and a Tescan Mira3 FESEM, also equipped with a Schottky field emission gun operating at 5 kV, and a chamber pressure of 3×10^{-2} Pa.

4.4.6 STM break junction

STM break junction (STMBJ) experiments were performed with a PicoSPM I microscope head controlled by a ‘Picoscan 2500’ controller, from Agilent. Data were acquired using a NI-DAQmx/BNC-2110 National Instruments data acquisition system and analysed with a code written with the LabVIEW software. Single-molecule conductivity measurements were performed using the STMBJ in the blinking

approach under fixed electrodes gap separation in a solution of mesitylene. The tunnelling current is first stabilized then current transients are captured. When a molecule bridges both electrodes, a sudden jump and ‘blink’ in the captured current is obtained. Conductance histograms were built by the accumulation of hundreds of individual blinks. The blinking histograms give information about the average conductivity of the single-molecule junctions that form spontaneously between the two electrodes, as well as information on their mechanical stability (blink lifetimes).

4.4.7 X-ray reflectometry (XRR)

Specular X-ray reflectometry was conducted as previously described^{19, 22, 35} on a Panalytical Ltd X’Pert Pro instrument. The instrument has a rotating anode source (Cu K α radiation, $\lambda = 1.54 \text{ \AA}$), has beam focusing using a Göbel mirror, and fixed collimation slits of 0.1 mm. Measurements were conducted at the solid-air interface under ambient conditions using angles of incidence from 0.05° to 5.00° in 0.01° steps for 20 seconds per step. The raw data was processed using in-house software so that the critical edge was normalised to a reflectivity of unity and the data was presented as reflectivity versus momentum transfer, Q , defined as:

$$Q = \frac{4\pi \sin \theta}{\lambda}$$

where λ is the X-ray wavelength and θ is the angle of incidence. Data analysis was conducted using the MOTOFIT software package, which utilises an Abele’s matrix method and a least-squares regression of varying the fitted parameters until a best fit that matches the experimental data is achieved.³⁶ The organic material was fitted using a single layer defined by its thickness, roughness, and scattering length density (SLD), ρ , defined as:

$$\rho = \frac{r_e \sum Z_i}{V_m}$$

where V_m is the total molecular volume (determined to be 237 \AA^3 for bis-diazo), Z_i is the atomic number of each atom in the species, and r_e is the Bohr electron radius ($2.818 \times 10^{-5} \text{ \AA}$). The theoretical SLD (ρ_t) of **bis-diazo** was determined to be $16.69 \times 10^{-6} \text{ \AA}^{-2}$. The number of molecules per cm^2 was determined from the fitted values as follows:

$$\text{molecules per cm}^2 = \frac{\tau \rho_f 10^{16}}{V_m \rho_t}$$

Where τ is the fitted thickness and ρ_f is the fitted SLD.

4.5 Results and Discussion

4.5.1 Electro- versus spontaneous-grafting of bis-diazo on gold

Multiple reduction peaks during the electrografting of diazonium salts on polycrystalline Au have been reported for several molecules and are often attributed to a range of different phenomena. One hypothesis is that multiple waves originates from the presence of different crystallographic facets present on the polycrystalline Au surface.³⁷⁻⁴⁰ To test this hypothesis we deliberately varied the crystallinity of the Au surface from a completely polycrystalline sample to a single crystal (111) surface (Figure 4.2a–c). The degree of crystallinity was estimated from the gold oxide anodic wave in cyclic voltammetry: a single oxidation peak indicates that the surface is 100% (111) while multiple or broad oxidation waves are ascribed to a polycrystalline sample (Figure 4.2a–c). For the reduction of **bis-diazo** on highly oriented single crystal Au(111), only a single wave is observed at –70 mV (Figure 4.2d). A second wave at more negative potentials (–350 mV) appears for the reduction of **bis-diazo** on other Au crystal orientations. For instance, the reduction of **bis-diazo** on a 70% Au(111) surface (Figure 4.2e) results in two waves, with that assigned to (111) being almost three folds larger than that centered at –350 mV (Figure 4.2e). Completely polycrystalline samples (Figure 4.2f) shows multiple broad waves between 0 and –400 mV, again highlighting the correlation between the crystallinity of the surface and the shifts in biases required to graft **bis-diazo**.

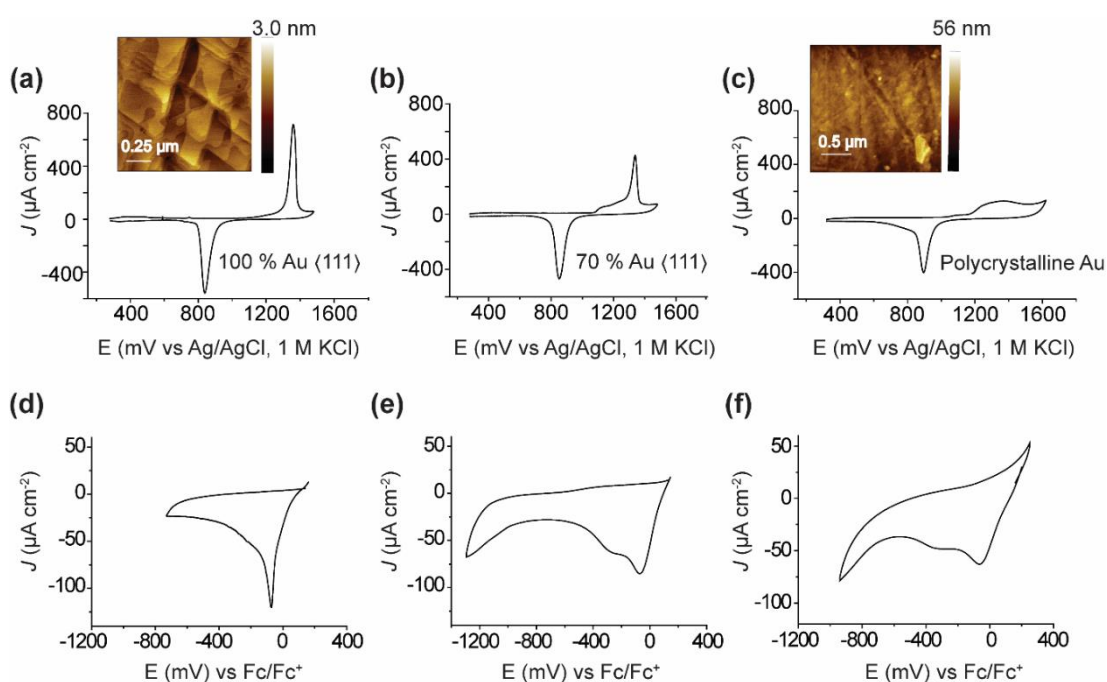


Figure 4. 2 Electrochemical grafting of **bis-diazo** on mono- and poly-crystalline gold surfaces. Cyclic voltammograms showing the oxidation and reduction waves of a) 100 % single crystal Au (111). The Inset in (a) shows an AFM topography image of the single crystal surface. b) 70% Au (111) and c) polycrystalline gold (0.5 M H₂SO₄ as the electrolyte) at scan rate 100 mV s⁻¹. The potential is expressed in mV against aq. Ag/AgCl electrode (1 M KCl). The inset in (c) shows an AFM topography image of the polycrystalline Au surface. The gold oxidation wave is a single peak at around +1300 mV for 100% Au (111). (b–c) Multiple oxidation waves between +1000 mV and +1400 mV appear for 70% Au (111)/30% polycrystalline in (b) and for a 100% polycrystalline surfaces in (c). (d–f) Electrochemical reduction waves for the grafting of **bis-diazo** (1 mM) with Bu₄NPF₆ (0.1 M) in a 1:49 (v/v) dimethyl sulfoxide/acetonitrile (DMSO/ACN) solvent mixture on the different gold surfaces shown in panels a–c. The scan rates in panels d–f are 50 mV s⁻¹ and the potential is expressed in mV against Fc/Fc⁺ (1 mM in ACN). The more polycrystalline the Au surface is the broader and the more split are the reduction waves.

The reduction potential of **bis-diazo** on Au(111) is relatively anodic (–70 mV vs Fc/Fc⁺, Figure 4.2), meaning the grafting could spontaneously occur even at open circuit. Following the reduction step, a radical intermediate will form a covalent bond

between the organic molecule and the gold surface,⁴¹⁻⁴² as schematized in Figure 4.3a. The surface-tethered molecule would still have a diazo group at the distal end, and this hypothesis was tested by resting a clean Au(111) sample at open circuit in a solution of **bis-diazo** for 2 h, after which the sample was transferred to a ferrocene solution. Ferrocene can act as sacrificial electron donor, reducing the diazonium to generate a radical⁴¹⁻⁴² that can in turn react with excess ferrocene in solution forming a covalent bond (see Figure 4.3a). The coupling reaction between the metallocene and the unreacted azo distal end of the monolayer formed at open circuit was then tested by means of measuring cyclic voltammograms. Cyclic voltammetry data for these films is shown in Figure 4.3c, and the amount of ferrocene units tethered on the surface are comparable to films formed by either spontaneous or potentiostatic electrolysis $2.30 (\pm 0.40) \times 10^{-10} \text{ mol cm}^{-2}$ equivalent to a $1.38 (\pm 0.24) \times 10^{14} \text{ molecule cm}^{-2}$ for the electrochemical grafting (Figure 4.3b) and $1.80 (\pm 0.29) \times 10^{-10} \text{ mol cm}^{-2}$ equivalent to $1.08 (\pm 0.17) \times 10^{14} \text{ molecule cm}^{-2}$ for the spontaneous process (Figure 4.3c).

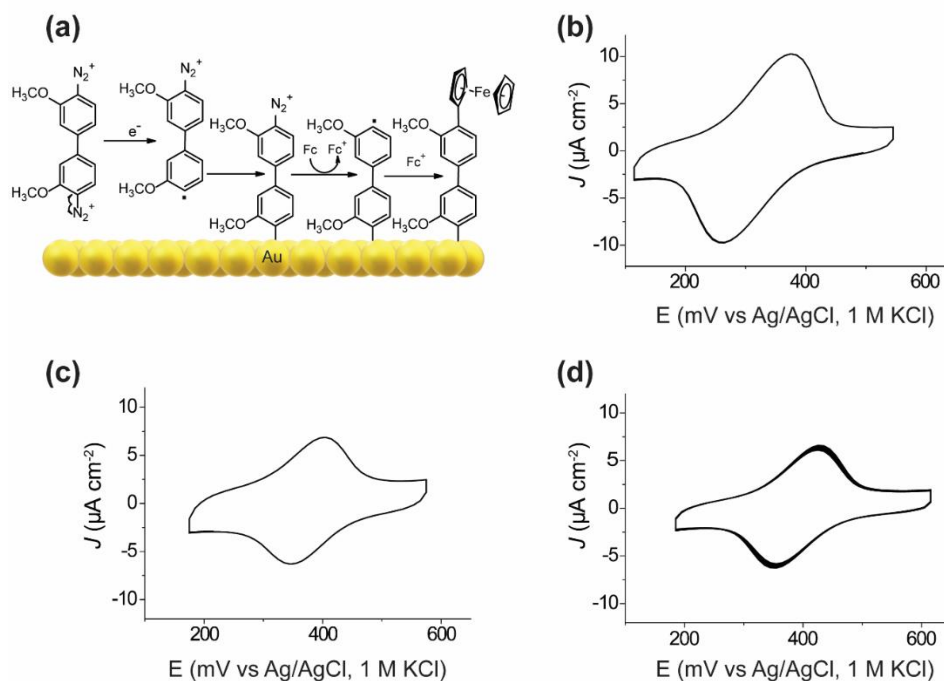


Figure 4. 3 Electrochemical and spontaneous grafting of **bis-diazo** on Au(111) followed by a reaction with ferrocene. a) Schematics describing the formation of a diazonium film on an Au surface and the reduction of the distal diazonium moiety by ferrocene molecules. b) Cyclic voltammogram for an Au(111) surface that was first modified with **bis-diazo** then exposed to a solution of ferrocene. The electrochemical reduction was first performed via 1 potential cycle (0 to -1 V vs Fc/Fc⁺) in a solution of **bis-diazo** (1mM) with Bu₄NPF₆ (0.1 M) in a 1:49 (v/v) DMSO/ACN solvent mixture. The surface was then exposed to a solution of ferrocene (1 mM in ACN) for 30 min at open circuit. Note that the schematic in (a) does not take into account the polymerization of the film, see Appendix C, Figure C–4–3 for details. c) Cyclic voltammogram for the spontaneous reduction of bis-diazo, by means of resting an Au(111) sample in a solution of **bis-diazo** for 2 h at open circuit, followed by the spontaneous reaction with ferrocene (30 min) to indirectly probe the presence of an intact unreacted diazo group at the distal end of the monolayer. The potential scan rate is 50 mVs⁻¹. d) Stability of the interface tested by means of 30 repetitive cyclic voltammograms scans for a surface that is prepared in a similar way to that described in (c), see Appendix C, Figure C–4–4 for details. The voltammograms in (b–d) were recorded in 1 M HClO₄ and the potential is expressed in mV against Ag/AgCl electrode (1 M KCl).

4.5.2 Electro-versus spontaneous-grafting of bis-diazo on silicon

Having established the formation of **bis-diazo** monolayers on gold surfaces, we then attempted to graft bis-diazo on silicon electrodes. Figure 4.4a shows that the wave for the electrochemical reduction of **bis-diazo** is centered at -650 and -830 mV on Si(111) and Si(100), respectively. Thickness of the films was determined using X-ray reflectometry (XRR) and was found to be 2.43 nm when one potential scan, between $+0.4$ and -1.8 V vs Fc/Fc⁺ with a scan rate of 50 mV s⁻¹, was applied. A thickness of 2.43 nm means that **bis-diazo** polymerizes and the film comprises about 3 repeated **bis-diazo** units (Figure C-4-3 and Table C-4-1, Appendix C).

As shown in Figure 4.4b, the electrochemical reduction of **bis-diazo** is scan rate-dependent, and digital simulations of the experimental voltammetry were used to gain quantitative insights on the heterogeneous electrochemical rate constant, k_{et} , values for the electrochemical reaction on both gold and silicon electrodes (Appendix C, Figures C-4-6-C-4-8). We assumed an EC_{irrev} mechanism (E is the homogeneous redox step, **bis-diazo**⁺/**bis-diazo**; C_{irrev} is the chemical homogeneous nitrogen loss, **bis-diazo** → **bis-diazo**[•] + N₂). The k_{et} best-fit values are 4.0×10^{-3} cm s⁻¹ for Au(111), 1.0×10^{-5} cm s⁻¹ for Au(100), 2.0×10^{-7} cm s⁻¹ for Si(111), and 5.0×10^{-9} cm s⁻¹ for Si(100). The electrochemical rate is significantly slower for silicon, and both for silicon and gold the k_{et} drops from (111) to (100) facets. Furthermore, it is apparent from the absence of a return wave that the reduced form of the diazonium salt expels nitrogen after its initial electrochemical reduction with a rather large chemical rate (best-fit k_f of 5.0×10^3 s⁻¹). The sluggish reduction kinetics on silicon indicates that for films of **bis-diazo** to form spontaneously at open circuit on silicon may require more time than that on gold. This was confirmed by measuring the ferrocene surface coverage vs time on both gold and silicon electrodes (Appendix C, Figures C-4-9-C-4-12). The ferrocene molecules coverage increase from $7.67 (\pm 1.15) \times 10^{11}$ molecule cm⁻² to $3.89 (\pm 0.58) \times 10^{12}$ molecule cm⁻² when the resting time of the Si-H surface in the solution of **bis-diazo** increased from 2 min to 8 h (Appendix C, Figures C-4-10). In contrast, on the gold electrode the reaction reached equilibrium after 2 h.

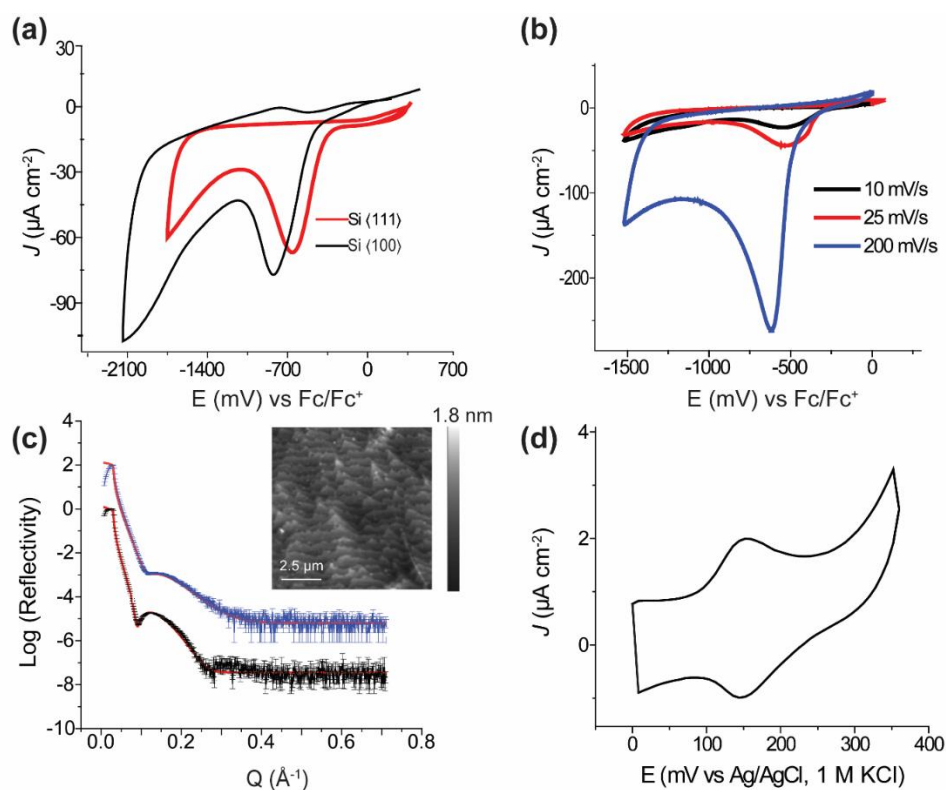


Figure 4. Electrochemical and spontaneous grafting of **bis-diazo** on silicon. a) Reductive grafting of **bis-diazo** (1 mM **bis-diazo** with 0.1 M Bu₄NPF₆ in a 1:49 (v/v) DMSO/ACN solvent mixture) on Si(111) (red line) and on Si(100) (black line) using one potential cycle (+0.4 V to -1.8 V for Si(111) and +0.5 V to -2.1 V for Si(100)) at scan rate of 50 mV s⁻¹. The second potential cycle is shown in Appendix C, Figure C-4-5. b) Reduction of **bis-diazo** on Si(111) using one potential cycle at different scan rates (10, 25 and 200 mV s⁻¹). c) XRR profiles for samples prepared by grafting **bis-diazo** on Si(111)-H electrochemically (black trace) or spontaneously (blue trace). The inset in (c) shows an AFM topography image of the Si(111)-H surface. The symbols with error bars are the collected data and the red solid lines are the fits to each data set. The data is vertically offset for clarity and the parameters used in the interpretation of the XRR data are listed in Appendix C, Table C-4-1. d) Cyclic voltammogram at a scan rate of 200 mV s⁻¹ of a film of **bis-diazo** spontaneously prepared by resting a hydrogen-terminated Si(111)-H surface in a solution of **bis-diazo** for 8 h and then exposing it to a solution of ferrocene for 30 min. The potential in (a-b) is expressed in mV against Fc/Fc⁺ (1 mM in ACN). The voltammogram in (d) was recorded in 1M HClO₄ and the potential is expressed in mV against Ag/AgCl electrode (1 M KCl).

As in the case of gold, a surface comprising both Si(111) and (100) facets should show two discrete waves. To verify this, we etched crystallographically oriented Si(111) pyramids on a Si(100) surface by anisotropic etching in KOH solutions.⁴³⁻⁴⁵ KOH etching creates samples with both (111) and (100) that can be used to probe *in-situ* the crystal-facets dependency of the electrochemical reduction.

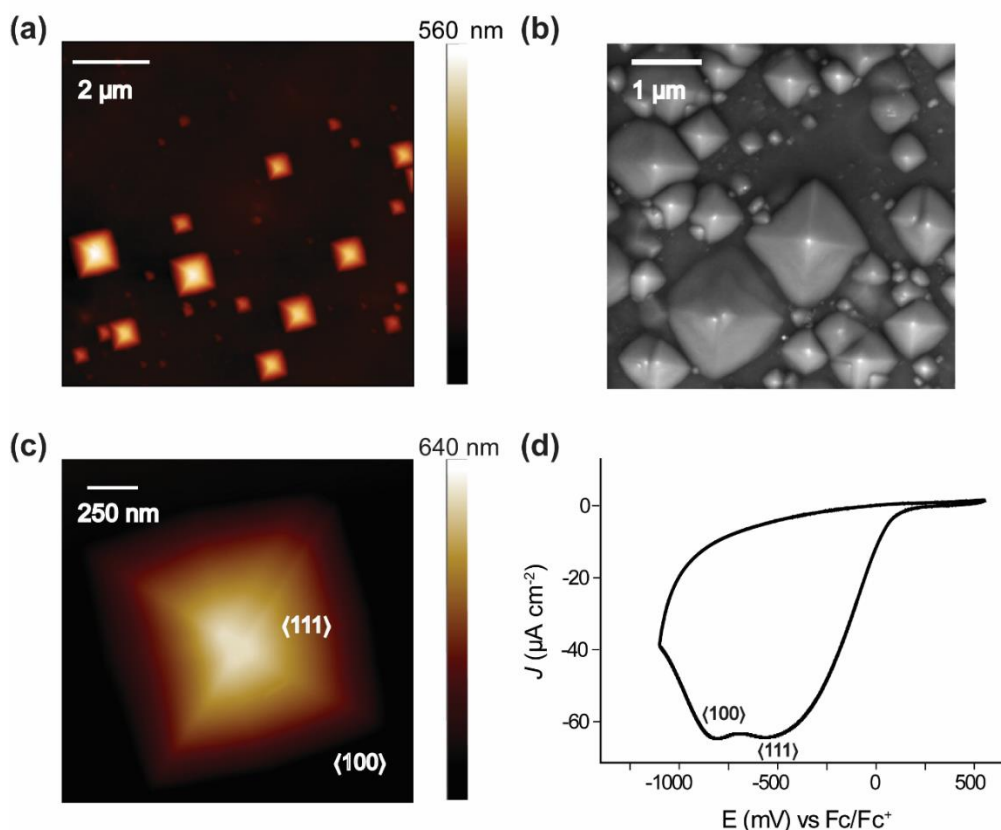


Figure 4. 5 Electrochemical grafting of **bis-diazo** on crystalline silicon: Si(100) vs Si(111). a) AFM image of Si(111) pyramids grown on Si(100) by anisotropic etching of the surface in a solution of KOH solution. b) SEM image for the same surface. c) A zoom-in AFM image of a single pyramid. d) The electrochemical reduction wave of **bis-diazo** (1 mM **bis-diazo** with 0.1 M Bu₄NPF₆ in a 1:49 v/v DMSO/ACN mixture) on the sample presented in (a) and (b). The potential scan rate in (d) is 50 mV s⁻¹ and the potential is expressed in mV against Fc/Fc⁺ (1 mM in ACN).

The difference in the peak position for the reduction waves of **bis-diazo** on separate samples of Si(111) and (100) is 180 mV, as in Figure 4.4a. Similar differences (ca. 200 mV) in the position of the reduction were observed for the mixed (111/100) (sample

with pyramids; (100) surface etched to expose (111) pyramids) (Figure 4.5b). The 200 mV difference is significant such that it can be used to control chemical reactivity on different silicon crystal orientation by controlling the applied reduction potential. The crystal-facet dependence is not restricted to the **bis-diazo** compound, and similar shifts in the diazo reduction wave were observed for 4-bromodiazonium salts electrochemically reduced on Si(111), Si(100) and on mixed (111)/(100) silicon surfaces (Appendix C, Figures C-4-13).

It is worth noting that since the source of electrons is not identified, the mechanism by which the spontaneous modification on both Au and Si occur is less clear than that when using the electrochemical method. The open circuit potential (OCP) measured for Au and Si electrode/electrolyte systems used in this study are -200 ± 100 mV and -300 ± 100 mV vs Fc/Fc⁺, respectively. These values are relatively cathodic, and the formal potential of the **bis-diazo** is relatively anodic making it easily reducible to the aryl radical. The most plausible electron donors are the gold and silicon surfaces. Unlike bulk gold, which can usually be regarded as inert, surface defects, step edges and nanoscale protrusions are known to oxidize at significantly lower potentials.⁴⁶⁻⁴⁷ Silicon oxidation can involve up to four electrons,⁴⁸ and the anodic growth of oxide can extend longitudinally away from the interface⁴⁹ meaning that the oxidation of limited surface areas can be sufficient to generate enough coulombs to reductively graft a **bis-diazo** monolayer. This scenario is in agreement with the slightly lower coverage measured by XRR (Appendix C, Table C-4-1) for the spontaneous versus electrochemical grafting. Another possibility or a contributor is the oxidation of adventitious impurities in the reaction solution; however this possibility is unlikely since the spontaneous reaction also occurred with an STM gold tip in a mesitylene solvent (section 4.5.3), a different environment to that used to form the **bis-diazo** films.

4.5.3 Single-molecule STMBJ studies

The monolayer results of the previous section verify the spontaneous attachment of an electron-poor diazonium salt (**bis-diazo**) to both gold and silicon electrodes. The distal diazonium group of the molecule is conserved upon attachment, which opens the possibility for the further spontaneous attachment of a redox active organic

molecule (e.g. ferrocene in Figure 4.3a), or more importantly, of a top metal point-contact to spontaneously close the electrical circuit. We proceeded to show this by forming Si-**bis-diazo**-Au junctions (Figure 4.6a). We performed single-molecule measurements using the scanning tunnelling microscopy (STM) junction technique in the “blinking approach”⁵⁰⁻⁵² in which a gold STM tip is brought within tunnelling distance to a silicon surface that was pre-modified with **bis-diazo** molecules. When a chemical bond is formed between the tip and the molecule a sudden current jump, or blink, appears in the current-time STM trace. A typical blink is shown in Figure 4.6b (inset) depicting the junction comprising a **bis-diazo** molecule passing a current of 3.5 ± 0.5 nA for 1.2 s. Figure 4.6b shows a histogram of the single-molecule conductance obtained from hundreds of blinks, with an average value of $90 \pm 35 \mu G_0$ ($G_0, 77.5 \mu S$, is the conductance of a single quantum channel). The relative uniform conductivity distribution indicates that these molecular circuits are reproducible and of similar chemical nature. A histogram of blink lifetimes is shown in Figure 4.6b with the average being centered at 1.1 ± 0.2 s. This lifetime is significantly higher than previously reported for single-molecule junctions between gold surfaces using other chemistries.⁵³ As a comparison, the lifetime of an Au-**bis-diazo**-Au junction is 0.75 ± 0.15 s (Appendix C, Figure C-4-14) which is 30% less than that of the Au-**bis-diazo**-Si system. The difference was unexpected, given that the lifetime of both junctions should be limited by the relatively weak Au-molecule contact. We attribute the superior stability of the Au-**bis-diazo**-Si system to the presence of at least one robust point of contact (the silicon side), which can enhance the robustness of the junction if the mechanical pull is distributed more heavily on the silicon side, which is a probable scenario as the STM tip is drifting away during measurements. The lifetime of the junctions was also compared on gold electrodes, but using a contact chemistry different than the Au-carbon of the Au-**bis-diazo**-Au junctions. The blinking lifetime for Au-molecule-Au system that relies on either Au-sulfur or Au-nitrogen contacts are 0.50 ± 0.10 s and 0.20 ± 0.05 s, respectively. These blinking lifetimes are several folds lower than that of the Au-**bis-diazo**-Au and Au-**bis-diazo**-Si contacts, highlighting the superior mechanical stability of the covalent Au-C and Si-C electrode contacts. (Appendix C, Figure C-4-14).

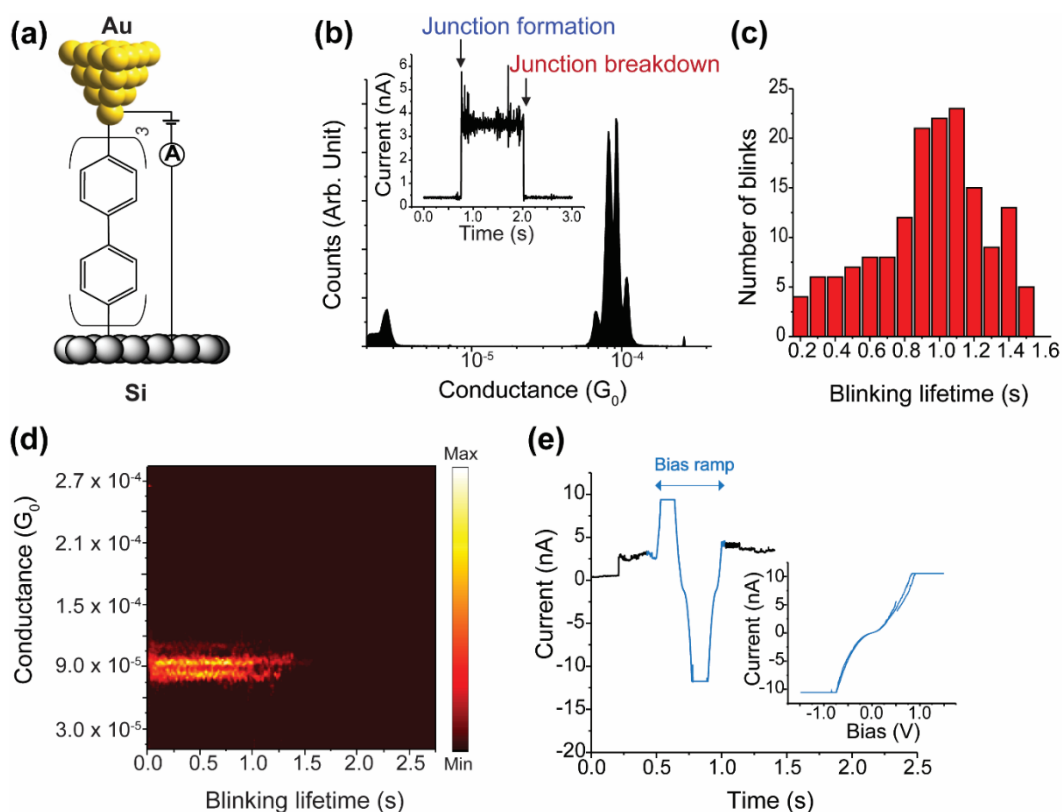


Figure 4.6 Single-molecule junction measurements of a Si(111) surface pre-modified electrochemically (one potential cycle from +0.4 V to -1.8 V Fc/Fc⁺) by a **bis-diazo** film with a gold tip forming the top contact. a) Schematic depicting the molecular junction formed. b) Conductance histogram built from ca. 200 blinks averaging $90 \pm 35 \mu G_0$. (inset). Representative Au–bis-diazo–Si blink, measured at a bias of 0.5 V. c) Histogram of blink lifetimes with the average being 1.1 ± 0.2 s d) Blinking color maps obtained by accumulating ca. 200 blinks and normalized to a common time origin. (e) Representative data for a voltage sweep applied during a blink of a single-molecule Au–bis-diazo–Si junction. Current is monitored before and after the voltage sweep to ensure the voltage is ramped while the molecular junction is still intact. (inset) shows the corresponding current-voltage curve. The STM experiments were performed at room temperature in mesitylene.

The superior duration of the blinks formed by **bis-diazo** molecules is owed to its covalent bonding to both electrodes (Si–C and Au–C). Figure 4.6e shows that these junctions can be subjected to a voltage ramp of ± 1.5 V, for a duration of 0.5 s, without rupture. The timescale for the collection of current-voltage (I–V) is well within the ~ 1 s of the lifetime of a **bis-diazo** junction. I–V curves are symmetrical around the origin

with very limited current rectification being observed. This is in contrast to the I–V curves measured on bare unmodified Si–H surfaces which showed current rectification (Figure 4.7a). Even when the molecule is not bridging the two electrodes a shift towards a non-rectifying I–V curves are observed (Figure 4.7b).

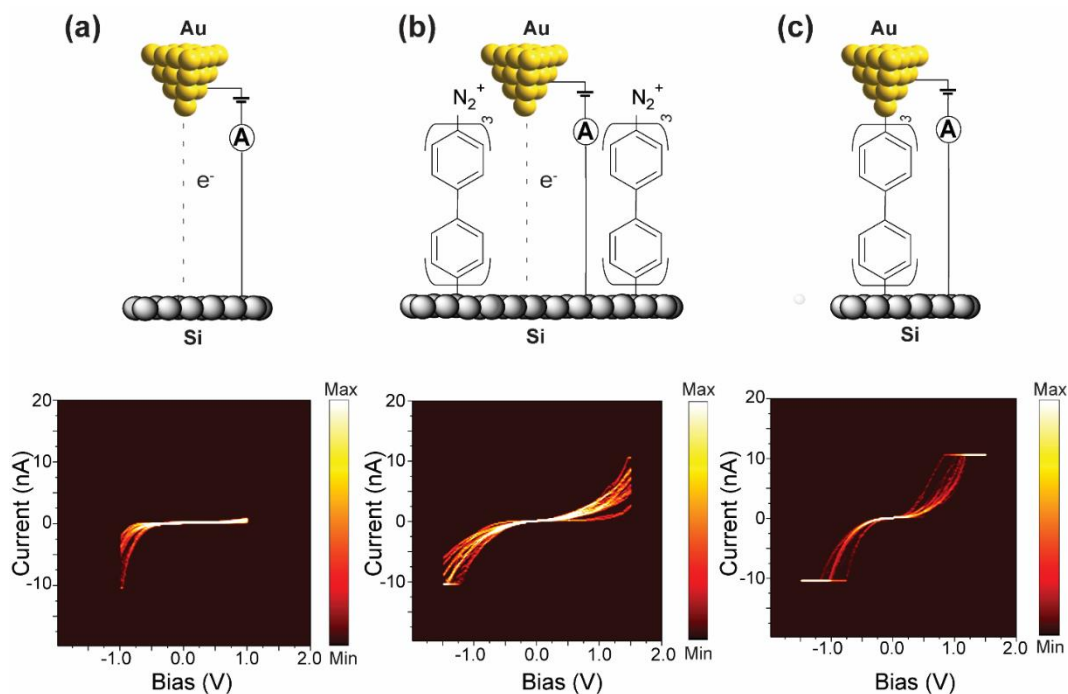


Figure 4. 7 STM-current-voltage measurements. a) Schematic and current-voltage measurements of Au-Si tunneling junctions in the absence of **bis-diazo** molecules. b) Schematic and current-voltage measurements Au--bis-diazo--Si junctions in the absence of a “blink” and therefore absence of covalent bonding to both electrodes. c) Schematic and current-voltage measurements of Au–bis-diazo–Si junctions in which the **bis-diazo** molecule is covalently bonded to both electrodes. The data for each set is the accumulation of 30 different voltage sweeps and the bias is applied to the silicon surface. The characteristics of the current-voltage curves changes from rectifying in (a) to ohmic in the presence of a top contact with the molecule in (c) where the path of charge transfer is restricted to within the molecule. If the electrons can tunnel in the gaps between the molecules the rectification characteristic is intermediate. The STM experiments were performed at room temperature in mesitylene.

Of a particular note is the gradual decrease in the current rectification ratio (RR) when the system switches from a tunneling through space (Figure 4.7a, RR = 10–20 at $\pm 1V$) to tunneling through the **bis-diazo** molecular film without a covalent attachment to the top gold electrode (therefore absence of a blink, Figure 4.7b, RR = $1-10 \pm 1V$), then to tunneling through the molecule when a blink forms (RR = $1-2 \pm 1V$). As a comparison we performed I–V curves on symmetrical Au–**bis-diazo**–Au junctions (Appendix C, Figure C–4–15). Although the I–V of Au–**bis-diazo**–Au junctions are also symmetrical, they are significantly different than the Au–**bis-diazo**–Si junctions. First, they are more conducting as evidenced by a larger I–V slope specifically in the small bias window of -0.5 to $+0.5$ V; and second there is no difference in the I–V curves shape nor in the non-rectifying properties of the junctions whether a molecule is connected between the gold electrodes or whether electrons are tunneling through space and not through a connecting **bis-diazo** molecule. This rules out the possibility of gold atom transferring to the silicon being the reason for the symmetric I–V curves for the Au–**bis-diazo**–Si junctions in Figure 4.7c. It also means that in Au–**bis-diazo**–Si junctions the covalently-connected molecule is providing a pathway for electrons to tunnel through the silicon’s band gap. Non-rectifying junctions were recently observed for Au–molecule–GaAs junctions by Nichols and co-workers¹⁷⁻¹⁸ in which the degree of rectification was found to depend on the molecules used to bridge the Au and the semiconducting GaAs electrodes: the more conjugated the molecules are (such as **bis-diazo**) the smaller the band gap and the more likely to have the lowest unoccupied molecular orbitals (LUMO) energy closer to the metal Fermi level enabling states for electron transport from the metal to the semiconductor under reverse bias. Another possible contributor to the high reverse bias current is the introduction of surface states that reduces the barrier height for electron transfer between the metal and the bottom of the conduction band.⁵⁴ This means that unlike conventional solid-state metal-semiconductor diodes, the metal–**bis-diazo**–semiconducting diodes can be tuned not only by the choice of the molecule but also by the nature of the top-contact (covalent versus non-contact).

4.6 Conclusion

We demonstrated that **bis-diazo** compounds form molecular films spontaneously, as well as electrochemically, on gold and silicon electrodes. The grafting is more sluggish on silicon than it is on gold and is crystal-facet dependent, being more favourable on (111) than it is on (100). This aspect of the work could become a way to address chemical reactivity at discrete locations, for example by forming molecular monolayers on Si(111) pyramids on a rather unmodified Si(100) surface. This can be of significant practical implications in molecular electronics. We also show that the formed molecular films enable for the further attachment of top molecules and/or electrodes. We utilized this approach to form metal–molecule–semiconductor junctions between silicon and gold electrodes using the STMBJ technique. The single-molecule wires are mechanically stable, owing to the strong Au–C and Si–C contacts, with an average life time of 1.1 s, which is 30–400 % more stable than previous molecular junctions on gold electrodes and which enables current-voltage properties of the devices to be measured while the molecule is intact. We demonstrate that unlike conventional metal-semiconductor diodes, the metal–**bis-diazo**–semiconducting diodes can be tuned by a single-molecule contact and by the nature of the top-contact being covalent versus non-contact. This study offers a viable way to make top/bottom contacts between semiconductors and metals in miniaturized electronic devices and open prospects for a hybrid silicon and single-molecule electronics technology.

4.7 Acknowledgement

This work was supported by the Australian Research Council for DE160101101, DE160100732 and DP190100735 grants. M. C. R Peiris would like to thank Curtin International Postgraduate Research Scholarship and Research Stipend Scholarship (CIPRS). This research was undertaken using the facilities (XPS, SEM) at the John de Laeter Centre, Curtin University, Department of Chemistry, Curtin University and Australian Nuclear Science and Technology Organization (ANSTO).

4.8 References

1. Ratner, M., A brief history of molecular electronics. *Nat. Nanotechnol.* **2013**, *8* (6), 378.
2. Tao, N. J., Electron transport in molecular junctions. *Nat. Nanotechnol.* **2006**, *1* (3), 173-181.
3. Xu, B.; Xiao, X.; Tao, N. J., Measurements of single-molecule electromechanical properties. *J. Am. Chem. Soc.* **2003**, *125* (52), 16164-16165.
4. Zhang, Y.; Zhao, Z.; Fracasso, D.; Chiechi, R. C., Bottom-up molecular tunneling junctions formed by self-assembly. *Isr. J. Chem.* **2014**, *54* (5-6), 513-533.
5. Jia, C.; Guo, X., Molecule–electrode interfaces in molecular electronic devices. *Chem. Soc. Rev.* **2013**, *42* (13), 5642-5660.
6. Darwish, N.; Paddon-Row, M. N.; Gooding, J. J., Surface-bound norbornylogous bridges as molecular rulers for investigating interfacial electrochemistry and as single molecule switches. *Acc. Chem. Res.* **2013**, *47* (2), 385-395.
7. Darwish, N.; Eggers, P. K.; Ciampi, S.; Tong, Y.; Ye, S.; Paddon-Row, M. N.; Gooding, J. J., Probing the effect of the solution environment around redox-active moieties using rigid anthraquinone terminated molecular rulers. *J. Am. Chem. Soc.* **2012**, *134* (44), 18401-18409.
8. Rascón-Ramos, H.; Artés, J. M.; Li, Y.; Hihath, J., Binding configurations and intramolecular strain in single-molecule devices. *Nat. Mater.* **2015**, *14* (5), 517.
9. Darwish, N.; Aragonès, A. C.; Darwish, T.; Ciampi, S.; Diez-Perez, I., Multi-responsive photo-and chemo-electrical single-molecule switches. *Nano Lett.* **2014**, *14* (12), 7064-7070.
10. Haiss, W.; Wang, C.; Grace, I.; Batsanov, A. S.; Schiffrin, D. J.; Higgins, S. J.; Bryce, M. R.; Lambert, C. J.; Nichols, R. J., Precision control of single-molecule electrical junctions. *Nat. Mater.* **2006**, *5* (12), 995.
11. Wang, L.; Gong, Z. L.; Li, S. Y.; Hong, W.; Zhong, Y. W.; Wang, D.; Wan, L. J., Molecular Conductance through a Quadruple-Hydrogen-Bond-Bridged Supramolecular Junction. *Angew. Chem., Int. Ed.* **2016**, *55* (40), 12393-12397.

12. Bensebaa, F.; Ellis, T. H.; Badia, A.; Lennox, R., Thermal treatment of n-alkanethiolate monolayers on gold, as observed by infrared spectroscopy. *Langmuir*. **1998**, *14* (9), 2361-2367.
13. Huang, Z.; Chen, F.; Bennett, P. A.; Tao, N., Single molecule junctions formed via au- thiol contact: stability and breakdown mechanism. *J. Am. Chem. Soc.* **2007**, *129* (43), 13225-13231.
14. Huang, C.; Jevric, M.; Borges, A.; Olsen, S. T.; Hamill, J. M.; Zheng, J.-T.; Yang, Y.; Rudnev, A.; Baghernejad, M.; Broekmann, P., Single-molecule detection of dihydroazulene photo-thermal reaction using break junction technique. *Nat. Commun.* **2017**, *8*, 15436.
15. Darwish, N.; Eggers, P. K.; Ciampi, S.; Zhang, Y.; Tong, Y.; Ye, S.; Paddon-Row, M. N.; Gooding, J. J., Reversible potential-induced structural changes of alkanethiol monolayers on gold surfaces. *Electrochem. Commun.* **2011**, *13* (5), 387-390.
16. McCreery, R. L.; Yan, H.; Bergren, A. J., A critical perspective on molecular electronic junctions: there is plenty of room in the middle. *Phys. Chem. Chem. Phys.* **2013**, *15* (4), 1065-1081.
17. Vezzoli, A.; Brooke, R. J.; Ferri, N.; Higgins, S. J.; Schwarzacher, W.; Nichols, R. J., Single-molecule transport at a rectifying GaAs contact. *Nano Lett.* **2017**, *17* (2), 1109-1115.
18. Vezzoli, A.; Brooke, R. J.; Ferri, N.; Brooke, C.; Higgins, S. J.; Schwarzacher, W.; Nichols, R. J., Charge transport at a molecular GaAs nanoscale junction. *Faraday Discuss.* **2018**, *210*, 397-408.
19. Vogel, Y. B.; Zhang, L.; Darwish, N.; Gonçalves, V. R.; Le Brun, A.; Gooding, J. J.; Molina, A.; Wallace, G. G.; Coote, M. L.; Gonzalez, J., Reproducible flaws unveil electrostatic aspects of semiconductor electrochemistry. *Nat. Commun.* **2017**, *8* (1), 2066.
20. Aragonès, A. C.; Darwish, N.; Ciampi, S.; Sanz, F.; Gooding, J. J.; Díez-Pérez, I., Single-molecule electrical contacts on silicon electrodes under ambient conditions. *Nat. Commun.* **2017**, *8*, 15056.
21. McCreery, R. L., Molecular Electronic Junctions. *Chem. Mater.* **2004**, *16* (23), 4477-4496.

22. Zhang, L.; Vogel, Y. B.; Noble, B. B.; Goncales, V. R.; Darwish, N.; Brun, A. L.; Gooding, J. J.; Wallace, G. G.; Coote, M. L.; Ciampi, S., TEMPO monolayers on Si (100) electrodes: electrostatic effects by the electrolyte and semiconductor space-charge on the electroactivity of a persistent radical. *J. Am. Chem. Soc.* **2016**, *138* (30), 9611-9619.
23. Ciampi, S.; Harper, J. B.; Gooding, J. J., Wet chemical routes to the assembly of organic monolayers on silicon surfaces via the formation of Si–C bonds: Surface preparation, passivation and functionalization. *Chem. Soc. Rev.* **2010**, *39* (6), 2158-2183.
24. Menanteau, T.; Dias, M. n.; Levillain, E.; Downard, A. J.; Breton, T., Electrografting via diazonium chemistry: the key role of the aryl substituent in the layer growth mechanism. *J. Phys. Chem. C* **2016**, *120* (8), 4423-4429.
25. Gooding, J. J., Advances in interfacial design for electrochemical biosensors and sensors: aryl diazonium salts for modifying carbon and metal electrodes. *Electroanalysis*. **2008**, *20* (6), 573-582.
26. Combellas, C.; Kanoufi, F.; Pinson, J.; Podvorica, F. I., Sterically hindered diazonium salts for the grafting of a monolayer on metals. *J. Am. Chem. Soc.* **2008**, *130* (27), 8576-8577.
27. Liu, G.; Liu, J.; Böcking, T.; Eggers, P. K.; Gooding, J. J., The modification of glassy carbon and gold electrodes with aryl diazonium salt: The impact of the electrode materials on the rate of heterogeneous electron transfer. *Chem. Phys.* **2005**, *319* (1-3), 136-146.
28. Mahouche-Chergui, S.; Gam-Derouich, S.; Mangeney, C.; Chehimi, M. M., Aryl diazonium salts: a new class of coupling agents for bonding polymers, biomacromolecules and nanoparticles to surfaces. *Chem. Soc. Rev.* **2011**, *40* (7), 4143-4166.
29. Chen, P.; McCreery, R. L., Control of Electron Transfer Kinetics at Glassy Carbon Electrodes by Specific Surface Modification. *Anal. Chem.* **1996**, *68* (22), 3958-3965.
30. Lehr, J.; Williamson, B. E.; Flavel, B. S.; Downard, A. J., Reaction of Gold Substrates with Diazonium Salts in Acidic Solution at Open-Circuit Potential. *Langmuir*. **2009**, *25* (23), 13503-13509.

31. Brooksby, P. A.; Downard, A. J., Electrochemical and atomic force microscopy study of carbon surface modification via diazonium reduction in aqueous and acetonitrile solutions. *Langmuir*. **2004**, *20* (12), 5038-5045.
32. Downard, A. J., Potential-dependence of self-limited films formed by reduction of aryldiazonium salts at glassy carbon electrodes. *Langmuir*. **2000**, *16* (24), 9680-9682.
33. Paulik, M. G.; Brooksby, P. A.; Abell, A. D.; Downard, A. J., Grafting aryl diazonium cations to polycrystalline gold: Insights into film structure using gold oxide reduction, redox probe electrochemistry, and contact angle behavior. *J. Phys. Chem. C*. **2007**, *111* (21), 7808-7815.
34. Hines, T.; Díez-Pérez, I.; Nakamura, H.; Shimazaki, T.; Asai, Y.; Tao, N., Controlling formation of single-molecule junctions by electrochemical reduction of diazonium terminal groups. *J. Am. Chem. Soc.* **2013**, *135* (9), 3319-3322.
35. Zhang, L.; Laborda, E.; Darwish, N.; Noble, B. B.; Tyrell, J. H.; Pluczyk, S.; Le Brun, A. P.; Wallace, G. G.; Gonzalez, J.; Coote, M. L., Electrochemical and electrostatic cleavage of alkoxyamines. *J. Am. Chem. Soc.* **2018**, *140* (2), 766-774.
36. Nelson, A., Co-refinement of multiple-contrast neutron/X-ray reflectivity data using MOTOFIT. *J. Appl. Crystallogr.* **2006**, *39* (2), 273-276.
37. Clavilier, J.; Armand, D.; Sun, S.; Petit, M., Electrochemical adsorption behaviour of platinum stepped surfaces in sulphuric acid solutions. *J. Electroanal. Chem.* **1986**, *205* (1-2), 267-277.
38. Clavilier, J.; El Achi, K.; Rodes, A., In situ probing of step and terrace sites on Pt (S)-[n (111)×(111)] electrodes. *Chem. Phys.* **1990**, *141* (1), 1-14.
39. Feliu, J.; Fernandez-Vega, A.; Aldaz, A.; Clavilier, J., New observations of a structure sensitive electrochemical behaviour of irreversibly adsorbed arsenic and antimony from acidic solutions on Pt (111) and Pt (100) orientations. *J. Electroanal. Chem. Interfacial Electrochem.* **1988**, *256* (1), 149-163.
40. Benedetto, A.; Balog, M.; Viel, P.; Le Derf, F.; Sallé, M.; Palacin, S., Electro-reduction of diazonium salts on gold: Why do we observe multi-peaks? *Electrochim. Acta*. **2008**, *53* (24), 7117-7122.

41. Beckwith, A.; Jackson, R.; Longmore, R., The intermediacy of free aryl radicals in the reaction of o-alkenyloxybenzenediazonium salts with ferrocene. *Aust. J. Chem.* **1992**, *45* (5), 857-863.
42. Zou, C.; Wrighton, M. S., Synthesis of octamethylferrocene derivatives via reaction of (octamethylferrocenyl) methyl carbocation with nucleophiles and application to functionalization of surfaces. *J. Am. Chem. Soc.* **1990**, *112* (21), 7578-7584.
43. Schröder, H.; Obermeier, E.; Steckenborn, A., Micropyramidal hillocks on KOH etched {100} silicon surfaces: formation, prevention and removal. *J. Micromech. Microeng.* **1999**, *9* (2), 139.
44. Palik, E.; Glembocki, O.; Heard Jr, I.; Burno, P.; Tenerz, L., Etching roughness for (100) silicon surfaces in aqueous KOH. *J. Appl. Phys.* **1991**, *70* (6), 3291-3300.
45. Powell, O.; Harrison, H. B., Anisotropic etching of {100} and {110} planes in (100) silicon. *J. Micromech. Microeng.* **2001**, *11* (3), 217.
46. Masitas, R. A.; Zamborini, F. P., Oxidation of Highly Unstable <4 nm Diameter Gold Nanoparticles 850 mV Negative of the Bulk Oxidation Potential. *Journal of the American Chemical Society* **2012**, *134* (11), 5014-5017.
47. Rodríguez-López, J.; Alpuche-Avilés, M. A.; Bard, A. J., Interrogation of Surfaces for the Quantification of Adsorbed Species on Electrodes: Oxygen on Gold and Platinum in Neutral Media. *Journal of the American Chemical Society* **2008**, *130* (50), 16985-16995.
48. Nohira, T.; Yasuda, K.; Ito, Y., Pinpoint and bulk electrochemical reduction of insulating silicon dioxide to silicon. *Nature Materials* **2003**, *2* (6), 397-401.
49. Kinser, C. R.; Schmitz, M. J.; Hersam, M. C., Conductive Atomic Force Microscope Nanopatterning of Hydrogen-Passivated Silicon in Inert Organic Solvents. *Nano Letters* **2005**, *5* (1), 91-95.
50. Nichols, R. J.; Higgins, S. J., Molecular junctions: Single-molecule contacts exposed. *Nat. Mater.* **2015**, *14* (5), 465.
51. Nichols, R. J.; Haiss, W.; Higgins, S. J.; Leary, E.; Martin, S.; Bethell, D., The experimental determination of the conductance of single molecules. *Phys. Chem. Chem. Phys.* **2010**, *12* (12), 2801-2815.

52. Aragonès, A. C.; Haworth, N. L.; Darwish, N.; Ciampi, S.; Bloomfield, N. J.; Wallace, G. G.; Diez-Perez, I.; Coote, M. L., Electrostatic catalysis of a Diels–Alder reaction. *Nature*. **2016**, *531* (7592), 88.
53. Pla-Vilanova, P.; Aragonès, A. C.; Ciampi, S.; Sanz, F.; Darwish, N.; Diez-Perez, I., The spontaneous formation of single-molecule junctions via terminal alkynes. *Nanotechnol.* **2015**, *26* (38), 381001.
54. Cowley, A.; Sze, S., Surface states and barrier height of metal-semiconductor systems. *J. Appl. Phys.* **1965**, *36* (10), 3212-3220.

Every reasonable effort has been made to acknowledge the owners of copyright material. I would like to apologise if any copyright owner who has been omitted or incorrectly acknowledged.

Chapter 5

Spontaneous S–Si bonding of alkanethiols to Si(111)–H: towards Si–molecule–Si circuits

Chandramalika R. Peiris, Simone Ciampi, Essam M. Dief, Jinyang Zhang, Peter J. Canfield, Anton P. Le Brun, Daniel S. Kosov, Jeffrey R. Reimers and Nadim Darwish
Chemical Science, Volume 11, 26th April 2020, Pages 5246–5256

DOI: <https://doi.org/10.1039/D0SC01073A>

“Reproduced with permission from (Chem. Sci 2020, 11, 5246–5256.) Copyright (2020) Royal Society of Chemistry.”

5.1 Summary of this chapter

This chapter reports the spontaneous formation of covalent Si–S bonds. The covalent bonding requires no heating, UV irradiation, or external catalysis, but is dependent on having ambient levels of dissolved O₂ in solution. The monolayers are mechanically robust and resist desorption under an electric field of 2 V/nm. DFT calculations indicate that thiyl (RS[•]) radicals form spontaneously in solution then react with H-terminated silicon surfaces to abstract a hydrogen. The resulting surface silicon radicals then combine with a thiol to form Si–S bonds. As similar to the Si–C bonds, thiol monolayers formed on Au and Si are comparable suggesting that Si–S contacts are highly conducting and a viable alternative to the widely used Au–S contacts in molecular electronics, opening new prospects for electrically transmissive molecule–semiconductor circuitry as shown in Figure 5.1. Further details are provided in the form of the published manuscript in *Chemical Science*, based on this work. The signed author contribution letter is provided in Appendix D (D–5–1).

5.2 Abstract

We report the synthesis of covalently linked self-assembled monolayers (SAMs) on silicon surfaces, using mild conditions, in a way that is compatible with silicon–electronics fabrication technologies. In Molecular Electronics, SAMs of functional molecules tethered to gold via sulfur linkages dominate, but these devices are not robust in design and not amenable to scalable manufacture. Whereas covalent bonding to silicon has long been recognized as an attractive alternative, only formation processes involving high temperature and/or pressure, strong chemicals, or irradiation are known. To make molecular devices on silicon under mild conditions with properties reminiscent of Au–S ones, we exploit the susceptibility of thiols to oxidation by dissolved O₂, initiating free-radical polymerization mechanisms without causing oxidative damage to the surface. Without thiols present, dissolved O₂ would normally oxidize the silicon and hence reaction conditions such as these have been strenuously avoided in the past. The surface coverage on Si(111)–H is measured to be very high, 75% of a full monolayer, with density-functional theory calculations used to profile spontaneous reaction mechanisms. The impact of the Si–S chemistry in single-molecule electronics is demonstrated using STM-junction approaches by forming Si–hexanedithiol–Si junctions. Si–S contacts result in single-molecule wires that are mechanically stable, with an average lifetime at room temperature of 2.7 s, which is five folds higher than that reported for conventional molecular junctions formed between gold electrodes. The enhanced “ON” lifetime of this single-molecule circuit enables previously inaccessible electrical measurements on single molecules.

5.3 Introduction

Self-assembled monolayers have captured the attention of the scientific community owing to their ease of formation and affinity to different types of substrates, with a vast range of established application in nano fabrications, sensors, biotechnology and molecular electronics. Considering electronics applications, thiol and dithiol SAMs, particularly on Au, have attracted considerable interest¹⁻¹³ owing to their ease of preparation from gas phase or from solution.¹⁴⁻¹⁵ Although widely used, thiols on Au suffer from major drawbacks, including the high mobility of the S–Au bonds and the availability of a wide range of possible thiol–gold bonding motifs at quite similar

energies.¹⁶ S–Au bonds are dominated by dispersion forces¹⁷⁻¹⁸ and are hence relatively weak,¹⁹ poorly directional, and can accommodate a wide range of coordination numbers.²⁰⁻²²

In the last few years, there has been increasing interest in expanding the use of SAMs in nanoelectronics from gold⁸ towards semiconducting platforms including GaAs²³⁻²⁵ and Si.²⁶⁻³¹ It is anticipated that combining the electrical properties of semiconductors with the chemical diversity of organic molecules, a variety of technological development can be achieved. Silicon, in particular, provides an attractive choice as an electrode because atomically flat silicon substrates are commercially available, are widely used in microelectronics industry, and their electronic properties can be controlled via doping and chemical variation.^{7, 16, 32-35}

SAMs built upon covalent bonds to silicon were first assembled³⁶ in 1993, utilizing Si–C bonds formed through activated free-radical chemistry. In one almost-trivial application, SAMs could replace SiO₂ as the insulating material in field-effect transistors and other devices, providing better structural and chemical control,^{33, 37-39} leading even to biomedical applications.⁴⁰ Devices in which the interface forms a critical component¹⁶ include: quantum-dot photonics,⁴¹ light harvesting and usage,⁴²⁻⁴³ photoluminescence,⁴⁴ general electrochemical applications⁴⁵ including sensing,⁴⁶ polymer engineering,⁴⁷ hydrophobicity,⁴⁸ general electrochemical sensors,⁴⁹ bioimaging, biosensing, and cancer treatment,⁵⁰⁻⁵¹ as well as molecular-electronics applications.^{32, 45, 52-56} Mostly the strategies used for making covalent bonds to silicon⁵⁷ have involved conditions considered harsh for silicon engineering, including: radical initiators,^{36, 58-59} Lewis acids,⁶⁰ Grignard reagents,^{35, 61} electrografting,⁶² and microwave⁶³ or UV-Visible irradiation,⁶⁴⁻⁶⁶ with many processes also requiring significant heating. Hence notable absences in the developed applications involving silicon–molecule interfaces are those that would involve integration into standard silicon–device fabrication.

We focus on covalent links between silicon and sulfur as a means of achieving this goal (Figure 5.1). Molecules tethered to silicon in this way were first synthesized using ultra–high vacuum technologies,⁶⁷⁻⁶⁸ followed by high–temperature solution chemistry^{27, 69} and even high–temperature high–pressure processes in supercritical CO₂,⁷⁰ as well as UV⁷¹⁻⁷³ and visible⁷⁴ photochemical approaches. Well-formed layers

have been produced that are resistive to chemicals that could be applied in subsequent stages of CMOS processing,²⁷ with junction characteristics useful for Molecular Electronics.^{32, 52, 75} Nevertheless, synthetic conditions involving the use of radical initiators, catalysts, high temperature and/or high pressure, or irradiation, are harsh, with even exposure to radiation known to induce SAM damage.⁷⁶ To date, there has been no technology developed, using Si–S or other types of covalent bonding, that could be readily applied to integrate molecular electronics into silicon engineering.

Typically, organic interfaces to silicon are dominated by surface–layer silicon oxides,⁷⁷ and hence device synthetic strategies often focus on conditions leading to oxide-free surfaces.^{16, 33, 35, 38, 40, 61, 70, 78-79} Indeed, dangling bonds on the surface that survive SAM formation, and other functionalities, are susceptible to attack from O₂, H₂O, and other common ambient species, demanding that functional SAMs assemble at high coverage with low levels of flaws. The explicit exclusion of oxygen from reactions has therefore been a priority. Most reactions with silicon are believed to proceed via radical mechanisms,^{36, 58-59, 73, 80-82} either through thermal or other production of surface radicals or else through the attack of radicals from solution on the surface. The presence of O₂ in solutions of thiols spontaneously leads to radical production, without the need for harsh conditions such as high temperature, pressure, added chemical radical initiators, or applied radiation.

We demonstrate that indeed such reactions can form high–quality SAMs on Si(111), synthesizing highly stable, low–oxygen-content monolayers with electrical properties akin to classic SAMs incorporating Au–S interfaces. The reactions performed are sketched in Figure 5.1 and involve reaction of two molecules (Figure 5.1a) with thiol groups (RSH) at least on one end, on H–terminated silicon (Figure 5.1b). The products are identified as densely-packed Si–S–linked SAMs (Figure 5.1d) based on extensive characterization X-ray reflectometry (XRR), atomic force microscopy (AFM), X-ray photoelectron spectroscopy (XPS) and cyclic voltammetry (CV) for determining SAM thickness, topography, surface composition and coverage. Reaction mechanisms (Figure 5.1c) and SAM properties are then understood using density-functional theory (DFT) modelling of the reaction pathways, depicting a set of reactions leading to spontaneous SAM formation under ambient conditions through free-radical

surface polymerization. Monolayers are formed using only mild conditions on Si containing different dopants (n- or p-type silicon), as well as on different crystal orientations (including (100) and (111)), indicating the versatility of the approach. Whilst **1** is used to form redox active monolayers, **2** containing thiol groups at both ends (Figure 5.1a), is utilized in forming single-molecule circuits connected to two silicon electrodes in scanning-tunneling microscopy (STM) break-junction (STM-BJ) experiments.

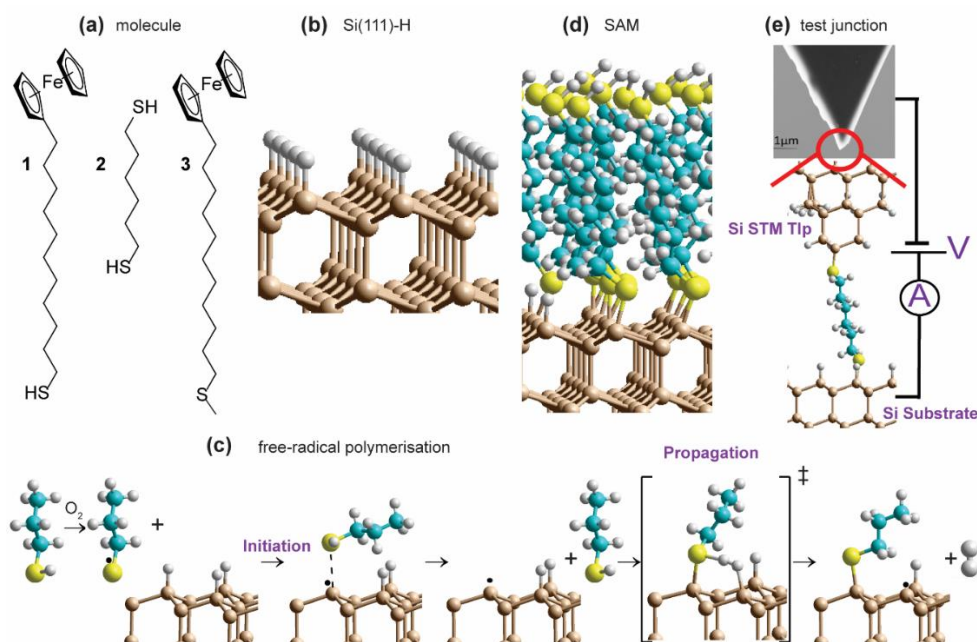


Figure 5. 1 (a) Molecular and SAM structures: **1** enables electrochemical studies while **2** enables STM-junction studies (a) molecules are reacted with H-terminated silicon surfaces (b) via a thiol free-radical polymerization (c), as illustrated for propanethiol, to form covalently bonded SAMs (d). (e) Si-molecule-Si junction formed from **2** using single-molecule STM-junction technology (e). S- yellow, Si- fawn, C- cyan, H- white.

5.4 Experimental methods

5.4.1 General chemicals and materials.

All chemicals were of analytical grade and used as received. Chemicals used in surface modification and electrochemical experiments were of high purity (>99%). Hydrogen peroxide (30 wt % in water), ammonium fluoride (Puranal TM, 40 wt % in water) and sulfuric acid (Puranal TM, 95–97%) used in wafer etching and cleaning procedures were of semiconductor grade from Sigma-Aldrich. Compound **1** (98 %) and **2** (98 %)

were purchased from Sigma-Aldrich; both were used without further purification. Milli-Q water ($>18 \text{ M}\Omega \text{ cm}$) was used to prepare electrolytes and for surface cleaning procedures. The DCM, 2-propanol, and ethanol solvents were redistilled prior to use. When required, dissolved O_2 was removed from the DCM by bubbling argon for 60 min. All silicon wafers were purchased from Siltronix, S.A.S. (Archamps, France). The thickness of the wafers was $500 \pm 25 \text{ }\mu\text{m}$, cut to be oriented $\pm 0.5^\circ$ away from the (100) or (111) plane. p-type silicon was boron doped with nominal resistivity of either $0.001 \text{ }\Omega \text{ cm}$ (for highly doped) or $10 \text{ }\Omega \text{ cm}$ (for low doped). n-type silicon was phosphorous doped with nominal resistivity of $0.001 \text{ }\Omega \text{ cm}$ (for highly doped) or $10 \text{ }\Omega \text{ cm}$ (for low doped).

5.4.2 Thiol-functionalized silicon (100) and (111) surfaces.

Assembly of **1** or **2** onto both n-type and p-type silicon proceeded as sketched in Figure 5. 1. Silicon wafers were cut into pieces (approximately $10 \times 10 \text{ mm}$), cleaned for 20–30 min in hot Piranha solution ($130 \text{ }^\circ\text{C}$, 3:1 (v/v)) mixture of concentrated sulfuric acid to 30 % hydrogen peroxide), rinsed with water and then etched with a deoxygenated 40 % aqueous ammonium fluoride solution for 13 min. The freshly etched Si–H surface was then covered by a 4 mM solution of the thiol in DCM for 24 h to allow spontaneous monolayer formation. Re-distilled DCM was used to clean samples before all subsequent analyses, followed by drying under a stream of Ar gas.

5.4.3 Electrochemical Measurements.

All the electrochemical measurements were performed with a CHI650 (CH Instruments, USA) electrochemical workstation and a conventional three-electrode system with a platinum wire as the auxiliary electrode, silicon wafer modified with **1** as the working electrode. An Ag/AgCl aqueous electrode (3.0 M KCl, CH Instruments, USA) served as the reference.

5.4.4 AFM Measurements.

Atomic force microscopy images were obtained using a Bruker dimension microscope operating in tapping mode. All images were obtained in air, at room temperature, and using silicon nitride cantilevers (TESPA from Bruker, with a spring constant of 20

N m⁻¹). Tip induced oxide formation was carried out by conductive AFM, current–voltage data were obtained using a Bruker ICON head with Peak Force Tuna module at room temperature with Pt (RMN) probes having a spring constant of 18 N m⁻¹. AFM–Pt tip induced SiO_x oxide patterns were obtained by varying the applied bias from 0.5 V to 5 V. The resolution was set to 256 points/line, the scan rate to 1 Hz and the peak force to 554 nN. During the local oxidation, the humidity, tip scan speed, and all other parameters were kept constant, except for the applied bias voltage. The local oxidation patterns were obtained for n–type Si(111) substrates, with the surface is modified with **2**. The oxidation rate of the SAM modified surface was compared to that for the Si(111)–H surface under identical conditions.

5.4.5 X-ray photoelectron spectroscopy (XPS) measurements.

X-ray photoelectron spectroscopy measurements were performed on a Kratos Axis Ultra DLD spectrometer using a monochromatic Al–K α (1486.6 eV) irradiation source operating at 150 W. Spectra of Si 2p (90–110 eV), C 1s (277–300 eV), N 1s (390–410 eV) and S2p (163–164 eV) were taken in normal emission at or below 7 \times 10⁻⁹ Torr. Data files were processed using CasaXPS[®] software and the reported XPS energies are binding energies expressed in eV. After background subtraction (Shirley), spectra were fitted with Voigt functions. To correct for energy shifts caused by adventitious charging, all peak energies were corrected with a rigid shift to bring the C 1s emission to 285.0 eV. X-ray Reflectometry (XRR) Specular X-ray reflectometry at the solid-air interface was conducted on a Panalytical Ltd X’Pert Pro instrument with a rotating anode source (Cu K α radiation, λ = 1.54 Å). The beam was focused using a Göbel mirror and collimated using fixed slits of 0.1 mm. The samples were mounted onto a motorized stage to adjust the sample into the optimal position for measurements. Angles of incidence were measured from 0.05° to 5.00° in 0.01° steps for 20 seconds per step. The raw data was reduced so that the critical edge was normalized to a reflectivity of unity and the data was presented as reflectivity versus momentum transfer, Q , which is equal to $4\pi \sin\theta/\lambda$, where θ is the angle of incidence and λ is the X-ray wavelength (1.54 Å). Structural parameters for the monolayer were refined in MOTOFIT reflectometry analysis software.

5.4.6 STM break junction.

STM experiments were carried out with PicoSPM 1 microscope head controlled by a “Picoscan 2,500 electronics, from Agilent”. The STM-junction data were collected using an NI-DAQmx/BNC-2,110 national instruments (LabVIEW data collection system) and analysed with code based on LabVIEW software.

In the blinking approach, the tunnelling current is first stabilized for 1 h until tunnelling current variation of $< 10\%$ is obtained. Current transients are then captured when a molecule connect between the STM tip and the surface in the presence of $4\ \mu\text{M}$ solution of **2**.

In the current-distance approach, the STM tip is moved in and out from a surface in the presence of the $4\ \mu\text{M}$ solution of **2**. 3000 current versus distance traces were collected and were all accumulated in the conductance histograms without selection.

5.4.7 DFT Calculations.

All periodic-slab calculations were performed using VASP 5.4.1, where the valence electrons were separated from the core by use of projector-augmented wave pseudo potentials (PAW) using “PREC=HIGH”. The energy tolerance for the electronic structure determinations was set at 10^{-7} eV to ensure accuracy. We used k-space grids of $2\times 2\times 1$ for 3×3 supercells and $1\times 1\times 1$ for 5×5 supercells. The PBE density functional was used, combined with Grimme’s “D3” empirical dispersion correction with Becke-Johnson damping; the dispersion force is known to be important in controlling properties of SAMs containing alkane chains.^{21, 83-84} The vacuum region between slabs was ca. $15\ \text{\AA}$ wide, with the silicon lattice vector being $5.412\ \text{\AA}$ ($4/3^{1/2}$ times $r_{\text{Si-Si}} = 2.34346\ \text{\AA}$). Dipole corrections were not used. Geometry optimizations were made for all structures, terminating when the forces on all atoms fell below $0.01\ \text{eV/\AA}$. The slabs were 4 silicon layers thick; for 3×3 supercells, the lower two layers were frozen.

The transition state was optimized first for a model cluster compound using Gaussian16⁸⁵ with the 6-31++G** basis set,⁸⁶ employing Hessian matrices analytically evaluated at each step. This was then transferred onto the 2D surface and optimized using aspects of the DUSHIN vibrational analysis package,⁸⁷ utilizing a numerically evaluated Hessian matrix weighted to favor coordinate updates to closely following

the imaginary Hessian eigenvalue up toward the transition state at the expense of following positive eigenvalues downhill. This guarantees the rapid and smooth convergence of the VASP calculations to the transition state. Free energies were evaluated using DUSHIN for all structures based on standard approaches.⁸⁸

5.4.8 STM tip preparation.

Silicon STM tips were mechanically cut from double-side polished silicon wafers oriented on the $((111) \pm 0.05^\circ)$ and of thickness 180 μm using a diamond cutter into ca. 3 mm size tips. Ohmic contact to the tips was made by connecting a gold wire 2 mm away from the apex of the tip. The gold wire connector serves as the connection to the STM scanner. The tips were then washed with DCM, 2-propanol, Milli-QTM water and cleaned for 30 min in hot Piranha solution (130 °C, a 3:1 (v/v) mixture of concentrated sulfuric acid to 30% hydrogen peroxide), rinsed with water and dried under a stream of Ar gas. Gold wires were then connected to the tips using gallium-indium eutectic to form an ohmic contact and conductive adhesive (Anders) to give mechanical stability. The tips were then etched in 3.50 M KOH solution at 65° C for 48 h. The silicon tips were then dipped in a 40% solution of NH_4F for 5 min to remove any remaining oxide and to expose Si-H at the apex of the tip. Tip apexes radius of < 1 μm was consistently obtained using the above method and is comparable to the mechanically cut gold STM tips routinely used in STM break junction experiments. Scanning electron-microscopy (SEM) images of the silicon tips are shown in Appendix E Figures. E-5-1d to E-5-1f. Similar images for the gold STM tips used are shown in Appendix E Figures. E-5-1a to E-5-1c.

5.5 Results and discussion

5.5.1 Synthesis.

SAMs of compound **1** and **2** was produced as described in Methods and summarized in Figure 5.1. All operations in this method are universally available in silicon fabrication laboratories, with, in particular, the reaction of the thiol with the surface being as easy to perform as is standard gold–thiol chemistry. Critically, no heating, UV irradiation or external catalysis is required; note that performing the experiments under ultra-low light conditions did not affect the outcome.

The aspect of the synthesis of most note is the O₂ content of the dichloromethane (DCM) solvent used in the reaction of the thiol and the prepared silicon surface. Using DCM as purchased and re-distilled, the reaction proceeds to completion on the 24-hour timescale. However, removal of O₂ from the solvent resulted in SAMs of only ca. one tenth the coverage after the same period of time (see Figure 5.2f). Hence the presence of dissolved O₂ is critical to the reaction mechanism.

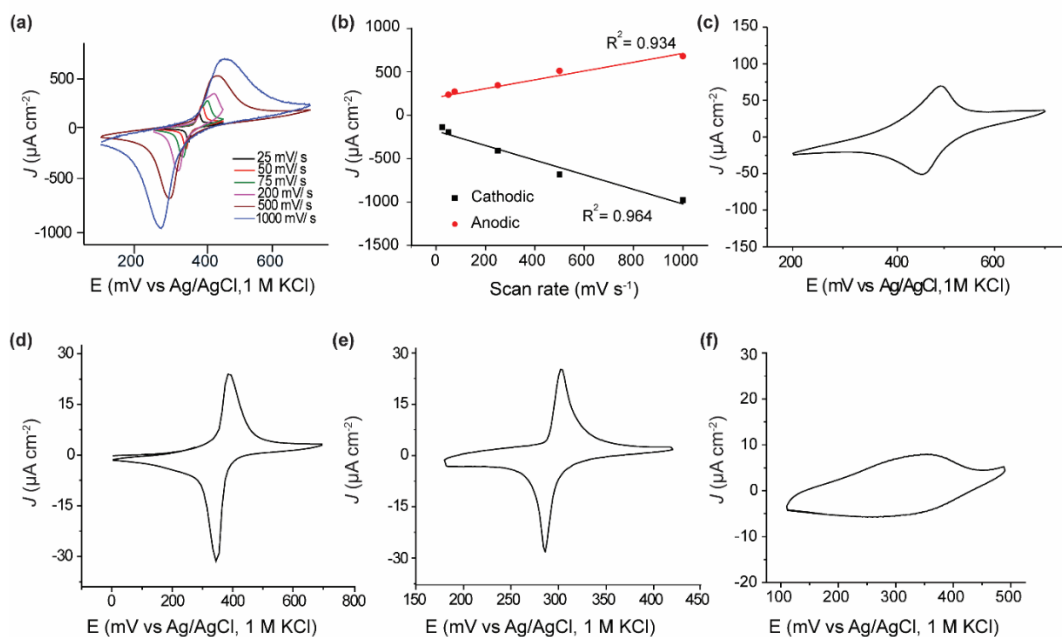


Figure 5. 2 Cyclic voltammetry. (a) Cyclic voltammetry at different scan rates for a SAM of **1** on p-type Si(111)–H of resistivity 0.001 Ω cm. The estimated surface coverage is 2.53×10^{14} molecules cm^{-2} . (b) Current versus scan rate for the SAM formed of **1**. The current increases linearly with scan rate, indicating a surface redox reaction. (c) Cyclic voltammetry for a SAM of **1** on Si(111)–H at 50 mV s^{-1} on n-type phosphorus doped of resistivity 0.001 Ω cm. Coverage is dopant independent, the results leading to coverages of 2.50×10^{14} molecules cm^{-2} and is comparable to that obtained on p-type boron doped silicon shown in (a). (d) Cyclic voltammetry at 50 mV s^{-1} for SAMs of **1** on Au(111), showing very similar appearances to those reported for Si in (a) at a similar scan rate. The deduced coverages are 2.20×10^{14} molecules cm^{-2} , slightly less than that for the corresponding monolayers on Si(111)–H. (e) Cyclic voltammetry at 50 mV s^{-1} for SAMs of **1** on Si(100)–H showing a similar appearances to those reported for Si(111)–H; however the surface coverage is lower and estimated at 9.3×10^{13} molecules cm^{-2} . (f) Cyclic voltammetry for SAMs of **1** on Si(111)–H prepared from fresh solid of **1** dissolved in deoxygenated DCM. Oxygen was removed by bubbling Ar for 60 min in the DCM solution containing **1** using a septum sealed vessel and a needle as a vent. The SAM reaction flask was kept under a positive pressure of Ar during the 24 h reaction time. The surface coverage is estimated to be 2.10×10^{13} molecules cm^{-2} and is about 10% of that produced under ambient conditions.

5.5.2 SAM characterization by cyclic voltammetry.

Figure 5.2a shows cyclic voltammograms obtained for SAM of **1** on p-type Si(111)–H. The estimated coverage of the ferrocenyl-terminated compound **1** is 2.53×10^{14} molecules cm^{-2} , about the highest coverage possible for a layer of ferrocene molecules. This translates to 0.32 bound molecules for every surface silicon atom, suggesting a high-quality SAM at 1:3 coverage, possibly on a $(\sqrt{3} \times \sqrt{3})$ supercell.

Results shown in Figures. 5.2a, 5.2c and Figure 5.2d indicate that this coverage is insensitive to doping (p-type or n-type) of the silicon. The shapes of the voltammetric waves and the surface coverage were comparable to a monolayer of the same molecule formed on Au(111) (Figure 5.2d). The voltammetric waves were stable after extensive voltammetric cycling. Similar to thiol–gold monolayers, the peak current in thiol–silicon monolayers increase linearly with the scan rate, indicating a surface-bound electrochemical process (Figure 5.2a and 5.2b).

Analogous results shown in Figure 5.2e indicate that, independent of doping, the adsorbate coverage on Si(100) is 9.3×10^{13} molecules cm^{-2} , one third of that observed on Si(111)–H. As a ratio of the number of surface Si atoms, this coverage is 1:7.3, a value difficult to understand based on the surface symmetry and adsorbate size which would suggest likely values of 1:2 or 1:4. The Si(100) surface used has not undergone its possible (2×1) reconstruction and hence two H atoms protrude from each surface Si atom, so only one in fifteen surface hydrogens were replaced. Hence, while the same chemical reaction is likely to be occurring independent of the silicon surface used, only Si(111)–H appears useful for the production of dense and regular SAMs, as is needed for large scale molecular electronics devices. It is possible that method modifications could yield higher coverages, however, as electronically functional alkane SAMs on Si(100), with a coverage of $3 \pm 1 \times 10^{14}$ molecules cm^{-2} , have been produced using UV irradiation,⁷² with high coverages also produced utilizing thermal surface-radical production.⁸⁹

5.5.3 SAM characterization by AFM and C-AFM.

Figure 5.3a and Appendix E, E-5-2 show $10 \times 10 \mu\text{m}^2$ and $20 \times 20 \mu\text{m}^2$ AFM images, respectively, of a p-type Si(111)-H surface covered by the dithiol **2**. The topography shows flat terraces separated by atomic steps. The peak-to-peak roughness measured within one Si(111) terrace is ca. 1.7 \AA , consistent with an atomically smooth alkyl monolayer on Si(111).⁹⁰ Further, the high-quality topography confirms that the SAMs are homogeneous monolayers at the nanoscale, free of any contaminants or oxidative products or etched regions. These properties parallel those of SAMs produced by other means,^{27, 70-71, 74, 80-81} despite the utilization of dissolved O_2 in the reaction mechanism.

The mechanical stability under electric fields of the monolayers were assessed by conductive AFM measurements using peak force tunneling mode (PF-TUNA) tip-induced local oxidation method. The topography and current-voltage (I-V) data show that unmodified bare H-terminated silicon can be oxidized by applying 2 V for a period of 8 min. In contrast, surface covered with a SAM of **2** provides a robust barrier to surface oxidation up to 2 V (see Appendix E, E-5-3).

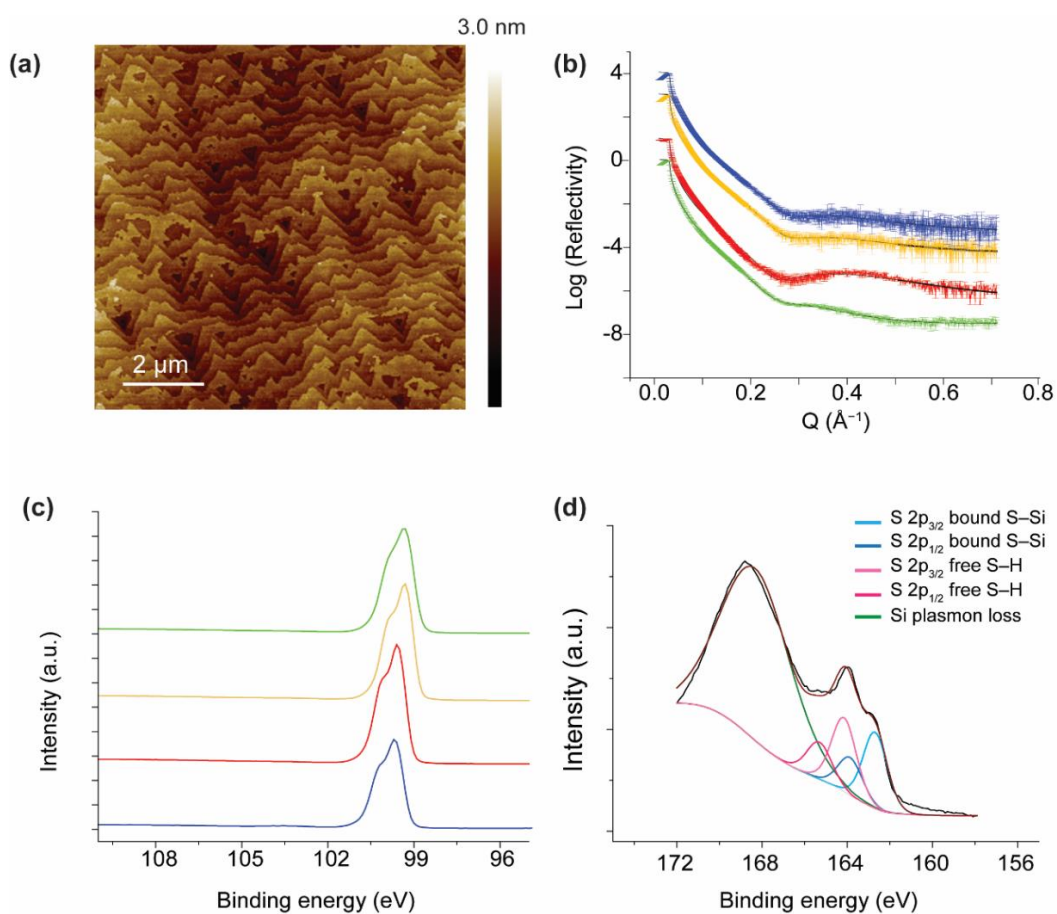


Figure 5. 3 Surface characterization. (a) $10 \times 10 \mu\text{m}^2$ of a p-type Si(111)–H surface covered by dithiol **2** on Si(111). (b) XRR measurements of **2** on Si(111)–H for various silicon dopant levels: high p-doped (green), low n-doped (red), low p-doped (yellow) and high n-doped (blue). The symbols with error bars are the collected data and the solid lines are the fits to each data set. The data is offset for clarity (c) XPS spectra showing the absence of Si–O_x at 102–104 eV for SAMs of **2** on high p-doped (green), low p-doped (yellow), low n-doped (red) and high n-doped (blue). The data is offset for clarity. (d) S2p narrow XPS scan of monolayers of **2** on Si (p-type, 0.001 Ω cm). Two sets of spin-orbit-split S2p peaks (2p_{1/2} and 2p_{3/2}, high and low binding energy, respectively), held 1.16 eV apart, are evident between 162 and 165 eV. The intensity ratio between the 3/2 and 1/2 emission is set to two, and values of full width at half maximum are 1.3 eV. The S2p emission centred at 164.7 eV is ascribed to thiols in a R–SH configurations, and the emission 163.3 eV is associated to thiols bound to Si (RS–Si)

5.5.4 SAM characterization by XPS and XRR.

The reflection of applied X-rays to a SAM of **2** on p-type and n-type Si is shown in Figure 5.3b, from which the thickness and surface coverage can be approximately extracted, see Section E-3, Appendix E. For Si(111)-H, the adsorbate volume fraction is estimated to be from 0.878 to 0.981. This corresponds to $5.36\text{--}6.64 \times 10^{14}$ molecules cm^{-2} , indicating 68–84 % coverage. Averaging over four samples of different doping levels, the coverage is 75 ± 8 %. The apparent height of the SAM is given in Appendix E, Tables E-5-1 and E-5-2, ranging from 8.5–11.1 Å. The height variation is due to the differences in surface coverage, the perceived surface roughness, and the angle of the molecules from the surface. Later DFT calculations perceive the C–C chain propagation direction as being closely parallel to the vector from the surface-bound Si atom to the distant S atom, a vector of length 11.1 Å at low coverage and 11.4 Å at 1:1 coverage. If the angle of chain propagation from the surface face is θ , then the SAM height is ca. $11.1 \sin \theta$. Using this relationship, the average chain angle obtained from this data is $66 \pm 16^\circ$, in rough agreement with previous measurements for alkanethiol SAMs on Si(111)-H of 57° for dodecanethiol,⁸¹ 75° for octadecanethiol,⁷⁰ and $60 \pm 2^\circ$ for hexanethiol and larger alkanethiols.⁹¹

XPS analyses of monolayers of **2** showed two sets of spin-orbit-split (SOS) S $2p_{1/2}$ and S $2p_{3/2}$ peaks, each 1.18 eV apart (Figure 5.3d). The SOS emissions at 162.7 eV and 163.9 eV correspond to S–Si bonding, whilst the emissions at 164.17 eV and 165.35 eV correspond to the distal free SH of **2**. The ratio of the two sets of SOS is 0.49:0.51 for the bound versus free thiol, respectively, indicating that the molecules do not hairpin and therefore do not bind with both thiols attached to the Si surface. The peak at 168 eV is attributed to Si plasmon loss.⁹² The absence of peaks in the 102–104 eV range indicate that negligible oxides or sub-oxides are present, a requirement of a well-formed monolayer that historically has not been expected when O_2 is present under reaction conditions.^{27, 33, 35, 54, 70, 81, 91}

5.5.5 DFT understanding of the SAM formation process.

DFT calculations for the test reagent C_3H_7SH attacking a $Si(111)-H$ surface, represented as a 3×3 supercell, produced no indication of a reaction pathway below an activation free energy of 90 kcal mol^{-1} . To account for the observed reaction, barrier heights must be much lower than this, presumably $< 20 \text{ kcal mol}^{-1}$. Hence some means for enhancing the reaction is required. The observation that SAM formation is greatly retarded in oxygen-depleted solutions indicates that O_2 is involved. It can act as an initiator as thiols RSH and O_2 in solution react to form disulfides $RSSR$, species always in equilibrium with thiyl radicals RS^\bullet (Figure 5.4a). Most significantly, this reaction consumes the available solution oxygen before it becomes exposed to silicon surfaces. DFT calculations (Figure 5.4b) then indicate that thiyls react with $Si(111)-H$ barrierlessly to abstract a surface hydrogen and form a thiol $RS-H$ physisorbed to a silicon-surface radical site; similar reactions on silicon compounds usually have a small barrier to abstraction.⁹³ The produced intermediate can then react quickly over a transition state free-energy barrier of 9 kcal mol^{-1} to form a covalent $Si-S$ bond and a neighbouring surface radical, releasing H_2 .

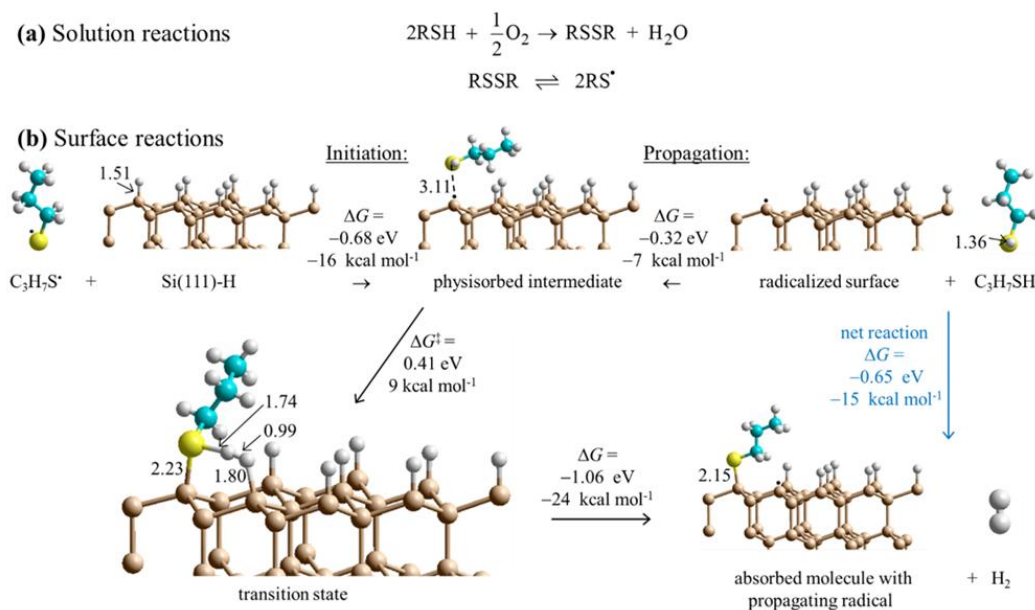


Figure 5. 4 Proposed reaction scheme for the consumption of ambient oxygen as an initiator leading to surface free-radical polymerization. (a) Known solution reactions of thiols (RSH). (b) DFT mechanism for surface SAM formation starting at low coverage. Calculations indicate that thiyl radicals (RS^* , with here $\text{R} = \text{C}_3\text{H}_7$) react with Si(111)-H to abstract hydrogen to form thiol physisorbed to a silicon surface radical (black dot). Reaction over a barrier then leads to chemisorption and radical regeneration. This provides initiation for a free-radical polymerization reaction that then covers the surface with adsorbate. Some critical bond lengths are shown, in Å; only one copy of the used 3×3 supercell is shown. These results show Gibbs free energy changes for surface reactions, while Appendix E, Figure E-5-4 provides analogous electronic energy changes, with detailed internal reaction coordinate descriptions provided in Appendix E, Figure E-5-7. Also, Figures. E-5-5 and E-5-6 provide analogous energies for a model compound.

The calculations indicate that thiols can barrierlessly react with silicon surface radicals, either a pre-existing radical or else one produced by the above thiyl attack. In either case, Figure 5.4 shows that this leads to a similar physisorbed intermediate and the same chemical reaction, making a new product surface radical. Hence, thiyl attachment can be considered as an initiation reaction for a subsequent free-radical polymerization process. The net free-energy change of the propagation reaction at low coverage is calculated to be $-24 \text{ kcal mol}^{-1}$. In simpler terms, the net reaction

occurs owing to the different bond strengths, calculated to be Si–S: 88 kcal mol⁻¹ and H–H: 103 kcal mol⁻¹ for the products, outcompeting Si–H: 78 kcal mol⁻¹ and S–H: 89 kcal mol⁻¹ for the reactants.⁸⁴

5.5.6 SAM completion at high coverage for the binding of **2** to Si(111)–H

Progress of SAM formation up to high coverage is described in detail in Section E–4 in Appendix E. There, calculations on a 3×3 supercell for the binding of **2** to Si(111)–H depict a complicated scenario, with many possible mechanisms for the formation of irregular, kinetically trapped SAMs. Key results are presented in Figure 5.5a shows a low coverage 1:9 SAM with the alkane chain at its native angle of 68° from the surface. Next, Figure 5.5b shows a SAM at 7:9 coverage producible quickly by free-radical polymerization, displaying six nearly vertically aligned chains and one chain lying over at 54°. Averaging the sine of these orientations indicates an average angle of 76°, consistent the observed XRR average value of 66±16°. This coverage is 78 %, close to the XRR observed value of 75±8 %. The inter-chain separations are near their optimal value of 4.3 Å, indicating near-maximum chain density. Finally, Figure 5.5c shows a SAM at full 1:1 coverage (inter-chain separation $(8/3)^{1/2}r_{\text{Si-Si}} = 3.827$ Å). The calculations indicate that increasing the coverage from 7:9 to 8:9 is endothermic, owing to increasing chain compression. A coverage of 1:1 could be producible, in principle, by repeated attack of solution thiyl radicals RS• on the 7:9 SAM.

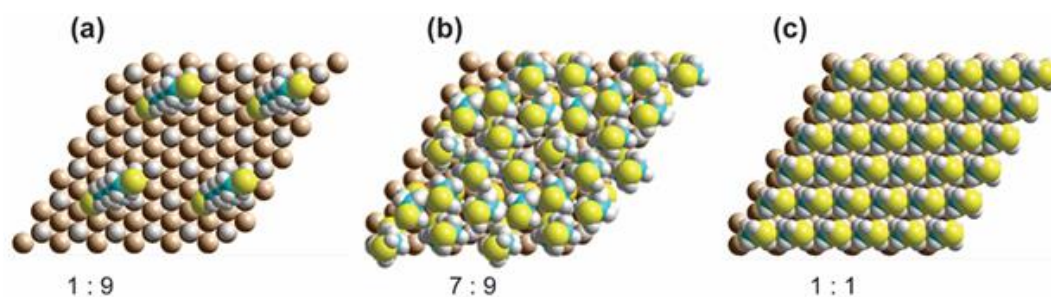


Figure 5. 5 DFT calculated SAM structures for **2** on Si(111)–H as a function of coverage, showing each four copies of the 3×3 supercell used in the calculations.

These results are consistent with the observed qualitative chemistry. The production of regular surfaces requires 24 hours owing to the low concentration of thiyls in

solution and the need for them to diffuse to the reaction sites, but, under most circumstances, regular SAMs of coverage ca. 75 % coverage, e.g., the calculated 7:9 SAM, not 1:1 SAMs. In deoxygenated solutions, SAM growth can still be initiated by intrinsic surface radical defects, defects produced if there is exposure to UV light, or by most any other radical species present in solution, utilizing well-known harsh technologies.^{36, 58-59, 73, 80-82, 89} Without such harsh conditions, SAM growth is erratic and easily inhibited, producing SAMs of at most 10 % coverage.

5.5.7 Control experiments using S-CH₃ contacts.

Control experiments using **3**, a methyl protected version of **1** showed that the SAM formation is not possible with S-CH₃ contacts (see Appendix E, Figures.E-5-8 - E-5-13. Unlike SAMs formed with **1** or **2**, Si(111)-H surface incubated in 4 mM solution of the methyl protected thiol (**3**) for 24 h showed no evidence of ferrocene signals in cyclic voltammetry and no evidence of S-Si bonding in XPS. These results are consistent with the DFT mechanism in that the reaction pathway of **1** or **2** with Si (111)-H involves the formation of disulfides RSSR (Figure 5.4a) which is not possible to form in the protected version of **1** (S-CH₃ contacts).

5.5.8 Single molecule STM-junction studies

The SAMs results in the previous sections demonstrate the mild conditions by which thiols are capable to covalently bond to Si electrodes. The distal thiol contacts in **2** is conserved upon attachment as shown in the XPS section, which opens the possibility of a top Si (or Au) contact to spontaneously connect, forming Si-molecule-Si circuits. We proceeded to show this by performing single-molecule measurements using the scanning tunneling microscopy (STM) junction technique in the current-time or "blinking approach"⁹⁴⁻⁹⁶ (Figure.5.6a-c) in which a Si STM tip is brought within tunneling distance to a Si surface in the presence of a dilute solution of **2**.

Figure 5.6b shows typical blinks of the Au-**2**-Au as compared to that of Au-**2**-Si and Si-**2**-Si junctions. The average conductance peaks occur at 180 μG_0 ($G_0 = 77.4 \mu S$ and is the conductance of a single open quantum channel) for Au-**2**-Au junctions, 120 μG_0 for Au-**2**-Si junctions, and 50 μG_0 for Si-**2**-Si junctions, with both Si electrodes

being p-type highly doped at 3.8×10^{19} dopant atoms per cm^3 . The conductivity of the junctions formed from the Si electrodes are only few folds less than those made using gold. Nevertheless, the slightly lower conductivity of Si–2–Si junctions is mild and is well within the accessible current range of typical STM–junction measurements for detecting single molecules between gold electrodes. The important advantage of the Si–2–Si junctions, however, is their enhanced mechanical stability, facilitating junctions lasting on average 5 times longer than the gold-molecule junctions. This increased “ON” lifetime will enable a range of external stimuli, such as light and electrochemical gating to be applied while a single molecule is connected between the source and drain electrodes.

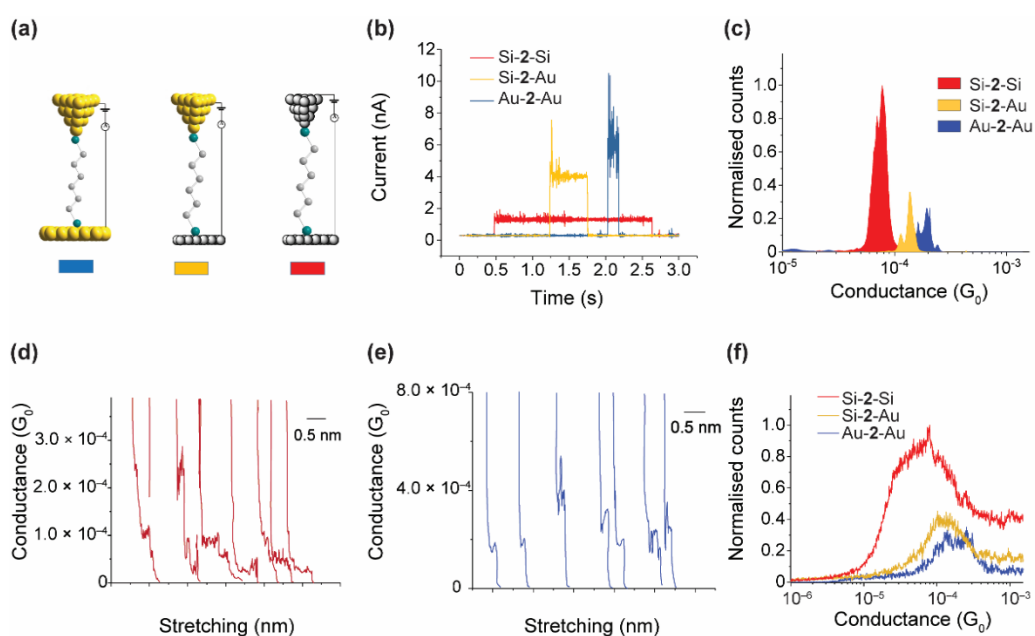


Figure 5. 6 (a) Cartoons of the junctions studied. (b) Representative blinks for single molecules of 2 bonded to two Au(111) electrodes (blue), one Au(111) and one Si(111)–H electrode (yellow), and two Si(111)–H electrodes (red). (c) Blinking histograms for the Au–2–Au, Au–2–Si and Si–2–Si junctions. The blinking histograms were constructed by the accumulation of 300 blinks for each system. The blinking histogram was normalised to the total number of blinks (d) Representative current–distance traces for the Si–2–Si junctions. (e) Representative current–distance traces for the Si–2–Si junctions. (f) Current–distance traces histograms constructed from the accumulation of 3000 curves for each system. The blinking histogram was normalised to the total number of traces.

Figures 5.6 d-f show the results obtained from the tapping method (current versus distance profiles), where the tip is driven into and out from the surface while the current versus distance is monitored. Three thousands of current versus distance traces (Figures 5.6 d and e) are collected and accumulated in conductance histograms and the peak maximum in the histograms represents the most probable conductance value for each system. The average conductance peaks (Figure 5.6f) occur at $170 \mu G_0$ for Au-2-Au junctions, $125 \mu G_0$ for Au-2-Si junctions, and $60 \mu G_0$ for Si-2-Si junctions, all of which are consistent with the conductance values obtained via the blinking method. Plateau length histograms for Au-2-Au and Si-2-Si junctions showed an average plateau length of 0.25 and 0.70 nm, respectively (Appendix E, Figure. E-5-14). This suggests that due to the enhanced mechanical stability, the Si-2-Si junctions are resistant to breakage during the entire pulling cycle while the typical Au-2-Au junctions break before a full molecular stretch.

5.6 Conclusions

We demonstrate that thiols can form stable covalent bonds to H-terminated silicon, leading to the nearly regular and dense SAMs, using reactions that are easy to perform and compatible with facilities available in silicon-manufacturing plants. They involve radical mechanisms, being initiated by O_2 present in the reaction solvent at ambient conditions. DFT calculations indicate that thiyl radicals produced in solution by the O_2 can react barrierlessly with Si(111)-H to initiate a subsequent free-radical polymerization reaction between the surface and solution thiols. They can also react with, and eliminate, SAM imperfections. The DFT results, obtained here for alkyl-radical attack on Si(111), are generally applicable for the description of many free-radical polymerization processes previously reported on Si(111)-H pertaining to the use of harsh reaction conditions.^{36, 58-59, 73, 80-82, 89} The important, unexpected, feature of the current work is that SAMs made under mild conditions in the presence of O_2 do not show oxidative damage to the silicon, a feature that would limit product usefulness and hence has been, historically, rigorously excluded. This results as the oxygen is consumed by the thiols in solution, which happens before the solution is exposed to the surface.

In principle, highly ordered pure alkanethiol SAMs with 1:1 coverage of adsorbate molecule to Si(111) surface sites are possible, but this requires compression of the alkane chains together, demanding specific circumstances to facilitate the compression. Observed SAM coverages of $\sim 75\%$ are found, in agreement with calculated results suggesting that 7:9 is the maximum achievable coverage under normal conditions. This coverage is high enough to generate a dense, if not perfectly regular, monolayer that will prevent further reactions with the silicon surface and hence sample degradation, similar to the best SAMs produced by other means. Ferrocene-terminated alkane thiols also form very regular SAMs on Si(111) at 1:3 coverage. The monolayers are mechanically robust and resist desorption under an electric field of 2 V/nm opening new prospects in molecular electronics. Single-molecule Si–molecule–Si junctions are mechanically stable, owed to the strong Si–S contacts, with an average life time of 2.7 s at room temperature, which is five times higher than molecular junctions formed between the typical gold electrodes. The Si–S chemistry offers a viable way to make top/bottom contacts between semiconductors in miniaturized electronics and open prospects for a hybrid technology that merges silicon and molecular electronics.

5.7 Acknowledgement

This work was supported by the Australian Research Council for grants DE160101101 and DE160100732. M.C.R Peiris also thank the National Natural Science Foundation of China (NSFC; Grant No. 11674212), and the Shanghai High-End Foreign Experts Grant for funding this research, as well as National Computational Infrastructure and Intersect. M. C. R Peiris thank Dr. Jean-Pierre Veder from the John de Laeter Centre for the assistance with XPS measurements, Curtin International Postgraduate Research Scholarship and Research Stipend Scholarship (CIPRS). and Australian Nuclear Science and Technology Organization (ANSTO).

5.8 References

1. Rieley, H.; Kendall, G. K., X-ray Studies of Self-Assembled Monolayers on Coinage Metals. 3. Angularly Resolved Near Edge X-ray Absorption Fine Structure Determination of the Orientation in 1-Octanethiol SAMs on Ag(111) and Cu(111). *Langmuir*. **1999**, *15* (26), 8867-8875.
2. Love, J. C.; Estroff, L. A.; Kriebel, J. K.; Nuzzo, R. G.; Whitesides, G. M., Self-Assembled Monolayers of Thiolates on Metals as a Form of Nanotechnology. *Chem. Rev.* **2005**, *105* (4), 1103-1170.
3. Heimel, G.; Romaner, L.; Zojer, E.; Brédas, J. L., Toward Control of the Metal–Organic Interfacial Electronic Structure in Molecular Electronics: A First-Principles Study on Self-Assembled Monolayers of π -Conjugated Molecules on Noble Metals. *Nano Lett.* **2007**, *7* (4), 932-940.
4. Van Alsten, J. G., Self-Assembled Monolayers on Engineering Metals: Structure, Derivatization, and Utility. *Langmuir*. **1999**, *15* (22), 7605-7614.
5. Haick, H.; Paz, Y., Long-Range Effects of Noble Metals on the Photocatalytic Properties of Titanium Dioxide. *J. Phys. Chem. B.* **2003**, *107* (10), 2319-2326.
6. Vericat, C.; Vela, M. E.; Benitez, G.; Carro, P.; Salvarezza, R. C., Self-assembled Monolayers of Thiols and Dithiols on Gold: New Challenges for a Well-Known System. *Chem. Soc. Rev.* **2010**, *39* (5), 1805-1834.
7. Vilan, A.; Aswal, D.; Cahen, D., Large-Area, Ensemble Molecular Electronics: Motivation and Challenges. *Chem. Rev.* **2017**, *117* (5), 4248-4286.
8. Darwish, N.; Eggers, P. K.; Ciampi, S.; Tong, Y.; Ye, S.; Paddon-Row, M. N.; Gooding, J. J., Probing the Effect of the Solution Environment Around Redox-Active Moieties Using Rigid Anthraquinone Aerminated Molecular Rulers. *J. Am. Chem. Soc.* **2012**, *134* (44), 18401-18409.
9. Dief, E. M.; Vogel, Y. B.; Peiris, C. R.; Le Brun, A. P.; Gonçalves, V. R.; Ciampi, S.; Reimers, J. R.; Darwish, N., Covalent Linkages of Molecules and Proteins to Si–H Surfaces Formed by Disulfide Reduction. *Langmuir* **2020**, *36* (49), 14999-15009.
10. Darwish, N.; Eggers, P. K.; Ciampi, S.; Zhang, Y.; Tong, Y.; Ye, S.; Paddon-Row, M. N.; Gooding, J. J., Reversible potential-induced structural changes of alkanethiol monolayers on gold surfaces. *Electrochem. Commun.* **2011**, *13* (5), 387-390.

11. Chen, X.; Luais, E.; Darwish, N.; Ciampi, S.; Thordarson, P.; Gooding, J. J., Studies on the Effect of Solvents on Self-Assembled Monolayers Formed from Organophosphonic Acids on Indium Tin Oxide. *Langmuir* **2012**, *28* (25), 9487-9495.
12. Tavallaie, R.; Darwish, N.; Gebala, M.; Hibbert, D. B.; Gooding, J. J., The Effect of Interfacial Design on the Electrochemical Detection of DNA and MicroRNA Using Methylene Blue at Low-Density DNA Films. *ChemElectroChem* **2014**, *1* (1), 165-171.
13. Parviz, M.; Darwish, N.; Alam, M. T.; Parker, S. G.; Ciampi, S.; Gooding, J. J., Investigation of the Antifouling Properties of Phenyl Phosphorylcholine-Based Modified Gold Surfaces. *Electroanalysis* **2014**, *26* (7), 1471-1480.
14. Pakiari, A. H.; Jamshidi, Z., Nature and Strength of M-S Bonds (M = Au, Ag, and Cu) in Binary Alloy Gold Clusters. *J. Phys. Chem. A* **2010**, *114* (34), 9212-9221.
15. Dief, E. M.; Brun, A. P. L.; Ciampi, S.; Darwish, N., Spontaneous Grafting of OH⁻ Terminated Molecules on Si-H Surfaces via Si-O-C Covalent Bonding. *Surfaces* **2021**, *4* (1), 81-88.
16. Vilan, A.; Cahen, D., Chemical Modification of Semiconductor Surfaces for Molecular Electronics. *Chem. Rev.* **2017**, *117* (5), 4624-4666.
17. Reimers, J. R.; Ford, M. J.; Halder, A.; Ulstrup, J.; Hush, N. S., Gold Surfaces and Nanoparticles are Protected by Au (0)-Thiyl Species and are Destroyed when Au (I)-Thiolates Form. *Proc. Natl. Acad. Sci. U. S. A.* 2016, pp E1424-E1433.
18. Reimers, J. R.; Ford, M. J.; Marcuccio, S. M.; Ulstrup, J.; Hush, N. S., Competition of Van der Waals and Chemical Forces on Gold-Sulfur Surfaces and Nanoparticles. *Nat. Rev. Chem.* **2017**, *1* (2), 1-25.
19. Darwish, N.; Eggers, P. K.; Ciampi, S.; Zhang, Y.; Tong, Y.; Ye, S.; Paddon-Row, M. N.; Gooding, J. J., Reversible Potential-Induced Structural Changes of Alkanethiol Monolayers on Gold Surfaces. *Electrochem. Commun.* **2011**, *13* (5), 387-390.
20. Wang, Y.; Chi, Q. J.; Zhang, J. D.; Hush, N. S.; Reimers, J. R.; Ulstrup, J., Chain-Branching Control of the Atomic Structure of Alkanethiol-Based Gold-Sulfur Interfaces. *J. Am. Chem. Soc.* **2011**, *133*, 14856-14859.
21. Yan, J.; Ouyang, R.; Jensen, P. S.; Ascic, E.; Tanner, D. A.; Mao, B.; Zhang, J.; Tang, C.; Hush, N. S.; Ulstrup, J.; Reimers, J. R., Controlling the stereochemistry and regularity of butanethiol self-assembled monolayers on Au(111) *J. Amer. Chem. Soc.* **2014**, *136*, 17087-17094.

22. Ouyang, R.; Yan, J.; Jensen, P. S.; Ascic, E.; Gan, S.; Tanner, D.; Mao, B.; Niu, L.; Zhang, J.; Tang, C., Intermixed Adatom and Surface-Bound Adsorbates in Regular Self-Assembled Monolayers of Racemic 2-Butanethiol on Au (111). *ChemPhysChem*. **2015**, *16* (5), 928-932.
23. McGuinness, C. L.; Shaporenko, A.; Mars, C. K.; Uppili, S.; Zharnikov, M.; Allara, D. L., Molecular Self-Assembly at Bare Semiconductor Surfaces: Preparation and Characterization of Highly Organized Octadecanethiolate Monolayers on GaAs(001). *J. Am. Chem. Soc.* **2006**, *128* (15), 5231-5243.
24. Zerulla, D.; Chassé, T., Scanning Tunneling Microscopy and Spectroscopy of UHV-Deposited Dodecanethiolate Films on InP(110) Surfaces at Consecutive Doses: A Single Domain System. *Langmuir*. **2002**, *18* (14), 5392-5399.
25. Vezzoli, A.; Brooke, R. J.; Ferri, N.; Higgins, S. J.; Schwarzacher, W.; Nichols, R. J., Single-Molecule Transport at a Rectifying GaAs Contact. *Nano Lett.* **2017**, *17* (2), 1109-1115.
26. Campos, M. A. C.; Paulusse, J. M.; Zuilhof, H., Functional Monolayers on Oxide-Free Silicon Surfaces via Thiol-ene Click Chemistry. *Chem. Commun.* **2010**, *46* (30), 5512-5514.
27. Sano, H.; Ohno, K.; Ichii, T.; Murase, K.; Sugimura, H., Alkanethiol Self-Assembled Monolayers Formed on Silicon Substrates. *Jpn. J. Appl. Phys.* **2010**, *49* (1S), 01-09.
28. Peiris, C. R.; Vogel, Y. B.; Le Brun, A. P.; Aragonès, A. C.; Coote, M. L.; Díez-Pérez, I.; Ciampi, S.; Darwish, N., Metal-Single-Molecule-Semiconductor Junctions Formed by a Radical Reaction Bridging Gold and Silicon Electrodes. *J. Am. Chem. Soc.* **2019**, *141* (37), 14788-14797.
29. de Sousa, J. A.; Bejarano, F.; Gutiérrez, D.; Leroux, Y. R.; Nowik Boltyk, E. M.; Junghoefer, T.; Giangrisostomi, E.; Ovsyannikov, R.; Casu, M. B.; Veciana, J.; Mast-Torrent, M.; Fabre, B.; Rovira, C.; Crivillers, N., Exploiting the Versatile Alkyne-Based Chemistry for Expanding the Applications of a Stable Triphenylmethyl Organic Radical on Surfaces. *Chem. Sci.* **2020**, *11*, 516-524.
30. Fabre, B., Functionalization of Oxide-Free Silicon Surfaces with Redox-Active Assemblies. *Chem. Rev.* **2016**, *116* (8), 4808-4849.

31. Fabre, B.; Hauquier, F., Boronic Acid-Functionalized Oxide-Free Silicon Surfaces for the Electrochemical Sensing of Dopamine. *Langmuir*. **2017**, *33* (35), 8693-8699.
32. Vilan, A.; Yaffe, O.; Biller, A.; Salomon, A.; Kahn, A.; Cahen, D., Molecules on Si: Electronics with Chemistry. *Adv. Mater.* **2010**, *22* (2), 140-159.
33. Ashkenasy, G.; Cahen, D.; Cohen, R.; Shanzer, A.; Vilan, A., Molecular Engineering of Semiconductor Surfaces and Devices. *Acc. Chem. Res.* **2002**, *35* (2), 121-128.
34. Buriak, J. M., Organometallic Chemistry on Silicon and Germanium Surfaces. *Chem. Rev.* **2002**, *102* (5), 1271-1308.
35. Puniredd, S. R.; Assad, O.; Haick, H., Highly Stable Organic Monolayers for Reacting Silicon with Further Functionalities: The Effect of the C-C Bond Nearest the Silicon Surface. *J. Am. Chem. Soc.* **2008**, *130* (41), 13727-13734.
36. Linford, M. R.; Chidsey, C. E. D., Alkyl Monolayers Covalently Bonded to Silicon Surfaces. *J. Am. Chem. Soc.* **1993**, *115* (26), 12631-12632.
37. McPherson, J. W., Time Dependent Dielectric Breakdown Physics - Models Revisited. *Microelectron. Reliab.* **2012**, *52* (9-10), 1753-1760.
38. Webb, L. J.; Michalak, D. J.; Biteen, J. S.; Brunschwig, B. S.; Chan, A. S. Y.; Knapp, D. W.; Meyer Iii, H. M.; Nemanick, E. J.; Traub, M. C.; Lewis, N. S., High-Resolution Soft X-ray Photoelectron Spectroscopic Studies and Scanning Auger Microscopy Studies of the Air Oxidation of Alkylated Silicon(111) Surfaces. *J. Phys. Chem. B.* **2006**, *110* (46), 23450-23459.
39. Wong, K. T.; Lewis, N. S., What a Difference a Bond Makes: The Structural, Chemical, and Physical Properties of Methyl-Terminated Si(111) Surfaces. *Acc. Chem. Res.* **2014**, *47* (10), 3037-3044.
40. Assad, O.; Haick, H. In *Chemically Sensitive Field Effect Transistors of Oxide-Free Silicon Nanowires -Towards Detection of Volatile Biomarkers of Cancer*, IEEE Int. Symp. Ind. Electron., 2008; pp 2040-2044.
41. Dasog, M.; Bader, K.; Veinot, J. G. C., Influence of Halides on the Optical Properties of Silicon Quantum Dots. *Chem. Mater.* **2015**, *27* (4), 1153-1156.
42. Fermi, A.; Locritani, M.; Di Carlo, G.; Pizzotti, M.; Caramori, S.; Yu, Y.; Korgel, B. A.; Bergamini, G.; Ceroni, P., Light-Harvesting Antennae Based on Photoactive

Silicon Nanocrystals Functionalized with Porphyrin Chromophores. *Faraday Discuss.* **2015**, *185*, 481-495.

43. Peng, W.; Rupich, S. M.; Shafiq, N.; Gartstein, Y. N.; Malko, A. V.; Chabal, Y. J., Silicon Surface Modification and Characterization for Emergent Photovoltaic Applications Based on Energy Transfer. *Chem. Rev.* **2015**, *115* (23), 12764-12796.

44. Debenedetti, W. J. I.; Chiu, S. K.; Radlinger, C. M.; Ellison, R. J.; Manhat, B. A.; Zhang, J. Z.; Shi, J.; Goforth, A. M., Conversion from Red to Blue Photoluminescence in Alcohol Dispersions of Alkyl-Capped Silicon Nanoparticles: Insight into the Origins of Visible Photoluminescence in Colloidal Nanocrystalline Silicon. *J. Phys. Chem. C.* **2015**, *119* (17), 9595-9608.

45. Kang, O. S.; Bruce, J. P.; Herbert, D. E.; Freund, M. S., Covalent Attachment of Ferrocene to Silicon Microwire Arrays. *ACS Appl. Mater. Interfaces.* **2015**, *7* (48), 26959-26967.

46. Wang, J.; Zhou, Y.; Watkinson, M.; Gautrot, J.; Krause, S., High-Sensitivity Light-Addressable Potentiometric Sensors Using Silicon on Sapphire Functionalized with Self-Assembled Organic Monolayers. *Sens. Actuators.* **2015**, *209*, 230-236.

47. Dasog, M.; Kehrlé, J.; Rieger, B.; Veinot, J. G. C., Silicon Nanocrystals and Silicon-Polymer Hybrids: Synthesis, Surface Engineering, and Applications. *Angew. Chem., Int. Ed.* **2016**, *55* (7), 2322-2339.

48. Brown, E. S.; Hlynchuk, S.; Maldonado, S., Chemically Modified Si(111) Surfaces Simultaneously Demonstrating Hydrophilicity, Resistance Against Oxidation, and Low Trap State Densities. *Surf. Sci.* **2016**, *645*, 49-55.

49. Yasseri, A. A.; Syomin, D.; Loewe, R. S.; Lindsey, J. S.; Zaera, F.; Bocian, D. F., Structural and Electron-Transfer Characteristics of O, S, and Se-Tethered Porphyrin Monolayers on Si(100). *J. Am. Chem. Soc.* **2004**, *126* (47), 15603-15612.

50. Peng, F.; Su, Y.; Zhong, Y.; Fan, C.; Lee, S. T.; He, Y., Silicon Nanomaterials Platform for Bioimaging, Biosensing, and Cancer Therapy. *Acc. Chem. Res.* **2014**, *47* (2), 612-623.

51. Cheng, X.; Lowe, S. B.; Reece, P. J.; Gooding, J. J., Colloidal Silicon Quantum Dots: From Preparation to the Modification of Self-Assembled Monolayers (SAMs) for Bio-Applications. *Chem. Soc. Rev.* **2014**, *43* (8), 2680-2700.

52. Yu, L. H.; Gergel-Hackett, N.; Zangmeister, C. D.; Hacker, C. A.; Richter, C. A.; Kushmerick, J. G., Molecule-Induced Interface States Dominate Charge Transport in Si-Alkyl-Metal Junctions. *J. Phys.: Condens. Matter.* **2008**, *20* (37).
53. Ciampi, S.; Choudhury, M. H.; Ahmad, S. A. B. A.; Darwish, N.; Brun, A. L.; Gooding, J. J., The Impact of Surface Coverage on the Kinetics of Electron Transfer Through Redox Monolayers on a Silicon Electrode Surface. *Electrochim. Acta.* **2015**, *186*, 216-222.
54. Vogel, Y. B.; Zhang, L.; Darwish, N.; Gonçalves, V. R.; Le Brun, A.; Gooding, J. J.; Molina, A.; Wallace, G. G.; Coote, M. L.; Gonzalez, J.; Ciampi, S., Reproducible Flaws Unveil Electrostatic Aspects of Semiconductor Electrochemistry. *Nat. Commun.* **2017**, *8* (1).
55. Aragonès, A. C.; Darwish, N.; Ciampi, S.; Sanz, F.; Gooding, J. J.; Diéz-Pérez, I., Single-Molecule Electrical Contacts on Silicon Electrodes Under Ambient Conditions. *Nat. Commun.* **2017**, *8*.
56. Allain, A.; Kang, J.; Banerjee, K.; Kis, A., Electrical Contacts to Two-Dimensional Semiconductors. *Nat Mater.* **2015**, *14* (12), 1195-1205.
57. Sugimura, H., Self-Assembled Monolayer Covalently Fixed on Oxide-Free Silicon. In *Nanocrystalline Materials: Their Synthesis-Structure-Property Relationships and Applications*, 2 ed.; Tjong, S.-C., Ed. Elsevier: 2013; pp 161-193.
58. Sieval, A. B.; Demirel, A. L.; Nissink, J. W. M.; Linford, M. R.; Van Der Maas, J. H.; De Jeu, W. H.; Zuilhof, H.; Sudhölter, E. J. R., Highly Stable Si-C Linked Functionalized Monolayers on the Silicon (100) Surface. *Langmuir.* **1998**, *14* (7), 1759-1768.
59. Buriak, J. M.; Sikder, M. D. H., From Molecules to Surfaces: Radical-Based Mechanisms of Si-S and Si-Se Bond Formation on Silicon. *J. Am. Chem. Soc.* **2015**, *137* (30), 9730-9738.
60. Buriak, J. M.; Stewart, M. P.; Geders, T. W.; Allen, M. J.; Choi, H. C.; Smith, J.; Raftery, D.; Canham, L. T., Lewis Acid Mediated Hydrosilylation on Porous Silicon Surfaces. *J. Am. Chem. Soc.* **1999**, *121* (49), 11491-11502.
61. Nemanick, E. J.; Hurley, P. T.; Webb, L. J.; Knapp, D. W.; Michalak, D. J.; Brunschwig, B. S.; Lewis, N. S., Chemical and Electrical Passivation of Single-Crystal

Silicon(100) Surfaces Through a Two-Step Chlorination/Alkylation Process. *J. Phys. Chem. B.* **2006**, *110* (30), 14770-14778.

62. Robins, E. G.; Stewart, M. P.; Buriak, J. M., Anodic and Cathodic Electrografting of Alkynes on Porous Silicon. *Chem. Commun.* **1999**, (24), 2479-2480.

63. Boukherroub, R.; Petit, A.; Loupy, A.; Chazalviel, J. N.; Ozanam, F., Microwave-Assisted Chemical Functionalization of Hydrogen-Terminated Porous Silicon Surfaces. *J. Phys. Chem. B.* **2003**, *107* (48), 13459-13462.

64. Soliman, A. I. A.; Utsunomiya, T.; Ichii, T.; Sugimura, H., 1,2-Epoxyalkane: Another Precursor for Fabricating Alkoxy Self-Assembled Monolayers on Hydrogen-Terminated Si(111). *Langmuir.* **2018**, *34* (44), 13162-13170.

65. Sun, Q. Y.; de Smet, L. C. P. M.; van Lagen, B.; Giesbers, M.; Thüne, P. C.; van Engelenburg, J.; de Wolf, F. A.; Zuilhof, H.; Sudhölter, E. J. R., Covalently Attached Monolayers on Crystalline Hydrogen-Terminated Silicon: Extremely Mild Attachment by Visible Light. *J. Am. Chem. Soc.* **2005**, *127* (8), 2514-2523.

66. Sun, Q. Y.; de Smet, L. C. P. M.; van Lagen, B.; Wright, A.; Zuilhof, H.; Sudhölter, E. J. R., Covalently Attached Monolayers on Hydrogen-Terminated Si(100): Extremely Mild Attachment by Visible Light. *Angew. Chem., Int. Ed.* **2004**, *43* (11), 1352-1355.

67. Coulter, S. K.; Schwartz, M. P.; Hamers, R. J., Sulfur Atoms as Tethers for Selective Attachment of Aromatic Molecules to Silicon(001) Surfaces. *J. Phys. Chem. B.* **2001**, *105* (15), 3079-3087.

68. Lai, Y. H.; Yeh, C. T.; Yeh, C. C.; Hung, W. H., Thermal Reactions of Methanethiol and Ethanethiol on Si(100). *J. Phys. Chem. B.* **2003**, *107* (35), 9351-9356.

69. Hacker, C. A., Modifying Electronic Properties at the Silicon-Molecule Interface Using Atomic Tethers. *Solid-State Electron.* **2010**, *54* (12), 1657-1664.

70. Bhartia, B.; Puniredd, S. R.; Jayaraman, S.; Gandhimathi, C.; Sharma, M.; Kuo, Y. C.; Chen, C. H.; Reddy, V. J.; Troadec, C.; Srinivasan, M. P., Highly Stable Bonding of Thiol Monolayers to Hydrogen-Terminated Si via Supercritical Carbon Dioxide: Toward a Super Hydrophobic and Bioresistant Surface. *ACS Appl. Mater. Interfaces.* **2016**, *8* (37), 24933-24945.

71. Vogel, Y. B.; Zhang, L.; Darwish, N.; Gonçalves, V. R.; Le Brun, A.; Gooding, J. J.; Molina, A.; Wallace, G. G.; Coote, M. L.; Gonzalez, J., Reproducible Flaws Unveil

Electrostatic Aspects of Semiconductor Electrochemistry. *Nat. Commun.* **2017**, *8* (1), 2066.

72. Gergel-Hackett, N.; Zangmeister, C. D.; Hacker, C. A.; Richter, L. J.; Richter, C. A., Demonstration of Molecular Assembly on Si (100) for CMOS-Compatible Molecule-Based Electronic Devices. *J. Am. Chem. Soc.* **2008**, *130* (13), 4259-4261.

73. Hu, M.; Liu, F.; Buriak, J. M., Expanding the Repertoire of Molecular Linkages to Silicon: Si-S, Si-Se, and Si-Te Bonds. *ACS Appl. Mater. Interfaces.* **2016**, *8* (17), 11091-11099.

74. Huang, Y. S.; Chen, C. H.; Chen, C. H.; Hung, W. H., Fabrication of Octadecyl and Octadecanethiolate Self-Assembled Monolayers on Oxide-Free Si (111) with a One-Cell Process. *ACS Appl. Mater. Interfaces.* **2013**, *5* (12), 5771-5776.

75. Walkey, M. C.; Peiris, C. R.; Ciampi, S.; C. Aragonès, A.; Domínguez-Espíndola, R. B.; Jago, D.; Pulbrook, T.; Skelton, B. W.; Sobolev, A. N.; Díez Pérez, I., Chemically and Mechanically Controlled Single-Molecule Switches Using Spiropyrans. *ACS Appl. Mater. Interfaces.* **2019**, *11* (40), 36886-36894.

76. Soliman, A. I. A.; Ichii, T.; Utsunomiya, T.; Sugimura, H., Chemical Conversion of Self-Assembled Hexadecyl Monolayers with Active Oxygen Species Generated by Vacuum Ultraviolet Irradiation in an Atmospheric Environment. *Soft Matter.* **2015**, *11* (28), 5678-5687.

77. Steinrück, H. G.; Schiener, A.; Schindler, T.; Will, J.; Magerl, A.; Konovalov, O.; Li Destri, G.; Seeck, O. H.; Mezger, M.; Haddad, J.; Deutsch, M.; Checco, A.; Ocko, B. M., Nanoscale Structure of Si/SiO₂/Organics Interfaces. *ACS Nano.* **2014**, *8* (12), 12676-12681.

78. McPherson, J. W.; Mogul, H. C., Underlying Physics of the Thermochemical Model in Describing Low-Field Time-Dependent Dielectric Breakdown in SiO₂ Thin Films. *J. Appl. Phys.* **1998**, *84* (3), 1513-1523.

79. Sieval, A. B.; Linke, R.; Zuilhof, H.; Sudhölter, E. J. R., High-Quality Alkyl Monolayers on Silicon Surfaces. *Adv. Mater.* **2000**, *12* (19), 1457-1460.

80. Hu, M.; Hauger, T. C.; Olsen, B. C.; Lubner, E. J.; Buriak, J. M., UV-Initiated Si-S, Si-Se, and Si-Te Bond Formation on Si (111): Coverage, Mechanism, and Electronics. *J. Phys. Chem. C.* **2018**, *122*, 13803-13814.

81. Lou, J. L.; Shiu, H. W.; Chang, L. Y.; Wu, C. P.; Soo, Y. L.; Chen, C. H., Preparation and Characterization of an Ordered 1-dodecanethiol Monolayer on Bare Si(111) Surface. *Langmuir*. **2011**, *27* (7), 3436-3441.
82. Linford, M. R.; Fenter, P.; Eisenberger, P. M.; Chidsey, C. E. D., Alkyl Monolayers on Silicon Prepared from 1-Alkenes and Hydrogen-Terminated Silicon. *J. Am. Chem. Soc.* **1995**, *117* (11), 3145-3155.
83. Arefi, H. H.; Nolan, M.; Fagas, G., Density functional theory with van der waals corrections study of the adsorption of alkyl, alkylthiol, alkoxy, and amino-alkyl chains on the H: Si (111) surface. *Langmuir*. **2014**, *30* (44), 13255-13265.
84. Reimers, J. R.; Panduwinata, D.; Visser, J.; Chin, Y.; Tang, C.; Goerigk, L.; Ford, M. J.; Santic, M.; Sum, T. J.; Coenen, M. J. J., A Priori Calculations of the Free Energy of Formation from Solution of Polymorphic Self-Assembled Monolayer. *Proc. Natl. Acad. Sci. U. S. A.* 2015, pp E6101-E6110.
85. Frisch, M. J.; Trucks, G. W.; Schlegel, H. B.; Scuseria, G. E.; Robb, M. A.; Cheeseman, J. R.; Scalmani, G.; Barone, V.; Petersson, G. A.; Nakatsuji, H.; Li, X.; Caricato, M.; Marenich, A. V.; Bloino, J.; Janesko, B. G.; Gomperts, R.; Mennucci, B.; Hratchian, H. P.; Ortiz, J. V.; Izmaylov, A. F.; Sonnenberg, J. L.; Williams, D.; Ding, F.; Lipparini, F.; Egidi, F.; Goings, J.; Peng, B.; Petrone, A.; Henderson, T.; Ranasinghe, D.; Zakrzewski, V. G.; Gao, J.; Rega, N.; Zheng, G.; Liang, W.; Hada, M.; Ehara, M.; Toyota, K.; Fukuda, R.; Hasegawa, J.; Ishida, M.; Nakajima, T.; Honda, Y.; Kitao, O.; Nakai, H.; Vreven, T.; Throssell, K.; Montgomery Jr., J. A.; Peralta, J. E.; Ogliaro, F.; Bearpark, M. J.; Heyd, J. J.; Brothers, E. N.; Kudin, K. N.; Staroverov, V. N.; Keith, T. A.; Kobayashi, R.; Normand, J.; Raghavachari, K.; Rendell, A. P.; Burant, J. C.; Iyengar, S. S.; Tomasi, J.; Cossi, M.; Millam, J. M.; Klene, M.; Adamo, C.; Cammi, R.; Ochterski, J. W.; Martin, R. L.; Morokuma, K.; Farkas, O.; Foresman, J. B.; Fox, D. J., *Gaussian 16 Revision B.01*. Gaussian Inc.: Wallingford, CT, 2016.
86. Hehre, W. J.; Ditchfield, R.; Pople, J. A., Self-Consistent Molecular Orbital Methods. XII. Further Extensions of Gaussian-Type Basis Sets for Use in Molecular Orbital Studies of Organic Molecules *J. Chem. Phys.* **1972**, *56*, 2257-61.
87. Reimers, J. R., A Practical Method for the Use of Curvilinear Coordinates in Calculations of Normal-Mode Projected Displacements and Duschinsky Rotation Matrices for Large Molecules. *J. Chem. Phys.* **2001**, *115*, 9103-9109.

88. Ochterski, J. W., Thermochemistry in gaussian. *Gaussian Inc.* **2000**, 1-19.
89. Sieval, A. B.; Opitz, R.; Maas, H. P. A.; Schoeman, M. G.; Meijer, G.; Vergeldt, F. J.; Zuilhof, H.; Sudhölter, E. J. R., Monolayers of 1-Alkynes on the H-Terminated Si(100) Surface. *Langmuir*. **2000**, *16* (26), 10359-10368.
90. Faucheux, A.; Gouget-Laemmel, A. C.; Henry de Villeneuve, C.; Boukherroub, R.; Ozanam, F.; Allongue, P.; Chazalviel, J. N., Well-Defined Carboxyl-Terminated Alkyl Monolayers Grafted onto H-Si (111): Packing Density from a Combined AFM and Quantitative IR Study. *Langmuir*. **2006**, *22* (1), 153-162.
91. Chang, L. Y.; Kuo, Y. C.; Shiu, H. W.; Wang, C. H.; Lee, Y. C.; Yang, Y. W.; Gwo, S.; Chen, C. H., N-Alkanethiols Directly Grown on a Bare Si(111) Surface: From Disordered to Ordered Transition. *Langmuir*. **2017**, *33* (50), 14244-14251.
92. Hassan, F. M.; Batmaz, R.; Li, J.; Wang, X.; Xiao, X.; Yu, A.; Chen, Z., Evidence of covalent synergy in silicon–sulfur–graphene yielding highly efficient and long-life lithium-ion batteries. *Nat. Commun.* **2015**, *6* (1), 8597.
93. Zavitsas, A. A.; Chatgililoglu, C., Energies of Activation. The Paradigm of Hydrogen Abstractions by Radicals. *J. Am. Chem. Soc.* **1995**, *117* (43), 10645-10654.
94. Nichols, R. J.; Higgins, S. J., Single-molecule contacts exposed. *Nat. Mater.* **2015**, *14* (5), 465-466.
95. Nichols, R. J.; Haiss, W.; Higgins, S. J.; Leary, E.; Martin, S.; Bethell, D., The experimental determination of the conductance of single molecules. *Phys. Chem. Chem. Phys.* **2010**, *12* (12), 2801-2815.
96. Aragones, A. C.; Haworth, N. L.; Darwish, N.; Ciampi, S.; Bloomfield, N. J.; Wallace, G. G.; Diez-Perez, I.; Coote, M. L., Electrostatic catalysis of a Diels–Alder reaction. *Nature*. **2016**, *531* (7592), 88-91.

Every reasonable effort has been made to acknowledge the owners of copyright material. I would like to apologise if any copyright owner who has been omitted or incorrectly acknowledged.

Chapter 6

Silicon oxide nanostructures formation using atomic force microscope tip induced oxidation. Revealing the mechanism and more.

6.1 Overview of this chapter

The previous two chapters discussed in detail developing new chemistry for molecular electronic devices on silicon (Si). As reported in chapters 4 and 5, diazonium and thiols on Si show a high density of molecules on the surface enabled by strong Si–C and Si–S bonds. After understanding how to modify Si with molecules in a way comparable to that with gold, this chapter demonstrates how Si oxidation can be used as an advantage or adversary to separate molecular arrays for molecular electronic circuits. Oxide on Si can be used as an insulator to separate arrays of molecules akin to a tunable diode that depends on the thickness of the oxide layer. The aim, of this chapter, is to first determine the threshold of the voltage needed to oxidize the Si surface to form a uniform and insulating dielectric layer of oxide on Si(111)–H compared to the isotope substituted Si(111)–D. Secondly, to study the current-voltage (I – V) properties of the thin oxide layers by using conductive atomic force microscope (c–AFM), peak force tunnelling current (PF–TUNA) mode. Importantly, this chapter demonstrates that topography is deceptive in visually assessing the oxide formation on Si as minimal changes in the oxide thickness lead to a large change in the electrical measurement. Therefore, current measurements can be used as a tool to read the less dense oxide patterns as shown in Figure 6.1.

This chapter reveals that the thin oxide layers behave as tunable Schottky diodes with different rectification ratios and the oxide formation rate is slower on the Si surface when hydrogen is replaced with deuterium. It is also found that the oxide layer height increases gradually for Si(111)–H surfaces with increasing the applied voltage and the Si(111)–D surface shows a very slow rate of oxidation up to +3 V when writing speed, humidity, temperature and peak force were kept constant. This isotopic effect is an advantage to Si-based nanofabrication since the isotope substitution can tailor the

surface properties such as the thickness of oxides on Si and electrical properties without complicating the controllability of other external factors.

Up to now, it is not clear whether it is electron tunnelling or the electric field that induces desorption of the H and the subsequent oxidation. To separate the effects of the electric field from electron tunnelling (electric current), we fabricated Pt–Si Schottky junctions with both n–type and p–type Si. Such junctions enabled blocking the current at the reverse bias (when +ve is applied to n–type Si or –ve applied to p–type Si) and i.e. allowed, for the first time, disentangling electric current and electric-field-induced effects. Results show that oxidation is dependent mainly on the electric field and not the current.

Importantly, this chapter illustrates that SiO_x structures show other behaviours rather than simply insulating and showed that the oxide layer can breakdown when applying a high bias using an AFM tip. With the applied high bias oxide layer develop conducting oxide channels and the properties of the oxide changed from insulating to ohmic. These conducting oxide channels can be reversed back to the insulator by applying a low bias voltage such as ± 2 V. This switching Schottky/ohmic properties can potentially be used as memory devices.

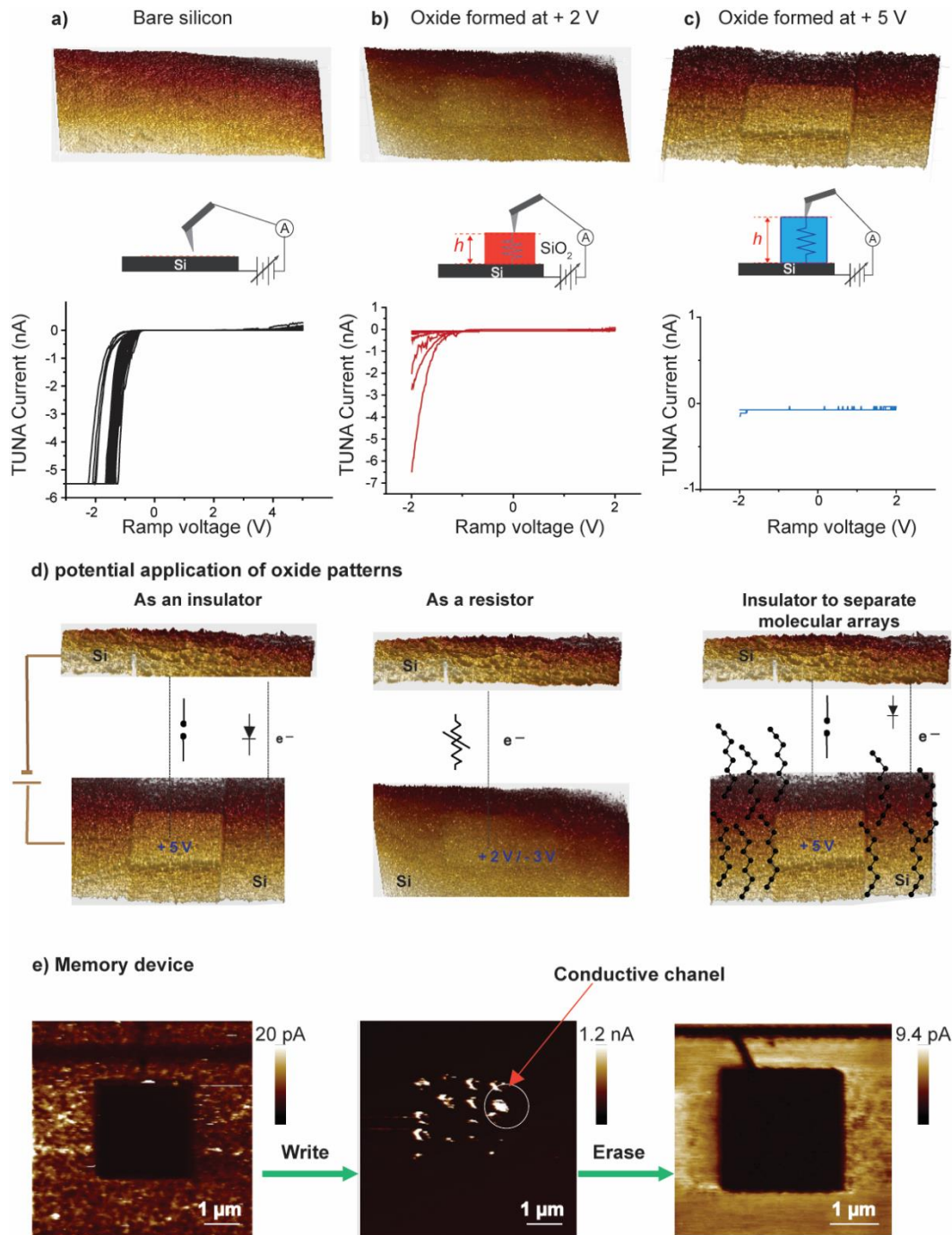


Figure 6. 1 Overview of the work and application of this project where a) metal-semiconductor junction behaving as a Schottky diode b) tunable Schottky diode and c) as a perfect dielectric (insulator) with the increase of positive bias voltages and d) potential application of oxide pattern formation by AFM tip induced oxidation where oxide zones are needed to separate molecular arrays in a molecular electronics device and e) as a potential memory device.

6.2 Introduction

The formation of surface oxide patterns within a nanometre scale has attracted significant interest for nanoelectronics devices such as single-electron transistors. With the invention of the scanning probe microscope (SPM), semiconductors such as Si can be oxidised by the electric field localized at the tip-surface interfaces promising low-cost nanolithography for electronic devices. Tip induced local anodic oxidation was originally demonstrated on Si surfaces with STM operating in the air by Dagata et al. in 1990¹ and followed by many other groups to develop oxide patterns.²⁻⁷ The height of the oxide pattern induced by the STM tip usually in the order of 1–10 nm, which is robust enough to be used as a mask for Si nanostructure fabrication.⁸ To avoid the disadvantages of STM such as applying a bias voltage to the tip without changing the feedback control,⁸ recent work has replaced STM with AFM to develop oxide patterns on surfaces. AFM tip-induced local anodic oxidation (ATLAO) has been applied for conducting materials such as Ti, Mg, and Ca^{5, 9} and semiconducting materials, such as Si^{4, 10-11} and GaAs.⁵⁻⁶ AFM has been used to locally oxidize the Si surface using both contact and non-contact modes. Notably, these oxide patterns can be used as a lithographic mask.

In ATLAO, there are few mechanisms proposed so far for the oxidation of H-terminated Si surfaces. One of the proposed mechanism is the depassivation of the Si surface by desorption of hydrogen assisted by the electric field above the threshold voltage, followed by converting into SiO_x in the presence of O₂.¹²⁻¹⁶ Si-H when exposed to dry O₂ or deoxygenated water gives a low oxide growth rates but, where a combination of H₂O and O₂ gives a significant faster oxide growth.^{15, 17} The formation of OH⁻ in the water meniscus between the tip and surface involves both electrochemical and dissolution process.^{6, 18} It was suggested that the migration of the OH⁻ is assisted by the electric field toward the SiO_x-Si interface which further accelerates the oxidation in the presence of a positive bias.¹⁹ As reported by Marchi et al.¹⁹ the oxide growth is dependant on both applied bias voltage and ambient air. So far, oxide formation experiments carried out in the literature are mainly focused on positive biases.^{6, 20-21} However, there are few reports of negative biases being able to produce oxide layers, thus the mechanism of the process and factors that control the rate are still debatable.²²⁻²³ Another suggested mechanism is an electric field that

can shift the vibrational excitation energy which is known as a “Stark shift”²⁴⁻²⁵ which can affect the desorption of Si–H. When this shift is larger than the bandwidth of the vibrational excitation, the bond can break, and H will be released from the surface creating reactive Si radicals.²⁶

However, understanding the desorption of hydrogen from Si is also a subject of significant technological importance.^{8, 27} Up to now, it is not known whether the AFM tip induced oxidation is due to electric current or an electric field that induces desorption of the H and the subsequent oxidation. The difficulty lies in the lack of experiments that can separate electric field from electric current effects which both are usually present simultaneously.

To separate the effects of the electric field from electric current, in this chapter, we address the mechanism of the AFM tip induced oxidation of H-terminated Si by designing junctions that comprise a platinum AFM tip which has a high work function (5.65 eV) and therefore creates a Schottky diode with Si p- and n-type (work function of Si is 4.05–5.15 eV). The diode current is low in the reverse bias and therefore applying a positive bias to n-type Si will lead to negligible current in the reverse bias and the inverse will happen with p-type Si in which a negative bias to the p-type surface will lead to a negligible current. Thus by applying negative and positive voltages on p- and n-type, these experiments can reveal the mechanism of oxide growth and distinguish the difference between the effects of electric field and electric current towards the oxidation of Si, respectively.

Oxides also have other applications for example electric-field-induced resistive-random-access-memories²⁸⁻³¹ (ReRAMs) have recently attracted increased attention as a promising candidate for the next generation of memory devices. Studying oxide resistive switching has been so far studied using capacitor-like structure composed of SiO_x or other oxide materials³² such as metal oxides sandwiched between two metal electrodes.³²⁻³⁷ For these studies normally the oxide layer is thermally grown. Thermal oxidation will not likely be the method of use for further miniaturization of electronics because of the complexity of controlling the dimensions of thermally grown oxide layers at the nanoscale.³⁸⁻⁴¹ Alternative methods are to use scanning probe techniques such as atomic force microscopy to form local silicon oxide zones on Si. Although much work has been devoted in investigating the growth conditions

of AFM induced SiO_x pattern on Si, little is known about the electrical properties of the AFM grown oxide. In this work, after determining the threshold voltage needed to create these oxide layers, switched to the low-resistance state by applying a second threshold high voltage stress. Applying a high bias such ± 6 V silicon oxide layer can undergo partial breakdown forming conducting channels and can reset this process by applying a lower voltage.

In contemplating future electronic devices on the nanoscale, materials required include conductors, tunable diodes, memory devices and insulators. One of the problems associated with using semiconductors for microelectronics is the difficulty of doping such small structures. So, one of the solutions for this problem is using tip induced oxidation to make oxide patterns which make a barrier to control the current passing through the semiconductor. In this chapter, we demonstrate that the thin oxide layers behave as a tunable Schottky diode with different rectification ratios and can act as a memory device with an applied high electric field. This chapter also compares the oxidation rate of H-terminated Si with D-terminated Si to examine the importance of isotope effects for the dynamics of the desorption process in the presence of the applied electric field. Where use AFM to study how the current-voltage (I-V) behaviour changes on the oxide of Si(111)-H/D surface with applied different bias voltages from -3 V to $+5$ V. The current maps are used to demonstrate which applied bias formed dense or thin layers of oxides on the surface where the topography is misleading in visually assessing the oxide formation. This chapter also investigates using SiO_x formation and breaking as write-erase memory devices.

6.3 Experimental methods

6.3.1 Chemicals and materials

Unless stated otherwise, all chemicals were of analytical grade and used as received. Hydrogen peroxide (30 wt% in water), sulfuric acid (PuranalTM, 95–97%), ammonium fluoride (PuranalTM, 40 wt% in water), ammonium sulfite monohydrate (Sigma-Aldrich, $(\text{NH}_4)_2\text{SO}_3$, 92%) used for wafer cleaning and Si modification procedures were obtained from Sigma Aldrich. Deuterated water (D_2O), deuterated dichloromethane (d_2 -DCM) and potassium fluoride (KF) were purchased from Sigma-Aldrich and used for wafer cleaning and etching to prepare deuterated Si surfaces. Milli-QTM water

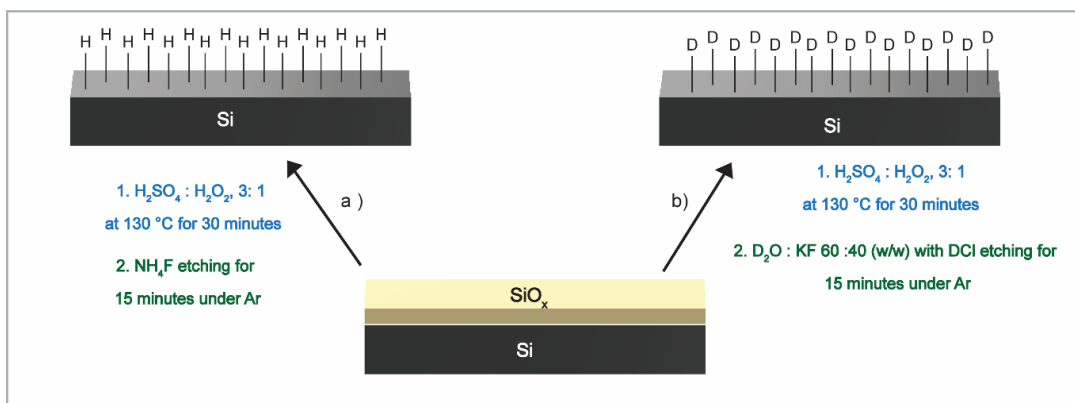
(>18 M Ω cm) was used for surface cleaning procedures. Prime-grade, single-side polished Si wafers were obtained from Siltronix, S.A.S. (Archamps, France) and were n-type (phosphorus doped), 500 ± 25 μm thick and either (111) $\pm 0.5^\circ$ (with a resistivity of 0.007–0.013 Ω cm), p-type (Boron doped), 500 ± 25 μm thick, (111) $\pm 0.5^\circ$ with a resistivity of 0.007–0.013 Ω cm.

6.3.2 Si(111)–H surface modification

Silicon electrodes were cleaned and etched by the following literature procedures.⁴² In brief, Si wafers were cut into pieces (approximately 10×10 mm), cleaned for 30 min in hot Piranha solution ($\text{H}_2\text{SO}_4 : \text{H}_2\text{O}_2$ 3 : 1) at 130 °C, rinsed with Milli-Q™ water and then etched with a deoxygenated 40 wt% aqueous ammonium fluoride (NH_4F) solution for 13 minutes (Scheme 6.1). This process leads to a hydrogen-terminated Si surface (Si(111)–H)). To the etching solution, added a small amount (ca. 5 mg) of ammonium sulfite to absorb oxygen. The etched samples were rinsed sequentially with Milli-Q™ water, dichloromethane (DCM) and blown dry in a stream of argon before analysis or further modifying the Si surface.

6.3.3 Si(111)–D surface modification

As in the preparation of Si(111)–H, Si wafers were cut into pieces (approximately 10×10 mm), cleaned for 30 min in hot Piranha solution, rinsed with Milli-Q™ water. For deuterating the surfaces, a solution of approximately 60 : 40 deuterated water (D_2O) and anhydrous potassium fluoride (KF) (w/w) were prepared and to this solution added few drops of 37% deuterated sulfuric acid (DCl) and a small quantity of sodium sulphite. The etching solutions were bubbled under argon for at least 15 minutes before use and surfaces were etched for 13 minutes under argon. The deuterated surfaces were rinsed once in D_2O and twice in deuterated dichloromethane(d_2 –DCM) and stored in distilled d_2 –DCM until use (Scheme 6.1).



Scheme 6. 1 a) schematic diagram of preparation Si(111)–H surface, b) Si(111)–D surface using Si wafers after piranha treatment.

6.3.4 Formation of Si oxide squares on Si(111)

Tip induced oxidation was performed in the ambient conditions with Bruker Dimension Icon atomic force microscopy (AFM) fitted with a PF–TUNA module operating in peak force tunnelling current (PF–TUNA) mode (Figure 6.1). All images and current-voltage (*I*–*V*) curves were obtained in air, at room temperature, and using solid Pt tips (RMN-25PT300B tip, nominal spring constant = 18 N/m, nominal resonant frequency = 20 kHz, tip radius < 20 nm) purchased from Rocky Mountain Nanotechnology. The 2 × 2 μm areas of Si(111) were oxidised to SiO_x by applied biases ranging from –3 to +5 V with the number of lines (256), the number of scans (2), scan rate (1 Hz), humidity (55%), peak force (554 nN) and temperature (21 °C) were kept as constants. *I*–*V* curves were measured by ramping 20 times in each position from a negative bias to positive bias to negative bias at 2.25 μN and 1 Hz ramp rate. The positive to negative bias ramps were averaged and plotted. For these preliminary experiments, a Si sample was mounted on the base plate of the AFM with carbon tape which acts as a pathway to electrical ground via the metal stage. The AFM and control software was set up to allow the sample to be biased whilst maintaining the tip at the ground. The data were processed using NanoScope Analysis v1.9.

6.3.5 Conducting oxide tunnels formation on SiO_x

After forming the SiO_x layer, the oxide tunnels were formed by ramping 10 times in 20 positions by applying –6 to +6 to –6 V biases at 2.25 μN and 1 Hz ramp rate. The positive to negative bias ramps were averaged and plotted. To check the reversibility of oxide formation, the oxide tunnels filled by ramping 20 times in the same 20 positions by applying –2 to +2 to –2 V biases at 2.25 μN and 1 Hz ramp rate. The positive to negative bias ramps were averaged and plotted.

6.4 Results and discussion

6.4.1 Conductivity change of the oxide hillocks on Si(111)–H formed by different positive bias voltages

The I–V characteristics have been studied as a function of bias voltages applied for the Si to form oxide when other parameters such as scan rate (1 Hz), humidity (55%), and peak force (554 nN) at 25 °C for 8 minutes (2 scans) were kept as constants. Height images corresponding to the bias applied on the fresh surfaces in the air are presented in Figure 6.2c, Figure 6.2e, Figure 6.2g, Figure 6.2i and their representative I–V's in Figure 6.2d, Figure 6.2f, Figure 6.2h and Figure 6.2j, respectively. These I–V characteristics are the average result of 20 I–V measurements obtained on 20 different regions as shown in Figure 6.2c in “X” marks. The voltage range has been applied on the substrate from –2 to +2 V (forward and reverse) with a ramp speed of 1 Hz and current sensitivity 100 nA / V. The I–V curves recorded on oxide hillocks were compared with the I–V behaviour of the bare Si(111)–H. In the absence of oxide, direct Pt–Si contact is made, showed high current rectification (RR) ~300 with the significant forward current higher than reverse current for Si(111)–H surface (Figure 6.2b) demonstrating the behaviour of a typical metal–semiconducting junction. The height of the oxide pattern is measured from the cross-section profiles for at least three sections, and then the average is calculated. The average oxide height plotted versus applied voltages are presented in Figure 6.3.

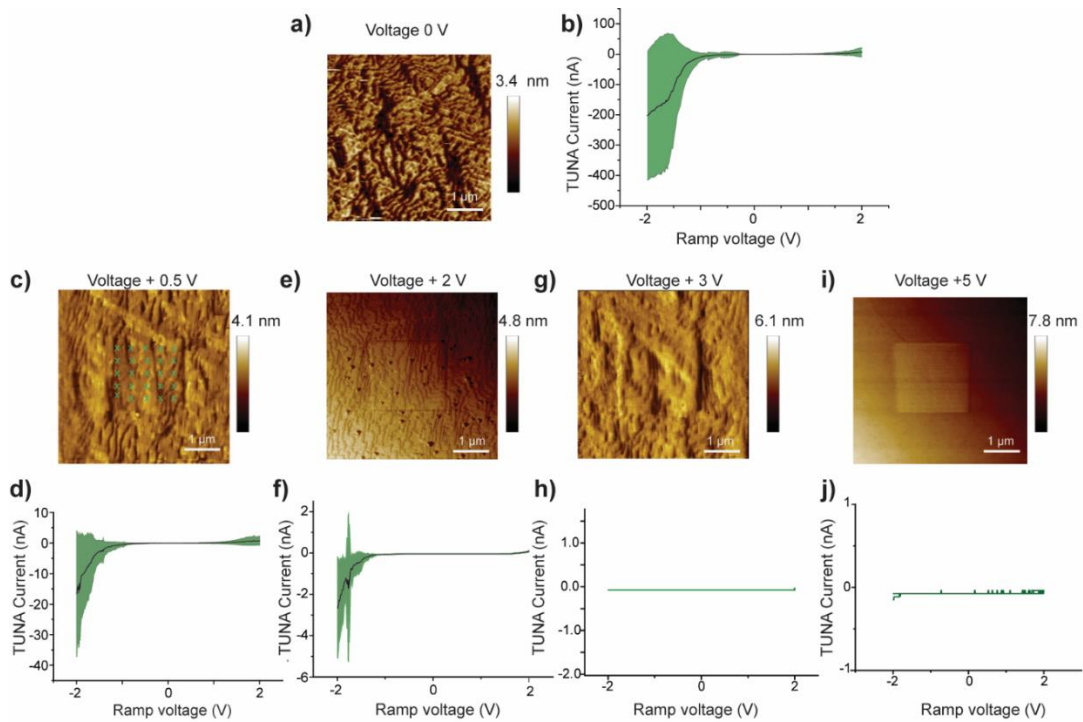


Figure 6. 2 AFM height topography of the oxide hillocks obtained on n-type Si–H with the AFM–tip induced oxidation at an applied positive bias voltage of 0 V (a), +0.5 V (c), +2 V (e), +3 V (g) and +5 V (i). The corresponding forward and reverse I–V characteristics recorded on the oxide hillocks are presented at current sensitivity 100 nA/ V, at 0 V (b) and after oxidation of Si(111)–H surface with +0.5 V (d), +2 V (f), +3 V (h), +5 V (j).

Oxide growth on Si(111)–H surfaces significantly increases with the voltage and one can see the oxide patterns visibly in AFM height images, however, they are not very prominent up to +3 V (Figure 6.2). At +3 V, the growth of oxide is prominent in the topography (Figure 6.2g). This illustrates that the threshold bias voltage for achieving a fully robust layer of oxide on Si(111)–H is +3 V or higher with the given conditions. Bias voltages of +0.5 V (Figure 6.2c), +1 V, +2 V (Figure 6.2e), +3 V (Figure 6.2g) and +5 V (Figure 6.2i) show average oxide height increases of 1.0 ± 0.36 nm, 1.6 ± 0.40 nm, 2.6 ± 0.19 , 4.3 ± 0.09 nm, 6.3 ± 0.37 nm, respectively.

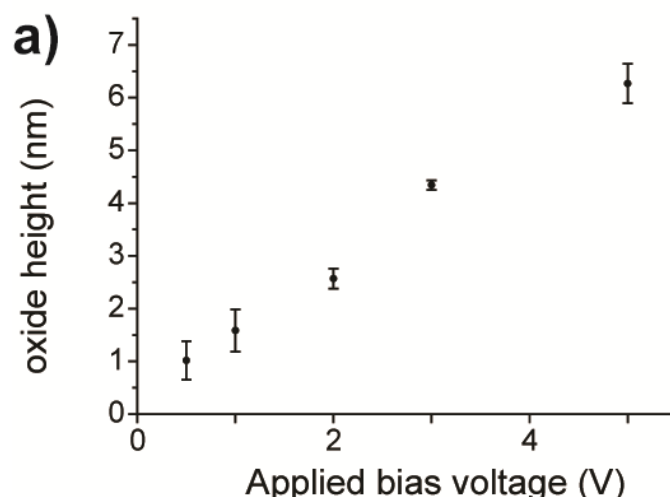


Figure 6. 3 Heights of the oxide hillocks on Si(111)–H surface as a function of applied positive bias voltage under a relative humidity ~55 % at 25 °C, scan rate 1 Hz, and peak force 554 nN for 8 minutes.

The I–Vs illustrate that oxide hillocks show less forward current when the oxide thickness is increasing with the function of bias voltage (Figure 6.2d, 6.2f) and after applying +3 V or higher the current is completely blocked in the –2 V to +2 V window (Figure 6.2h, 6.2j). Moreover, the topography images demonstrate the difference in the hillocks’ heights which increase from 1 nm to 6 nm when the voltage is increased from +0.5 V to +5 V. According to the I–Vs and height topography, it clearly shows that the 4 nm thickness of oxide is enough to show a complete insulator where the threshold bias is +3 V. Slightly positive tip bias such as +0.5 V develop a thin oxide layer which does not completely block the current but yield a diode with a lower forward current.

6.4.2 Conductivity of the oxide hillocks formed on Si(111)–H by negative bias voltages

The I–V characteristics have been studied as a function of negative voltages applied on Si(111)–H as shown in Figure 6.4. The height topography after oxidation with negative biases are shown in Figure 6.4c, 6.4e, 6.4g and 6.4i.

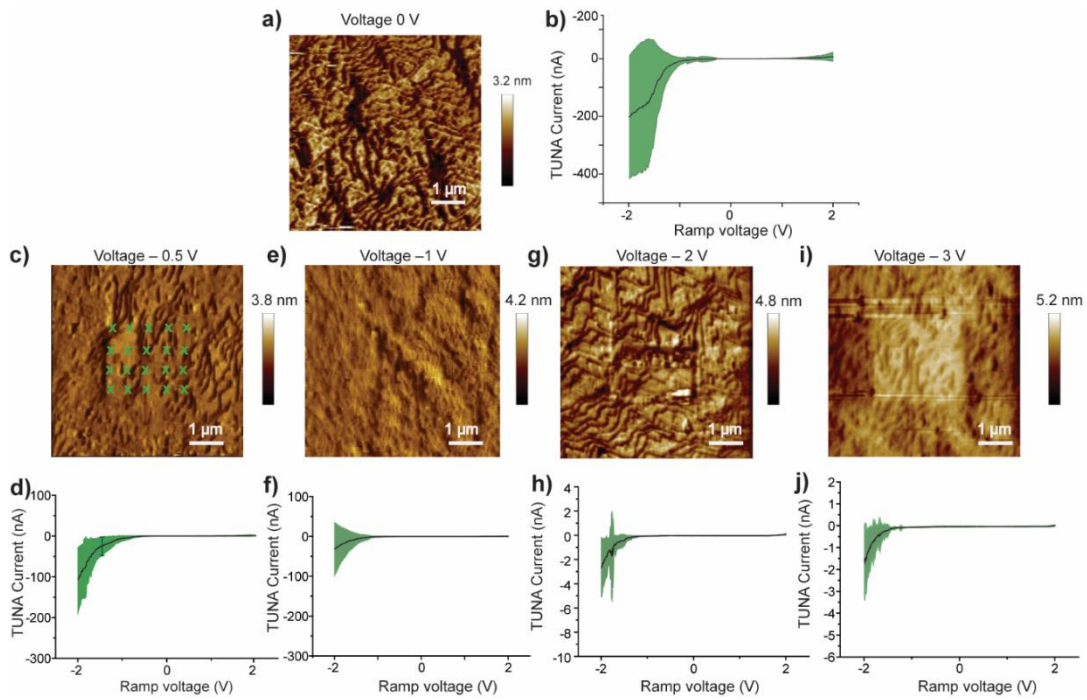


Figure 6. 4 AFM height topography of the oxide hillocks obtained for the n-type Si–H with the AFM–tip induced oxidation at an applied negative bias voltage of 0 V (a), –0.5 V (c), –1 V (e), –3 V (g) and –5 V (i). The corresponding forward and reverse I–V characteristics on the oxide hillocks are presented (current sensitivity 100 nA/ V) at 0 V (b), after oxidation of Si(111)–H surface at –0.5 V (d), –1 V (f), –3 V (h) and –5 V (j).

The I–Vs illustrate that the oxide hillocks formed by negative biases show higher forward current compared to the oxides formed by positive biases (Figure 6.4d, 6.4f, 6.4h and 6.4i).

To confirm this oxide formation on Si surface, TUNA current images were recorded for the two different positive and negative bias voltages. After forming of oxide hillocks with two positive biases (+0.5 V, +3 V) and two negative biases (–0.5 V, –3 V), the TUNA current was measured by applying –1 V and +1 V to illustrate the conductivity of the oxide hillocks formed under different biases. These TUNA current images are shown in (Figure 6.5) at positive and negative biases.

With the applied bias where the topography is misleading in visually assessing the oxide formation (low biases as +0.5 V or negative biases which formed very thin layers of oxides), minimum changes in the oxide thickness lead to a measurable change in the electrical measurement. Therefore, current images are more conclusive than

height images. These current maps demonstrate which applied bias formed dense or thin layers of oxides on the surface.

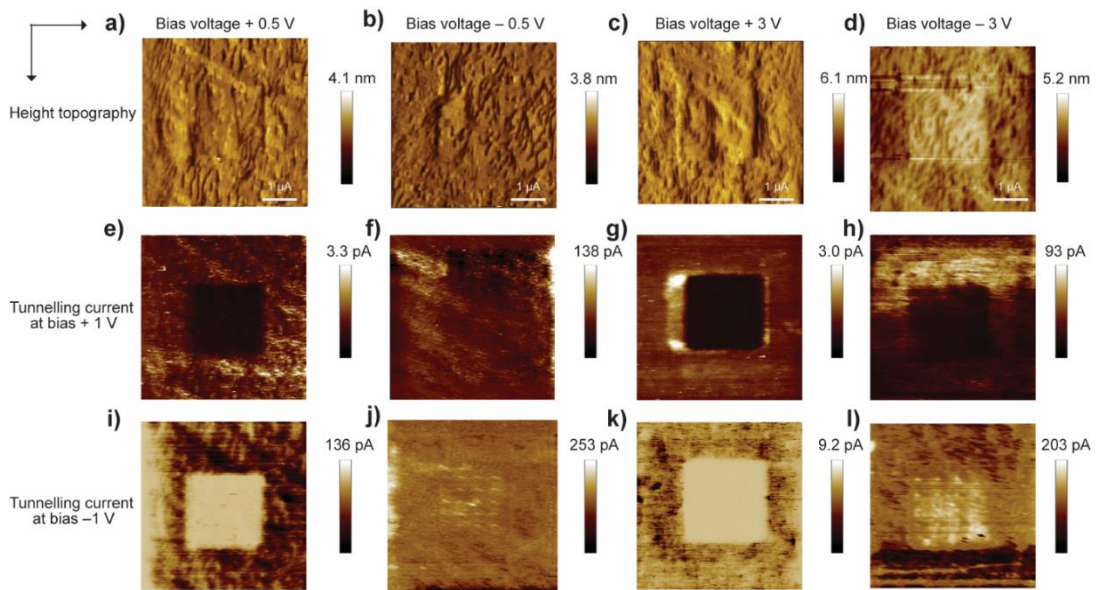


Figure 6. 5 Height topography of the oxide hillocks for the n-type Si-H formed by different bias +0.5 V, -0.5 V, +3 V and -3 V (a, b, c, d) for 8 minutes, TUNA current was measured by AFM-PF TUNA mode by applying +1 V bias (e, f, g, h) and -1 V (i, j, k, l) at scan rate 1 Hz and peak force 554 nN for 4 minutes.

The oxide is barely visible in the topography images in Figure 6.5a, 6.5c but it is visible in the TUNA current images (Figure 6.5e, 6.5g). The greater the oxide density, the less TUNA current is observed. TUNA current images recorded for the oxide hillocks read with applying +1 V (Figure 6.5e), and -1 V (Figure 6.5i), after oxidising with +0.5 V shows that the hillocks show more forward current compared to the oxide hillocks formed with +3 V (Figure 6.5f, Figure 6.5j). This is similar to the I-V plots shown in Figure 6.2. TUNA current maps for the -0.5 V (Figure 6.5g, Figure 6.5k), +0.5 V (Figure 6.5e, Figure 6.5i) and -3 V (Figure 6.5h, Figure 6.5l) recorded in the same environment demonstrate that the oxide hillocks heights are not visible at very low bias voltages but, TUNA current confirms the existence of the different oxide heights of the hillocks, indicating the oxide height sensitivity of the TUNA images

To distinguish the difference between the effect of electric field and electron tunnelling towards the oxidation of Si, the same experiment was repeated with p-type Si(111) highly doped surface. The I–V characteristics have been studied as a function of positive and negative voltages applied on p-type Si(111)–H to check the oxide formation. The height topography for p-type, Si(111) after oxidation with positive and negative bias is shown in Figure 6.6 and 6.7, respectively.

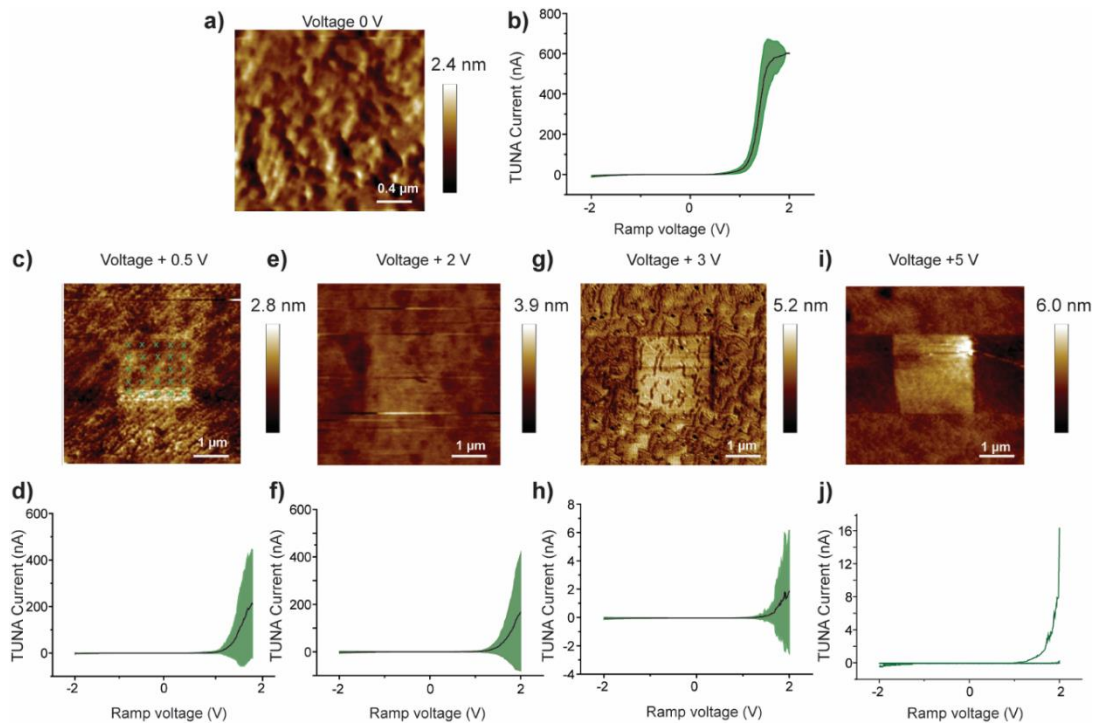


Figure 6. 6 AFM height topography (p-type) of the oxide hillocks obtained for the p-type Si–H with the AFM–tip induced oxidation at an applied positive bias voltage of 0 V (a), +0.5 V (c), +2 V (e), +3 V (g) and +5 V (i). The corresponding forward and reverse I–V characteristics recorded on the oxide hillocks are presented at current sensitivity 100 nA/ V, 0 V (b) and after oxidation of p-type Si(111)–H surface at +0.5 V (d), +2 V (f), +3 V (h), +5 V (j), respectively.

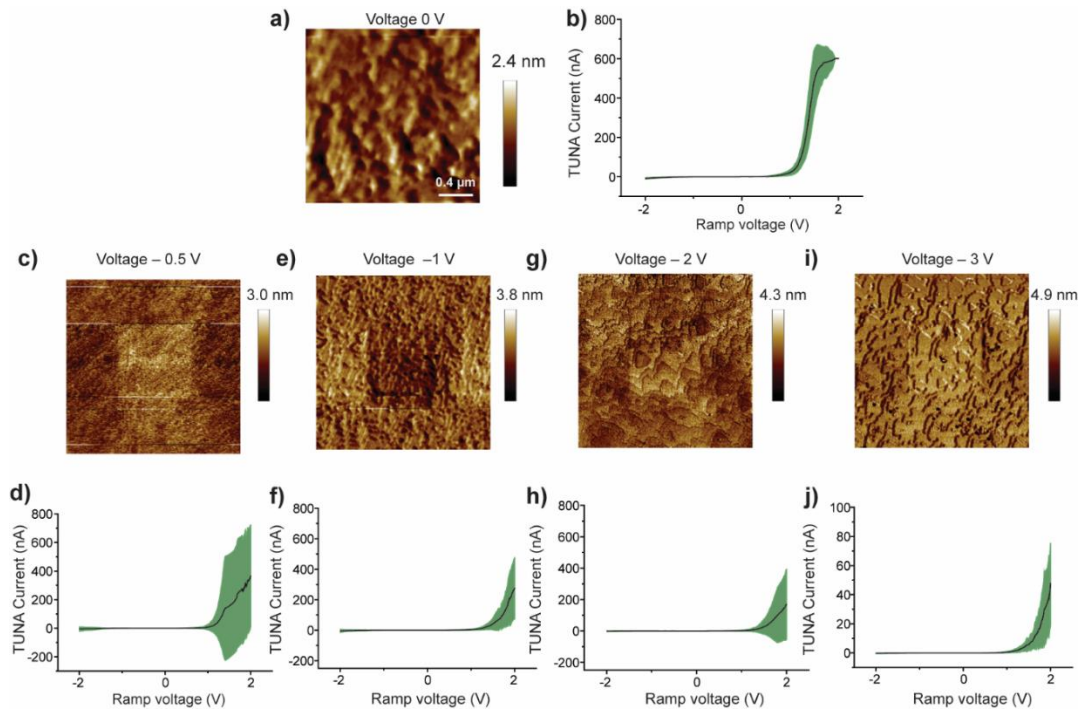


Figure 6. 7 AFM height topography of the oxide hillocks obtained for the p-type Si-H with the AFM-tip induced oxidation at an applied negative bias voltage of 0 V (a), -0.5 V (c), -1 V (e), -2 V (g) and -3 V (i). The corresponding forward and reverse I-V characteristics on the oxide hillocks are presented (current sensitivity 100 nA/V) at 0 V (b), after oxidation of p-type Si(111)-H surface at 0 (b), -0.5 V (d), -1 V (f), -2 V (h) and -3 V (j), respectively.

The I-Vs illustrate that the p-type oxide hillocks show higher forward current due to a thinner oxide layer compared to the oxides formed on n-type Si and less tendency to oxidise with applied positive and negative bias. Similar to n-type, to confirm this oxide formation on the Si surface, TUNA current images were recorded on p-type for different applied positive and negative bias voltages. After forming oxide hillocks with two positive bias (+0.5 V, +3 V) and negative bias (-0.5 V, -3 V) the TUNA current was measured by applying +1 V to illustrate the conductivity of the oxide hillocks formed under different biases (Figure 6.8). Although p-type has more current at positive bias, the oxide thickness is more similar to n-type Si (see section 6.4.6 for more details)

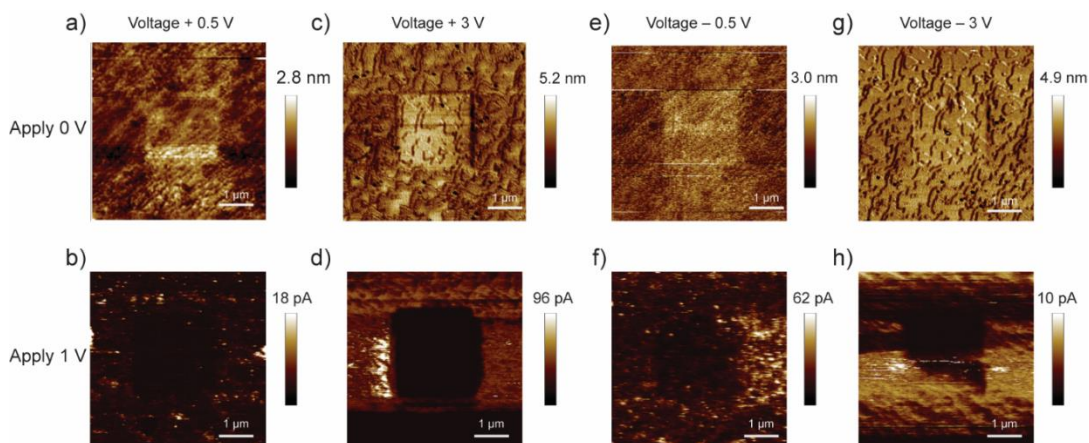


Figure 6. 8 The height topography of the oxide hillocks formed on p-type Si by different bias +0.5 V, -0.5 V, +3 V and -3 V (a, c, e, g) for 8 minutes and TUNA current was read by AFM-PF TUNA mode by applying +1 V bias (b, d, f, h) at scan rate 1 Hz and peak force 554 nN for 4 minutes (one scan)

6.4.3 Si-D versus Si-H

To further examine the effect of electric field versus electric current, we have replaced the H on the Si-H surfaces with Deuterium (Si-D). The D is a heavier atom and therefore it will significantly affect the vibration of the Si-D bond as compared to that of the Si-H bond. Both Si-H and Si-D have a similar capability towards OH⁻ adsorption that is suggested to initiate oxidation at positive biases. Hence, comparing the oxide formation on Si-D and Si-H surfaces will give information about whether electric fields or an electrochemical process is the dominant mechanism of oxide formation. Figure 6.9 shows the height topography and I-Vs for the oxidation of Si-D.

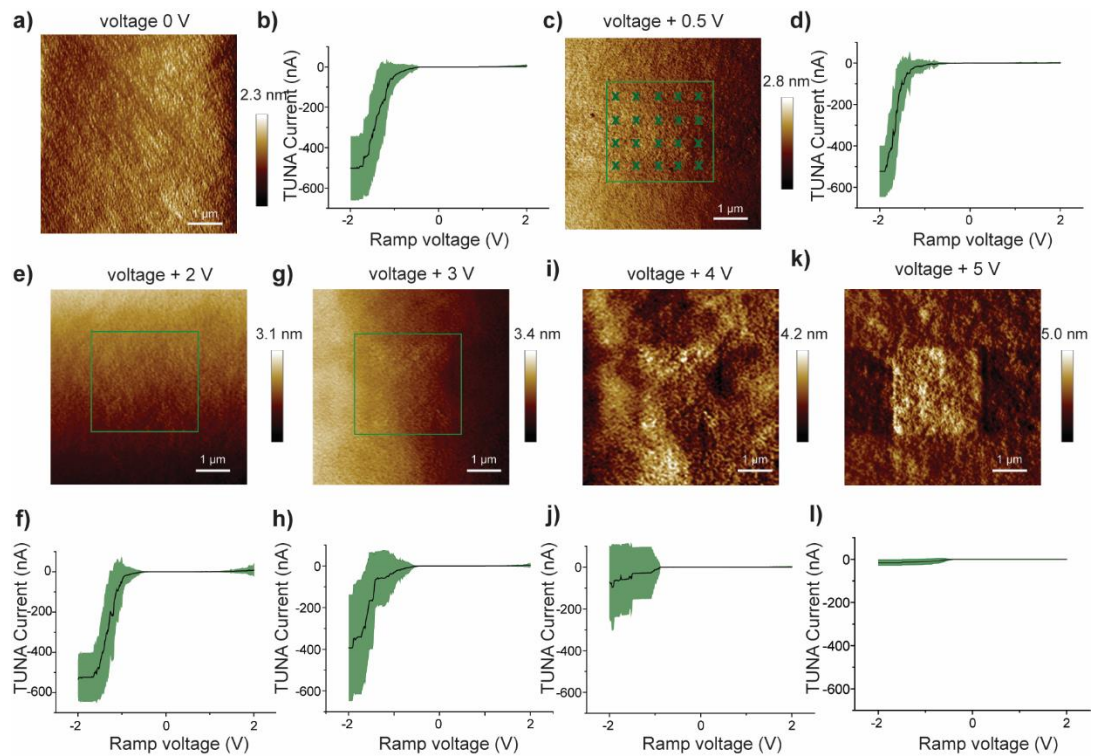


Figure 6. 9 AFM height topography of the oxide hillocks obtain for the n-type Si-D with positive applied bias voltage at 0 V (a), +0.5 V (c), +2 V (e), +3 V (g) and +5 V (i). The corresponding forward and reverse I–V characteristics are presented on the oxide hillocks at 0 V (b), after oxidation of Si(111)–D surface at +0.5 V (d), +2 V (f), +3 V (h) and +5 V (j), respectively with current sensitivity 100 nA/V.

The I–Vs illustrate that the oxide hillocks formed on Si–D show a higher forward current due to the formation of a thinner oxide layer compared to the oxides formed on n– and p–type Si–H and less tendency to oxidise with applied positive bias. Figure 6.10 shows the TUNA Current measured by applying +1 V to illustrate the conductivity of the oxide hillocks formed under different positive biases on Si–D surface.

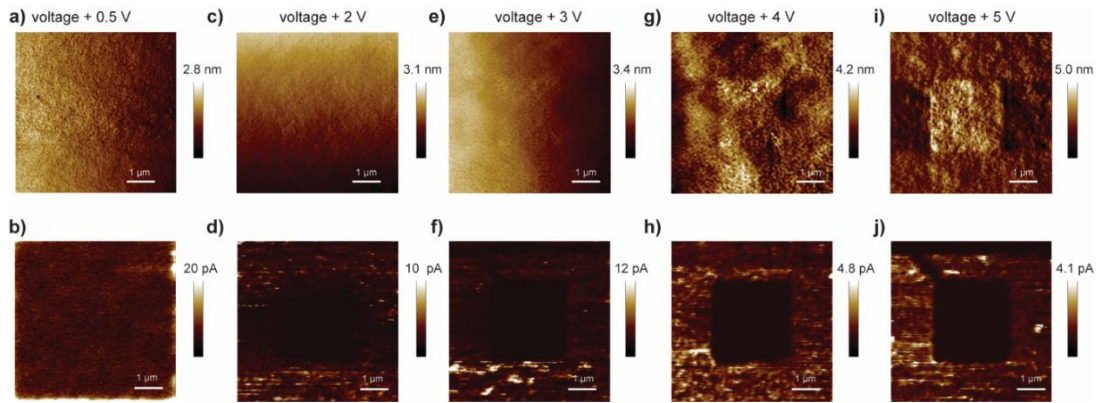


Figure 6. 10 The height topography of the oxide hillocks formed on the n-type Si–D by different bias +0.5 V, +2 V, +3 V, +4 V and +5 V (a, c, e, g, i) for 8 minutes (two scans) and TUNA current was measured by AFM–PF TUNA mode by applying +1 V bias (b, d, f, h, j) at scan rate 1 Hz and peak force 554 nN for 4 minutes (one scan)

According to Figures 6.9 and 6.10, the threshold voltage of Si(111)–D oxidation is +4 V. High forward current observed for the I–Vs of thin oxide hillocks formed below +5 V as shown in Figures 6.9d, 6.9f and 6.9h. The thickness of the oxide is 5 fold less than in n-type, Si(111)–H up to +3 V of applied bias as shown in Figure 6.9. The oxide growth rate of for Si–D is slow compares to Si–H with applied bias as shown in Figure 6.11. Thickness of the oxides are 0.2 ± 0.03 nm, 0.3 ± 0.01 nm, 0.5 ± 0.01 nm, 1.4 ± 0.02 nm, 3.8 ± 0.34 nm and 4.7 ± 0.34 nm for the applied bias of +0.5, +1, +2, +3, +4 V and +5 V, respectively. At the applied bias of +3 V, Si(111)–H surface is completely oxidised and act as an insulator, but Si(111)–D still can pass current in the forward bias (acting as a diode) after applying +3 V, which agrees with the observation that the Si(111)–D oxide hillocks (1.4 ± 0.02 nm, at +3.0 V) are thinner compared to Si(111)–H (4.3 ± 0.09 nm, at +3 V).

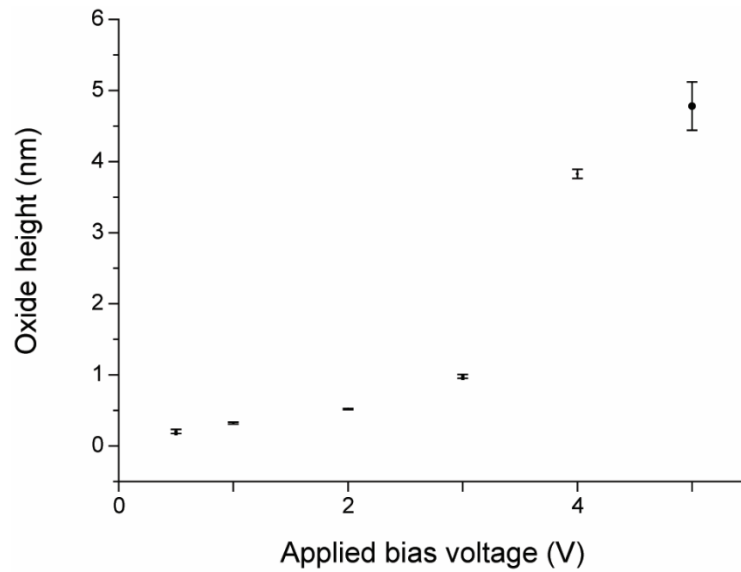


Figure 6. 11 Oxide hillocks heights for n-type Si(111)-D surface as a function of applied positive bias voltage. The oxide thickness is smaller than that of Si(111)-H at the same bias range (see Figure 6.3)

6.4.4 Advanced oxide architecture using different writing bias voltages

The oxide formation can be used to perform advanced lithography where oxide thickness is controlled to give a specific current response. We use both voltage and time to control the oxide thickness as shown in Figure 6.12. The TUNA current and I-V changes of the oxide hillocks forms with the duration of bias applied on Si, oxides were formed on n-type Si at different bias, time and the current was read by applying a negative bias.

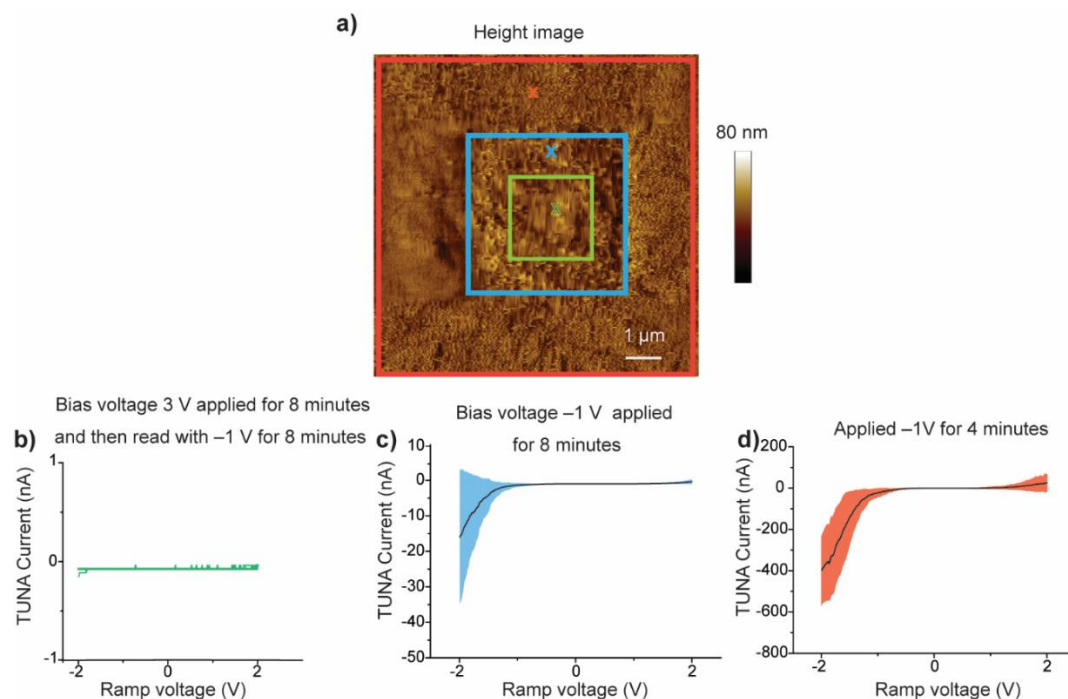


Figure 6. 12 (a) height topography for the area of $10\ \mu\text{m} \times 10\ \mu\text{m}$ Si(111)-H surface oxidised first with +3 V ($2\ \mu\text{m} \times 2\ \mu\text{m}$, 8 minutes), then read with -1 V ($5\ \mu\text{m} \times 5\ \mu\text{m}$, 4 minutes) and finally read again with applying -1 V ($10\ \mu\text{m} \times 10\ \mu\text{m}$, 4 minutes). (b), (d) and (f) are the corresponding I-V curves for the area of A, B and C. Differences of the forward current shows that oxide growth can be controlled to a degree that current-voltage can be predicted in nanodevices.

At the end of the experiment, the area marked in green has been exposed to a total of 16 (four scans) minutes, 8 minutes (two scans) of which are +3 V and -1 V. The area marked in blue has accumulated to a total of 8 minutes of -1 V and the area marked in red is exposed to 4 minutes (one scan) of -1 V. The difference between the blue and red area shows that time at a constant voltage can be used to control the thickness of the oxide. The oxide patterning with different levels of oxide thicknesses on the same surface has practical implications in the design of nanodevices to develop molecular arrays and resistors with different conductivity. Characteristic I-Vs recorded for this study illustrate that the three surface areas exposed to the different voltages have different forward currents as shown in Figures 6.12b, 6.12c and 6.12d. The I-Vs demonstrate that area A is acting as an insulator because of the applied high positive bias (+3 V for 8 minutes and exposed to -1 V for another 8

minutes). Section C shows more forward current than B because -1 V was applied twice (8 minutes) for area B than C (-1 V for 4 minutes).

The experiment results shown in Figure 6.13 was recorded by applying only negative bias voltages. This experiment was carried out by first applying -1 V on the $2 \times 2\ \mu\text{m}$ area for 8 minutes and reading the area by increasing the size to $5\ \mu\text{m}$ with -1 V for 4 minutes, then again increasing the size of the scan area to $10\ \mu\text{m}$ and reading it with -1 V for 4 minutes.

At the end of the experiment, zone "A" has been exposed to a total of 16 minutes with -1 V . The area marked in green has accumulated to a total of 8 minutes of -1 V and the area marked in red is exposed to 4 minutes of -1 V . The tunnelling current changes with the applied voltage as shown in Figure 6.13. TUNA currents are tabulated in Table. 6.1.

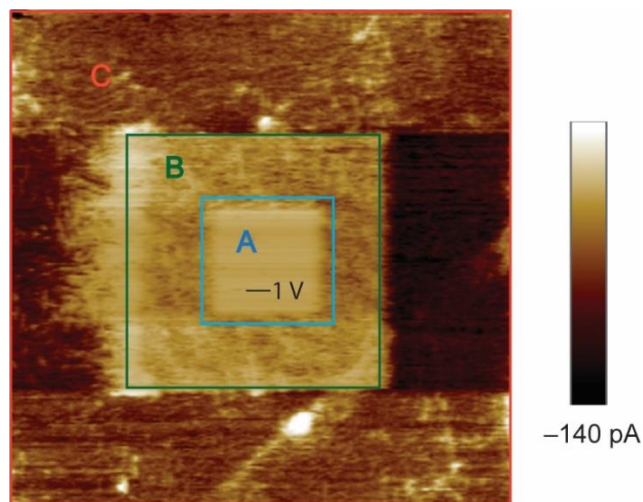


Figure 6. 13 TUNA image for the area of $10 \times 10\ \mu\text{m}$ Si(111)-H surface oxidised first with -1 V ($2 \times 2\ \mu\text{m}$, 8 minutes), then enlarge the area and read with applying -1 V ($5 \times 5\ \mu\text{m}$, 4 minutes) and finally reading the whole image ($10 \times 10\ \mu\text{m}$, 4 minutes) with -1 V .

Table 6.1 TUNA currents recorded for the areas A, B and C of the oxide hillocks formed by negative bias (-1 V).

Area	A voltage applied is -1V	TUNA current/ μA	SD
A	16 accumulated minutes	-1.95	0.80
B	8 accumulated minutes	-21.30	6.61
C	4 minutes	-78.90	9.73

As in Table 6.1, the forward current gradually changes due to the oxide layer formed by the applied negative bias. When the voltage is applied for a long period (16 minutes in total for area A) the forward current is less than areas B (8 minutes) and C (4 minutes). The important observation here is that the thickness of the oxide layer not only depends on the applied bias but also with writing time. Therefore, to a certain degree oxide growth is controlled by writing time when the bias is constant.

6.4.5 Tunable Schottky diodes

Next, we used a platinum AFM tip which has a high work function creates a Schottky diode with Si. In these experiments, the primary aim is to design tunable Schottky diodes using different thicknesses of oxide. Therefore, by oxidising the Si using a range of positive and negative bias to form an oxide layer between this metal–semiconductor junction, the oxide acts as a resistor to change the properties of the Schottky diode as shown in Figure 6.14. Ultimately these metal–oxide–semiconductor junctions can act as future electronic devices on the nanoscale as tunable diodes and insulators. Here, according to the I – V s, the oxide thickness changes only the forward current, not the reverse current. The reason for this behaviour can be attributed to the oxide layer only changing the magnitude of the resistance in the forward current while the reverse current is dominated by the depletion region of the Schottky Pt–Si junction.

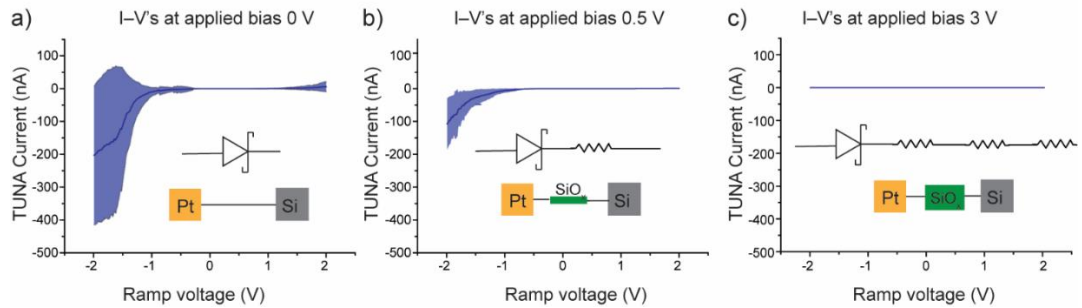


Figure 6. 14 Shows the accumulation of 20 I–V curves of a) Pt–Si (n–type) and Pt–oxide–Si (n–type) junctions (b, c), formed with the applied voltages of (b) +0.5 V and (c) +3 V. The I–V curves averaged from 20 I–Vs of Pt–oxide–Si (n–type) junctions showing a change in the slope beyond an applied forward bias of ca. ± 0.5 V which behave as a tunable Schottky diode. Analogue behaviour was observed with the Pt–oxide–Si (p–type) junctions as shown in Figure 6.6, 6.7.

6.4.6 Possible mechanisms of oxide formation

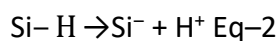
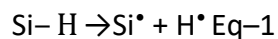
For the n–type, the current is negligible in the reverse bias and therefore applying a positive bias to n–type Si will lead to negligible current and the inverse will happen with p–type Si in which a negative bias to the p–type surface will lead to a negligible current. These I–V plots can be used to identify whether it is the current or the electric field that creates the oxide on Si when a bias is applied between a metallic tip and Si.

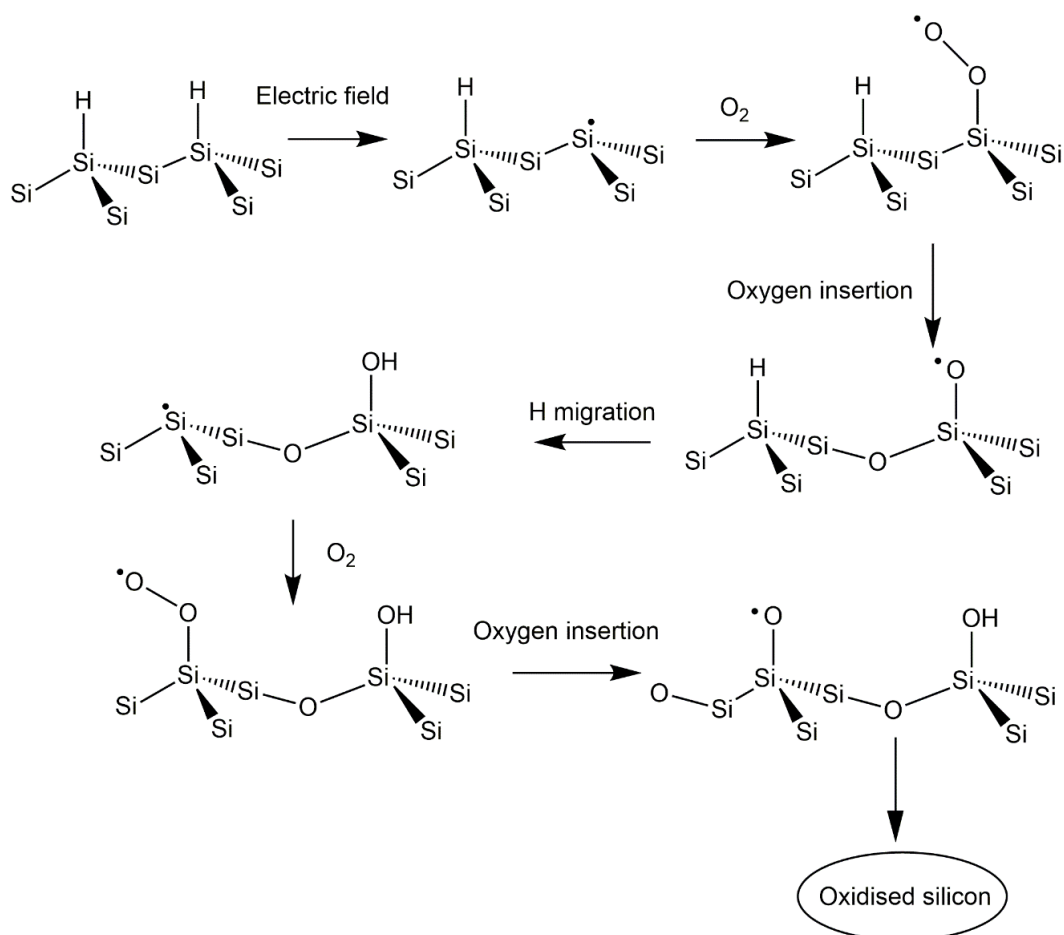
Herein, forward current is affected by both electric current and electric field for both n– and p–type. However, in the reverse current (at reverse bias), there is only electric fields effects in the depletion region with the current between tip and surface being negligible. Applying a positive bias to p–type Si causes a significant increase in the current (under accumulation, forward-biased) however, the opposite happens with the n–type Si (applying positive to n–type Si brings the junction into depletion and negligible current can pass). Hence, it is expected that at significant positive biases (example +3 and +5 V), the p–type Si should show higher oxide formation than n–type if the current is the dominant factor in the formation of the oxide. However, Figure 6.8, shows the oxide layer formed is less in p–type Si at +3, +5 V and junctions allows current to tunnel through the oxide layer. This shows that the forward current in the p–type does not affect the growth of oxide. The thickness of oxide is in a similar

range to that observed with the n-type where the positive voltage gives a negligible forward current. The I-V plots and topography images also show that n-type Si grows less oxide at negative biases (-3 V) than in positive biases (+3 V) where the reverse current is insignificant at positive bias. This shows that even higher current at positive biases is not making a difference for the oxidation of Si, so its effects of electric fields is dominant over current effects.

The electric field can split Si-H bonds either forming ions such as Si⁻, H⁺ or radicals (Si[•] and H[•]) by heterolytic or homolytic cleavage (Eq-1, 2) which then react with molecular oxygen^{15-17, 43-45} to form SiO₂ and Si-OH. For example, silyl radicals can react with the molecular oxygen to form peroxy radicals, that can abstract neighbouring hydrogen to produce a new surface dangling bond as shown in scheme 6.2.

As shown by the experiments on H-terminated Si, oxide formation begins to occur at a bias of +0.5 V and -0.5 V (Figures 6.2, 6.3), which can be attributed to Si-H bond cleavage induced by the electric field when there is a minimal current in the reverse bias.

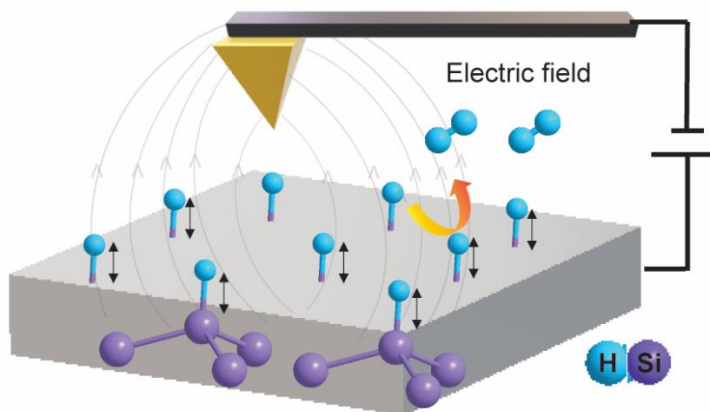




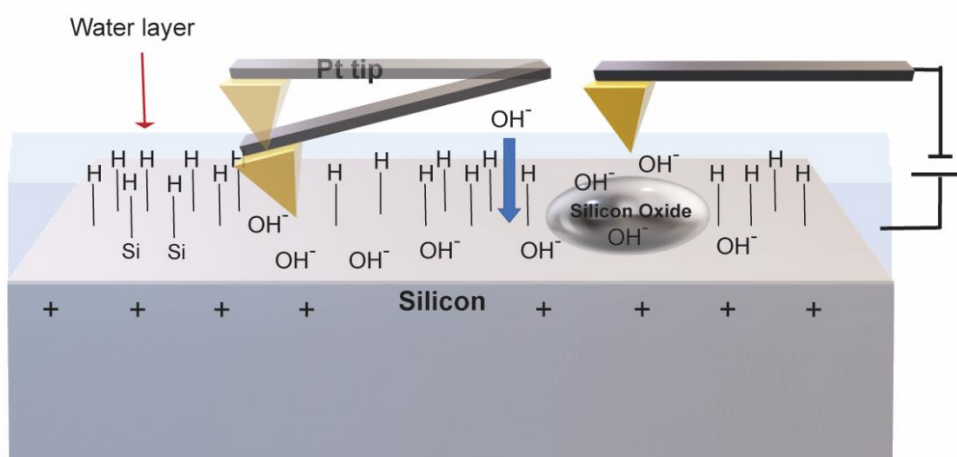
Scheme 6. 2. A possible mechanism for the oxidation of silicon surface by molecular oxygen

The Si–H oxidation in an air of Si(111)–H surface is humidity dependent. Therefore the oxidation of Si–H to Si–OH, H_2O also affecting the rate-limiting step in the native oxide formation.⁴⁴ In addition to the depassivation mechanism by an applied electric field, electrochemical oxidation occurs spontaneously on the Si surface, which accelerated by the positive bias applied on the Si substrate thus it explains a thinner oxide layer formed on Si when applying a negative bias on the Si substrate. The OH^- in the water layer migrates towards the Si surface under a positive applied bias and further induces the oxidation on the Si substrate.^{3, 19, 46} The oxide growth mechanisms under positive bias are schematically presented in Scheme 6.3.

a) Electric field effect



b) Electric field assisted OH^- migration towards Si surface



Scheme 6. 3 Schematic diagram of tip induced oxidation on Si(111)–H surface with a conductive Pt tip keeps in and out contact (tapping) with the sample surface. The surface under the tip is locally oxidized to produce oxide hillocks simultaneously when the tip is moving across the Si(111)–H surface with applied bias voltage. a) illustrate the mechanism of oxidation with the applied electric field and b) represent the electric field-assisted OH^- migration and electrochemical oxidation of Si.

Another indication of electric field effects comes from replacing Si–H by Si–D. When the experiment is repeated with deuterium terminated Si, an isotope effect was observed: the deuterium substituted surface shows two times lower oxidation rate than the hydrogen-terminated Si. The influencing factor for Si oxidation on the D-terminated surface is the electric field effect since the electrochemical oxidation rate is the same for both surfaces when applying a positive voltage on the surface. With

defect creation by the complete replacement of hydrogen with deuterium, the only substantial difference between the isotopes is their mass, leading to a change in their dynamical or vibrational properties. Both H and D feel the same repulsion moving on the excited-state potential energy curve. However, D moves more slowly due to the higher mass of D and, as a result, it stays in the surface longer. Si-D has a shorter vibrational lifetime than Si-H.⁴⁷⁻⁴⁸ The vibrational frequency of the bending mode for Si-H is 650 cm^{-1} compared to 460 cm^{-1} for Si-D.⁴⁹⁻⁵⁰ Therefore, breaking the bond of Si-D is much more difficult than Si-H. At the same time applied external electric field gradually reduced the binding forces between H/D and Si and at one point, the interaction region is mainly dominated by purely repulsive forces that result in desorption of H/ D atoms from the Si surface at a constant temperature where applied electric field redistributes the charges in the system and rearranges to a favourable environment for desorption. Therefore, the dominating factor on oxidation is the electric field effect⁵¹ rather than the electrochemical process. Results obtained in this experiment illustrate that it is possible that substituting with D slows down the rate of depassivation. The desorption yield of deuterium is a strong function of leakage current. The rate of oxidation of Si-D surfaces is slow compared to Si-H which is clearly illustrated in the topography and I-Vs obtained for this system.

6.4.7 Forming conducting oxide channels/ memory devices

Recently, there have been reports of an intrinsic reversible breakdown of silicon oxides, produced by the field-induced movement of oxygen ions in silicon oxide,^{28, 37, 40} which is usually ascribed to the formation of chains of oxygen vacancies. In this chapter, we demonstrate that by applying a high electric field using AFM we can break down the oxide layer in a specific location. This can induce the movement of oxygen ions which can change the electrical properties of oxides changing from an insulator to ohmic contact from the underneath Si.³⁷

The I-V measurements are one of the most sensitive techniques available to probe the formation of defects states in oxides. Therefore, the electrical properties and current images were recorded on oxide before and after applying an electric field on the oxide layer. Conductive AFM images show the correlation between surface

distortion and regions of increased conductivity due to the formation of oxide tunnels as shown in Figure 6.15i. and both polarities can influence the breakage of the oxide layer.^{28, 32, 34}

According to the data obtained, we proposed a mechanism for the formation of these conductive oxide channels on silicon oxide with the applied electric field. Previous work related to the oxide-forming and breaking reported that the rapid oxygen movement through the bulk SiO_x under electrical stress and subsequent deformation of the Si surface underneath. These vacancies act as a mediator for the electron transport between the tip and the surface; however, the mechanisms of the formation of these defect are still being investigated by many groups.

These vacancies in the SiO_x which act as a conducting channel for the electron transfer from bulk silicon to the surface, as supported by observations that can increase current in these channels compared to the surrounding SiO_x as shown in Figure 6.15i. Figure 6.15e and 6.15h show the topography changes before and after applying high electric fields and corresponding I-Vs changes for each stage before and during applying electrical fields as is shown in Figure 6.15f and 6.15j.

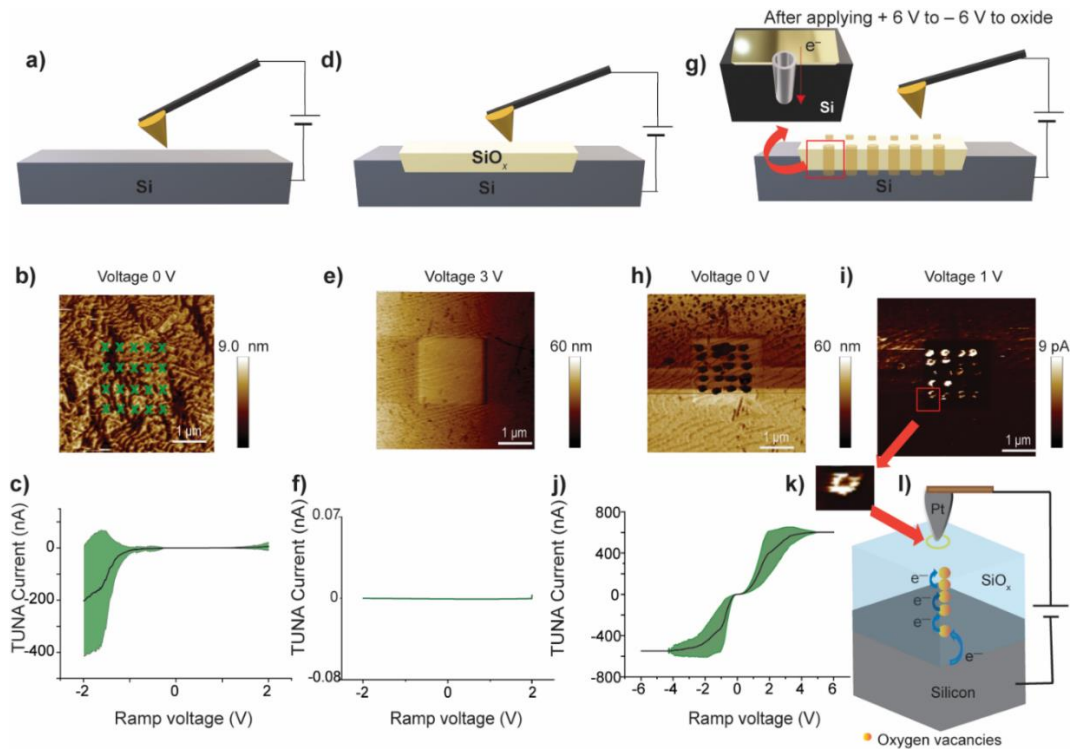


Figure 6.15 a) Schematic representation of the Schottky junction between Pt and Si. b) height topography of the area of $5\ \mu\text{m} \times 5\ \mu\text{m}$ Si(111)-H surface before the oxidation. c) corresponding I-V curves for the area representing in "X" marks in Figure 6.15b. d) Schematic representation of the dense oxide layer formation on Si. e) height topography of the area of $5\ \mu\text{m} \times 5\ \mu\text{m}$ Si(111)-H surface oxidised by applying +3 V f) corresponding I-V curves for the area marked in "X". g) Schematic representation of the formation of electric field-induced defects (conductive tunnels) on oxide by the AFM tip. h) corresponding height image for the area of $5\ \mu\text{m} \times 5\ \mu\text{m}$ Si(111)-H surface oxidised with +3 V and defects formed by 20, -6 to +6 to -6 V ramps i) TUNA current image at an applied bias of +1 V, for the area of $5\ \mu\text{m} \times 5\ \mu\text{m}$ Si(111)-H surface of the oxide tunnels). j) corresponding I-V curves for the creation of oxide defects in h). k) enlarged TUNA current image of one oxide tunnel as seen in i). l) schematic diagram representing the movement of electrons through the low-density oxide with oxygen vacancies.

After the creation of these conducting tunnels onto the oxidised surface, the site of interest was cut out by a focused ion beam (FIB) and the cross-section of one single conductive channel was examined by transmission electron microscopy (TEM) as shown in Figure 6.16. The dark hemisphere appeared around the oxide channel (Figure 6.16e) implies the structural changes of the bulk Si³³ after forming conductive oxide channels, which was not observed in the silicon oxide structure without the formation of these channels. Figure 6.16 d and 6.16 e show the TEM cross-section of oxide channels formed after applying ± 6 V. The white spots in the SEM represent the edge of the oxide holes (blue circle in Figure 6.16c) and larger white regions are the oxide produced by the applied electric field (green circle in Figure 6.16c) instead of forming conductive channels. The nanometer-scale hemisphere appeared under the oxide channel inhomogeneity is evident as contrast variation of the silicon where the size of one oxide channel is ~ 50 nm and depth of the oxide channel is 2–3 nm which is sufficient to reach the bulk silicon to change the properties of the Si–Pt contact from insulating to ohmic.

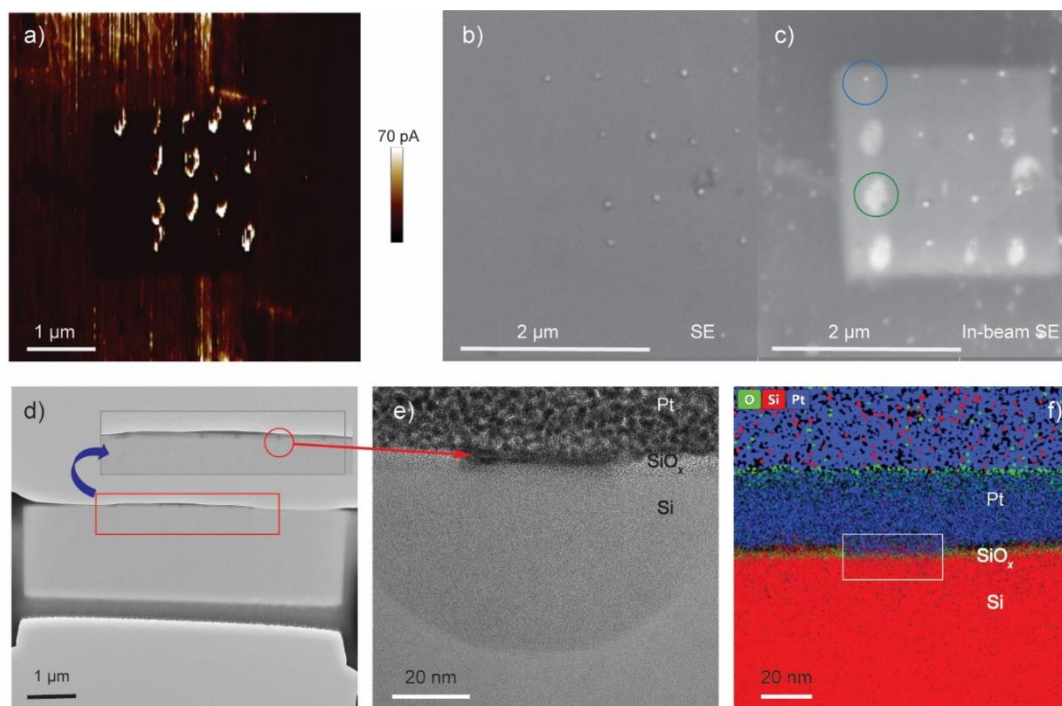


Figure 6.16 Structural changes of the oxide when forming a conducting oxide channel by applying an electrical field a) AFM TUNA current image after forming conductive oxide structures b, c) FIB-SEM images of a with SE detector and in-beam SE detector, respectively. d) dark-field TEM cross-sectional image of the sample after forming oxide channels. e) corresponding image of one oxide channel, showing removal of SiO_x (f) EDX image of one oxide channel. The area marked with the white rectangle indicates the conductive oxide channel, which shows a decrease in oxygen concentration inside the channel

To check the reversibility of the formation of conductive oxide channels by applying a bias back to holes formed on the oxide. The typical I–V curves show switching behaviour as shown in Figure 6.17. The system begins in a high resistance “off” state as shown in Figure 6.17 a-d. The applied bias from –6 to +6 to –6 V, 10 times shows a high conductance and thus a switch to a low resistance “on” state as seen in Figure 6.17 e-h. An applied bias from –2 to +2 to –2 V, 20 times switches this low resistance state to the initial high resistance “off” state as shown in Figure 6.17 i-l. The switching to an “off” state is likely to be silicon oxidation driven by applying a positive bias which is sufficient enough to oxidise the surface. The application of a voltage range greater than ±4V breaks the oxide, switching to the “on” state.

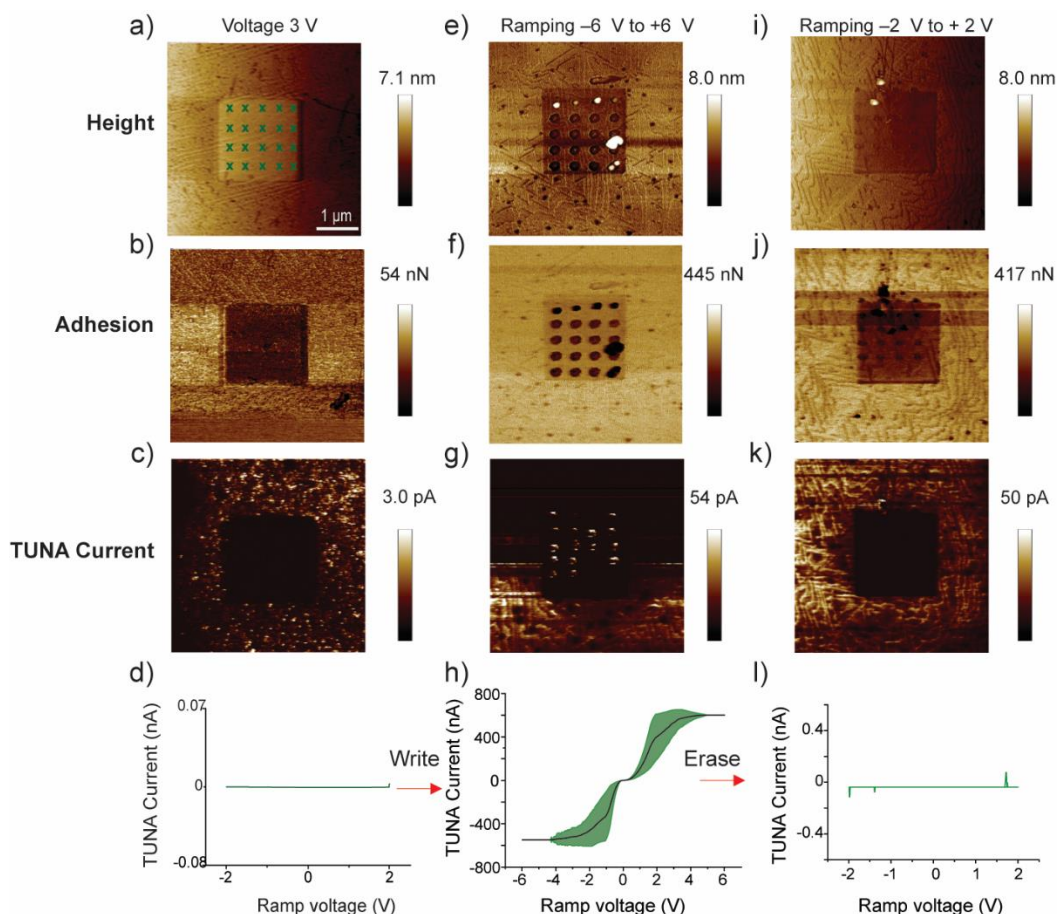


Figure 6.17 a) height image for Si(111)–H surface oxidised with 3 V b) and c) are the adhesion and TUNA current images of a. d) is the corresponding I–V curves for the area marked in “X”. e) corresponding height image for the formation of electric field-induced defects (conductive tunnels) on oxides by AFM tip where the defects formed by ramped with +6 V– (–6 V). f) and g) are the corresponding Adhesion and TUNA current images of e and h) is the corresponding I–V curves for the area conductive channels formed. i) disappearance of the conductive channels in the height topography (5 μm \times 5 μm) after oxidising the conductive channels by applying $\pm 2\text{V}$, where electric field-induced defects (conducting tunnels) formed with applying +6 V– (–6 V). j) and k) are the corresponding Adhesion and TUNA current images of i and d) is the corresponding I–V curves for the area marked in ramps after oxidising the channels with $\pm 2\text{V}$.

To confirm whether these conducting channels formed due to the break down of the oxide, the same voltage range ($\pm 6\text{ V}$) was applied to the freshly prepared Si–H surface without forming the SiO_x . Applying the same voltage range to Si–H shows the

formation of oxide on the particular locations where voltage is applied rather than the formation of conductive channels as shown in Figure 6.18. This behaviour confirmed that to develop oxide channels, first, we have to grow an oxide layer (~2-3 nm) on the surface (Figure 6.18) and break down the SiO_x layer.

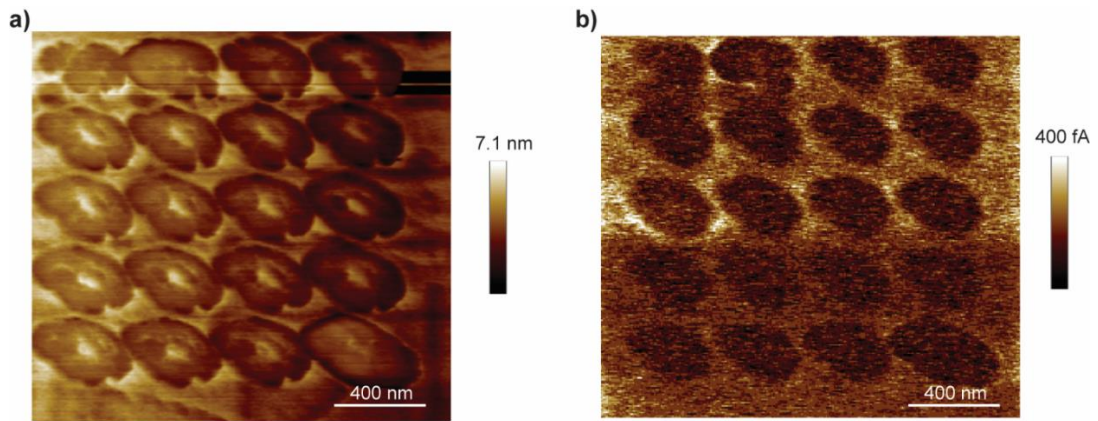


Figure 6.18 a) corresponding height image for the area of $2 \mu\text{m} \times 2 \mu\text{m}$ Si(111)-H surface oxidised by 20, -6 to $+6$ to -6 V ramps b) TUNA current image at an applied bias of $+1$ V, for the area of $2 \mu\text{m} \times 2 \mu\text{m}$ Si(111)-H surface of the oxides showing that without holes there is no conducting channels.

The evidence obtained from conductive AFM, FIB-SEM and TEM shows that by applying high electric fields (± 6 V) we can break down the oxide layer. This process can be reset by applying a smaller bias range (± 2 V) which regrows the oxide again. This work provides evidence of the ability to form reversibly switchable Schottky/ohmic contacts in a highly localised fashion. This has potential applications in future write-erase memory devices.

6.5 Conclusion

The AFM-tip induced oxidation has been performed on both n- and p-type Si(111)-H and, n-type Si(111)-D surfaces to produce protuberant oxide hillock patterns using the AFM-PF TUNA mode. The current-voltage properties of these oxide hillocks have been investigated by recording the I-V plots and TUNA current images. Here, the AFM tip induced oxidation method is used to construct oxide patterns with different thicknesses, where it can act as a tunnelling barrier to control the current passing through the metal-semiconductor junction, demonstrating that the thin oxide layers

can behave as a tunable Schottky diode with different rectification ratios. By examining the I–V data and oxide growth, the mechanism of the AFM tip induced oxidation of H–terminated Si was studied by separating the effect of the electric field from the electric current by forming Schottky diodes with a platinum AFM tip with both n–type and p–type Si. At the positive voltages, p–type formed an oxide layer which is not thick and it allows current to pass through the oxide layer. This proves that the forward current in the p–type does not affect the growth of oxide. Similar behaviour was observed with the n–type when applying negative voltages. Hence, I–Vs showed that there is zero contribution from tunnelling and oxidation is based only on the electric field. It is also found that the oxide hillocks height increase gradually for Si(111)–H and Si(111)–D surfaces with increasing the applied voltage when writing speed, humidity, temperature and peak force are kept constant. Compared to Si–H, Si–D surfaces show a very slow rate of oxidation up to +3 V. This indicates that the substitution of H with D strongly influences the oxidation process on Si. The D–terminated Si surfaces possess a similar oxidation mechanism to that on a H substituted Si surface, but the rate of oxidation is lower due to the difference between the masses, leading to a change in their dynamical or vibrational properties. This allows D to stay on the surface longer in the presence of an electric field aside from an additional degradation of the Si bulk due to the electrochemical oxidation. The threshold voltage differences of these two surfaces is a great advantage to Si–based nanofabrication since the isotope substitution can tailor the surface oxidation rate. This study also demonstrates that voltages can be used for patterning of Si surfaces with different thicknesses and electrical properties. In contrast to Si(111)–H, Si(111)–D surface threshold voltage is high (+4 V). Therefore, lower voltages below +2 V and negative voltages up to –3 V with the same writing speed can induce oxidation on the Si substrates which can act as tunable Schottky diodes and also can avoid the negative effects on the electrical characteristics of the adjacent region, which is of great benefit to the fabrication of integrated nanometre-sized oxide height based electronic devices such as nanowires and resistors in future molecular electronic devices.

After developing different oxide densities, results showed that applying a high voltage such as (–6 V to +6 V) can break the insulating oxide layer. The insulating

properties of the oxide changed into ohmic properties. By applying a low voltage back to these conducting channels, oxygen vacancies get blocked by the SiO_x and this process becomes reversible. This can be used as a potential application for future memory devices. These conducting channels were investigated by using the AFM peak force tunnelling current (PF-TUNA) technique and focussed ion beam milling combined with scanning electron microscopy (FIB-SEM). A cross-section of one single conducting channel was examined by transmission electron microscopy (TEM) and energy dispersive X-ray analysis (EDX). Results show that that the thin oxide layers can form a tunable Schottky diode with different rectification ratios and also this work proves that SiO_x structures can have other behaviours than simply insulating and that oxide formation and breakdown with potential for use in developing memory devices.

6.6 Acknowledgement

This work was supported by the Australian Research Council for grants DE160101101 and DE160100732. M.C.R Peiris also thank John de Laeter Centre for the assistance with TEM, FIB-SEM measurements, Curtin International Postgraduate Research Scholarship and Research Stipend Scholarship (CIPRS) and Department of Chemistry, Curtin University (SPM facilities).

6.7 References

1. Dagata, J. A.; Schneir, J.; Harary, H. H.; Evans, C.; Postek, M. T.; Bennett, J., Modification of hydrogen-passivated silicon by a scanning tunneling microscope operating in air. *Appl. Phys. Lett.* **1990**, *56* (20), 2001-2003.
2. Yasutake, M.; Ejiri, Y.; Hattori, T., Modification of silicon surface using atomic force microscope with conducting Probe. *Jpn. J. Appl. Phys.* **1993**, *32* (Part 2, No. 7B), L1021-L1023.
3. Gordon, A.; Fayfield, R.; Litfin, D.; Higman, T., Mechanisms of surface anodization produced by scanning probe microscopes. *J. Vac. Sci. Technol., B: Microelectron. Nanometer Struct.--Process., Meas., Phenom.* **1995**, *13* (6), 2805-2808.
4. Bernal, A. G. Á.; Bonilla, R. S., Local anodic oxidation on silicon (100) substrates using atomic force microscopy. *Dyna* **2012**, *79* (174), 58-61.
5. Avouris, P.; Martel, R.; Hertel, T.; Sandstrom, R., AFM-tip-induced and current-induced local oxidation of silicon and metals. *Appl. Phys. A: Mater. Sci. Process.* **1998**, *66*, S659-S667.
6. Avouris, P.; Hertel, T.; Martel, R., Atomic force microscope tip-induced local oxidation of silicon: kinetics, mechanism, and nanofabrication. *Appl. Phys. Lett.* **1997**, *71* (2), 285-287.
7. Tello, M.; García, R., Nano-oxidation of silicon surfaces: Comparison of noncontact and contact atomic-force microscopy methods. *Appl. Phys. Lett.* **2001**, *79* (3), 424-426.
8. Avouris, P.; Walkup, R. E.; Rossi, A. R.; Shen, T. C.; Abeln, G. C.; Tucker, J. R.; Lyding, J. W., STM-induced H atom desorption from Si(100): Isotope effects and site selectivity. *Chem. Phys. Lett.* **1996**, *257* (1), 148-154.
9. Maynor, B. W.; Li, Y.; Liu, J., Au "Ink" for AFM "Dip-Pen" nanolithography. *Langmuir*. **2001**, *17* (9), 2575-2578.
10. Li, Y.; Maynor, B. W.; Liu, J., Electrochemical AFM "Dip-Pen" nanolithography. *J. Am. Chem. Soc.* **2001**, *123* (9), 2105-2106.
11. Buyukkose, S.; Okur, S.; Aygun, G., Local oxidation nanolithography on HF thin films using atomic force microscopy (AFM). *J. Phys. D: Appl. Phys.* **2009**, *42* (10), 105302.

12. Monreal, R.; Apell, S. P., Electromagnetic-field-enhanced desorption of atoms. *Phys. Rev. B* **1990**, *41* (11), 7852-7855.
13. Tománek, D.; Kreuzer, H. J.; Block, J. H., Tight-binding approach to field desorption: N₂ on Fe(111). *Surf. Sci. Lett.* **1985**, *157* (1), L315-L322.
14. Surya, V. J.; Iyakutti, K.; Mizuseki, H.; Kawazoe, Y., First principles study on desorption of chemisorbed hydrogen atoms from single-walled carbon nanotubes under external electric field. *Int. J. Hydrogen Energy* **2011**, *36* (21), 13645-13656.
15. Chatgililoglu, C.; Timokhin, V. I., 2 Silyl radicals in chemical synthesis. *Adv. Organomet. Chem.* **2008**, *57*, 117.
16. Harper, J.; Sailor, M. J., Photoluminescence quenching and the photochemical oxidation of porous silicon by molecular oxygen. *Langmuir*. **1997**, *13* (17), 4652-4658.
17. Miura, T. a.; Niwano, M.; Shoji, D.; Miyamoto, N., Kinetics of oxidation on hydrogen-terminated Si(100) and (111) surfaces stored in air. *J. Appl. Phys.* **1996**, *79* (8), 4373-4380.
18. Sugimura, H.; Nakagiri, N., Chemical approach to nanofabrication: Modifications of silicon surfaces patterned by scanning probe anodization. *Jpn. J. Appl. Phys.* **1995**, *34* (6S), 3406.
19. Marchi, F.; Bouchiat, V.; Dallaporta, H.; Safarov, V.; Tonneau, D.; Doppelt, P., Growth of silicon oxide on hydrogenated silicon during lithography with an atomic force microscope. *J. Vac. Sci. Technol., B: Microelectron. Nanometer Struct.--Process., Meas., Phenom.* **1998**, *16* (6), 2952-2956.
20. Jorgensen, P. J., Effect of an electric field on silicon oxidation. *J. Chem. Phys.* **1962**, *37* (4), 874-877.
21. Avouris, P.; Martel, R.; Hertel, T.; Sandstrom, R., AFM-tip-induced and current-induced local oxidation of silicon and metals. *Applied Physics A: Materials Science & Processing* **1998**, *66* (7).
22. Snow, E.; Campbell, P., AFM fabrication of sub-10-nanometer metal-oxide devices with in situ control of electrical properties. *Science* **1995**, *270* (5242), 1639-1641.
23. Matsumoto, K.; Takahashi, S.; Ishii, M.; Hoshi, M.; Kurokawa, A.; Ichimura, S.; Ando, A., Application of STM nanometer-size oxidation process to planar-type MIM diode. *Jpn. J. Appl. Phys.* **1995**, *34* (2S), 1387.

24. Foley, E. T.; Kam, A. F.; Lyding, J. W.; Avouris, P., Cryogenic UHV-STM study of hydrogen and deuterium desorption from Si(100). *Phys. Rev. Lett.* **1998**, *80* (6), 1336-1339.
25. Palik, E.; Holm, R.; Stella, A.; Hughes, H., Stark effect of SiOH and SiH molecules in SiO₂. *J. Appl. Phys.* **1982**, *53* (12), 8454-8461.
26. Luo, Y.-R.; Kerr, J., Bond dissociation energies. *CRC Handbook of Chemistry and Physics* **2012**, *89*, 89.
27. Menzel, D.; Gomer, R., Desorption from surfaces by slow-electron impact. *J. Chem. Phys.* **1964**, *40* (4), 1164-1165.
28. Cario, L.; Vaju, C.; Corraze, B.; Guiot, V.; Janod, E., Electric-field-induced resistive switching in a family of Mott insulators: Towards a new class of RRAM memories. *Adv. Mater.* **2010**, *22* (45), 5193-5197.
29. Zhu, L.; Zhou, J.; Guo, Z.; Sun, Z., An overview of materials issues in resistive random access memory. *J. Materiomics* **2015**, *1* (4), 285-295.
30. Shang, J.; Liu, G.; Yang, H.; Zhu, X.; Chen, X.; Tan, H.; Hu, B.; Pan, L.; Xue, W.; Li, R. W., Thermally stable transparent resistive random access memory based on all-oxide heterostructures. *Adv. Funct. Mater.* **2014**, *24* (15), 2171-2179.
31. Liu, C.; Wang, L.-G.; Qin, K.; Cao, Y.-Q.; Zhang, X.-J.; Wu, D.; Li, A.-D., Impact of metal nanocrystal size and distribution on resistive switching parameters of oxide-based resistive random access memories. *IEEE Trans. Electron Devices* **2018**, *65* (10), 4674-4678.
32. Jiang, W.; Miao, J.; Li, T., Silicon mode-selective switch via horizontal metal-oxide-semiconductor capacitor incorporated with ENZ-ITO. *Sci. Rep.* **2019**, *9* (1), 1-12.
33. Mehonic, A.; Buckwell, M.; Montesi, L.; Munde, M. S.; Gao, D.; Hudziak, S.; Chater, R. J.; Fearn, S.; McPhail, D.; Bosman, M., Nanoscale transformations in metastable, amorphous, silicon-rich silica. *Adv. Mater.* **2016**, *28* (34), 7486-7493.
34. Kamiya, K.; Young Yang, M.; Park, S.-G.; Magyari-Köpe, B.; Nishi, Y.; Niwa, M.; Shiraishi, K., ON-OFF switching mechanism of resistive-random-access-memories based on the formation and disruption of oxygen vacancy conducting channels. *Appl. Phys. Lett.* **2012**, *100* (7), 073502.
35. Yao, J.; Sun, Z.; Zhong, L.; Natelson, D.; Tour, J. M., Resistive switches and memories from silicon oxide. *Nano Lett.* **2010**, *10* (10), 4105-4110.

36. Bakan, G.; Gokirmak, A.; Silva, H., Suppression of thermoelectric Thomson effect in silicon microwires under large electrical bias and implications for phase-change memory devices. *J. Appl. Phys.* **2014**, *116* (23), 234507.
37. Li, C.; Jiang, H.; Xia, Q., Low voltage resistive switching devices based on chemically produced silicon oxide. *Appl. Phys. Lett.* **2013**, *103* (6), 062104.
38. Starodub, D.; Gusev, E.; Garfunkel, E.; Gustafsson, T., Silicon oxide decomposition and desorption during the thermal oxidation of silicon. *Surf. Rev. Lett.* **1999**, *6* (01), 45-52.
39. Deal, B. E.; Grove, A., General relationship for the thermal oxidation of silicon. *J. Appl. Phys.* **1965**, *36* (12), 3770-3778.
40. Deaton, R.; Massoud, H., Manufacturability of rapid-thermal oxidation of silicon: oxide thickness, oxide thickness variation, and system dependency. *IEEE Trans. Semiconductor manufacturing* **1992**, *5* (4), 347-358.
41. Hopper, M.; Clarke, R.; Young, L., Thermal oxidation of silicon: In situ measurement of the growth rate using ellipsometry. *J. Electrochem. Soc.* **1975**, *122* (9), 1216.
42. Vogel, Y. B.; Zhang, L.; Darwish, N.; Gonçalves, V. R.; Le Brun, A.; Gooding, J. J.; Molina, A.; Wallace, G. G.; Coote, M. L.; Gonzalez, J., Reproducible flaws unveil electrostatic aspects of semiconductor electrochemistry. *Nat. Commun.* **2017**, *8* (1), 2066.
43. Salazar, K. L.; Nicholas, K. M., (Alkynyl)dicobalt hexacarbonyl-mediated radical cyclizations. *Tetrahedron* **2000**, *56* (15), 2211-2224.
44. Miura, T. a.; Niwano, M.; Shoji, D.; Miyamoto, N., Kinetics of oxidation on hydrogen-terminated Si (100) and (111) surfaces stored in air. *Journal of applied physics* **1996**, *79* (8), 4373-4380.
45. Morse, K. A.; Pianetta, P., Room temperature photo-oxidation of NH₄F-prepared H-Si(111)(1×1) and H_x-Si(100). *J. Appl. Phys.* **2004**, *96* (11), 6851-6858.
46. Ma, Y. R.; Yu, C.; Yao, Y. D.; Liou, Y.; Lee, S. F., Tip-induced local anodic oxidation on the native SiO₂ layer of Si(111) using an atomic force microscope. *Phys. Rev. B* **2001**, *64* (19), 195324.
47. Guyot-Sionnest, P.; Dumas, P.; Chabal, Y.; Higashi, G., Lifetime of an adsorbate-substrate vibration: H on Si (111). *Phys. Rev. Lett.* **1990**, *64* (18), 2156.

48. Guyot-Sionnest, P.; Lin, P.; Hiller, E., Vibrational dynamics of the Si–H stretching modes of the Si (100)/H: 2× 1 surface. *J. Chem. Phys.* **1995**, *102* (10), 4269-4278.
49. Lucovsky, G.; Yang, J.; Chao, S.; Tyler, J.; Czubytyj, W., Oxygen-bonding environments in glow-discharge-deposited amorphous silicon-hydrogen *J. Non-Cryst. Solids* **1983**, *59* (60), 609-612.
50. Lucovsky, G.; Chao, S.; Yang, J.; Tyler, J.; Czubytyj, W., Coupled local mode vibrations in a-Si alloy films. *J. Vac. Sci. Technol., A* **1984**, *2* (2), 353-357.
51. Ciampi, S.; Darwish, N.; Aitken, H. M.; Díez-Pérez, I.; Coote, M. L., Harnessing electrostatic catalysis in single molecule, electrochemical and chemical systems: a rapidly growing experimental tool box. *Chem. Soc. Rev.* **2018**, *47* (14), 5146-5164.

Every reasonable effort has been made to acknowledge the owners of copyright material. I would like to apologise if any copyright owner who has been omitted or incorrectly acknowledged.

Chapter 7

Conclusions and future outlook

7.1 Conclusions

Using a single molecule as a component in an electronic device offers a solid answer to the quest of extending Moore's law into the 21st century. Molecules are advantageous not only because of their smaller size but also because of their diversity that offers properties beyond the reach of current electronics technology. This research discussed factors that govern the discovery and exploitation of the electronic properties of molecules on semiconductors as building blocks for nanoscale electronics.

Molecular electronics in its current state suffers from a few drawbacks. The majority of work to date has been restricted to highly specialised and expensive materials such as gold. However, gold is unlikely to be implemented in molecular electronics at a practical level. Another challenge of using molecules as electrical entities is to make stable contacts at ambient conditions. This thesis addressed these issues by developing stable molecule contacts on the micro (monolayers) and single-molecular level which can be separated using insulating SiO_x developed by AFM.

While Chapter One provided a brief overview of the thesis, Chapter Two presented a comprehensive literature review. The characterization techniques and experimental details were described in Chapter Three.

Chapter Four described the fabrication of stable molecular junctions on a non-gold substrate material by using diazonium salts on silicon surfaces. Here, a Si–C top-to-bottom single-molecule device was developed with the mechanical stability of 1.1 ± 0.2 s, a significant advancement in terms of stability and substrate material. This study showed that molecular contacts of diazonium salt derivated monolayers on silicon can be synthesised electrochemically and spontaneously. The monolayers on gold and silicon substrates were modified by spontaneously attaching ferrocene to the distal end of the diazonium molecule. This was further characterised by various spectroscopic and electrochemical techniques.

Furthermore, the electrochemical reduction of diazonium salts on different crystalline facets of Si was studied. Results showed that the grafting of diazonium salts was crystal-facet dependent and more favourable on Si(111) than Si(100). To confirm these assignments, microstructures of Si (111) were created on Si (100) surface by anisotropic etching. By doing so, the surfaces were used to probe in-situ the difference in the electrochemical reduction between the two crystal facets. This find is of great significance in terms of practical implications such as patterning of molecules for electronic devices.

Chapter Five described Si–S contacts developed using 1,6-hexanedithiol on a silicon substrate. These contacts showed a record lifetime for single-molecule junctions with a lifetime of 2.7 s at room temperature. This brings the field of single-molecule electronics into a workable timescale. For example, I–Vs can be obtained while a single-molecule in contact or light can be used to stimulate switching while the molecule is between two silicon electrodes.

Analogous to diazonium salts, thiols reacted spontaneously when the thiol is exposed to ambient oxygen. When thiols are exposed to oxygen, thiols are converted to a disulfide, which is in equilibrium with thiyl radicals. DFT calculations indicated that thiyl radicals produced in solution by the O_2 can react barrierlessly with Si(111)–H to initiate a subsequent free-radical reaction between the surface and solution thiols.

Thiol modified surfaces were characterized by various techniques, including X-ray photoelectron spectroscopy (XPS). XPS showed SAMs of 1,6-hexanedithiol on silicon with the presence of distal free thiol groups (R-S-H) and R-S-Si bonds. This is important because now thiols that have been long used on Au can be implemented on Si to merge silicon and molecular electronics.

Chapter Six demonstrates that SiO_x structures can have other behaviours than simply insulating. The oxide structures on Si can be used as an insulator to separate arrays of molecules. These structures can also act as a tunable diode that depends on the thickness of the oxide layer, demonstrating that the thin oxide layers can behave as a tunable Schottky diode with different rectification ratios. Chapter Six also showed an isotope effect where the bias voltage needed to oxidize the Si surface to form a uniform and insulating dielectric layer of oxide on Si(111)-H is lower than compared to the isotope substituted Si(111)-D. Therefore, the difference of the threshold voltage of these surfaces is an advantage when developing oxide-free monolayers on Si and for Si-based nanofabrication. This isotope substitution can tailor the surface properties such as the thickness of oxides on Si and electrical properties without complicating the controllability of other external factors.

Examining the I-V data and oxide growth for different types of silicon showed that there is an insignificant contribution from tunnelling current for the oxidation and that oxidation is based only on the applied electric field. Importantly, this chapter demonstrated that topography is deceptive in visually assessing the oxide formation on Si as minimal changes in the oxide thickness lead to a large change in the electrical measurement. Therefore, current measurements can be used as a tool to read the less dense oxide patterns which is a turning point of this work and allowed us to study unknown electrical properties of oxides.

Another important aspect of this work illustrated that SiO_x structures have switching behaviours where insulating SiO_x can be changed to conducting offering prospects as a memory device for nanoelectronics. This work showed that the oxide layer can break down by applying a high bias using an AFM tip. With the applied high bias, the oxide layer develops conducting oxide channels and the properties of the oxide changed from insulating to ohmic. These conductive oxide channels can be blocked by applying a low bias voltage, reversing the process. This switching between

Schottky and ohmic contacts can potentially be used for nanoscale memory devices and shows that the insulating behaviour of the oxide is not a fixed property; but rather is dynamic. This tunable oxide layer can have potential applications in advanced nanoelectronic devices where it can be used as a tunable diode, memory device or insulator.

7.2 Future outlook

The work in this thesis achieved a remarkable single-molecule junction lifetime by using flexible molecules. This junction lifetime can further be increased by using long and rigid yet conductive molecules connecting between silicon electrodes. However, as the molecular length increases so does the resistivity which dissipates energy in the form of heat, so the use of highly conductive molecules is critical. The rigidity of the molecule is also important as rigid molecules prevent rotation or the attachment of both ends of the molecules to the same surface. These factors prevent mechanical instability ensuring good control of the molecular junction and allow us to graft trillions of molecular wires, transistors and switches on to a semiconducting surface. Therefore, in future by using long, rigid and conductive molecules such as norbornylogous bridges (NB) with anthraquinone, oligophenyls, oligonaphthalenes, oligonaphthalenediimide, oligoperylenediimides or carbon nanostructures like carbon nanotubes or fullerenes, these issues in molecular electronics can be overcome.

Another suggestion is by combining stable contacts with metal nanostructures or quantum dots that support light-driven coherent collective electron oscillations called plasmons. This combination of conjugated molecules with plasmonic nanostructures will increase the length of the molecular wire without decreasing its conductivity. It will allow greater tuning of the properties of the molecule leading to the development of efficient electron transfer through the longest available molecular wires for electronic circuits.

This thesis presents a new chemical technology that allows reproducible silicon–molecule–silicon contacts to be built, utilizing strong Si–S and Si–C covalent bonding to fabricate Si–molecule–Si devices into future different doping of Si can be used to form P–N junctions. P–N junctions are usually made by doping one piece of silicon with n- and p-type dopants. P–molecule–N devices are the next step for this work. Various P–N heterojunctions can be constructed to obtain high rectification ratios. In addition, irradiation with light can be used to create a current inside the silicon offering more control of the junction. This is a fertile field for study, as shown in Figure 7.1. This will provide a way for the merging of silicon electronics with molecular electronics to provide the ultimate in component design.

As in Chapter Six, Si oxides show very promising properties which can replace molecules in electronic circuitry. In particular, the switchable conducting channels provide a promising avenue for applications in electronic devices and future work will investigate how this switching will depend on different dopings of silicon type and concentration. Similar to molecules, oxides also can be used as electronic components in nanoscale devices.

Future directions of molecular electronics

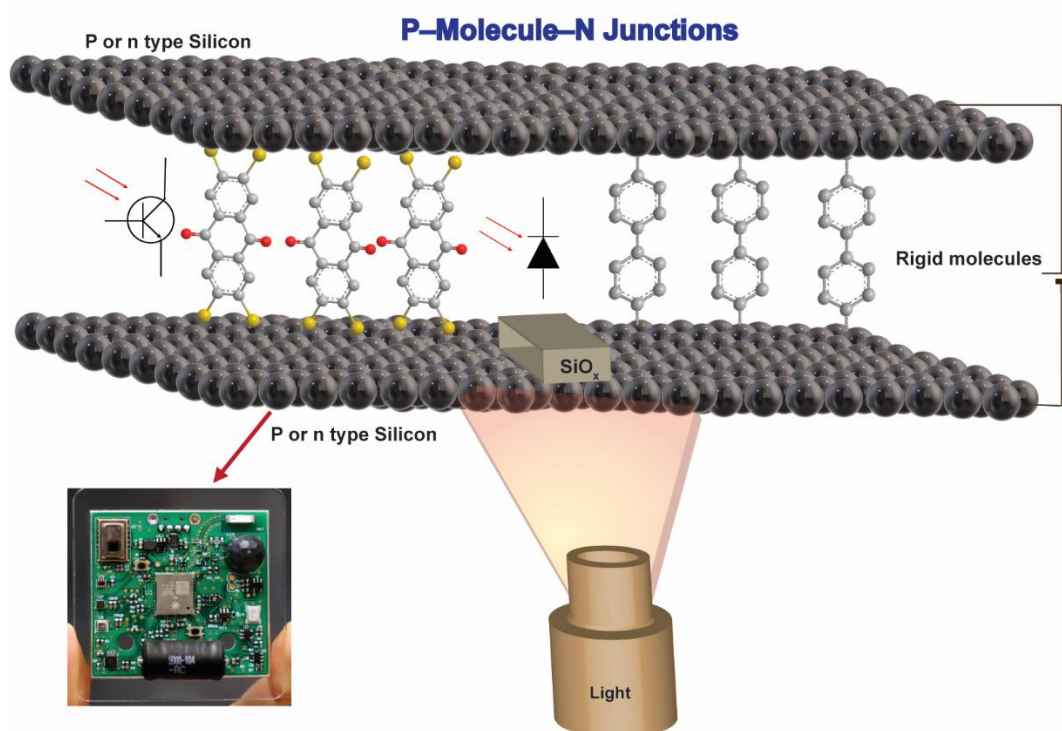


Figure 7.1 P–molecule–N devices for the nanoscale molecular electronic devices

Appendix A

Figure 2.2

RE: Permission Request Form: Malwattage

CONTRACTS-COPYRIGHT (shared) <Contracts-Copyright@rsc.org>

Fri 20/09/25 2:33 PM

To:

Chandramalika Peiris <m.c.peiris@postgrad.curtin.edu.au>

Dear Matwattage

The Royal Society of Chemistry hereby grants permission for the use of the material specified below in the work described and in all subsequent editions of the work for distribution throughout the world, in all media including electronic and microfilm. You may use the material in conjunction with computer-based electronic and information retrieval systems, grant permissions for photocopying, reproductions and reprints, translate the material and to publish the translation, and authorize document delivery and abstracting and indexing services. The Royal Society of Chemistry is a signatory to the STM Guidelines on Permissions (available on request).

Please note that if the material specified below or any part of it appears with credit or acknowledgement to a third party then you must also secure permission from that third party before reproducing that material.

Please ensure that the published article carries a credit to The Royal Society of Chemistry (see <http://rsc.li/permissions> for details) and that any electronic version of the work includes a hyperlink to the article on the Royal Society of Chemistry website.

Regards

Gill Cockhead

Contracts & Copyright Executive

Gill Cockhead

Figure 2.4

LSEVIER LICENSE TERMS AND CONDITIONS

Sep 23, 2020

This Agreement between Curtin University ("You") and Elsevier ("Elsevier") consists of your license details and the terms and conditions provided by Elsevier and Copyright Clearance Center.

License Number	4914691395150
License date	Sep 23, 2020
Licensed Content Publisher	Elsevier
Licensed Content Publication	Bioelectrochemistry
Licensed Content Title	DNA biosensors based on gold nanoparticles-modified graphene oxide for the detection of breast cancer biomarkers for early diagnosis
Licensed Content Author	Ayman Ali Saeed,Josep Lluís Acero Sánchez,Ciara K. O'Sullivan,Mohammed Nooredeen Abbas
Licensed Content Date	Dec 1, 2017
Licensed Content Volume	118
Licensed Content Issue	n/a
Licensed Content Pages	9
Start Page	91
End Page	99
Type of Use	reuse in a thesis/dissertation
Portion	figures/tables/illustrations
Number of figures/tables/illustrations	1
Format	both print and electronic
Are you the author of this Elsevier article?	No
Will you be translating?	No
Title	Covalently linked molecule–electrode contacts toward robust molecular-electronics circuits
Institution name	Curtin
Expected presentation date	Oct 2020
Portions	1
Requestor Location	Curtin University Kent street
	Bentley, Western Australia 6102 Australia Attn: Curtin University
Publisher Tax ID	GB 494 6272 12
Total	0.00 AUD
Terms and Conditions	

Figure 2.6

The screenshot displays the RightsLink interface. At the top, there are logos for the Copyright Clearance Center and RightsLink, along with navigation links for Home, Help, Email Support, and a user profile for Malwattage Peiris. The main content area features a white box with the following information:

Binding Motif of Terminal Alkynes on Gold Clusters
Author: Prasenjit Maity, Shinjiro Takano, Seiji Yamazoe, et al
Publication: Journal of the American Chemical Society
Publisher: American Chemical Society
Date: Jun 1, 2013
Copyright © 2013, American Chemical Society

Below this, a section titled "PERMISSION/LICENSE IS GRANTED FOR YOUR ORDER AT NO CHARGE" explains that this type of permission is granted because no fee is charged. It lists the following conditions:

- Permission is granted for your request in both print and electronic formats, and translations.
- If figures and/or tables were requested, they may be adapted or used in part.
- Please print this page for your records and send a copy of it to your publisher/graduate school.
- Appropriate credit for the requested material should be given as follows: "Reprinted (adapted) with permission from (COMPLETE REFERENCE CITATION), Copyright (YEAR) American Chemical Society." Insert appropriate information in place of the capitalized words.
- One-time permission is granted only for the use specified in your request. No additional uses are granted (such as derivative works or other editions). For any other uses, please submit a new request.

If credit is given to another source for the material you requested, permission must be obtained from that source. At the bottom of the white box are two buttons: "BACK" and "CLOSE WINDOW".

At the very bottom of the page, there is a footer with the following text: © 2020 Copyright - All Rights Reserved | Copyright Clearance Center, Inc. | Privacy statement | Terms and Conditions. Comments? We would like to hear from you. E-mail us at customercare@copyrights.com

Figure 2.7

The screenshot displays a web interface for RightsLink. At the top, there are logos for Copyright Clearance Center and RightsLink, along with navigation links for Home, Help, Email Support, and a user profile for Malwattage Peiris. The main content area is divided into two sections. The first section, titled 'Self-Assembled Monolayers of Terminal Alkynes on Gold', includes the ACS Publications logo and provides the following information: Author: Sheng Zhang, Kusum L. Chandra, Christopher B. Gorman; Publication: Journal of the American Chemical Society; Publisher: American Chemical Society; Date: Apr 1, 2007; and Copyright © 2007, American Chemical Society. The second section, titled 'PERMISSION/LICENSE IS GRANTED FOR YOUR ORDER AT NO CHARGE', explains that this type of permission is granted instead of standard terms and conditions. It lists several conditions: permission is granted for print and electronic formats and translations; figures and tables may be adapted; users should print the page for records and send a copy to their publisher/graduate school; appropriate credit should be given as follows: "Reprinted (adapted) with permission from (COMPLETE REFERENCE CITATION). Copyright (YEAR) American Chemical Society."; and one-time permission is granted only for the use specified in the request. A 'BACK' button is located at the bottom left of this section, and a 'CLOSE WINDOW' button is at the bottom right. At the very bottom of the page, there is a footer with copyright information: © 2020 Copyright - All Rights Reserved | Copyright Clearance Center, Inc. | Privacy statement | Terms and Conditions. Comments? We would like to hear from you. E-mail us at customercare@copyright.com.

Figure 2.8

The screenshot displays a web interface for RightsLink. At the top left, there are logos for the Copyright Clearance Center and RightsLink. On the top right, there are navigation links for Home, Help, Email Support, and a user profile for Malwattage Peiris. The main content area is divided into two sections. The first section, titled 'Self-Assembled Monolayers of Terminal Alkynes on Gold', includes the ACS Publications logo and provides the following information: Author: Sheng Zhang, Kusum L. Chandra, Christopher B. Gorman; Publication: Journal of the American Chemical Society; Publisher: American Chemical Society; Date: Apr 1, 2007; and Copyright © 2007, American Chemical Society. The second section, titled 'PERMISSION/LICENSE IS GRANTED FOR YOUR ORDER AT NO CHARGE', explains that this type of permission is granted instead of standard terms and conditions because no fee is charged. It lists several conditions: permission is granted in both print and electronic formats; figures and tables may be adapted; users should print the page for records; appropriate credit should be given as 'Reprinted (adapted) with permission from (COMPLETE REFERENCE CITATION), Copyright (YEAR) American Chemical Society.'; and one-time permission is granted only for the specified use. A 'BACK' button is located at the bottom left of this section, and a 'CLOSE WINDOW' button is at the bottom right. At the very bottom of the page, there is a footer with copyright information: © 2020 Copyright - All Rights Reserved | Copyright Clearance Center, Inc. | Privacy statement | Terms and Conditions. Comments? We would like to hear from you. E-mail us at customercare@copyright.com.

Figure 2.9

License 1014876-1.pdf

128 KB



Dear Malwattage Peiris,

Thank you for your email. I have checked our system and can see that you placed two orders for the same figure. I can confirm that the permission was gratis granted at checkout. You are now free to use the content in accordance with the terms and conditions set-forth by the publisher. For your convenience, I have attached the corresponding license agreement to this email.

Have a great day!

If you have any further questions please don't hesitate to contact a Customer Account Specialist at 855-239-3415 Monday-Friday, 24 hours/day.

Kind regards,

Nathan

Nathan Tomlinson
Customer Account Specialist
Copyright Clearance Center
222 Rosewood Drive
Danvers, MA 01923
www.copyright.com
Toll Free US +1.855.239.3415
International +1.978-646-2600
[Facebook](#) - [Twitter](#) - [LinkedIn](#)

ref:_00D30oeGz._5004Q25SIVK:ref



Marketplace™

IOP Publishing, Ltd - License Terms and Conditions

This is a License Agreement between Pepita Pla-Vilanova ("You") and IOP Publishing, Ltd ("Publisher") provided by Copyright Clearance Center ("CCC"). The license consists of your order details, the terms and conditions provided by IOP Publishing, Ltd, and the CCC terms and conditions.

All payments must be made in full to CCC.

Order Date	22-Jan-2020	Type of Use	Republish in a thesis/dissertation
Order license ID	1014876-1	Publisher Portion	IOP Publishing
ISSN	0957-4484		Image/photo/illustration

LICENSED CONTENT

Publication Title	Nanotechnology	Country	United Kingdom of Great Britain and Northern Ireland
Author/Editor	American Institute of Physics., Institute of Physics (Great Britain)	Rightsholder	IOP Publishing, Ltd
Date	01/01/1990	Publication Type	Journal
Language	English		

REQUEST DETAILS

Portion Type	Image/photo/illustration	Distribution	Worldwide
Number of images / photos / illustrations	1	Translation	Original language of publication
Format (select all that apply)	Print, Electronic	Copies for the disabled?	No
Who will republish the content?	Not-for-profit entity	Minor editing privileges?	No
Duration of Use	Current edition and up to 10 years	Incidental promotional use?	No
Lifetime Unit Quantity	Up to 499	Currency	AUD
Rights Requested	Main product		

NEW WORK DETAILS

Title	Mechanically robust single molecule-circuits	Institution name	Curtin University
Instructor name	Nadim Darwish	Expected presentation date	2020-04-23

ADDITIONAL DETAILS

Order reference number	N/A	The requesting person / organization to appear on the license	Pepita Pla-Vilanova
------------------------	-----	---	---------------------

Figure 2.10

ELSEVIER ORDER DETAILS

Sep 23, 2020

This Agreement between Malwattage CR Peiris ("You") and Elsevier ("Elsevier") consists of your order details and the terms and conditions provided by Elsevier and Copyright Clearance Center.

Order Number	501590167			
Order date	Aug 11, 2020			
Licensed Content Publisher	Elsevier			
Licensed Content Publication	Electrochimica Acta			
Licensed Content Title	Electro-reduction of diazonium salts on gold: Why do we observe multi-peaks?			
Licensed Content Author	Alessandro Benedetto, Mirela Balog, Pascal Viel, Franck Le Derf, Marc Sallé, Serge Palacin			
Licensed Content Date	15 October 2008			
Licensed Content Volume	53			
Licensed Content Issue	24			
Licensed Content Pages	6			
Start Page	7117			
End Page	7122			
Type of Use	reuse in a thesis/dissertation			
Portion	figures/tables/illustrations			
Number of figures/tables/illustrations	4			
Format	both print and electronic			
Are you the author of this Elsevier article?	No			
Will you be translating?	Yes, including English rights			
Number of languages	>10			
Title	Covalently linked molecule–electrode contacts toward robust molecular-electronics circuits			
Institution name	Curtin			
Expected presentation date	Oct 2020			
Portions	Figure 4			
Specific Languages	english			
	Curtin			University street
	Kent			
Requestor Location	Bentley,	Western	Australia	6102
	Australia			
	Attn: Curtin University			
Publisher Tax ID	GB 494 6272 12			
Billing Type	Invoice			
	Curtin			University street
	Kent			
Billing Address	Bentley,		Australia	6102
	Attn: Curtin University			
Total	0.00 USD			
Terms and Conditions				

Table 2.1

RE: Permission Request Form: Malwattage

CONTRACTS-COPYRIGHT (shared) <Contracts-Copyright@rsc.org>

Fri 20/09/25 2:39 PM

To: Chandramalika Peiris <m.c.peiris@postgrad.curtin.edu.au>

Dear Malwattage

The Royal Society of Chemistry hereby grants permission for the use of the material specified below in the work described and in all subsequent editions of the work for distribution throughout the world, in all media including electronic and microfilm. You may use the material in conjunction with computer-based electronic and information retrieval systems, grant permissions for photocopying, reproductions and reprints, translate the material and to publish the translation, and authorize document delivery and abstracting and indexing services. The Royal Society of Chemistry is a signatory to the STM Guidelines on Permissions (available on request).

Please note that if the material specified below or any part of it appears with credit or acknowledgement to a third party then you must also secure permission from that third party before reproducing that material.

Please ensure that the published article carries a credit to The Royal Society of Chemistry (see <http://rsc.li/permissions> for details) and that any electronic version of the work includes a hyperlink to the article on the Royal Society of Chemistry website.

Regards

Gill Cockhead

Contracts & Copyright Executive

Gill Cockhead

Contracts & Copyright Executive

Royal Society of Chemistry,

Thomas Graham House,

Science Park, Milton Road,

Cambridge, CB4 0WF, UK

From: m.c.peiris@postgrad.curtin.edu.au <m.c.peiris@postgrad.curtin.edu.au>

Sent: 25 September 2020 03:04

To: CONTRACTS-COPYRIGHT (shared) <Contracts-Copyright@rsc.org>

Subject: Permission Request Form: Malwattage

Name: Malwattage

Institution: Curtin university

Email: m.c.peiris@postgrad.curtin.edu.auAddress:

Unit 3/29 Stannard Street

Bentley

6102

Australia

I am preparing the following work for publication:

Article/chapter title: Chapter-Introduction

Journal/book title: Covalently linked molecule–electrode contacts toward robust molecular-electronics circuits

Editor/author(s): M. C. R Peiris

Publisher: Curtin University

Is this request for a thesis?: Yes

I would very much appreciate your permission to use the following material:

Journal/book title: Fabrication of patterned silane based self-assembled monolayers by photolithography and surface reactions on silicon-oxide substrates

Editor/author(s): Nicole Herzer, Stephanie Hoepfner and Ulrich S. Schubert

ISBN/DOI: <https://doi.org/10.1039/C0CC00674B>

Year of publication: 12010

Page(s): 5634-5652

Type of material: Table 1

Figure/image number (if relevant): Table 1 List of abbreviations, structures and names of the used self-assembly molecules

Any additional comments:

Dear Sir/ Madam I would like to reuse the table 1 of the article name "Fabrication of patterned silane-based self-assembled monolayers by photolithography and surface

reactions on silicon-oxide substrates" for my thesis introduction. I would appreciate if you can grant me permission to reuse this table. Thank you Malwattage

Agree to terms: I agree

This communication is from The Royal Society of Chemistry, a company incorporated in England by Royal Charter (registered number RC000524) and a charity registered in England and Wales (charity number 207890). Registered office: Burlington House, Piccadilly, London W1J 0BA. Telephone: +44 (0) 20 7437 8656.

The content of this communication (including any attachments) is confidential, and may be privileged or contain copyright material. It may not be relied upon or disclosed to any person other than the intended recipient(s) without the consent of The Royal Society of Chemistry. If you are not the intended recipient(s), please (1) notify us immediately by replying to this email, (2) delete all copies from your system, and (3) note that disclosure, distribution, copying or use of this communication is strictly prohibited.

Any advice given by The Royal Society of Chemistry has been carefully formulated but is based on the information available to it. The Royal Society of Chemistry cannot be held responsible for accuracy or completeness of this communication or any attachment. Any views or opinions presented in this email are solely those of the author and do not represent those of The Royal Society of Chemistry. The views expressed in this communication are personal to the sender and unless specifically stated, this e-mail does not constitute any part of an offer or contract. The Royal Society of Chemistry shall not be liable for any resulting damage or loss as a result of the use of this email and/or attachments, or for the consequences of any actions taken on the basis of the information provided. The Royal Society of Chemistry does not warrant that its emails or attachments are Virus-free; The Royal Society of Chemistry has taken reasonable precautions to ensure that no viruses are contained in this email, but does not accept any responsibility once this email has been transmitted. Please rely on your own screening of electronic communication.

More information on The Royal Society of Chemistry can be found on our website:
www.rsc.org

Figure 2.13

JOHN WILEY AND SONS LICENSE

TERMS AND CONDITIONS

Sep 23, 2020

This Agreement between Curtin University ("You") and John Wiley and Sons ("John Wiley and Sons") consists of your license details and the terms and conditions provided by John Wiley and Sons and Copyright Clearance Center.

License Number	4915100657365
License date	Sep 23, 2020
Licensed Content Publisher	John Wiley and Sons
Licensed Content Publication	Angewandte Chemie International Edition
Licensed Content Title	Engineering Silicon Oxide Surfaces Using Self-Assembled Monolayers
Licensed Content Author	David N. Reinhoudt, Bart Jan Ravoo, Steffen Onclin
Licensed Content Date	Sep 30, 2005
Licensed Content Volume	44
Licensed Content Issue	39
Licensed Content Pages	23
Type of use	Dissertation/Thesis
Requestor type	University/Academic
Format	Print and electronic
Portion	Figure/table
Number of figures/tables	1
Will you be translating?	No
Title	Covalently linked molecule–electrode contacts toward robust molecular-electronics circuits
Institution name	Curtin
Expected presentation date	Oct 2020
Portions	1
Requestor Location	Curtin University Kent street Bentley, Western Australia 6102 Attn: Curtin University
Publisher Tax ID	EU826007151
Total	0.00 AUD
Terms and Conditions	

Figure 2.16

ELSEVIER
TERMS AND CONDITIONS
Sep 23, 2020

LICENSE

This Agreement between Curtin University ("You") and Elsevier ("Elsevier") consists of your license details and the terms and conditions provided by Elsevier and Copyright Clearance Center.

License Number	4915111466494		
License date	Sep 23, 2020		
Licensed Content Publisher	Elsevier		
Licensed Content Publication	Surface Science		
Licensed Content Title	Electrochemically driven organic monolayer formation on silicon surfaces using alkylammonium and alkylphosphonium reagents		
Licensed Content Author	Dong Wang, Jillian M. Buriak		
Licensed Content Date	Oct 1, 2005		
Licensed Content Volume	590		
Licensed Content Issue	2-3		
Licensed Content Pages	8		
Start Page	154		
End Page	161		
Type of Use	reuse in a thesis/dissertation		
Portion	figures/tables/illustrations		
Number of figures/tables/illustrations	1		
Format	both print and electronic		
Are you the author of this Elsevier article?	No		
Will you be translating?	No		
Title	Covalently linked molecule–electrode contacts toward robust molecular–electronics circuits		
Institution name	Curtin		
Expected presentation date	Oct 2020		
Portions	Figure 6		
Requestor Location	Bentley, Western Australia Attn: Curtin University	University street	6102
Publisher Tax ID	GB 494 6272 12		
Total	0.00 AUD		
Terms and Conditions			

Figure 2.17

The screenshot shows a web interface for RightsLink. At the top left are the Copyright Clearance Center and RightsLink logos. On the top right are navigation links for Home, Help, Email Support, and a user profile for Malwattage Peiris. The main content area is divided into two sections. The first section displays the title of a journal article: "TEMPO Monolayers on Si(100) Electrodes: Electrostatic Effects by the Electrolyte and Semiconductor Space-Charge on the Electroactivity of a Persistent Radical". Below the title, it lists the author (Long Zhang, Yan Boris Vogel, Benjamin B. Noble, et al), the publication (Journal of the American Chemical Society), the publisher (American Chemical Society), and the date (Aug 1, 2016). The ACS Publications logo is also present. The second section is titled "PERMISSION/LICENSE IS GRANTED FOR YOUR ORDER AT NO CHARGE" and contains a list of conditions for the permission, such as the requirement for credit and the prohibition of derivative works. At the bottom of this section are "BACK" and "CLOSE WINDOW" buttons. A footer at the very bottom contains copyright information for 2020 and contact details for the Copyright Clearance Center.

Copyright Clearance Center RightsLink[®] Home ? Email Support Malwattage Peiris

TEMPO Monolayers on Si(100) Electrodes: Electrostatic Effects by the Electrolyte and Semiconductor Space-Charge on the Electroactivity of a Persistent Radical

Author: Long Zhang, Yan Boris Vogel, Benjamin B. Noble, et al
Publication: Journal of the American Chemical Society
Publisher: American Chemical Society
Date: Aug 1, 2016
Copyright © 2016, American Chemical Society

PERMISSION/LICENSE IS GRANTED FOR YOUR ORDER AT NO CHARGE

This type of permission/license, instead of the standard Terms & Conditions, is sent to you because no fee is being charged for your order. Please note the following:

- Permission is granted for your request in both print and electronic formats, and translations.
- If figures and/or tables were requested, they may be adapted or used in part.
- Please print this page for your records and send a copy of it to your publisher/graduate school.
- Appropriate credit for the requested material should be given as follows: "Reprinted (adapted) with permission from (COMPLETE REFERENCE CITATION). Copyright (YEAR) American Chemical Society." Insert appropriate information in place of the capitalized words.
- One-time permission is granted only for the use specified in your request. No additional uses are granted (such as derivative works or other editions). For any other uses, please submit a new request.

If credit is given to another source for the material you requested, permission must be obtained from that source.

[BACK](#) [CLOSE WINDOW](#)

© 2020 Copyright - All Rights Reserved | Copyright Clearance Center, Inc. | Privacy statement | Terms and Conditions
Comments? We would like to hear from you. E-mail us at customercare@copyright.com

Figure 2.18

The screenshot displays the RightsLink interface for a copyright clearance request. At the top, the Copyright Clearance Center and RightsLink logos are visible, along with navigation links for Home, Help, Email Support, and Malwattage Peris. The main content area is divided into two sections. The first section, titled "UV-Induced Grafting of Alkenes to Silicon Surfaces: Photoemission versus Excitons", provides metadata for the article, including the author (Xiaoyu Wang, Rose E. Ruther, Jeremy A. Streifer, et al), publication (Journal of the American Chemical Society), publisher (American Chemical Society), and date (Mar 1, 2010). The second section, titled "PERMISSION/LICENSE IS GRANTED FOR YOUR ORDER AT NO CHARGE", contains a notice stating that the permission is granted at no charge and lists specific conditions for use, such as the requirement for appropriate credit and the prohibition of derivative works. At the bottom of the page, there is a footer with copyright information and contact details.

Copyright Clearance Center RightsLink[®] Home ? Email Support Malwattage Peris v

UV-Induced Grafting of Alkenes to Silicon Surfaces: Photoemission versus Excitons
Author: Xiaoyu Wang, Rose E. Ruther, Jeremy A. Streifer, et al
Publication: Journal of the American Chemical Society
Publisher: American Chemical Society
Date: Mar 1, 2010
Copyright © 2010, American Chemical Society

PERMISSION/LICENSE IS GRANTED FOR YOUR ORDER AT NO CHARGE
This type of permission/license, instead of the standard Terms & Conditions, is sent to you because no fee is being charged for your order. Please note the following:

- Permission is granted for your request in both print and electronic formats, and translations.
- If figures and/or tables were requested, they may be adapted or used in part.
- Please print this page for your records and send a copy of it to your publisher/graduate school.
- Appropriate credit for the requested material should be given as follows: "Reprinted (adapted) with permission from (COMPLETE REFERENCE CITATION), Copyright (YEAR) American Chemical Society," insert appropriate information in place of the capitalized words.
- One-time permission is granted only for the use specified in your request. No additional uses are granted (such as derivative works or other editions). For any other uses, please submit a new request.

If credit is given to another source for the material you requested, permission must be obtained from that source.

[BACK](#) [CLOSE WINDOW](#)

© 2020 Copyright - All Rights Reserved | Copyright Clearance Center, Inc. | Privacy statement | Terms and Conditions
Comments? We would like to hear from you. E-mail us at customerscare@copyright.com

Figure 2.19

The screenshot displays the RightsLink interface. At the top, the Copyright Clearance Center logo and RightsLink branding are visible on the left, and navigation links for Home, Help, Email Support, and Malwattage Peiris are on the right. The main content area features a white box with the following information:

Light-Induced Reactions of Porous and Single-Crystal Si Surfaces with Carboxylic Acids
Author: Eric J. Lee, Theodore W. Bitner, James S. Ha, et al
Publication: Journal of the American Chemical Society
Publisher: American Chemical Society
Date: Jan 1, 1996
Copyright © 1996, American Chemical Society

Below this, a section titled "PERMISSION/LICENSE IS GRANTED FOR YOUR ORDER AT NO CHARGE" contains the following text:

This type of permission/license, instead of the standard Terms & Conditions, is sent to you because no fee is being charged for your order. Please note the following:

- Permission is granted for your request in both print and electronic formats, and translations.
- If figures and/or tables were requested, they may be adapted or used in part.
- Please print this page for your records and send a copy of it to your publisher/graduate school.
- Appropriate credit for the requested material should be given as follows: "Reprinted (adapted) with permission from (COMPLETE REFERENCE CITATION). Copyright (YEAR) American Chemical Society." Insert appropriate information in place of the capitalized words.
- One-time permission is granted only for the use specified in your request. No additional uses are granted (such as derivative works or other editions). For any other uses, please submit a new request.
- If credit is given to another source for the material you requested, permission must be obtained from that source.

At the bottom of this section are two buttons: "BACK" and "CLOSE WINDOW".

At the very bottom of the page, a footer contains the following text:

© 2020 Copyright - All Rights Reserved | Copyright Clearance Center, Inc. | Privacy statements | Terms and Conditions
Comments? We would like to hear from you. E-mail us at customer@copyright.com

Figure 2.20

HomeHelpEmail SupportMalwattage Peiris



Covalently Attached Monolayers on Crystalline Hydrogen-Terminated Silicon: Extremely Mild Attachment by Visible Light
Author: Qiao-Yu Sun, Louis C. P. M. de Smet, Barend van Lagen, et al
Publication: Journal of the American Chemical Society
Publisher: American Chemical Society
Date: Mar 1, 2005
Copyright © 2005, American Chemical Society

PERMISSION/LICENSE IS GRANTED FOR YOUR ORDER AT NO CHARGE

This type of permission/license, instead of the standard Terms & Conditions, is sent to you because no fee is being charged for your order. Please note the following:

- Permission is granted for your request in both print and electronic formats, and translations.
- If figures and/or tables were requested, they may be adapted or used in part.
- Please print this page for your records and send a copy of it to your publisher/graduate school.
- Appropriate credit for the requested material should be given as follows: "Reprinted (adapted) with permission from (COMPLETE REFERENCE CITATION). Copyright (YEAR) American Chemical Society." Insert appropriate information in place of the capitalized words.
- One-time permission is granted only for the use specified in your request. No additional uses are granted (such as derivative works or other editions). For any other uses, please submit a new request.

If credit is given to another source for the material you requested, permission must be obtained from that source.

[BACK](#) [CLOSE WINDOW](#)

© 2020 Copyright - All Rights Reserved | Copyright Clearance Center, Inc. | [Privacy statement](#) | [Terms and Conditions](#)
Comments? We would like to hear from you. E-mail us at customercare@copyright.com

Figure 2.21

The screenshot displays the RightsLink interface. At the top, there are logos for Copyright Clearance Center and RightsLink, along with navigation links for Home, Help, Email Support, Sign in, and Create Account. The main content area features a white box with the following information:

Hidden Electrochemistry in the Thermal Grafting of Silicon Surfaces from Grignard Reagents
Author: Samira Fellah, Rabah Boukherroub, François Ozanam, et al
Publication: Langmuir
Publisher: American Chemical Society
Date: Jul 1, 2004
Copyright © 2004, American Chemical Society

Below this, a section titled "PERMISSION/LICENSE IS GRANTED FOR YOUR ORDER AT NO CHARGE" provides details. It states that this type of permission/license is sent because no fee is being charged. The following conditions apply:

- Permission is granted for your request in both print and electronic formats, and translations.
- If figures and/or tables were requested, they may be adapted or used in part.
- Please print this page for your records and send a copy of it to your publisher/graduate school.
- Appropriate credit for the requested material should be given as follows: "Reprinted (adapted) with permission from (COMPLETE REFERENCE CITATION). Copyright (YEAR) American Chemical Society." Insert appropriate information in place of the capitalized words.
- One-time permission is granted only for the use specified in your request. No additional uses are granted (such as derivative works or other editions). For any other uses, please submit a new request.

If credit is given to another source for the material you requested, permission must be obtained from that source.

At the bottom of the white box are two buttons: "BACK" and "CLOSE WINDOW".

At the very bottom of the page, there is a footer with the following text: © 2020 Copyright - All Rights Reserved | Copyright Clearance Center, Inc. | Privacy statement | Terms and Conditions. Comments? We would like to hear from you. E-mail us at customer care@copyright.com

Figure 2.22

The screenshot shows a web interface for RightsLink. At the top left, there are logos for Copyright Clearance Center and RightsLink. On the top right, there are navigation links: Home, Help, Email Support, and Malwattage Peirs. The main content area is divided into two sections. The first section, titled "Lewis Acid Mediated Hydrosilylation on Porous Silicon Surfaces", provides metadata for a publication: Author (Jillian M. Buriak, Michael P. Stewart, Todd W. Geders, et al), Publication (Journal of the American Chemical Society), Publisher (American Chemical Society), and Date (Dec 1, 1999). It also includes the ACS Publications logo and a copyright notice for 1999. The second section, titled "PERMISSION/LICENSE IS GRANTED FOR YOUR ORDER AT NO CHARGE", explains that this type of permission is sent because no fee is charged. It lists several conditions: permission is granted in print and electronic formats; figures and tables may be adapted; users should print the page and send a copy to their publisher; credit should be given as "Reprinted (adapted) with permission from (COMPLETE REFERENCE CITATION), Copyright (YEAR) American Chemical Society"; and one-time permission is granted only for the specified use. A "BACK" button is located at the bottom left of this section, and a "CLOSE WINDOW" button is at the bottom right. At the very bottom of the page, there is a footer with copyright information and contact details for Copyright Clearance Center, Inc.

Copyright Clearance Center RightsLink®

Home Help Email Support Malwattage Peirs

Lewis Acid Mediated Hydrosilylation on Porous Silicon Surfaces
Author: Jillian M. Buriak, Michael P. Stewart, Todd W. Geders, et al
Publication: Journal of the American Chemical Society
Publisher: American Chemical Society
Date: Dec 1, 1999
Copyright © 1999, American Chemical Society

PERMISSION/LICENSE IS GRANTED FOR YOUR ORDER AT NO CHARGE

This type of permission/license, instead of the standard Terms & Conditions, is sent to you because no fee is being charged for your order. Please note the following:

- Permission is granted for your request in both print and electronic formats, and translations.
- If figures and/or tables were requested, they may be adapted or used in part.
- Please print this page for your records and send a copy of it to your publisher/graduate school.
- Appropriate credit for the requested material should be given as follows: "Reprinted (adapted) with permission from (COMPLETE REFERENCE CITATION), Copyright (YEAR) American Chemical Society." Insert appropriate information in place of the capitalized words.
- One-time permission is granted only for the use specified in your request. No additional uses are granted (such as derivative works or other editions). For any other uses, please submit a new request.

If credit is given to another source for the material you requested, permission must be obtained from that source.

[BACK](#) [CLOSE WINDOW](#)

© 2020 Copyright - All Rights Reserved | Copyright Clearance Center, Inc. | Privacy statement | Terms and Conditions
Comments? We would like to hear from you. E-mail us at customer@copyright.com

Figure 2.23

The screenshot shows the RightsLink interface. At the top, there are logos for Copyright Clearance Center and RightsLink®, along with navigation links for Home, Help, Email Support, and Malwattage Peiris. The main content area displays the following information:

Electrical Conduction of Conjugated Molecular SAMs Studied by Conductive Atomic Force Microscopy

ACS Publications
Most Trusted. Most Cited. Most Read.

Author: Takao Ishida, Wataru Mizutani, Yoichiro Aya, et al
Publication: The Journal of Physical Chemistry B
Publisher: American Chemical Society
Date: Jun 1, 2002
Copyright © 2002, American Chemical Society

PERMISSION/LICENSE IS GRANTED FOR YOUR ORDER AT NO CHARGE

This type of permission/license, instead of the standard Terms & Conditions, is sent to you because no fee is being charged for your order. Please note the following:

- Permission is granted for your request in both print and electronic formats, and translations.
- If figures and/or tables were requested, they may be adapted or used in part.
- Please print this page for your records and send a copy of it to your publisher/graduate school.
- Appropriate credit for the requested material should be given as follows: "Reprinted (adapted) with permission from (COMPLETE REFERENCE CITATION). Copyright (YEAR) American Chemical Society." Insert appropriate information in place of the capitalized words.
- One-time permission is granted only for the use specified in your request. No additional uses are granted (such as derivative works or other editions). For any other uses, please submit a new request.

If credit is given to another source for the material you requested, permission must be obtained from that source.

Buttons: **BACK** and **CLOSE WINDOW**

© 2020 Copyright - All Rights Reserved | Copyright Clearance Center, Inc. | Privacy statement | Terms and Conditions
Comments? We would like to hear from you. E-mail us at customer@copyright.com

Figure 2.24

The screenshot shows the RightsLink interface. At the top, there are logos for Copyright Clearance Center and RightsLink®, along with navigation links for Home, Help, Email Support, and Malwattage Peiris. The main content area displays the following information:

Electrical Conduction of Conjugated Molecular SAMs Studied by Conductive Atomic Force Microscopy

ACS Publications
Most Trusted. Most Cited. Most Read.

Author: Takao Ishida, Wataru Mizutani, Yoichiro Aya, et al
Publication: The Journal of Physical Chemistry B
Publisher: American Chemical Society
Date: Jun 1, 2002
Copyright © 2002, American Chemical Society

PERMISSION/LICENSE IS GRANTED FOR YOUR ORDER AT NO CHARGE

This type of permission/license, instead of the standard Terms & Conditions, is sent to you because no fee is being charged for your order. Please note the following:

- Permission is granted for your request in both print and electronic formats, and translations.
- If figures and/or tables were requested, they may be adapted or used in part.
- Please print this page for your records and send a copy of it to your publisher/graduate school.
- Appropriate credit for the requested material should be given as follows: "Reprinted (adapted) with permission from (COMPLETE REFERENCE CITATION). Copyright (YEAR) American Chemical Society." Insert appropriate information in place of the capitalized words.
- One-time permission is granted only for the use specified in your request. No additional uses are granted (such as derivative works or other editions). For any other uses, please submit a new request.

If credit is given to another source for the material you requested, permission must be obtained from that source.

Buttons: **BACK** and **CLOSE WINDOW**

© 2020 Copyright - All Rights Reserved | Copyright Clearance Center, Inc. | Privacy statement | Terms and Conditions
Comments? We would like to hear from you. E-mail us at customer@copyright.com

Figure 2.25



Measurement of Single-Molecule Resistance by Repeated Formation of Molecular Junctions

Author: Bingqian Xu, Nongjian J. Tao

Publication: Science

Publisher: The American Association for the Advancement of Science

Date: Aug 29, 2003

Copyright © 2003, American Association for the Advancement of Science

Order Completed

Thank you for your order.

This Agreement between Curtin University ("You") and The American Association for the Advancement of Science ("The American Association for the Advancement of Science") consists of your license details and the terms and conditions provided by The American Association for the Advancement of Science and Copyright Clearance Center.

Your confirmation email will contain your order number for future reference.

License Number 4913930081608

[Printable Details](#)

License date Sep 21, 2020

Licensed Content

Licensed Content Publisher :The American Association for the Advancement of Science

Licensed Content Publication: Science

Licensed Content Title :Measurement of Single-Molecule Resistance by Repeated Formation of Molecular Junctions

Licensed Content Author ;Bingqian Xu, Nongjian J. Tao

Licensed Content Date :Aug 29, 2003

Licensed Content Volume: 301

Licensed Content Issue: 5637

Order Details

Type of Use :Thesis / Dissertation

Requestor type : Scientist/individual at a research institution

Format: Print and electronic

Portion: Figure

Number of figures/tables:1

About Your Work

Title: Covalently linked molecule–electrode contacts toward robust molecular-electronics circuits

Institution name: Curtin

Expected presentation date: Oct 2020

Price Total 0.00 AUD

Figure 2.26

The screenshot displays a web interface for RightsLink. At the top left, there are logos for Copyright Clearance Center and RightsLink. On the top right, there are links for Help and Email Support. The main content area is divided into two sections. The first section, titled "Single-molecule electrical contacts on silicon electrodes under ambient conditions", includes the author "Albert C. Aragonés et al", the publisher "Springer Nature", and the date "Apr 13, 2017". The second section, titled "Creative Commons", explains that the article is distributed under a Creative Commons CC BY license and provides instructions on how to request permission for reuse.

Copyright Clearance Center | RightsLink®

? Help | Email Support

Single-molecule electrical contacts on silicon electrodes under ambient conditions

Author: Albert C. Aragonés et al
Publication: Nature Communications
Publisher: Springer Nature
Date: Apr 13, 2017
Copyright © 2017, Springer Nature

SPRINGER NATURE

Creative Commons

This is an open access article distributed under the terms of the [Creative Commons CC BY](#) license, which permits unrestricted use, distribution, and reproduction in any medium, provided the original work is properly cited.

You are not required to obtain permission to reuse this article.
To request permission for a type of use not listed, please contact [Springer Nature](#)

© 2020 Copyright - All Rights Reserved | [Copyright Clearance Center, Inc.](#) | [Privacy statement](#) | [Terms and Conditions](#)
Comments? We would like to hear from you. E-mail us at customer-care@copyright.com

Figure 2.27

Figure 2.27a

The screenshot shows the RightsLink interface for a Springer Nature article. At the top, there are logos for Copyright Clearance Center and RightsLink, along with navigation links for Help and Email Support. The main content area displays the article title: "Tuning the electrical conductance of metalloporphyrin supramolecular wires". Below the title, it lists the author (Mohammed Noori et al), publication (Scientific Reports), publisher (Springer Nature), and date (Nov 21, 2016). A Creative Commons section explains that the article is distributed under a CC BY license, allowing unrestricted use with proper citation. At the bottom, there is a footer with copyright information and contact details for the Copyright Clearance Center.

Figure 2.27b

The screenshot shows the RightsLink interface for a Wiley article. At the top, there are logos for Copyright Clearance Center and RightsLink, along with navigation links for Home, Help, Email Support, and a user profile for Malwattage Peiris. The main content area displays the article title: "Observation of Electrochemically Controlled Quantum Interference in a Single Anthraquinone-Based Norbornylogous Bridge Molecule". Below the title, it lists the authors (Nadim Darwish, Ismael Díez-Pérez, Paulo Da Silva, et al), publication (Angewandte Chemie International Edition), publisher (John Wiley and Sons), and date (Feb 14, 2012). A green box contains a "Thank you for your order" message and a link to "Printable Details". Below this, there is a table with license details and a table with order details.

License Number	4913530927405	Printable Details	
License date	Sep 21, 2020		
Licensed Content		Order Details	
Licensed Content Publisher	John Wiley and Sons	Type of use	Dissertation/Thesis
Licensed Content Publication	Angewandte Chemie International Edition	Requestor type	University/Academic
Licensed Content Title	Observation of Electrochemically Controlled Quantum Interference in a Single Anthraquinone-Based Norbornylogous Bridge Molecule	Format	Print and electronic
Licensed Content Author	Nadim Darwish, Ismael Díez-Pérez,	Portion	Figure/table
		Number of figures/tables	1
		Will you be translating?	No

Figure 2.27c

The screenshot shows the RightsLink interface for a Springer Nature article. At the top, there are logos for Copyright Clearance Center and RightsLink, along with navigation links: Home, Help, Email Support, and Malwattage Peiris. The main content area features the article title "Dependence of single-molecule junction conductance on molecular conformation" and its metadata: Author: Latha Venkataraman et al, Publication: Nature, Publisher: Springer Nature, Date: Aug 24, 2006, and Copyright © 2006, Springer Nature. Below this is a "Welcome to RightsLink" section with a message from Springer Nature and a dropdown menu labeled "I would like to..." with the option "make a selection". At the bottom, there is a footer with copyright information and contact details.

Figure 2.27d

The screenshot shows the RightsLink interface for an ACS Publications article. At the top, there are logos for Copyright Clearance Center and RightsLink, along with navigation links: Home, Help, Email Support, and Malwattage Peiris. The main content area features the article title "Tuning Rectification in Single-Molecular Diodes" and its metadata: Author: Arunabh Batra, Pierre Darancet, Qishui Chen, et al, Publication: Nano Letters, Publisher: American Chemical Society, Date: Dec 1, 2013, and Copyright © 2013, American Chemical Society. Below this is a section titled "PERMISSION/LICENSE IS GRANTED FOR YOUR ORDER AT NO CHARGE" with a message explaining the type of permission and a list of conditions. At the bottom, there are "BACK" and "CLOSE WINDOW" buttons. At the bottom of the page, there is a footer with copyright information and contact details.

Figure 2.27e

Home ? Help Email Support Sign in Create Account

Multi-Responsive Photo- and Chemo-Electrical Single-Molecule Switches

Author: Nadim Darwish, Albert C. Aragonès, Tamim Darwish, et al

Publication: Nano Letters

Publisher: American Chemical Society

Date: Dec 1, 2014

Copyright © 2014, American Chemical Society



PERMISSION/LICENSE IS GRANTED FOR YOUR ORDER AT NO CHARGE

This type of permission/license, instead of the standard Terms & Conditions, is sent to you because no fee is being charged for your order. Please note the following:

- Permission is granted for your request in both print and electronic formats, and translations.
- If figures and/or tables were requested, they may be adapted or used in part.
- Please print this page for your records and send a copy of it to your publisher/graduate school.
- Appropriate credit for the requested material should be given as follows: "Reprinted (adapted) with permission from (COMPLETE REFERENCE CITATION), Copyright (YEAR) American Chemical Society." Insert appropriate information in place of the capitalized words.
- One-time permission is granted only for the use specified in your request. No additional uses are granted (such as derivative works or other editions). For any other uses, please submit a new request.

If credit is given to another source for the material you requested, permission must be obtained from that source.

[BACK](#) [CLOSE WINDOW](#)

© 2020 Copyright - All Rights Reserved | Copyright Clearance Center, Inc. | [Privacy statement](#) | [Terms and Conditions](#)
Comments? We would like to hear from you. E-mail us at customer@copyright.com

Appendix B

B-4-1 Statement of contribution to a co-authored paper

Chapter 4 is the co-authored paper "Metal–single-molecule–semiconductor junctions formed by a radical reaction bridging gold and silicon electrodes" which was published in *Journal of the American Chemical Society*. The details of this article is given below

Chandramalika R. Peiris, Yan B. Vogel, Anton P. Le Brun, Albert C. Aragonès, Michelle L. Coote, Ismael Díez-Pérez, Simone Ciampi and Nadim Darwish. *Journal of the American Chemical Society*, Volume 141, Issue 37, 27th August 2019, Pages 14788–14797

DOI: <https://doi.org/10.1021/jacs.9b07125>

I, Malwattage Chandramalika Rukmali Peiris, as the primary author, conducted all of the experimental work and data analysis, creating tables, figures, writing and editing of the manuscript.

Contribution of other co-authors is as follows:

Anton P. Le Brun contributes to the paper by doing X-ray refractometry and Yan B. Vogel contributes by capturing scanning electron microscope images of the surfaces. Albert C. Aragonès, Michelle L. Coote, Ismael Díez-Pérez, Simone Ciampi contribute by ideas, co-supervision and manuscript editing. Nadim Darwish contributes by helping with scanning tunnelling microscopic experiments, supervision, data analysis and editing of the manuscript.

I, as a co-author of the article name "Metal–single-molecule–semiconductor junctions formed by a radical reaction bridging gold and silicon electrodes" confirms that the contribution by the M. C. R Peiris indicated above is correct

- 1) Yan B. Vogel
- 2) Anton P. Le Brun (attached)
- 3) Albert C. Aragonès (attached)
- 4) Michelle L. Coote
- 5) Ismael Díez-Pérez
- 6) Simone Ciampi
- 7) Nadim Darwish

Statement of Contributions for **"Metal-Single-Molecule-Semiconductor Junctions Formed by a Radical Reaction Bridging Gold and Silicon Electrodes"**

17th July 2020

To whom it may concern

I, Anton Le Brun, contributed by XRR data interpretation for the paper/publication entitled "Metal-Single-Molecule-Semiconductor Junctions Formed by a Radical Reaction Bridging Gold and Silicon Electrodes " undertaken by Malwattage Chandramalika Rukmali Peiris.

Signature of Co-Author

Anton Le Brun

Signature of First Author

M. Chandramalika Rukmali Peiris



Statement of Contributions for "Metal-Single-Molecule-Semiconductor Junctions Formed by a Radical Reaction Bridging Gold and Silicon Electrodes"

17th July 2020

To whom it may concern

I, Albert C. Aragonès, contributed by data interpretation and manuscript editing for the paper/publication entitled "Metal-Single-Molecule-Semiconductor Junctions Formed by a Radical Reaction Bridging Gold and Silicon Electrodes" undertaken by Malwattage Chandramalika Rukmalie Peiris.

Signature of Co-Author

Albert C. Aragonès

Reproduced with permission from (Journal of the American Chemical Society, Volume 141, Issue 37, 27th August 2019, Pages 14788–14797.) Copyright (2019) American Chemical Society.”

HomeHelpEmail SupportMalwattage Peiris ▾



Metal-Single-Molecule-Semiconductor Junctions Formed by a Radical Reaction Bridging Gold and Silicon Electrodes

Author: Chandramalika R. Peiris, Yan B. Vogel, Anton P. Le Brun, et al
Publication: Journal of the American Chemical Society
Publisher: American Chemical Society
Date: Sep 1, 2019

Copyright © 2019, American Chemical Society

PERMISSION/LICENSE IS GRANTED FOR YOUR ORDER AT NO CHARGE

This type of permission/license, instead of the standard Terms & Conditions, is sent to you because no fee is being charged for your order. Please note the following:

- Permission is granted for your request in both print and electronic formats, and translations.
- If figures and/or tables were requested, they may be adapted or used in part.
- Please print this page for your records and send a copy of it to your publisher/graduate school.
- Appropriate credit for the requested material should be given as follows: "Reprinted (adapted) with permission from (COMPLETE REFERENCE CITATION). Copyright (YEAR) American Chemical Society." Insert appropriate information in place of the capitalized words.
- One-time permission is granted only for the use specified in your request. No additional uses are granted (such as derivative works or other editions). For any other uses, please submit a new request.

[BACK](#) [CLOSE WINDOW](#)

© 2020 Copyright - All Rights Reserved | [Copyright Clearance Center, Inc.](#) | [Privacy statement](#) | [Terms and Conditions](#)
Comments? We would like to hear from you. E-mail us at customer@copyright.com

Appendix C

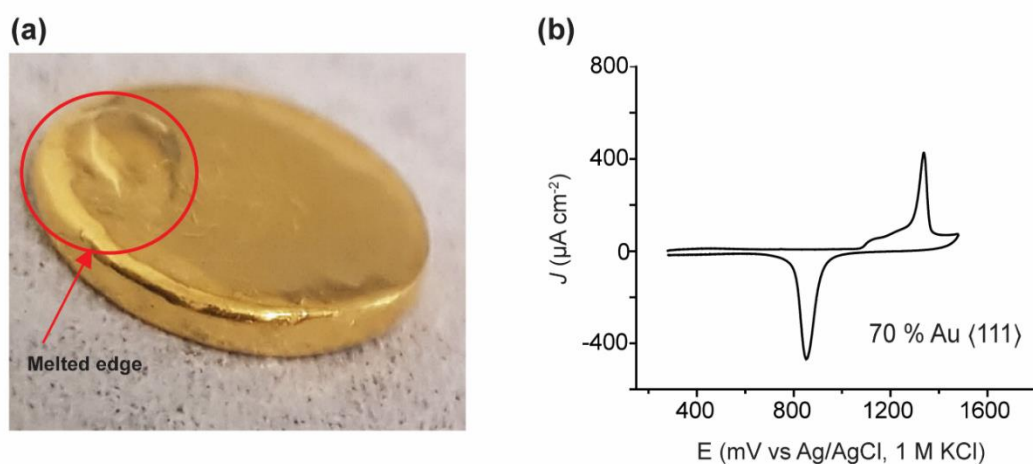


Figure C-4-1 a) An image of the 70% Au (111) single crystal. The melted edge is circled in red. b) Cyclic voltammogram for the 70% Au (111) oxidation/reduction showing two waves between +1150 mV and +1350 mV.

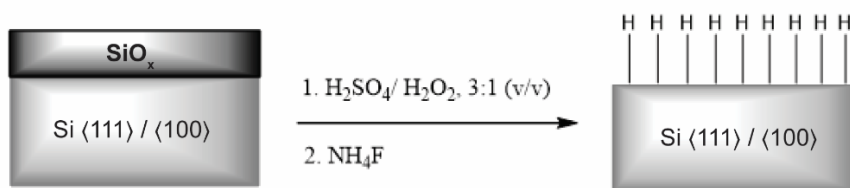


Figure C-4-2 Schematic describing the formation of Si(111)-H and Si(100)-H surfaces via surface oxidation of Si(111) and Si(100) surfaces for 30 min in a 3:1 H₂SO₄: H₂O₂ piranha mixture followed by oxide etching with ammonium fluoride.

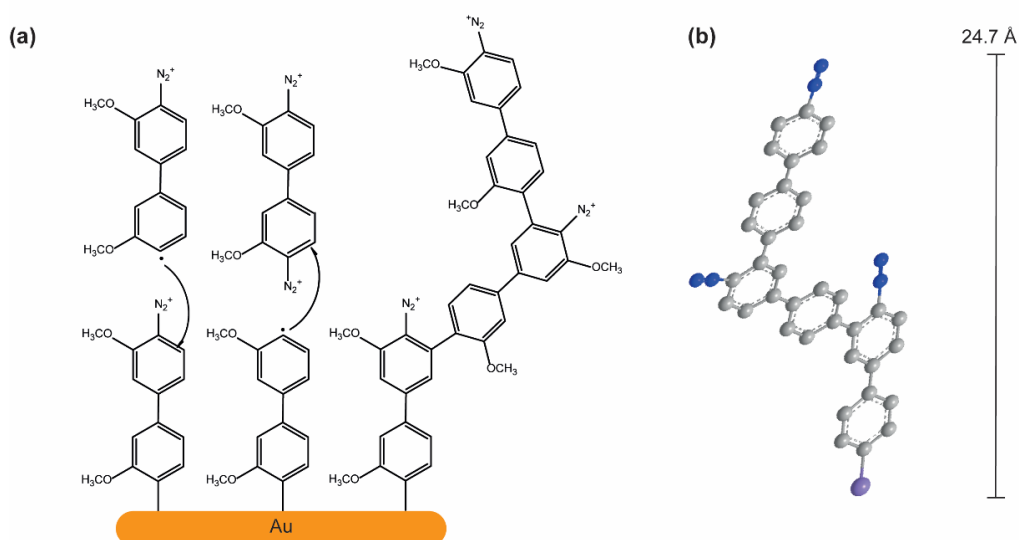


Figure C-4-3 a) Schematics diagram describing the possible polymerization outcome during one cycle of electro-reduction of the **bis-diazo** compound. This mechanism describes the formation of a covalent bond between the free **bis-diazo** radicals in solution with the **bis-diazo** grafted on the surface. A companion reaction is that between the radicals of **bis-diazo** attached to the electrode surface with excess **bis-diazo** in solution. This results in 3 polymerized units which has a thickness of ca. 2.43 nm comparable to the thickness of the film obtained via XRR measurements. b) Theoretical 3D Structure of the **bis-diazo** molecules with 3 polymerized units (Si-purple, C-grey, N-blue).

Table C-4-1. Fitted SAM thickness and surface roughness (in Å), and fitted SLD (in 10^{-6} \AA^{-2}) for **bis-diazo** on Si(111)-H for the electrochemical and spontaneous grafting as determined from XRR data (see XRR curves in Figure 4.4 in the main text).

Sample	Thickness / Å	Fitted SLD / $\times 10^{-6} \text{ \AA}^{-2}$	Air-monolayer / monolayer-silicon roughness / Å	Volume fraction	Molecules per cm^2 / $\times 10^{14}$
Electrochemically grafted	24.3 ± 1.2	10.1 ± 0.4	10.7 / 9.0	0.606 ± 0.024	6.21 ± 0.06
Spontaneous grafting (12 h)	23.8 ± 2.5	9.28 ± 0.41	5.5 / 11.7	0.556 ± 0.025	5.58 ± 0.11

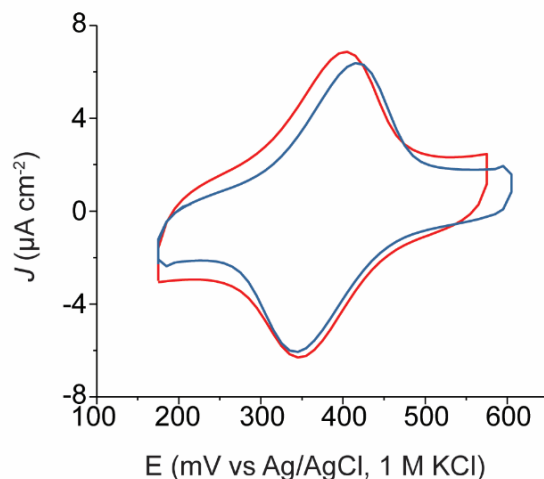


Figure C-4-4 Testing the stability of the interface. The red curve shows a cyclic voltammogram of the spontaneous reduction of **bis-diazo** by means of resting an Au(111) sample in a solution of **bis-diazo** for 2 h at open circuit, followed by the reaction with ferrocene (30 min). The blue curve shows a cyclic voltammogram of a spontaneously reduced diazo-film that was held at +1 V vs Ag/AgCl for 300 s before being exposed to a solution of ferrocene (30 min). The efficiency of ferrocene reaction with the pre-biased **bis-diazo** film (blue trace) is comparable to that on the fresh unbiased diazonium film (red trace) both being $1.08 (\pm 0.17) \times 10^{14}$ molecule cm^{-2} , testifying for the stability of the interface. The potential scan rate is 50 mVs^{-1} and the potential is expressed in mV against an aqueous Ag/AgCl (1.0 M KCl) reference electrode.

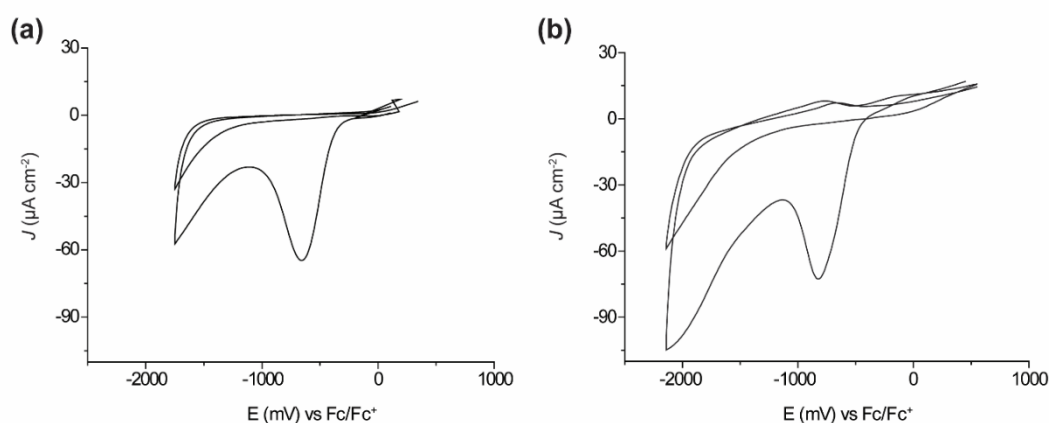


Figure C-4-5 Cyclic voltammograms for the 1st and 2nd reduction cycles at a scan rate of 50 mV s^{-1} of **bis-diazo** (1 mM) and Bu_4NPF_6 (0.1 M) in a 1:49 (v/v) mixture of DMSO and ACN) on a) Si(111) and b) Si(100).

Digital simulations of cyclic voltammetry were performed in DigiElch-Professional v7 (ElchSoft). Butler-Volmer kinetics was used to estimate charge transfer parameters and we assumed a semi-infinite 1D diffusion. Simulated kinetic, thermodynamic and transport parameters for the electrode reaction were determined from fittings of experimental data sets that covered a range of sweep rates and assuming an EC_{irre} mechanism (E , **bis-diazo**⁺/**bis-diazo** and C_{irre} , **bis-diazo** \rightarrow **bis-diazo**[•] + N_2). The cell iR drop was not compensated during measurement. Values of cell resistance were measured by electrochemical impedance spectroscopy and used in the simulations (130Ω for ACN/ Bu_4NPF_6). The double-layer capacitance was set to $10 \mu\text{F}$. Adsorption steps were neglected in the simulations and the transfer coefficients for the heterogeneous electron transfer reaction (the E step) was assumed as a constant (α , 0.5) for fitting purposes. In the simulation the heterogeneous adsorption step was not considered as this has no effect on the quality of the fits. For the chemical step (C_{irrev}) only the forward (k_f) constant is considered. The diffusivity of molecular nitrogen is high and the value of k_f large enough so that the second-order backward (k_b) constant tends to zero (i.e. backward chemical reaction is not operative in the time scale of the experiments).

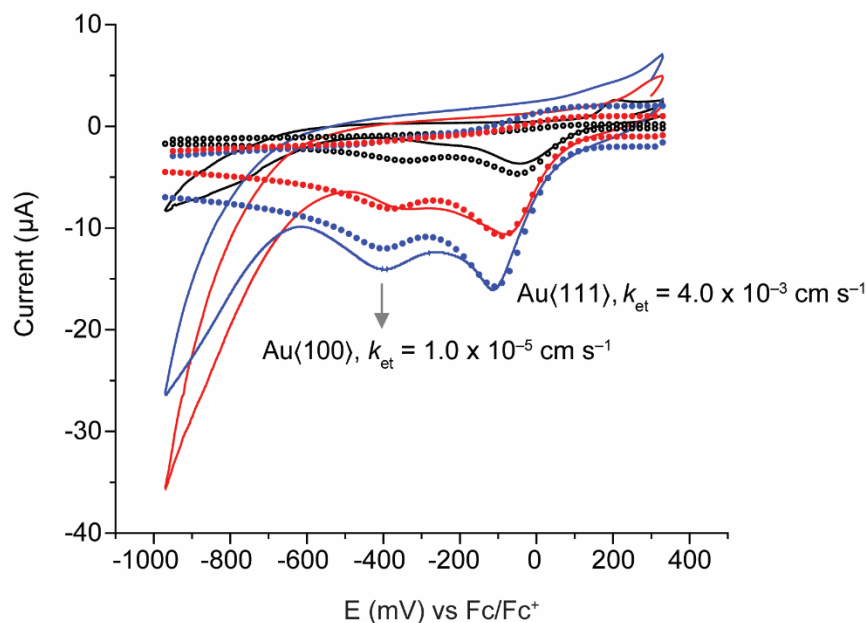


Figure C-4-6 Cyclic voltammograms of 1 mM **bis-diazo** salt in 0.1 M ACN/ Bu_4NPF_6 at polycrystalline gold electrodes (0.13 cm^2). Experimental (solid lines) and simulated (empty symbols) curves for an EC_{irrev} mechanism. The best-fit kinetics parameters for the heterogeneous E step (the one electron process for the **bis-diazo**⁺/**bis-diazo** couple) are $k_{\text{et}} = 4.0 \times 10^{-3} \text{ cm s}^{-1}$ on Au(111) facets, and $k_{\text{et}} = 1.0 \times 10^{-5} \text{ cm s}^{-1}$ on Au(100) facets. For the C_{irrev} step, that is the **bis-diazo** \rightarrow **bis-diazo**[•] + N_2 homogeneous chemical reaction, the k_f is $5 \times 10^3 \text{ s}^{-1}$. The apparent formal potential is 0 mV. The optimized diffusivity (D) for **bis-diazo**, **bis-diazo**⁺ and **bis-diazo**[•] is $3.0 \times 10^{-6} \text{ cm}^2 \text{ s}^{-1}$ and $2.5 \times 10^{-4} \text{ cm}^2 \text{ s}^{-1}$ for nitrogen. The voltage sweep rate is changed between 10 mV s^{-1} (black traces), 50 mV s^{-1} (red traces) and 100 mV s^{-1} (blue traces). The experimental reduction peak is at -37 mV at 10 mV s^{-1} , -70 mV at 50 mV s^{-1} and -105 mV at 100 mV s^{-1} .

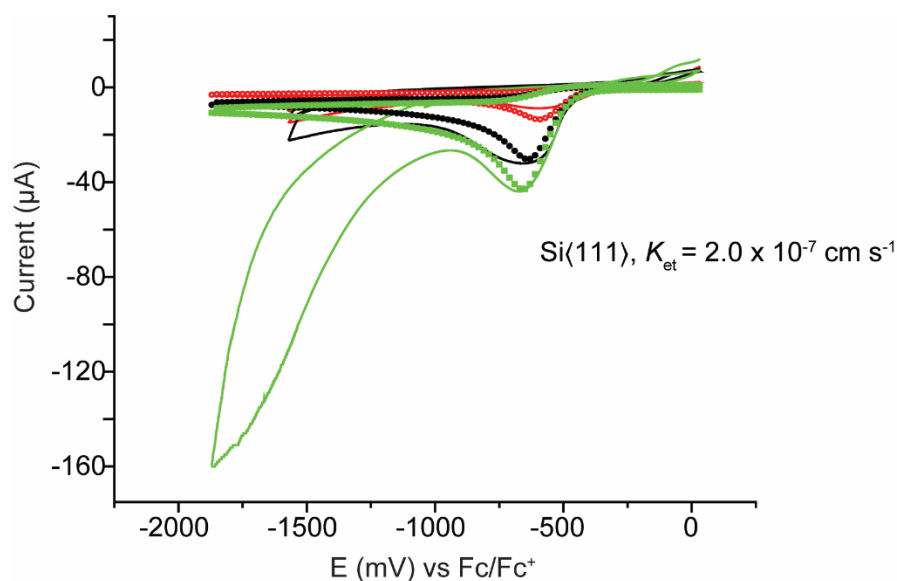


Figure C-4-7 Cyclic voltammograms of 1 mM **bis-diazo** salt in 0.1 M ACN/Bu₄NPF₆ at Si(111). Experimental (solid lines) and simulated (empty symbols) curves for an ECirrev mechanism. The best-fit kinetics parameters for the heterogeneous E step (the one electron redox process for the **bis-diazo**⁺/**bis-diazo** couple) are $k_{\text{et}} = 2.0 \times 10^{-7} \text{ cm s}^{-1}$ for Si(111). The k_f for the Cirrev step, that is the **bis-diazo** → **bis-diazo**[•] + N₂ homogeneous chemical reaction, is $5.0 \times 10^3 \text{ s}^{-1}$ and the apparent formal potential is 0 mV. The optimized diffusivity (D) for bis-diazo, **bis-diazo**⁺ and **bis-diazo**[•] is $3.0 \times 10^{-6} \text{ cm}^2 \text{ s}^{-1}$ and D for nitrogen is set to $2.5 \times 10^{-4} \text{ cm}^2 \text{ s}^{-1}$. The electrode area is 0.35 cm². The voltage sweep rate is changed between 10 mV s⁻¹ (red traces), 50 mV s⁻¹ (black traces) and 100 mV s⁻¹ (green traces). The experimental reduction peak is at -564 mV at 10 mV s⁻¹, -650 mV at 50 mV s⁻¹ and -671 mV at 100 mV s⁻¹.

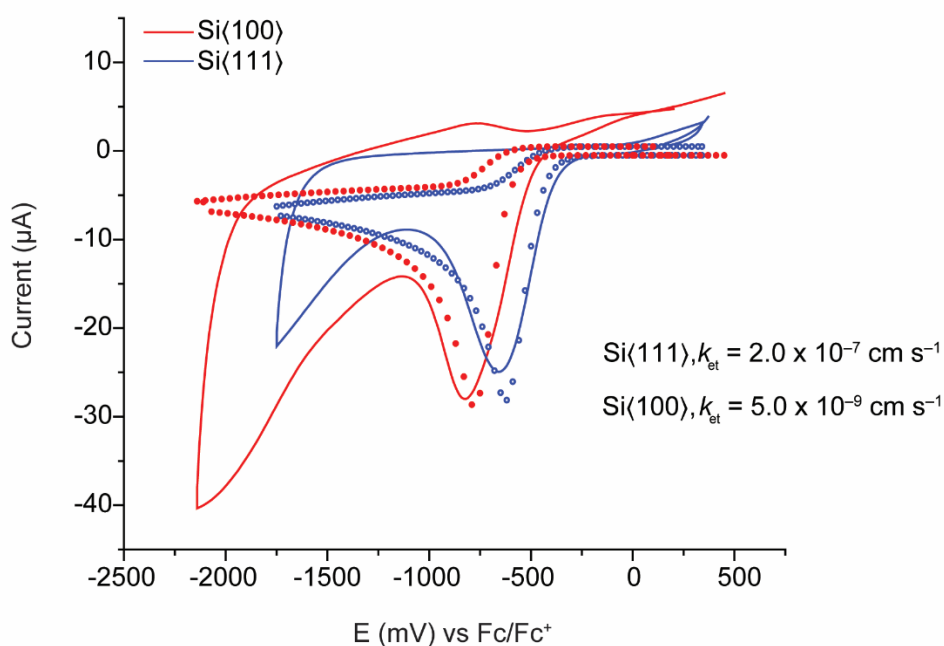


Figure C-4-8 Cyclic voltammograms of 1 mM **bis-diazo** salt in 0.1 M ACN/ Bu_4NPF_6 at Si(111) or Si(100) electrodes (blue and red trace, respectively). Experimental (solid lines) and simulated (empty symbols) curves for an EC_{irrev} mechanism. The best-fit kinetics parameters for the heterogeneous E step (the one electron redox process for the **bis-diazo**⁺/**bis-diazo** couple) are $k_{\text{et}} = 2.0 \times 10^{-7} \text{ cm s}^{-1}$ for Si(111) and $k_{\text{et}} = 5.0 \times 10^{-9} \text{ cm s}^{-1}$ for Si(100). The k_{f} for the C_{irrev} step, that is the **bis-diazo** \rightarrow **bis-diazo**[•] + N_2 homogeneous chemical reaction, is $5.0 \times 10^3 \text{ s}^{-1}$ and the apparent formal potential is 0 mV. The optimized diffusivity (D) for **bis-diazo**, **bis-diazo**⁺ and **bis-diazo**[•] is $3.0 \times 10^{-6} \text{ cm}^2 \text{ s}^{-1}$ and D for nitrogen is set to $2.5 \times 10^{-4} \text{ cm}^2 \text{ s}^{-1}$. The electrode area is 0.35 cm^2 and the voltage sweep rate is 50 mV s^{-1} .

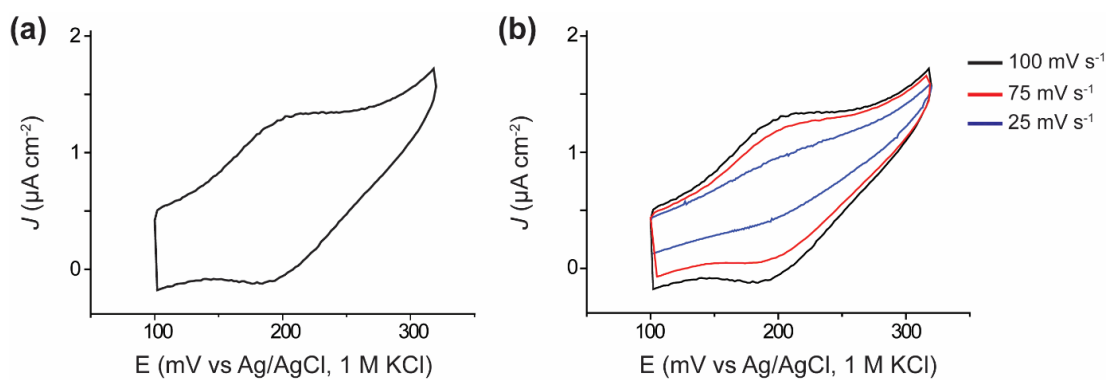


Figure C-4-9 Cyclic voltammogram of a film of **bis-diazo** electrochemically reduced on Si(111) and then exposed to a solution of ferrocene for 30 min at a scan rate of 100 mV s^{-1} . b) Cyclic voltammograms at different scan rates for the surface in (a).

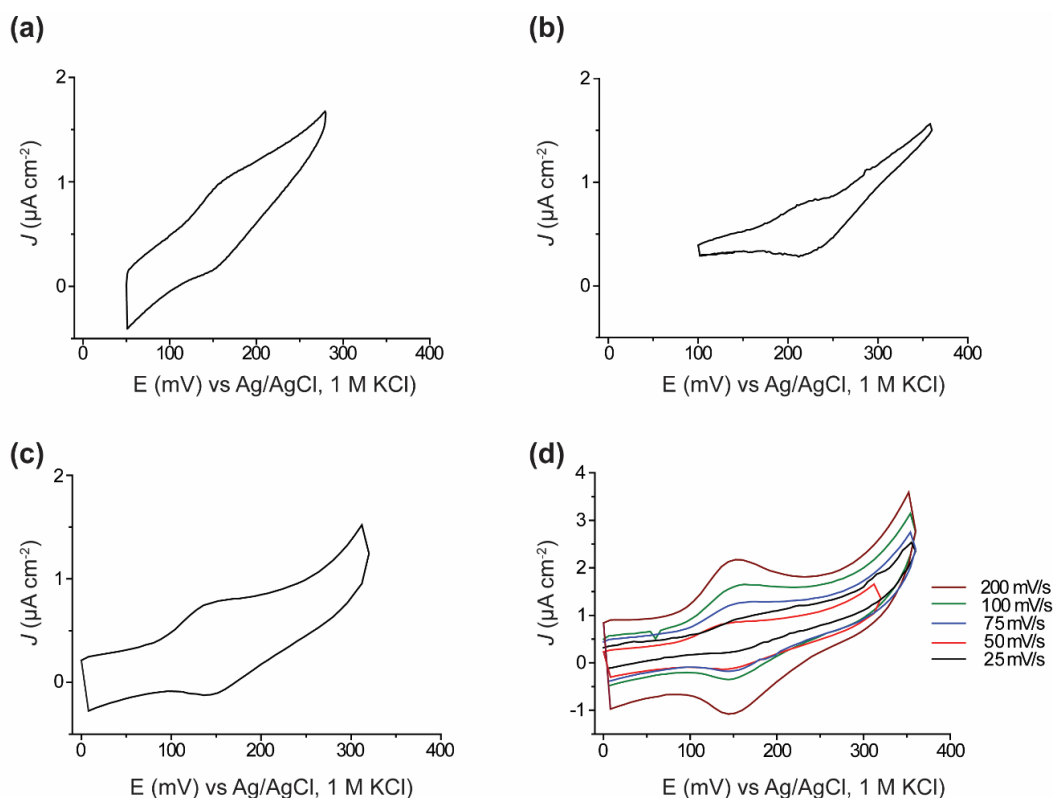


Figure C-4-10 Cyclic voltammogram of a film of **bis-diazo** spontaneously grafted on Si(111) by resting a Si(111)-H surface in a solution of bis-diazo and then exposed to a solution of ferrocene at a scan rate of 50 mV s^{-1} . The surfaces were rested in a **bis-diazo** compound for a) 2 h, b) 5 h and c) 8 h. d) Cyclic voltammograms at different scan rates for the surface in (c). Due to the low coverage in (a) and (b) of $7.67 (\pm 1.15) \times 10^{11} \text{ molecule cm}^{-2}$, the current increases significantly at anodic potentials (more anodic than + 100 mV) which is attributed to the oxidation of silicon. The current-increase at anodic potentials is relatively lower in (c) and (d) which is attributed to the surface having a relatively higher molecular coverage of $3.89 (\pm 0.58) \times 10^{12} \text{ molecule cm}^{-2}$.

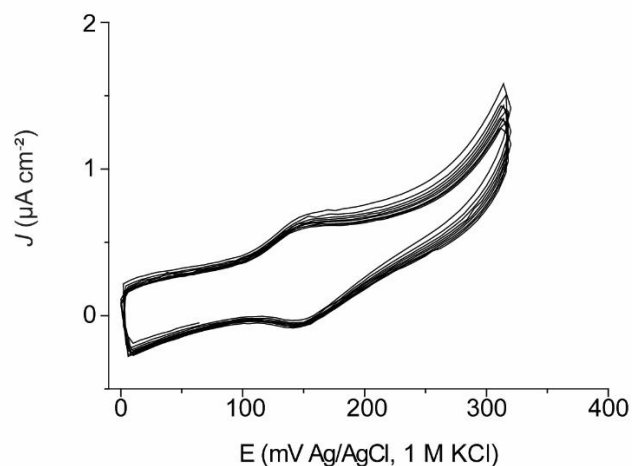


Figure C-4-11 Repetitive cyclic voltammograms at a scan rate 50 mV s^{-1} of a film of bis-diazo spontaneously reduced (resting a Si(111)-H surface in a solution of **bis-diazo** for 8 h and then exposed to a solution of ferrocene for 30 min).

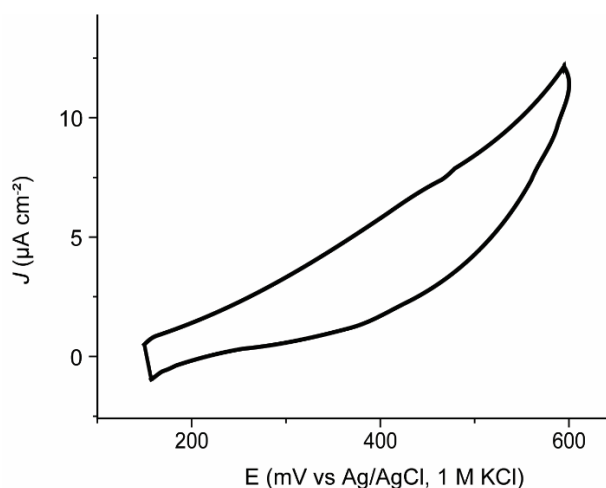


Figure C-4-12 Cyclic voltammogram of a film of **bis-diazo** spontaneously reduced on Si(100)-H surface (resting in a solution of **bis-diazo** for 2 h and then exposed to a solution of ferrocene for 30 min at a scan rate 50 mV s^{-1}). Due to the very low coverage of the **bis-diazo** on Si(100), no clear ferrocene signals are detected and the current increases significantly at anodic potentials (more anodic than + 100 mV) which is attributed to the oxidation of the silicon substrate. The absence of ferrocene signals is attributed to the rate of reduction of **bis-diazo** being slower on Si(100) than it is on Si(111)

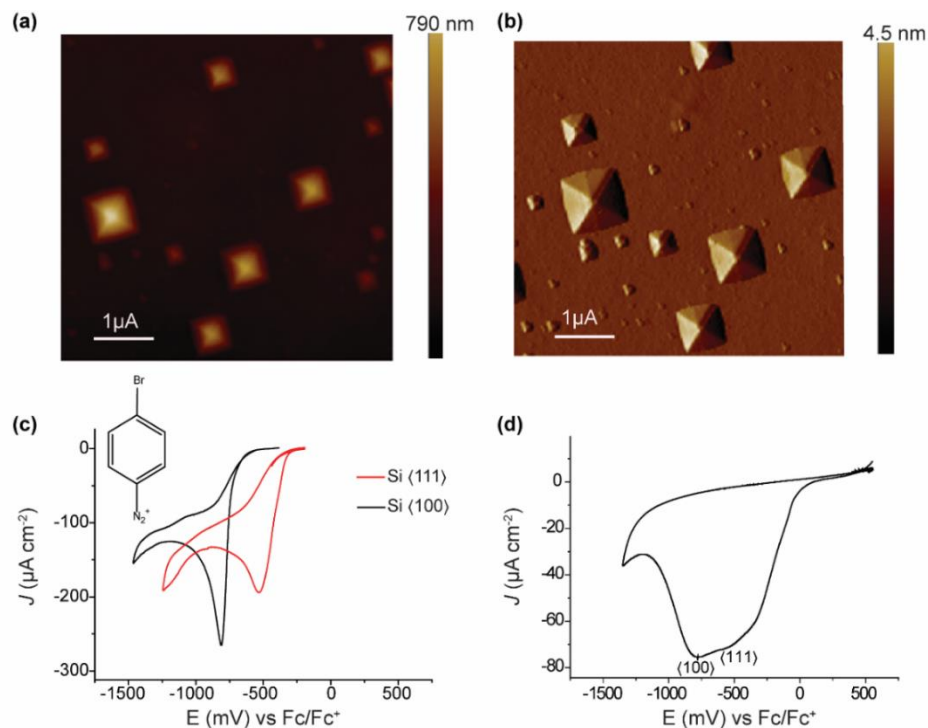


Figure C-4-13 a) AFM (height) image showing the Si(111) pyramids on Si(100) surface obtained by anisotropic etching of a Si(100) surface in 20% KOH solution. b) AFM (amplitude error) image for the same surface. c) The electrochemical reduction wave of **4-bromobenzene diazonium** on separate Si(111) and Si(100) surfaces are at -540 and -808 mV, respectively. d) The electrochemical reduction wave of **4-bromobenzene diazonium** on the mixed Si(111)/Si(100) surfaces showing two waves at -570 and -805 mV corresponding to the reduction of **4-bromobenzene diazonium** on Si(111) and Si(100), respectively.

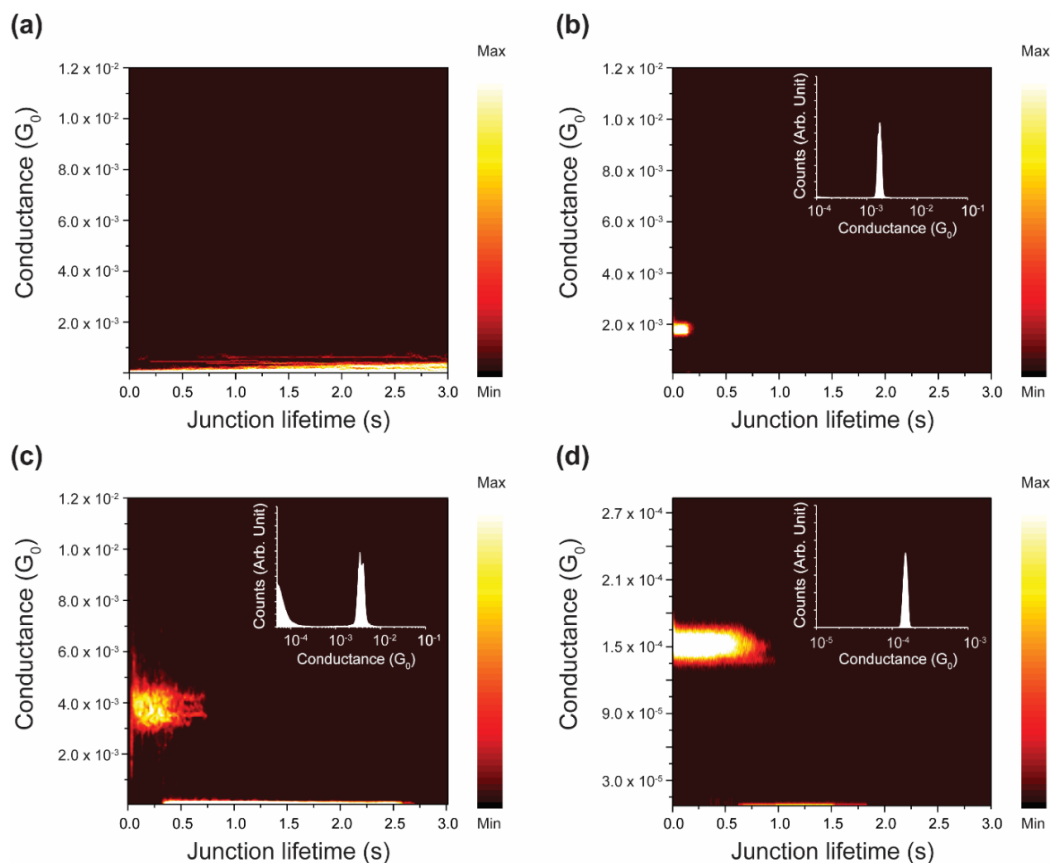


Figure C-4-14 2D conductance histograms of blinking experiments between a gold STM tip and a gold electrode using either (a) neat mesitylene, with an accumulation time of 2 h, (b) 1,4-phenylenediamine (Au-molecule-Au) (c) benzene-1,4-dithiol (Au-molecule-Au) (d) **bis-diazo** (Au-C-Si). The 2D maps in (b-d) are obtained from the accumulations of ca. 250 blinks and an accumulation time of 2-3 h. Insets in (b-d) show the corresponding 1D linear histograms obtained from the same data used to accumulate the 2D maps. The average blinking lifetime was 0.20, 0.50 and 0.75 s for 1,4-phenylenediamine, benzene-1,4-dithiol and **bis-diazo**, respectively.

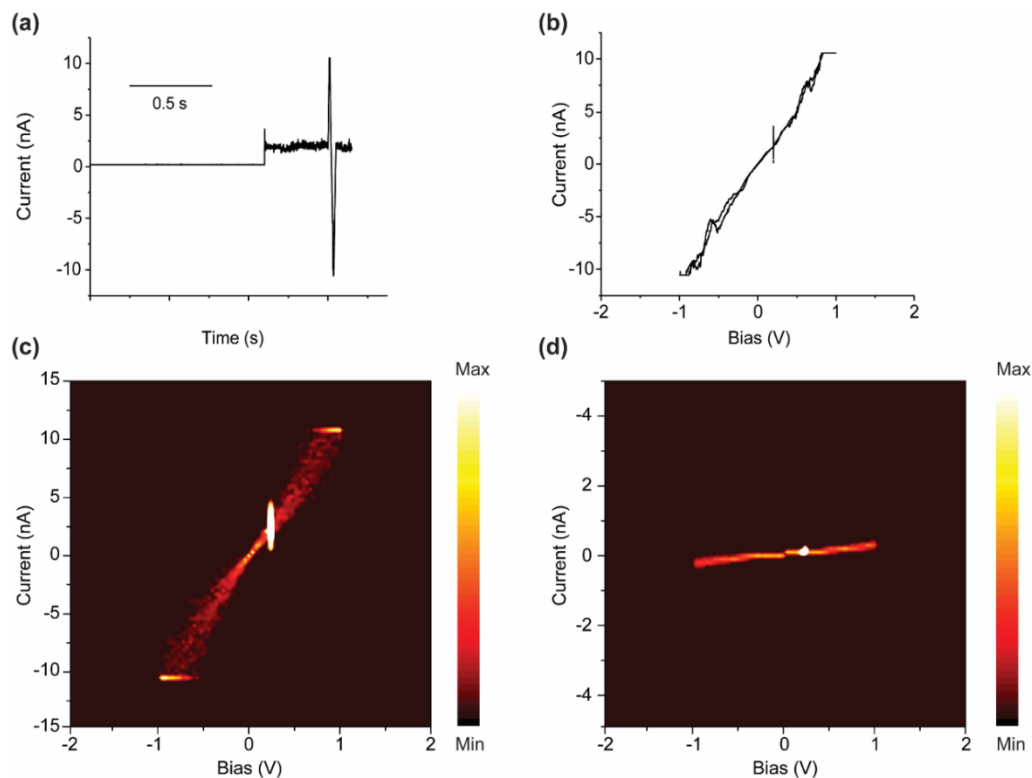


Figure C-4-15 (a) A representative Au-**bis-diazo**-Au blink measured at a bias of 0.2 V, with a bias sweep (-1 to +1 V) applied during the lifetime of the blink. (b) Current-voltage data acquired during a blink of the Au-**bis-diazo**-Au systems shown in panel (a). (c) Current-voltage measurements of Au-**bis-diazo**-Au junctions in which the **bis-diazo** molecule is covalently bound to both electrodes. (d) Current-voltage measurements of Au-Au tunneling junctions in the absence of **bis-diazo** molecules. Each data set is the accumulation of 30 different voltage sweeps.

Appendix D

C-5-1 Statement of contribution to a co-authored paper

Chapter 5 is the co-authored paper "Spontaneous S–Si bonding of alkanethiols to Si(111)–H: towards Si–molecule–Si circuits" which was published in Chemical Science.

The details of this article is given below

Chandramalika R. Peiris, Simone Ciampi, Essam M. Dief, Jinyang Zhang, Peter J. Canfield, Anton P. Le Brun, Daniel S. Kosov, Jeffrey R. Reimers and Nadim Darwish
Chemical Science, Volume 11, 26th April 2020, Pages 5246–5256

DOI: <https://doi.org/10.1039/D0SC01073A>

I, Malwattage Chandramalika Rukmali Peiris, as the primary author, conducted all of the experimental work and data analysis, creating tables, figures, writing and editing of the manuscript

Contribution of other co-authors is as follows:

Simone Ciampi contributes by co-supervision, data interpretation and manuscript editing for the paper. Essam M. Dief contributes with the synthesis of molecules, Jinyang Zhang contributes by capturing the scanning electron microscopic images of the Si surfaces, Anton P. Le Brun contributes by doing X-ray refractometry, Peter J. Canfield, Daniel S. Kosov, Jeffrey R. Reimers contribute by ideas, theoretical calculation and editing the manuscript. Nadim Darwish contributes by helping with scanning tunneling microscopic experiments, data analysis, supervision and editing of the manuscript.

I, as a co-author of the article name "Spontaneous S–Si bonding of alkanethiols to Si(111)–H: towards Si–molecule–Si circuits " confirms that the contribution by the M. C. R Peiris indicated above is correct

- 1) Simone Ciampi
- 2) Essam M. Dief
- 3) Jinyang Zhang
- 4) Peter J. Canfield
- 5) Anton P. Le Brun
- 6) Daniel S. Kosov
- 7) Jeffrey R. Reimers
- 8) Nadim Darwish

“Reproduced with permission from (Chem. Sci 2020, 11, 5246–5256.) Copyright (2020) Royal Society of Chemistry.”

RE: Permission Request Form: Chandramalika R. Peiris

CONTRACTS-COPYRIGHT (shared) <Contracts-Copyright@rsc.org>

Tue 20/09/15 6:16 PM

To: Chandramalika Peiris <m.c.peiris@postgrad.curtin.edu.au>

Dear Dr Peiris

The Royal Society of Chemistry (RSC) hereby grants permission for the use of your paper(s) specified below in the printed and microfilm version of your thesis. You may also make available the PDF version of your paper(s) that the RSC sent to the corresponding author(s) of your paper(s) upon publication of the paper(s) in the following ways: in your thesis via any website that your university may have for the deposition of theses, via your university's Intranet or via your own personal website. We are however unable to grant you permission to include the PDF version of the paper(s) on its own in your institutional repository. The Royal Society of Chemistry is a signatory to the STM Guidelines on Permissions (available on request).

Please note that if the material specified below or any part of it appears with credit or acknowledgement to a third party then you must also secure permission from that third party before reproducing that material.

Please ensure that the thesis includes the correct acknowledgement (see <http://rsc.li/permissions> for details) and a link is included to the paper on the Royal Society of Chemistry's website.

Please also ensure that your co-authors are aware that you are including the paper in your thesis.

Regards

Gill Cockhead

Contracts & Copyright Executive

Gill Cockhead

Contracts & Copyright Executive

Royal Society of Chemistry,

Thomas Graham House,

Science Park, Milton Road,
Cambridge, CB4 0WF, UK

From: m.c.peiris@postgrad.curtin.edu.au <m.c.peiris@postgrad.curtin.edu.au>

Sent: 15 September 2020 03:18

To: CONTRACTS-COPYRIGHT (shared) <Contracts-Copyright@rsc.org>

Subject: Permission Request Form: Chandramalika R. Peiris

Name: Chandramalika R. Peiris

Institution: Curtin University

Email: m.c.peiris@postgrad.curtin.edu.au

Address: Unit 3/29 Stannard Street

Bentley

6102

Australia

I am preparing the following work for publication:

Article/chapter title: Chapter 5

Journal/book title: Covalently linked molecule–electrode contacts toward robust molecular-electronics circuits

Editor/author(s): Malwattage Chandramalika R Peiris

Publisher: Curtin University

Is this request for a thesis?: Yes

I would very much appreciate your permission to use the following material:

Journal/book title: Spontaneous S–Si bonding of alkanethiols to Si(111)–H: towards Si–molecule–Si circuits

Editor/author(s): Chandramalika R. Peiris, Simone Ciampi, Essam M. Dief, Jinyang Zhang, Peter J. Canfield, Anton P. Le Brun, Daniel S. Kosov, Jeffrey R. Reimers and Nadim Darwish

ISBN/DOI: <https://doi.org/10.1039/D0SC01073A>

Year of publication: 2020

Page(s): 5246-5256

Type of material: Full paper

Figure/image number (if relevant):

Any additional comments:

I am the first author for this paper

Agree to terms: I agree

This communication is from The Royal Society of Chemistry, a company incorporated in England by Royal Charter (registered number RC000524) and a charity registered in England and Wales (charity number 207890). Registered office: Burlington House, Piccadilly, London W1J 0BA. Telephone: +44 (0) 20 7437 8656.

The content of this communication (including any attachments) is confidential, and may be privileged or contain copyright material. It may not be relied upon or disclosed to any person other than the intended recipient(s) without the consent of The Royal Society of Chemistry. If you are not the intended recipient(s), please (1) notify us immediately by replying to this email, (2) delete all copies from your system, and (3) note that disclosure, distribution, copying or use of this communication is strictly prohibited.

Any advice given by The Royal Society of Chemistry has been carefully formulated but is based on the information available to it. The Royal Society of Chemistry cannot be held responsible for accuracy or completeness of this communication or any attachment. Any views or opinions presented in this email are solely those of the author and do not represent those of The Royal Society of Chemistry. The views expressed in this communication are personal to the sender and unless specifically stated, this e-mail does not constitute any part of an offer or contract. The Royal Society of Chemistry shall not be liable for any resulting damage or loss as a result of the use of this email and/or attachments, or for the consequences of any actions taken on the basis of the information provided. The Royal Society of Chemistry does not warrant that its emails or attachments are Virus-free; The Royal Society of Chemistry has taken reasonable precautions to ensure that no viruses are contained in this email, but does not accept any responsibility once this email has been transmitted. Please rely on your own screening of electronic communication. More information on The Royal Society of Chemistry can be found on our website: www.rsc.org

Appendix E

E-1 Silicon STM tip preparation

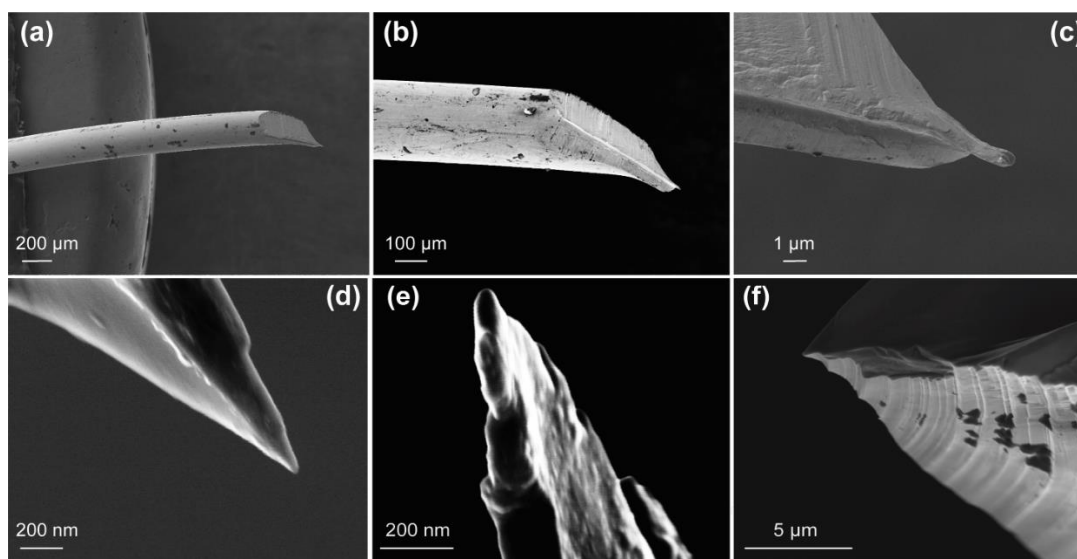


Figure E-5-1 (a-c) SEM images of mechanically cut gold STM tips at different scales. The radius of these conventional gold tips is comparable to that formed with silicon (111) tips shown in (d-f). SEM images of typical silicon (111) tips prepared by etching in 3.50 M KOH solution for 48 h at 65 °C. The tip preparation procedure consistently led to tip radii less than 1 μm and is comparable to that of gold STM tips.

E-2 AFM characterization

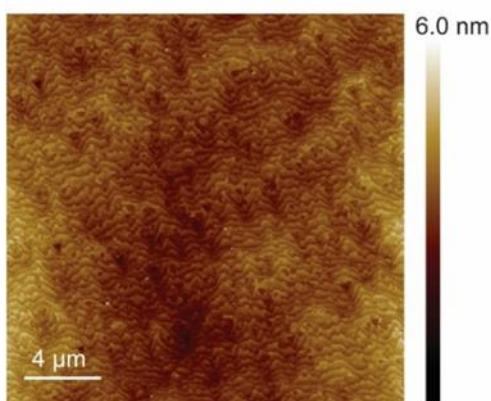


Figure E-5-2 AFM characterisation of 20× 20 μm of a p-type Si(111)-H surface covered by dithiol **2**. The topography shows flat terraces separated by atomic steps. The peak-to-peak roughness measured within one Si(111) terrace is ca. 1.7 Å, consistent with an atomically smooth alkyl monolayer on Si(111). The high-quality topography confirms that the SAMs are homogeneous monolayers at the nanoscale, free of any contaminants or oxidative damage. AFM images of the same surfaces kept for 7 days under ambient condition did not show any sign of deterioration.

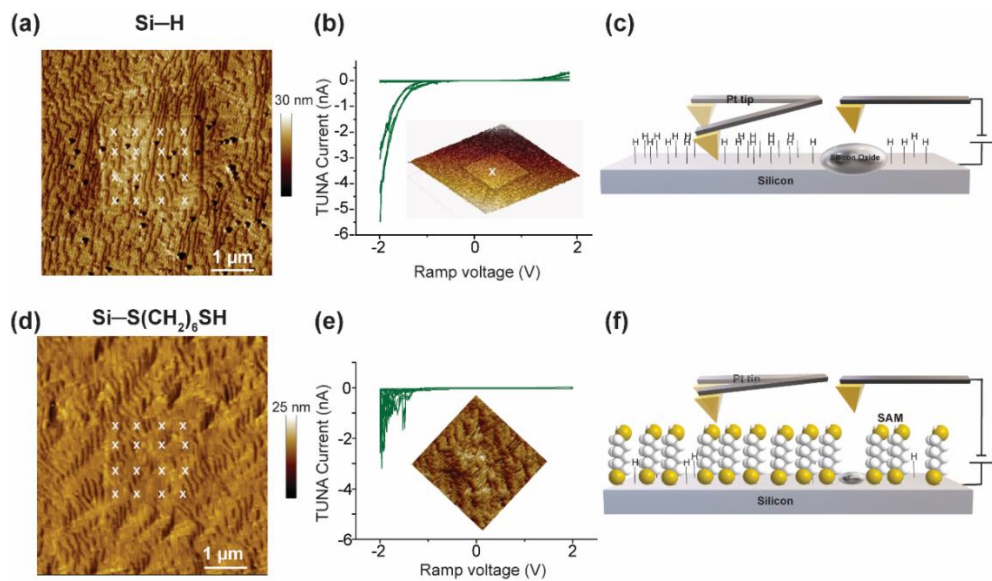


Figure E-5-3 (a) and (d) show the topography images ($5 \times 5 \mu\text{m}$) of the Si-H and the Si-S(CH₂)₆SH after a squared (2×2) μm area in the center of the Si surface was held at +2 V for a period of 8 min with constant peak force of 554 nN . The “x” labels indicate the location where a bias sweep was applied. (b) and (e) show the current-voltage (I - V) sweeps applied on the bias-treated areas at the center of the surfaces. The I - V curves of the Si-S(CH₂)₆SH surface are almost all rectifying (e) as expected for a platinum- n -type Si Schottky junction indicating that the hexanethiol monolayer prevent the surface from oxidation; however, after oxidation of the Si-H surface (b) a clearly AFM-visible oxide layer forms ($3.0 \pm 0.6 \text{ nm}$) which significantly blocks the current passing through the surface in more than 75% of the collected current-voltage curves meaning that the thin layer of oxide acts as dielectric film. Since the first step of oxidation of the Si surface requires the desorption of the -H or the -S(CH₂)₆SH, we conclude that the high density Si-S(CH₂)₆SH monolayers are exceptional in preventing silicon oxidation. (c) and (f) are schematic diagrams of the studied surfaces.

E-3 X-ray Reflectometry (XRR)

Specular X-ray reflectometry at the solid-air interface was conducted on a Panalytical Ltd X’Pert Pro instrument with a rotating anode source (Cu $K\alpha$ radiation, $\lambda = 1.54 \text{ \AA}$). The beam was focused using a Göbel mirror and collimated using fixed slits of 0.1 mm. The samples were mounted onto a motorised stage to adjust the sample into the optimal position for measurements. Angles of incidence were measured from

0.05° to 5.00° in 0.01° steps for 20 seconds per step. The raw data was reduced so that the critical edge was normalised to a reflectivity of unity and the data was presented as reflectivity versus momentum transfer, Q , defined as:

$$Q = \frac{4\pi \sin \theta}{\lambda}$$

where λ is the X-ray wavelength and θ is the angle of incidence. The data was analysed using MOTOFIT which utilises an Abele's matrix method. The monolayer was fitted using a single layer model with fitting parameters of thickness, roughness, and scattering length density (SLD), ρ , defined as:

$$\rho = \frac{r_e \sum Z_i}{V_m}$$

where V_m is the total molecular volume (determined to be 149 Å³ for compound **2**), Z_i is the atomic number of each atom in the species, and r_e is the Bohr electron radius (2.818 × 10⁻⁵ Å). The theoretical SLD (ρ_t) of compound **2** was determined to be 15.6 × 10⁻⁶ Å⁻². The fitting parameters were varied using least-squares regression until the calculated reflectivity from the fit suitably matched the collected data. The number of molecules per cm² was determined from the fitted values as follows:

$$\text{molecules per cm}^2 = \frac{\tau \rho_f 10^{16}}{V_m \rho_t}$$

Where τ is the fitted thickness and ρ_f is the fitted SLD.

Table E-5-1 Theoretical parameters used in the modelling.

Molecule	Calculated SLD / × 10 ⁻⁶ Å ⁻²	Estimated maximum thickness / Å	Estimated volume / Å ³
1,6-hexanedithiol	15.6	11.3	149

Table E-5-2 Fitted SAM thickness and surface roughness (in Å), and fitted SLD (in 10^{-6} \AA^{-2}) for **2** on Si(111)-H as determined from XRR data (see XRR curves in Figure. 5.2c).

Monolayer	Thickness / Å	Fitted SLD / $\times 10^{-6} \text{ \AA}^{-2}$	Volume fraction	Molecules per cm^2	coverage %	Roughness of Si-monolayer interface/ Å	Roughness of monolayer-air interface / Å
Low doped n	9.1 ± 0.2	13.7 ± 0.2	0.878 ± 0.013	5.36×10^{14}	68	0.6 ± 0.1	4.4 ± 0.1
Low doped p	10.4 ± 0.5	13.8 ± 0.2	0.885 ± 0.012	6.17×10^{14}	78	1.1 ± 0.2	4.6 ± 0.1
High doped n	8.5 ± 0.6	15.3 ± 0.1	0.981 ± 0.006	5.59×10^{14}	71	3.9 ± 0.1	13.3 ± 0.3
High doped p	11.1 ± 0.4	13.9 ± 0.3	0.891 ± 0.019	6.64×10^{14}	84	2.9 ± 0.1	7.3 ± 0.2

The SLD of air and silicon was fixed to 0 and $20.1 \times 10^{-6} \text{ \AA}^{-2}$ respectively.

E-4 Initiation and then propagation of a free-radical polymerization process

This section provides more details of the initiation and propagation reactions depicted in Figure 5.4, involving the model compound RSH ($R = \text{C}_3\text{H}_7$) reacting with Si(111)-H.

Figure 5.4 shows a reaction scheme involving initiation of the surface reaction and then propagation of a free-radical polymerization process at low coverage, showing calculated Gibbs free energies. The corresponding figure showing the purely electronic energy differences is Figure E-5-4.

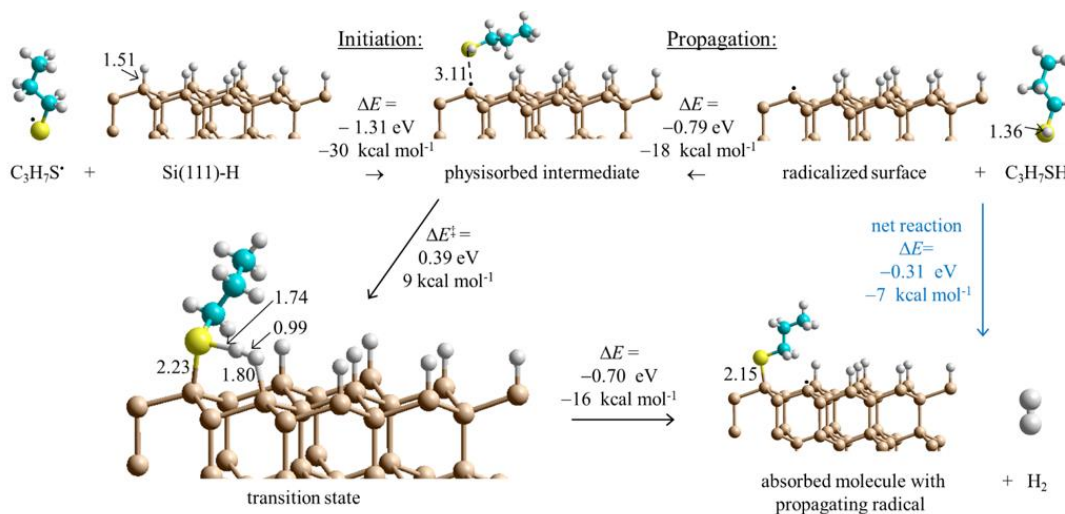


Figure E-5-4 DFT mechanism for SAM formation starting at low coverage. Calculations indicate that thiyl radicals (RS^\bullet , with here $R = C_3H_7$) produced by attack of solution O_2 on the thiol reactants (RSH) react with $Si(111)-H$ to abstract hydrogen and for thiol physisorbed to a silicon surface radical (black dot). Reaction over a barrier then leads to chemisorption and radical regeneration. This provides initiation for a free-radical polymerization reaction that then covers the surface with adsorbate. Some critical bond lengths are shown, in \AA ; only one copy of the used 3×3 supercell is shown. These results show the electronic energy changes coming from the VASP calculations that are analogous to the Gibbs free energy changes shown in Figure 5.4.

The transition state shown in these figures is a very complex one involving simultaneous motion involving changes to the $Si-S$, $S-H$, $H-H$, and $Si-H$ bond lengths: the reaction involves the near-synchronous breaking of two bonds and reformation of another two. Initial calculations were performed on a model compound, freezing the coordinates of the external silicon atoms to coincide with locations on the 2D $Si(111)-H$ surface. This cluster, as well as the energetics analogous to those shown in Figure E-5-5, are provided in Figure E-5-4. The results are quite similar to those subsequently optimized for the 2D surface. Indeed, the optimization of the transition structure for the 2D materials was made starting at the results for the model compound.

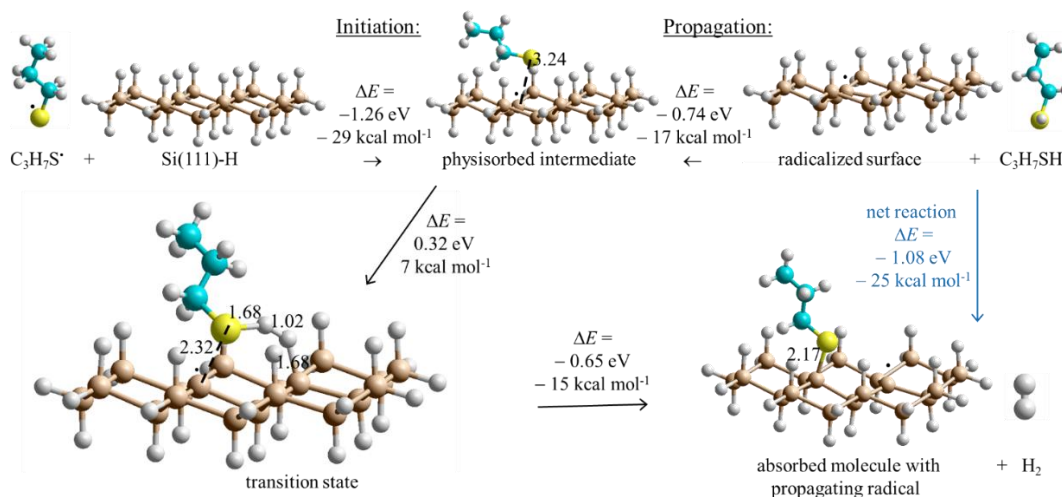


Figure E–5–5 DFT mechanism for SAM formation based on the properties of a model compound. Calculations indicate that thiyl radicals (RS^\bullet , with here $R = C_3H_7$) produced by attack of solution O_2 on the thiol reactants (RSH) react with $Si(111)-H$ to abstract hydrogen and for thiol physisorbed to a silicon surface radical (black dot). Reaction over a barrier then leads to chemisorption and radical regeneration. This provides initiation for a free-radical polymerization reaction that then covers the surface with adsorbate. Some critical bond lengths are shown, in \AA .

There is one significant difference found between the results for the model compound and the 2D surface: a second intermediary species was found for the 2D surface, displaying a chemisorbed thiol with in which sulfur forms three covalent bonds. It is only a shallow minimum on the potential-energy surface and hence was not depicted in the primary results in Figure 5.4. Its structure and properties are given in Figure E–5–5.

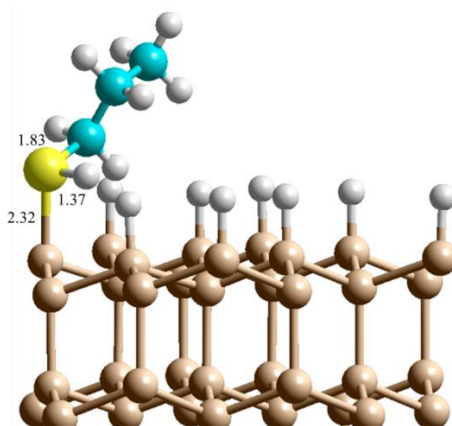


Figure E-5-6 A chemisorbed intermediate found on the 2D surface, showing the covalent-bond lengths to sulfur, in Å.

Notwithstanding this difference, the reaction profiles for the model cluster and 2D surface are similar. The energy profiles and key coordinate changes as a function of an internal reaction coordinate (defines as the integral of the accumulated bond-length changes in the 4 key bonds) are shown in Figure E-5-7. The Si-S and H-H bonds are largely formed at the transition state whilst the Si-H and S-H bonds are just beginning to break. On the 2D surface, the transition state occurs slightly later than it does for the model cluster.

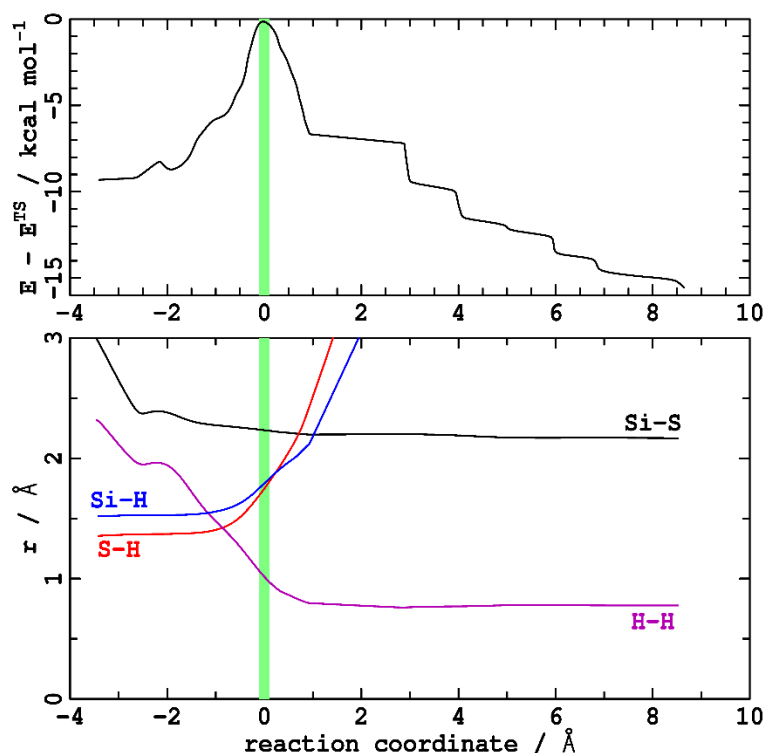


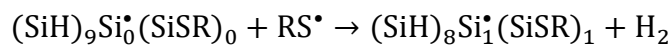
Figure E-5-7 The top frame shows the energy calculated for the indicated model cluster system as a function of a continuous reaction coordinate, going from the physisorbed intermediate over the transition state to form products. The lower frame shows the critical Si-S, S-H, H-H, and H-Si bond lengths (see Figure 5.4) along this reaction coordinate. While at the transition state, the H-H and Si-S bonds are largely formed whilst the S-H and Si-H are largely unbroken, critical changes to all 4 bond lengths do occur at this structure. The reaction coordinate follows the eigenvector of the hessian matrix with imaginary eigenvalue away from the transition state (green region), but afterwards becomes the results of unconstrained geometry optimization. The reaction profile for the model compound is similar.

E-5 SAM completion at high coverage for the binding of **2** to Si(111)-H

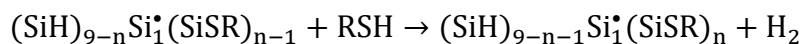
Calculations on a 3×3 supercell for the binding of **2** to Si(111)-H at high coverage are reported. In this lattice, the chemical state of the 9 surface silicon atoms can be represented by the formula

$$(\text{SiH})_i \text{Si}_j^* (\text{SiSR})_k \text{ where } i + j + k = 9$$

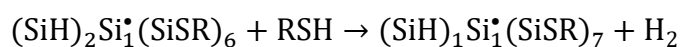
and $R = S(CH_2)_6SH$. At the low coverage of 1:9, the structure of $(SiH)_8Si_0^*(SiSR)_1$, shown in Figure 5.5a, has the alkane chains oriented at an angle of 70° to the surface. On this surface, initiation occurs through the reaction (akin to Figure 5.5)



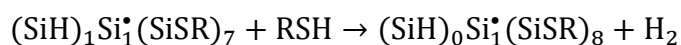
followed by the free-radical polymerization reaction



which can, in principle, occur for $n = 2$ to 8 , the final product being the isolated surface radical $(SiH)_0Si_1^*(SiSR)_8$. Figure 5.5b shows the species with $n = 7$ that forms part of this sequence, $(SiH)_1Si_1^*(SiSR)_7$. DFT predicts the reaction leading to its production



to be exothermic, with $\Delta E = -15 \text{ kcal mol}^{-1}$. However, as Frame c in Figure 5.5 shows, in this structure six chains are forced to align vertically whilst one slightly lays over, taking on an orientationally partially disordered structure in which the 7 chains quickly adjust to become roughly equally spaced. The inter-chain separation is ca. 4.3 \AA , close to the optimal distances found in 3D alkane materials and in monolayers on surfaces. Adding more ligands to this structure, therefore requires compression of the ligands, with effectively all of the compression energy of all of the ligands needed to be costed during the next step in the polymerization process. As a result, the calculated reaction energy for the next step,



is predicted to be endothermic, with $\Delta E = +44 \text{ kcal mol}^{-1}$. The free-radical polymerization mechanism therefore cannot proceed beyond a coverage of 7:9.

Also, free-radical polymerization can only proceed if the silicon free radical Si^\bullet is located on an adjacent site to a SiH bond. During SAM polymerization, several Si-H bonds could be located adjacent to Si^\bullet , meaning that the path that the polymerization takes across the 2D surface is not controlled. Hence it is possible to produce silicon radicals that are not adjacent to Si-H, prematurely terminating chain propagation. Similarly, the SAM may grow in ways that leave one or more Si-H bonds surrounded by SiSR and hence unavailable for a chain-propagation reaction. It is therefore likely that the chain propagation reaction will lead to a SAM containing many defects.

If the SAM is in thermodynamic equilibrium, then such defects would be healed by annealing. Even in SAMs held together only by Van der Waals forces, thermodynamic equilibrium is difficult to establish, making final compositions controlled by kinetic rather than thermodynamic factors. However, key steps in the formation process may be under thermodynamic control, and these can manifest to control some key final outcomes. In this case, calculations indicate that the transition state for the addition of the eighth ligand above remains accessible from the intermediate state (by analogy to Figure 5.5c), it is just that the precursor state itself becomes energetically unattainable. Understanding SAM properties then comes down to understanding the energetics of reactions that would anneal the SAM.

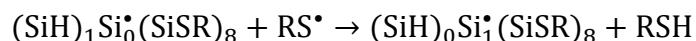
We have considered two processes for the model compound with R = C₃H₇, a species for which annealing reactions would be thought to be easier than for **2**. First, we examined the interchange of the ligand from an SiSR site to a neighbouring Si* site. Accurate transition-state energies were not obtained, but many possible paths were examined with estimated barriers in the 40-50 kcal mol⁻¹ range. To anneal SAMs at room temperature within 24 hours, barriers of at most 25 kcal mol⁻¹ could be envisaged. Second, we considered processes in which the ligand on an SiSR site interchanges with the hydrogen on a neighbouring Si-H site, possible through a self-catalysed thiol intermediate. Again, no pathway under 40 kcal mol⁻¹ could be envisaged. These results suggest that produced SAMs are kinetically trapped post production.

If the reactions are performed in solutions containing molecular oxygen and thiols, then small amount of thiols present in solution could continue to react with partially formed SAMs. Of most significance, the most difficult reaction to complete, the reaction of a radical SAM at 8:9 coverage to form a SAM at 1:1 coverage, i.e.



is predicted to be exothermic, with $\Delta E = -45$ kcal mol⁻¹ for R = (CH₂)₆SH. The energy released by the fusing of the two radicals to form a Si-S bond is sufficient to compress the SAM into the extremely tight structure shown in Figure. 5.4c. If that silicon surface radical can react with solution radicals, then so can any other similar species have produced during the SAM formation process.

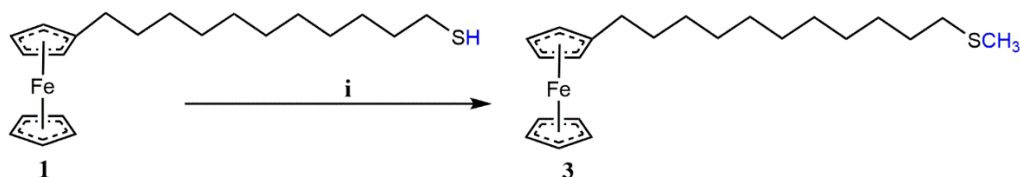
Next, we consider the reaction of an isolated SiH group with an RS[•] radical from solution. The hydrogen abstraction reaction



is predicted to be exothermic, with $\Delta E = -12 \text{ kcal mol}^{-1}$. This reaction introduces no new compression to the SAM and gains its exothermicity from the difference in S–H and Si–H bond strengths. After it is completed, a silicon surface radical is produced that can then react with a second thiol from solution to complete the SAM.

The difficulty in doing these reactions, controlling their transition-state energies, will be the compression of the SAM that must be introduced prior to the meeting of the reacting atoms. These barriers will be strongly ligand-size dependent, suggesting that an optimum chain length will exist for producing regular SAMs. They will also strongly depend on the precise chemical structure of the defect being attacked by the radical. Basically, reactions on defects in SAMs at below 7:9 coverage will be expected to proceed based only on the availability of surface radicals, whereas reactions involving species at 1:1 coverage will experience high barriers. These high barriers may well exceed 25 kcal mol^{-1} and hence prevent SAMs forming at these coverages.

E-6 Synthesis of 11-(Ferrocenyl)undecyl methyl sulphide (**3**)



Scheme E-5-1 Synthesis of compound **3**

Reagents: 240) MeOH, DMF, NaOH, CH₃I, 0 °C, 10 min.

All chemicals used for the synthesis of 11-(Ferrocenyl)undecyl methyl sulphide (**3**) were of analytical grade and used as received. 11-(Ferrocenyl)undecanethiol (**1**), 95.0%), iodomethane (99.0%), methanol (97.0%), deuteriochloroform (99.8%), N,N-dimethylformamide (99.8%), chloroform (98.0%) and hexane (98.0%) were purchased from Sigma-Aldrich and sodium hydroxide (97.0%) was purchased from Ajax fine chem. Milli-Q water (>18 MΩ cm) was used for cleaning and the preparation of solutions. The synthesis of **3** is based on a procedure reported by Yasuhiro. M et al. (Ann. Nucl. Med. 1993, 7, 173-177). Briefly, to a solution **1** (74.4 mg, 0.1 mmol) in 10 mL of MeOH: DMF (1:1) was added 10 mL of NaOH (1 M). Iodomethane (0.11 mmol, 13.68 μL) was cooled down to 0 °C and added to the mixture with continuous stirring for 10 min at 0 °C (Scheme E-5-1). The organic phase was then extracted using chloroform, evaporated and purified by gradient column chromatography using hexane. The purified form of **3** is then dried under vacuum resulting in a pale-yellow solid (46.4 mg, 60% yield). ¹H NMR 400 MHz (CDCl₃): δ (ppm) = 4.08 (s, 5H), 4.02 (s, 4H), 2.47 (m, 2H), 2.30 (t, 2H), 2.11 (s, 3H) for the added methyl group, 1.55 (m, 4H), 1.47 (m, 2H), 1.36(m, 2H), 1.28 (m, 10H). ¹³C{¹H} NMR (101 MHz, CDCl₃): δ (ppm) = 15.61(CH₃), 28.85(CH₂), 29.21(CH₂), 29.27(CH₂), 29.54(CH₂), 29.61(CH₂), 29.67(CH₂), 31.14(CH₂), 34.38 (CH₂), 53.41 (CH₂, next to ferrocene ring), 67.05 (CH), 68.14 (CH), and 68.50 (CH). HRMS m/z calculated for **3** [M+H]⁺ 386.1725, found 386.1720.

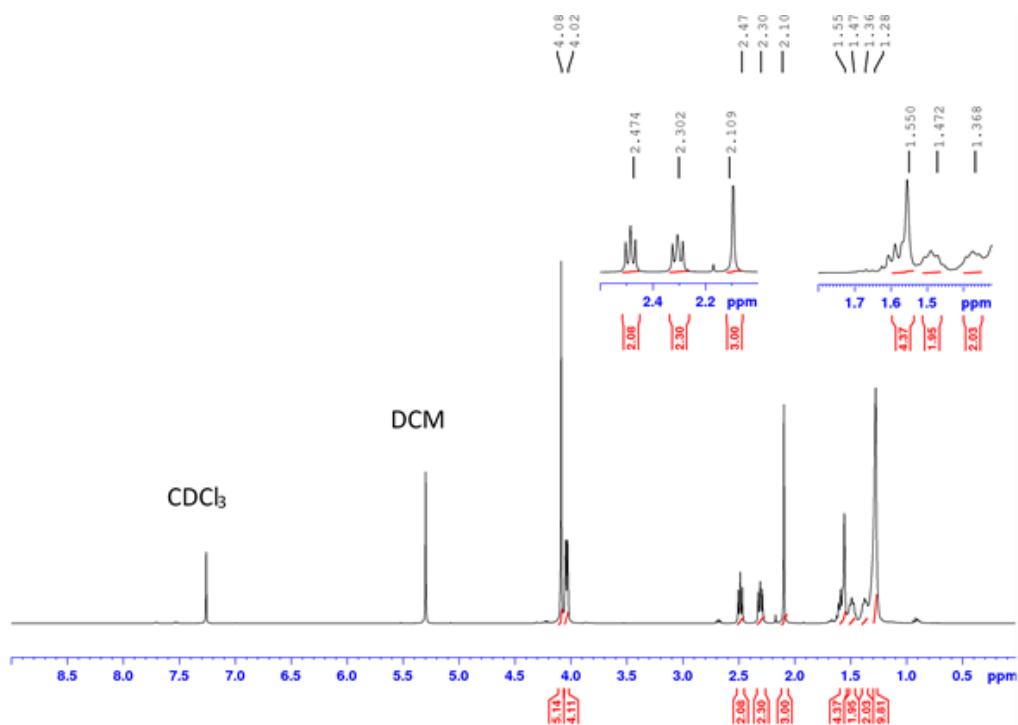


Figure E-5-8 ¹H NMR 400 MHz (CDCl₃) spectrum of **3**

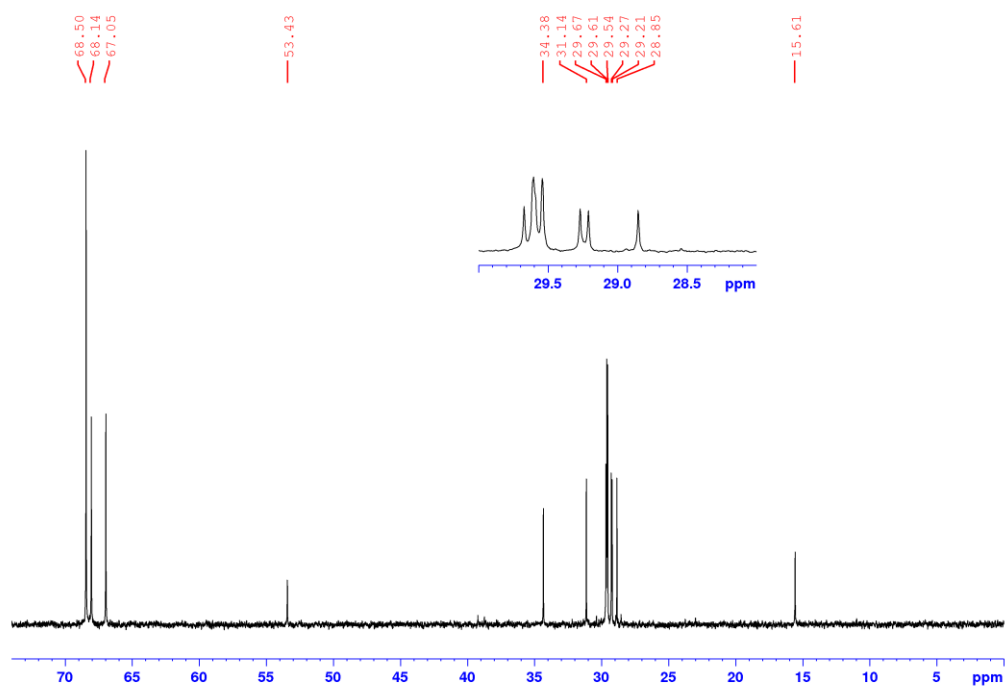


Figure E-5-9 ^{13}C NMR (CDCl_3 , 101 MHz) spectrum of **3**

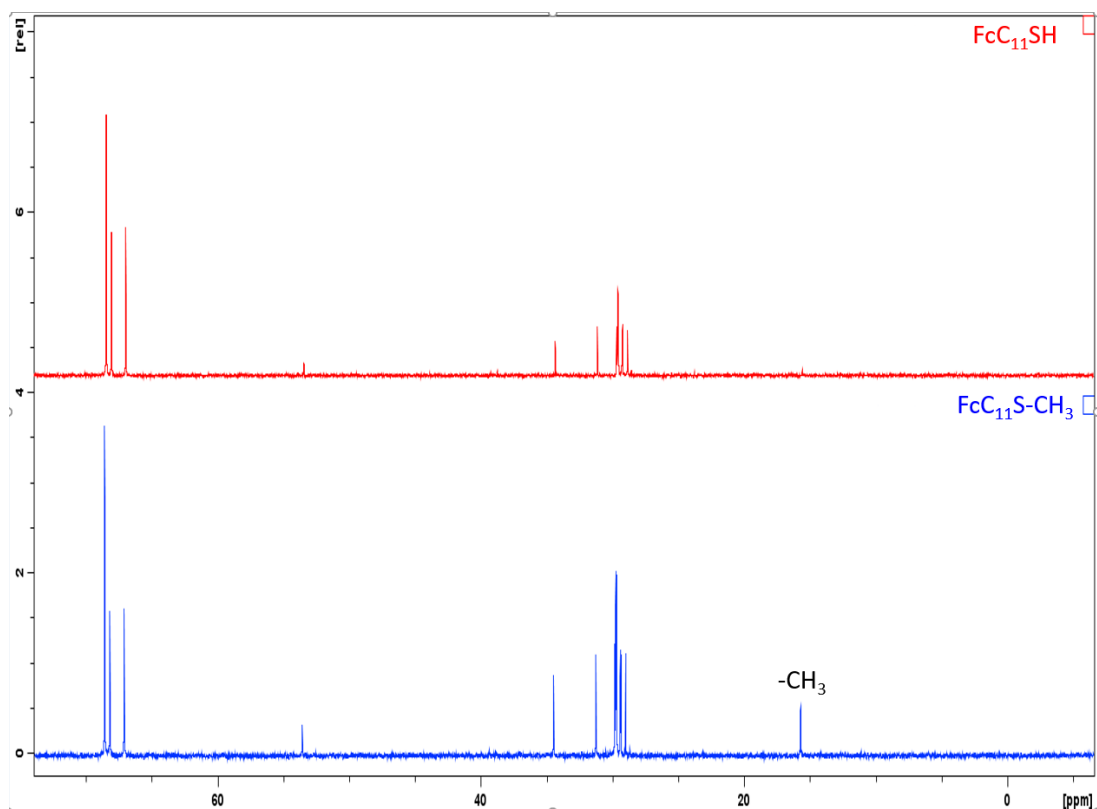


Figure E-5-10 ^{13}C NMR spectra for **3** (blue) and **1** (red) with the methyl signal in **3** at $\delta=15.7$.

E-7 XPS analysis

The XPS spectra Si(111)-H, incubated in 4 mM solution of **3** for 24 h showed an absence of the S-Si bonding at 162 eV. The observed noise between 162-164 eV is related to the Si plasmon loss background as it is also present in untreated Si(111)-H (Figure E-5-12). Further, the high resolution of the Si 2p envelope showed in addition to an emission centred at 99.5 eV that is assigned to the Si-Si bonding, an additional weak emission at 103 eV that is assigned to the growth of SiO_x suggesting that the Si(111)-H surface is prone to oxidation in the absence of a monolayer. This indicates that **3** does not form a monolayer.

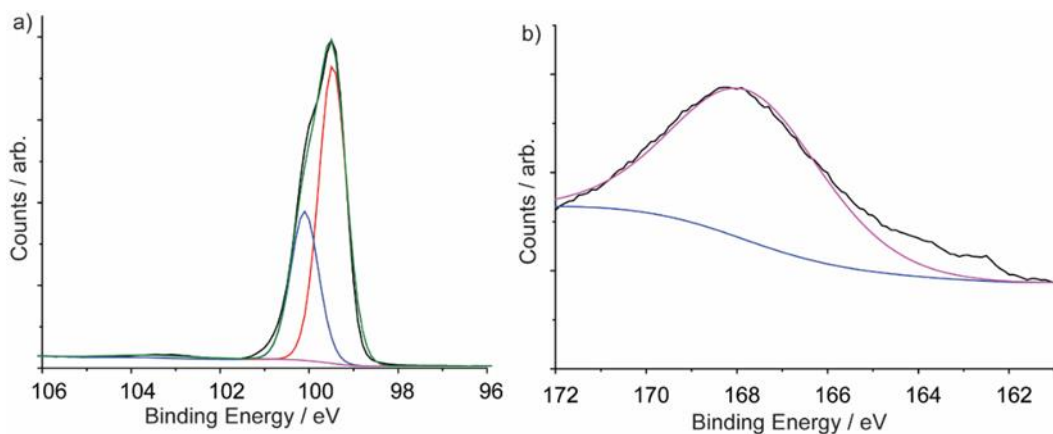


Figure E-5-11 a) XPS High-resolution Si 2p emission and b) S 2p emission for a Si(111)-H surface incubated in 4 mM solution of **3** for 24 h.

As a control measurement on the background signal of the Si electrode surface, we performed an XPS measurement for a freshly etched, unmodified Si(111)-H electrode (see Figure E-5-12 below). Si 2p emission showed a background emission alongside the high intensity Si plasmon loss peak at 168 eV.

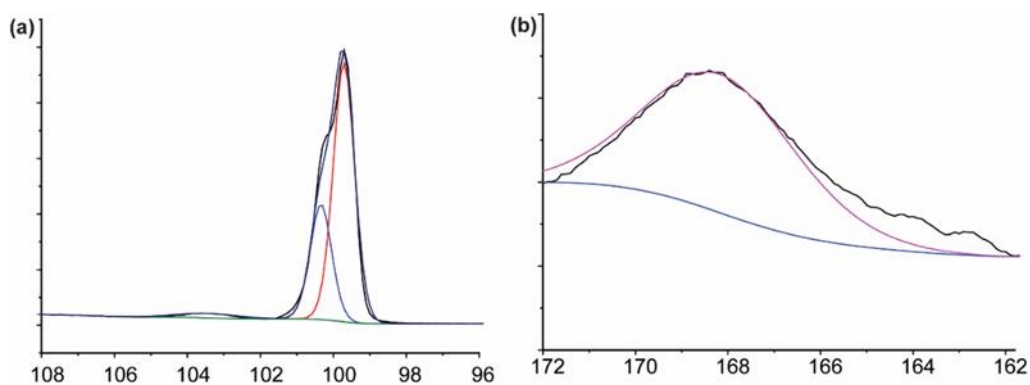


Figure E-5-12 a) XPS high resolution Si 2p emission and b) S 2p emission for untreated Si(111)-H electrode stored in DCM for 24 h.

E-8 Electrochemical characterisation of **3**

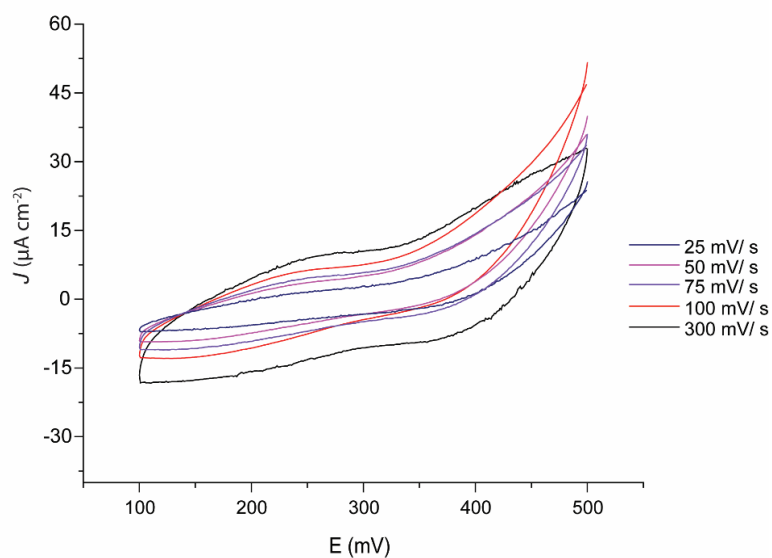


Figure E-5-13 Cyclic voltammograms of Si(111)-H surface incubated in 4 mM solution of **3** for 24 h. The voltammograms show absence of ferrocene signals and an increase in current beyond + 400 mV, indicating surface oxidation in the absence of a monolayer, suggesting that **3** does not form a monolayer on Si(111)-H surfaces.

E-9 STM-Plateau length histograms

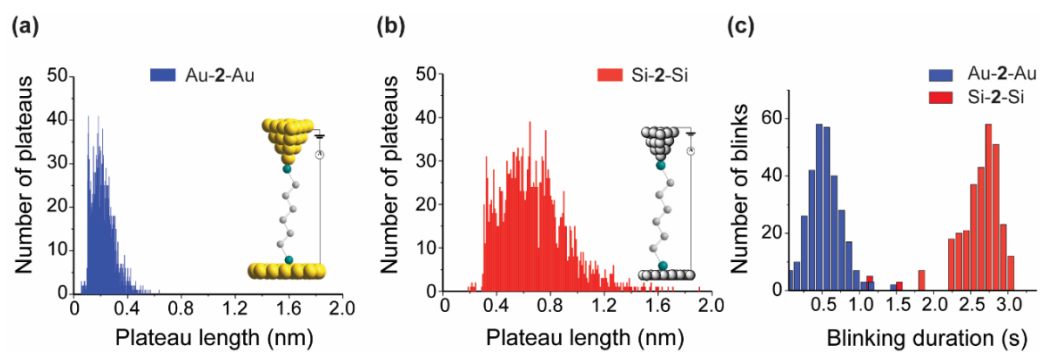


Figure E-5-14 Plateau length histogram for (a) Au-2-Au with average plateau length of 0.25 nm and (b) Si-2-Si junctions with average plateau length of 0.70 nm. This suggests that due to the enhanced mechanical stability, the Si-2-Si junctions are resistant to breakage during the entire pulling cycle while the typical Au-2-Au junctions break before a full molecular stretch (c) Blinking duration histograms when 2 is bonded to two Au electrodes (blue) versus when bonded to two Si electrodes (red) with average lifetime of 0.56 s and 2.70 s, respectively.

E–10 DFT optimized coordinates for all optimized 2D structures and associated molecules.

Table of Contents:

1. H₂
 2. C₃H₇SH
 3. C₃H₇S
 4. Si(111)-H 3x3
 5. Si(111)-H 3x3 radical, with one removed H
 6. Si(111)-H 3x3 radical, physisorbed intermediate with C₃H₇SH
 7. Si(111)-H 3x3 radical, chemisorbed intermediate with C₃H₇SH
 8. Si(111)-H 3x3 radical, transition state for chain propagation reaction
 9. Si model compound radical, transition state for chain propagation reaction
 10. Si(111)-H 3x3 radical after first ligand addition
 11. C₆H₁₃SH
 12. Si(111)-H 3x3 1:9 (SiH)₈(Si.)₀(SiSC₆H₁₂SH)₁
 13. Si(111)-H 3x3 1:1 (SiH)₀(Si.)₀(SiSC₆H₁₂SH)₉
 14. Si(111)-H 3x3 8:9 (SiH)₀(Si.)₁(SiSC₆H₁₂SH)₈
 15. Si(111)-H 3x3 8:9 (SiH)₁(Si.)₀(SiSC₆H₁₂SH)₈
 16. Si(111)-H 3x3 7:9 (SiH)₁(Si.)₁(SiSC₆H₁₂SH)₅
 17. Si(111)-H 3x3 2:3 (SiH)₂(Si.)₁(SiSC₆H₁₂SH)₆
 18. Au-2-Au Flat-S
 19. Au-2-Au Flat-SH
 20. Au-2-Au Tip-S
 21. Au-2-Au Tip-SH
 22. Si-2-Au Flat S
 23. Si-2-Au Flat SH
 24. Si-2-Au Tip S
 25. Si-2-Au Tip SH
 26. Si-2-Si
-
-

1. H2



E= -6.7341 eV, Ggas= -6.7704 eV, Gsoln= -6.6905 eV

box: 20.000000 0 0 0 20.000000 0 0 0 20.000000

Kpoints: 1 1 1

basis: NGX= 120 NGY= 120 NGZ= 120 NGXF= 180 NGYF= 180 NGZF= 180

Low Frequencies (cm⁻¹)= 4444.

1 0.000000 0.000000 19.624900

1 0.000000 0.000000 0.375100

2. C3H7SH

E= -60.9807 eV, Ggas= -59.0376 eV, Gsoln= -58.9577 eV

box: 25.000000 0 0 0 25.000000 0 0 0 25.000000

Kpoints: 1 1 1

basis: NGX= 192 NGY= 192 NGZ= 192 NGXF= 280 NGYF= 280 NGZF= 280

Low Frequencies (cm⁻¹)= 113. 207. 221. 248. 356. 689.

16 5.774760 3.958660 3.929870

6 1.578410 4.072160 4.007270

6 2.991270 3.492330 3.929180

6 4.063410 4.566480 4.082810

1 1.408350 4.583690 4.967520

1 0.819210 3.282340 3.911090

1 1.402680 4.804700 3.204090

1 3.129040 2.733510 4.717890

1 3.140860 2.970610 2.970600



1 3.951590 5.103470 5.037250
1 3.975140 5.316540 3.280420
1 5.728320 3.096880 4.969450

3. C3H7S

E= -55.9896 eV, Ggas= -54.3086 eV, Gsoln= -54.2287 eV

box: 25.000000 0 0 0 25.000000 0 0 0 25.000000

Kpoints: 1 1 1

basis: NGX= 192 NGY= 192 NGZ= 192 NGXF= 280 NGYF= 280 NGZF= 280

Low Frequencies (cm⁻¹)= 114. 224. 226. 357. 477. 724.



16 5.763980 3.981500 3.960160
6 1.579950 4.072510 4.007240
6 2.988330 3.483920 3.926860
6 4.070660 4.554140 4.061620
1 1.411880 4.583810 4.968070
1 0.816290 3.287340 3.910580
1 1.406070 4.806390 3.204560
1 3.134310 2.730300 4.716850
1 3.128180 2.958110 2.969160
1 3.977130 5.097910 5.021530
1 3.954570 5.336900 3.287330

4. Si(111)-H 3x3

E= -468.8368 eV, Ggas= -463.5937 eV, Gsoln= -463.5138 eV

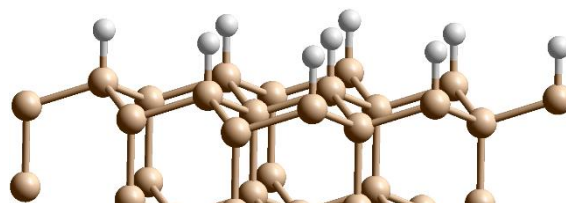
box: 11.480586 0 0 5.740293 9.942479 0 0 0 30.000000

Kpoints: 2 2 1

basis: NGX= 70 NGY= 70 NGZ= 180 NGXF= 100 NGYF= 100 NGZF= 270

Low Frequencies (cm⁻¹)= 44. 44. 77. 77. 77. 77.

14	2.613431	3.861800	2.000000
14	6.440293	3.861800	2.000000
14	10.267155	3.861800	2.000000
14	4.526862	7.175959	2.000000
14	8.353724	7.175959	2.000000
14	12.180586	7.175959	2.000000
14	0.700000	0.547640	2.000000
14	4.526862	0.547640	2.000000
14	8.353724	0.547640	2.000000
14	10.267155	1.652360	2.781155
14	2.613431	1.652360	2.781155
14	6.440293	1.652360	2.781155
14	12.180586	4.966520	2.781155
14	4.526862	4.966520	2.781155
14	8.353724	4.966520	2.781155
14	14.094017	8.280679	2.781155
14	6.440293	8.280679	2.781155
14	10.267155	8.280679	2.781155
14	10.267155	1.652360	5.124620
14	2.613431	1.652360	5.124620
14	6.440293	1.652360	5.124620
14	12.180586	4.966520	5.124620
14	4.526862	4.966520	5.124620
14	8.353724	4.966520	5.124620
14	14.094017	8.280679	5.124620
14	6.440293	8.280679	5.124620



14	10.267155	8.280679	5.124620
14	12.180586	2.757080	5.905775
14	4.526862	2.757080	5.905775
14	8.353724	2.757080	5.905775
14	14.094017	6.071239	5.905775
14	6.440293	6.071239	5.905775
14	10.267155	6.071239	5.905775
14	16.007448	9.385399	5.905775
14	8.353724	9.385399	5.905775
14	12.180586	9.385399	5.905775
14	12.180586	2.757080	8.249553
14	4.526862	2.757080	8.249553
14	8.353724	2.757080	8.249553
14	14.094017	6.071239	8.249553
14	6.440293	6.071239	8.249553
14	10.267155	6.071239	8.249553
14	16.007448	9.385399	8.249553
14	8.353724	9.385399	8.249553
14	12.180586	9.385399	8.249553
14	2.613431	3.861800	9.033240
14	6.440293	3.861800	9.033240
14	10.267155	3.861800	9.033240
14	4.526862	7.175959	9.033240
14	8.353724	7.175959	9.033240
14	12.180586	7.175959	9.033240
14	0.700000	0.547640	9.033240
14	4.526862	0.547640	9.033240
14	8.353724	0.547640	9.033240
14	2.613431	3.861800	11.378206
14	6.440293	3.861800	11.378206
14	10.267155	3.861800	11.378206
14	4.526862	7.175959	11.378206

14	8.353724	7.175959	11.378206
14	12.180586	7.175959	11.378206
14	0.700000	0.547640	11.378206
14	4.526862	0.547640	11.378206
14	8.353724	0.547640	11.378206
14	10.267155	1.652360	12.145176
14	2.613431	1.652360	12.145176
14	6.440293	1.652360	12.145176
14	12.180586	4.966520	12.145176
14	4.526862	4.966520	12.145176
14	8.353724	4.966520	12.145176
14	14.094017	8.280679	12.145176
14	6.440293	8.280679	12.145176
14	10.267155	8.280679	12.145176
1	2.613431	3.861800	0.495623
1	6.440293	3.861800	0.495623
1	10.267155	3.861800	0.495623
1	4.526862	7.175959	0.495623
1	8.353724	7.175959	0.495623
1	12.180586	7.175959	0.495623
1	0.700000	0.547640	0.495623
1	4.526862	0.547640	0.495623
1	8.353724	0.547640	0.495623
1	10.267155	1.652360	13.650245
1	2.613431	1.652360	13.650245
1	6.440293	1.652360	13.650245
1	12.180586	4.966520	13.650245
1	4.526862	4.966520	13.650245
1	8.353724	4.966520	13.650245
1	14.094017	8.280679	13.650245
1	6.440293	8.280679	13.650245
1	10.267155	8.280679	13.650245

5. Si(111)-H 3x3 radical, with one removed H

E= -464.3662 eV, Ggas= -459.2202 eV, Gsoln= -459.1403 eV

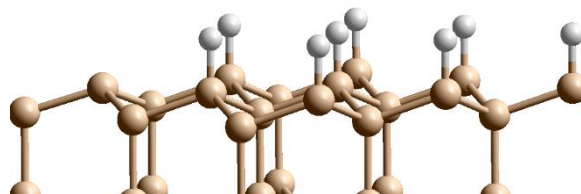
box: 11.480586 0 0 5.740293 9.942479 0 0 0 30.000000

Kpoints: 2 2 1

basis: NGX= 70 NGY= 70 NGZ= 180 NGXF= 100 NGYF= 100 NGZF= 270

Low Frequencies (cm⁻¹)= 53. 53. 76. 76. 85. 85.

14	2.613431	3.861800	2.000000
14	6.440293	3.861800	2.000000
14	10.267155	3.861800	2.000000
14	4.526862	7.175959	2.000000
14	8.353724	7.175959	2.000000
14	12.180586	7.175959	2.000000
14	0.700000	0.547640	2.000000
14	4.526862	0.547640	2.000000
14	8.353724	0.547640	2.000000
14	10.267155	1.652360	2.781155
14	2.613431	1.652360	2.781155
14	6.440293	1.652360	2.781155
14	12.180586	4.966520	2.781155
14	4.526862	4.966520	2.781155
14	8.353724	4.966520	2.781155
14	14.094017	8.280679	2.781155
14	6.440293	8.280679	2.781155
14	10.267155	8.280679	2.781155
14	10.267155	1.652360	5.124620
14	2.613431	1.652360	5.124620



14	6.440293	1.652360	5.124620
14	12.180586	4.966520	5.124620
14	4.526862	4.966520	5.124620
14	8.353724	4.966520	5.124620
14	14.094017	8.280679	5.124620
14	6.440293	8.280679	5.124620
14	10.267155	8.280679	5.124620
14	12.180586	2.757080	5.905775
14	4.526862	2.757080	5.905775
14	8.353724	2.757080	5.905775
14	14.094017	6.071239	5.905775
14	6.440293	6.071239	5.905775
14	10.267155	6.071239	5.905775
14	16.007448	9.385399	5.905775
14	8.353724	9.385399	5.905775
14	12.180586	9.385399	5.905775
14	12.181217	2.756716	8.254655
14	4.526231	2.756716	8.254655
14	8.353724	2.757175	8.251226
14	14.094017	6.073097	8.248484
14	6.440375	6.071192	8.251226
14	10.267073	6.071192	8.251226
14	16.005839	9.384470	8.248484
14	8.353724	9.386128	8.254655
14	12.182195	9.384470	8.248484
14	2.613431	3.863995	9.034570
14	6.440675	3.862020	9.036921
14	10.266773	3.862020	9.036921
14	4.526760	7.176018	9.033783
14	8.353724	7.175518	9.036921
14	12.180688	7.176018	9.033783
14	0.698099	0.546543	9.034570

14	4.528763	0.546543	9.034570
14	8.353724	0.547522	9.033783
14	2.613431	3.866698	11.386741
14	6.440742	3.862059	11.382304
14	10.266706	3.862059	11.382304
14	4.527466	7.175610	11.378639
14	8.353724	7.175441	11.382304
14	12.179982	7.175610	11.378639
14	0.695758	0.545191	11.386741
14	4.531104	0.545191	11.386741
14	8.353724	0.548337	11.378639
14	10.264803	1.653773	12.150988
14	2.613431	1.652360	12.080753
14	6.442645	1.653773	12.150988
14	12.178186	4.967851	12.150988
14	4.529262	4.967851	12.150988
14	8.353724	4.966520	12.148100
14	14.094017	8.280679	12.142359
14	6.440341	8.277935	12.150988
14	10.267107	8.277935	12.150988
1	2.613431	3.861401	0.495677
1	6.440134	3.861708	0.495643
1	10.267314	3.861708	0.495643
1	4.527850	7.175389	0.495642
1	8.353724	7.176142	0.495643
1	12.179598	7.175389	0.495642
1	0.700345	0.547839	0.495677
1	4.526517	0.547839	0.495677
1	8.353724	0.548781	0.495642
1	10.262957	1.652800	13.655456
1	6.444491	1.652800	13.655456
1	12.178106	4.969936	13.655456

1	4.529342	4.969936	13.655456
1	8.353724	4.966520	13.652730
1	14.094017	8.280679	13.647456
1	6.438575	8.276824	13.655456
1	10.268873	8.276824	13.655456

6. Si(111)-H 3x3 radical, physisorbed intermediate with C3H7SH

E= -526.1381 eV, Ggas= -518.5026 eV, Gsoln= -518.4227 eV

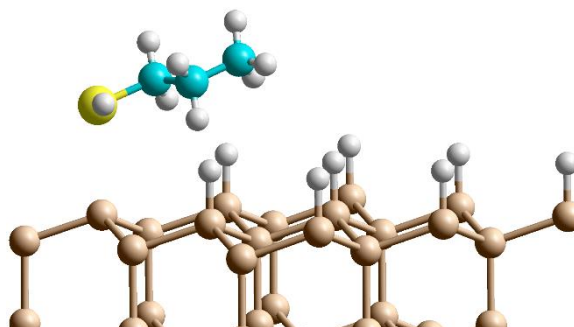
box: 11.480586 0 0 5.740293 9.942479 0 0 0 30.000000

Kpoints: 2 2 1

basis: NGX= 84 NGY= 84 NGZ= 224 NGXF= 126 NGYF= 126 NGZF= 336

Low Frequencies (cm⁻¹)= -44. 15. 36. 47. 53. 54.

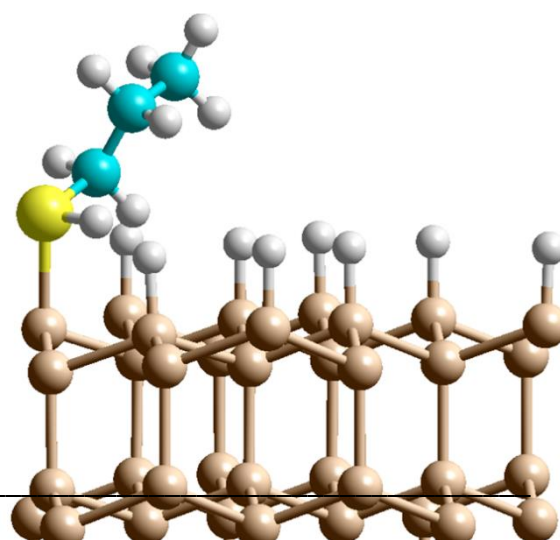
16	2.234068	0.514056	8.150558
14	13.143242	3.243510	25.245284
14	1.664560	1.034511	26.012848
14	3.576818	4.350877	26.004793
14	16.971882	9.877126	25.238685
14	9.318983	9.871774	25.248394
14	1.668513	1.034603	28.358865
14	5.491394	3.243456	25.245242
14	15.061482	6.552707	25.218236
14	3.580712	4.356943	28.349647
14	5.493139	1.034566	26.012861
14	3.582181	2.148475	29.133083
14	7.404009	4.348974	26.014619
14	5.487452	7.663117	25.991587
14	5.494607	5.463409	29.132731



14	13.146818	9.877443	25.235712
14	5.496955	1.035978	28.359296
14	3.597594	2.155068	1.479786
14	9.317071	3.246182	25.245720
14	7.408952	6.557759	25.245444
14	7.407660	4.351009	28.360946
14	5.487330	7.665827	28.335751
14	5.508016	5.473827	1.479750
14	9.318423	1.036751	26.010827
14	7.412508	2.139364	29.142077
14	13.165705	3.247012	2.266591
14	5.513273	3.260056	2.240611
14	9.331151	9.866209	2.151727
14	11.231290	4.349394	26.013695
14	9.321218	7.663235	26.017159
14	9.324686	5.455811	29.138218
14	7.397222	8.762566	29.128892
14	15.076935	6.572923	2.254537
14	7.425071	6.558738	2.259247
14	9.324567	1.035777	28.357198
14	7.423790	2.144227	1.490409
14	11.229516	6.556343	25.238821
14	11.240113	4.353369	28.359979
14	9.326940	7.668736	28.363483
14	9.336953	5.456733	1.484908
14	7.397082	8.758965	1.472800
14	15.091236	6.591990	4.597374
14	7.433296	6.558470	4.604354
14	11.238881	2.142034	29.141586
14	9.339030	3.248381	2.259941
14	13.153910	9.888191	2.292966
14	7.439763	4.355333	5.381008

14	13.151444	7.661435	25.983796
14	13.153108	5.466738	29.136787
14	11.257556	8.764107	29.130858
14	11.253044	6.559541	2.254301
14	5.531969	7.663226	5.391115
14	9.350698	7.662121	5.348108
14	11.250747	2.143942	1.490115
14	9.343612	3.247415	4.604701
14	13.162014	7.666796	28.328179
14	13.165037	5.459254	1.487335
14	11.267510	8.765506	1.477362
14	11.265036	6.558186	4.597524
14	9.355441	1.058089	5.414751
14	11.247028	4.356851	5.380604
14	15.063493	8.769769	29.140716
14	13.169415	7.650740	5.399433
14	15.069413	8.781875	1.492862
14	1.743326	1.033044	5.244644
14	9.347004	9.822910	4.459355
14	13.184406	3.284801	4.623547
14	5.465239	1.055265	5.191620
14	3.622587	4.391413	5.370526
14	5.519665	3.292048	4.580181
14	13.188662	9.868230	4.663138
14	16.992396	9.873919	4.635515
14	16.989776	9.883237	2.274849
6	1.705039	2.200317	8.594209
6	2.458964	2.808106	9.771524
6	13.416918	4.209184	10.096277
1	13.140609	3.241105	23.741833
1	16.975489	9.890959	23.735030
1	9.320177	9.872005	23.744539

1	5.497832	3.243405	23.741503
1	15.069132	6.540261	23.714787
1	13.147551	9.901292	23.732142
1	9.318842	3.249770	23.742056
1	7.424214	6.550606	23.742028
1	11.212810	6.548908	23.735200
1	7.424305	4.349613	6.884787
1	5.526719	7.638509	6.894659
1	9.348747	7.740931	6.850567
1	9.367150	1.085394	6.919051
1	11.230932	4.371282	6.885496
1	13.166926	7.613269	6.903132
1	5.367318	1.048060	6.705109
1	3.645277	4.384802	6.876966
1	3.517436	0.815331	7.838937
1	1.787037	2.837480	7.701061
1	12.112702	2.096369	8.816806
1	3.531635	2.855423	9.523982
1	2.368543	2.148582	10.648146
1	13.529338	4.883881	9.234879
1	13.962588	4.648851	10.941955
1	12.350035	4.182497	10.362646



7. Si(111)-H 3x3 radical, chemisorbed intermediate with C3H7SH

E= -526.1173 eV, Ggas= -518.4443 eV, Gsoln= -518.3644 eV

box: 11.480586 0 0 5.740293 9.942479 0 0 0 30.000000

Kpoints: 2 2 1

basis: NGX= 84 NGY= 84 NGZ= 224 NGXF= 126 NGYF= 126 NGZF= 336

Low Frequencies (cm⁻¹)= -27. 36. 49. 62. 63. 65.

16	2.140239	0.786674	7.515142
14	13.134096	3.251484	25.233628
14	1.653520	1.042044	26.014761
14	3.566925	4.356173	26.014757
14	16.960976	9.879856	25.233683
14	9.307251	9.879802	25.233616
14	1.653532	1.042056	28.358411
14	5.480384	3.251469	25.233624
14	15.047507	6.565595	25.233682
14	3.566958	4.356157	28.358386
14	5.480353	1.042031	26.014772
14	3.566964	2.146718	29.139301
14	7.393789	4.356165	26.014751
14	5.480280	7.670384	26.014751
14	5.480357	5.460734	29.139359
14	13.134077	9.879833	25.233643
14	5.480388	1.042073	28.358385
14	3.597594	2.155068	1.479786
14	9.307248	3.251495	25.233658
14	7.393868	6.565604	25.233738
14	7.393852	4.356187	28.358414
14	5.480494	7.670307	28.358725
14	5.508016	5.473827	1.479750
14	9.307241	1.042023	26.014737
14	7.393734	2.146706	29.139254
14	13.165705	3.247012	2.266591
14	5.513273	3.260056	2.240611
14	9.331151	9.866209	2.151727
14	11.220687	4.356177	26.014762
14	9.307251	7.670393	26.014750

14	9.307251	5.460928	29.139318
14	7.393889	8.775160	29.139310
14	15.076935	6.572923	2.254537
14	7.425071	6.558738	2.259247
14	9.307245	1.042161	28.358417
14	7.423790	2.144227	1.490409
14	11.220644	6.565616	25.233678
14	11.220636	4.356206	28.358423
14	9.307239	7.670318	28.358436
14	9.336953	5.456733	1.484908
14	7.397082	8.758965	1.472800
14	15.091236	6.591990	4.597374
14	7.433296	6.558470	4.604354
14	11.220729	2.146747	29.139246
14	9.339030	3.248381	2.259941
14	13.153910	9.888191	2.292966
14	7.439763	4.355333	5.381008
14	13.134119	7.670383	26.014727
14	13.134103	5.460792	29.139295
14	11.220572	8.775216	29.139287
14	11.253044	6.559541	2.254301
14	5.531969	7.663226	5.391115
14	9.350698	7.662121	5.348108
14	11.250747	2.143942	1.490115
14	9.343612	3.247415	4.604701
14	13.134043	7.670331	28.358590
14	13.165037	5.459254	1.487335
14	11.267510	8.765506	1.477362
14	11.265036	6.558186	4.597524
14	9.355441	1.058089	5.414751
14	11.247028	4.356851	5.380604
14	15.047343	8.775361	29.139281

14	13.169415	7.650740	5.399433
14	15.069413	8.781875	1.492862
14	1.743326	1.033044	5.244644
14	9.347004	9.822910	4.459355
14	13.184406	3.284801	4.623547
14	5.465239	1.055265	5.191620
14	3.622587	4.391413	5.370526
14	5.519665	3.292048	4.580181
14	13.188662	9.868230	4.663138
14	16.992396	9.873919	4.635515
14	16.989776	9.883237	2.274849
6	1.619569	2.368757	8.272582
6	2.400430	2.681957	9.541560
6	1.948767	4.021754	10.126947
1	13.132662	3.249238	23.730336
1	16.961246	9.882397	23.730312
1	9.306717	9.877926	23.730343
1	5.480468	3.249183	23.730309
1	15.044241	6.562847	23.730233
1	13.133329	9.878996	23.730415
1	9.307452	3.251141	23.730400
1	7.396568	6.563886	23.730470
1	11.218905	6.564103	23.730466
1	7.421698	4.348472	6.886741
1	5.521149	7.658092	6.897469
1	9.349886	7.755847	6.852570
1	9.378177	1.074012	6.922046
1	11.230457	4.381041	6.887025
1	13.165878	7.613121	6.905037
1	5.329272	1.048177	6.714563
1	3.635677	4.383030	6.880926
1	3.474105	1.072851	7.380199

1	1.742350	3.153516	7.514457
1	12.024532	2.239445	8.460732
1	3.475302	2.723489	9.301980
1	2.266244	1.873266	10.276036
1	13.588735	4.838655	9.408644
1	2.514466	4.256213	11.038174
1	12.361192	4.005117	10.387130

8. Si(111)-H 3x3 radical, transition state for chain propagation reaction

E= -525.7470 eV, Ggas= -518.0951 eV, Gsoln= -518.0152 eV

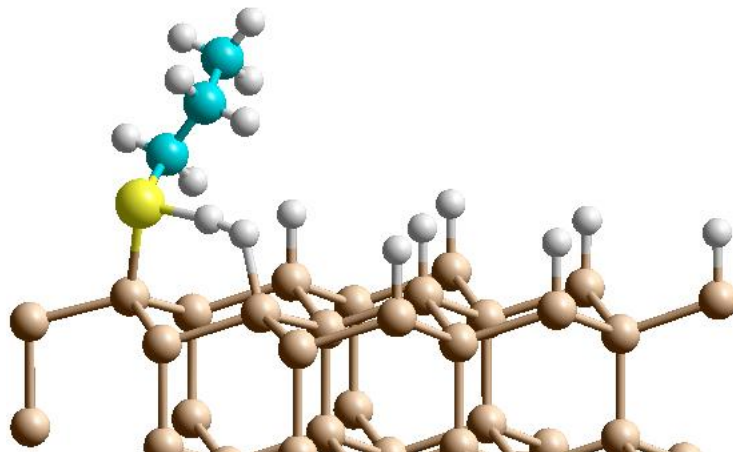
box: 11.480586 0 0 5.740293 9.942479 0 0 0 30.000000

Kpoints: 2 2 1

basis: NGX= 84 NGY= 84 NGZ= 224 NGXF= 126 NGYF= 126 NGZF= 336

Low Frequencies (cm⁻¹)= -901. 6. 29. 46. 61. 72.

16	3.232460	1.364710	14.162920
14	2.613430	3.861800	2.000000
14	2.613430	1.652360	2.781160
14	4.526860	4.966520	2.781160
14	0.700000	0.547640	2.000000
14	4.526860	0.547640	2.000000
14	2.613430	1.652360	5.124620
14	6.440290	3.861800	2.000000
14	4.526860	7.175960	2.000000
14	4.526860	4.966520	5.124620
14	6.440290	1.652360	2.781160
14	4.526860	2.757080	5.905780
14	8.353720	4.966520	2.781160



14	6.440290	8.280680	2.781160
14	6.440290	6.071240	5.905780
14	8.353720	0.547640	2.000000
14	6.440290	1.652360	5.124620
14	4.549140	2.761590	8.244710
14	10.267160	3.861800	2.000000
14	8.353720	7.175960	2.000000
14	8.353720	4.966520	5.124620
14	6.440290	8.280680	5.124620
14	6.463720	6.081930	8.245010
14	10.267160	1.652360	2.781160
14	8.353720	2.757080	5.905780
14	2.635650	3.855880	9.025560
14	6.462710	3.868490	9.007460
14	4.548830	0.531320	8.918560
14	12.180590	4.966520	2.781160
14	10.267160	8.280680	2.781160
14	10.267160	6.071240	5.905780
14	8.353720	9.385400	5.905780
14	4.552680	7.181380	9.020770
14	8.378540	7.167770	9.027610
14	10.267160	1.652360	5.124620
14	8.373760	2.753730	8.255270
14	12.180590	7.175960	2.000000
14	12.180590	4.966520	5.124620
14	10.267160	8.280680	5.124620
14	10.289880	6.065700	8.251950
14	8.353540	9.367420	8.237980
14	4.566730	7.197980	11.363780
14	8.384570	7.162560	11.373550
14	12.180590	2.757080	5.905780
14	10.289420	3.857270	9.027410

14	8.370260	0.555290	9.058610
14	8.392350	4.958570	12.148370
14	14.094020	8.280680	2.781160
14	14.094020	6.071240	5.905780
14	12.180590	9.385400	5.905780
14	12.207810	7.167530	9.021360
14	6.485260	8.270980	12.161120
14	10.304510	8.264970	12.114550
14	12.200040	2.752520	8.254130
14	10.297910	3.854380	11.372370
14	14.094020	8.280680	5.124620
14	14.121070	6.068870	8.251970
14	12.225020	9.373420	8.242800
14	12.222500	7.165540	11.364100
14	10.311800	1.664020	12.181810
14	12.205810	4.961960	12.142020
14	16.007450	9.385400	5.905780
14	14.126460	8.259350	12.164830
14	16.025730	9.389950	8.257030
14	2.697460	1.638940	12.010490
14	4.562720	0.484530	11.227430
14	2.659710	3.888590	11.378300
14	6.424900	1.657080	11.952160
14	4.574530	4.996330	12.132750
14	6.472930	3.894900	11.346740
14	8.403740	0.534520	11.428270
14	0.725310	0.538000	11.397560
14	0.724080	0.548470	9.038830
6	2.756150	2.889200	15.056750
6	3.661800	3.108920	16.264500
6	3.200440	4.308910	17.092380
1	2.618240	3.859180	0.496860

1	0.705520	0.548140	0.496830
1	4.531170	0.546170	0.496870
1	6.444770	3.859140	0.496840
1	4.530770	7.172260	0.496700
1	8.357020	0.546680	0.496920
1	10.271540	3.861090	0.496880
1	8.360920	7.173700	0.496900
1	12.183780	7.174540	0.496910
1	8.370410	4.951770	13.652910
1	6.475530	8.261750	13.665050
1	10.314890	8.347180	13.616030
1	10.326670	1.677450	13.687050
1	12.201300	4.976170	13.647940
1	14.129340	8.233100	13.669610
1	5.877060	1.761940	13.661990
1	4.599670	4.995790	13.639640
1	4.929490	1.681840	13.921940
1	2.808780	3.736330	14.359980
1	1.706270	2.755070	15.353920
1	4.693890	3.266650	15.913710
1	3.676000	2.200830	16.887920
1	3.191840	5.227940	16.489040
1	3.869110	4.473320	17.947970
1	13.665550	4.153540	17.484640

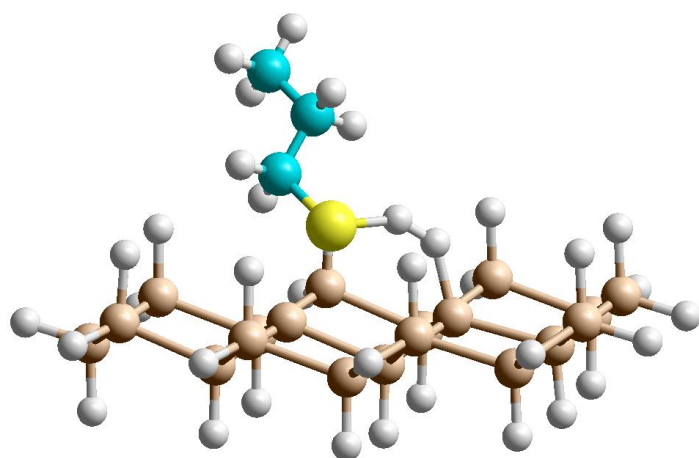
9. Si model compound radical, transition state for chain propagation reaction

#P pbepbe/6-31++g** empiricaldispersion=gd3bj nosym

Full point group C1 NOp 1

SCF Done: E(UPBE-PBE) = -6031.84792005 A.U. after 19 cycles

14	4.489419	-1.613341	11.972749
14	2.639589	-2.767888	11.081333
14	6.449149	-2.762395	11.366665
14	4.528939	0.639077	11.279070
14	2.663200	-4.987559	11.864983
14	0.763992	-1.703279	12.015471
1	2.592856	-2.657802	9.579806
14	8.353402	-1.662095	12.145599
14	6.438855	-4.975197	12.144188
1	6.505912	-2.797708	9.861752
14	2.614312	1.650985	12.144834
14	6.439657	1.651485	12.145366
1	4.530402	0.719559	9.772933
14	4.610112	-6.132438	11.236409
14	0.672389	-6.100817	11.303644
1	2.967452	-4.768661	13.506186
14	0.700059	0.547707	11.378411
14	-1.213682	-2.766499	11.377993
1	0.896547	-1.783830	13.511072
14	8.353581	0.547726	11.378251
1	8.337246	-1.663393	13.649371
1	9.597795	-2.386452	11.710933
1	6.306938	-4.990464	13.641277
1	7.744418	-5.640001	11.803985
1	2.685031	1.535849	13.641338
1	2.587904	3.114974	11.798626
1	6.373309	1.534135	13.643476
1	6.488464	3.115852	11.807454
14	4.526838	-8.289106	12.145512
1	4.760450	-6.209467	9.740627



14	0.700335	-8.288832	12.145549
14	-1.211520	-4.976502	12.145128
1	0.544623	-6.181437	9.802844
1	0.664265	0.616482	9.877418
1	-0.550693	1.204504	11.895537
1	-2.407205	-2.003929	11.886152
1	-1.283468	-2.773225	9.876447
1	9.604585	1.269395	11.799917
1	8.324279	0.524121	9.875670
14	2.613157	-9.395070	11.378131
1	4.459547	-8.152100	13.641159
1	5.773830	-9.062270	11.814341
1	0.728872	-8.224992	13.646668
1	-0.549538	-9.019777	11.739109
1	-1.131446	-4.979463	13.645659
1	-2.460544	-5.713621	11.746585
1	2.618244	-10.838980	11.801522
1	2.616232	-9.364348	9.875197
1	3.431985	-4.053778	14.058223
16	3.906161	-2.440829	14.060093
6	5.467073	-2.477669	15.049055
6	5.328612	-3.392249	16.267461
1	6.289907	-2.814969	14.399423
1	5.671260	-1.437890	15.351782
6	6.609897	-3.380555	17.111504
1	5.109207	-4.419817	15.926591
1	4.465766	-3.070233	16.877130
1	7.476624	-3.730314	16.525255
1	6.507800	-4.040984	17.987552
1	6.838552	-2.365721	17.479001

10. Si(111)-H 3x3 radical after first ligand addition

E= -519.7153 eV, Ggas= -512.3831 eV, Gsoln= -512.3032 eV

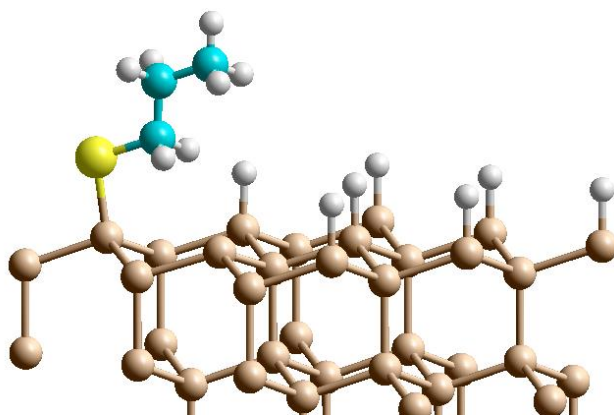
box: 11.480586 0 0 5.740293 9.942479 0 0 0 35.000000

Kpoints: 2 2 1

basis: NGX= 84 NGY= 84 NGZ= 256 NGXF= 126 NGYF= 126 NGZF= 392

Low Frequencies (cm⁻¹)= 28. 38. 54. 61. 65. 77.

16	8.134370	4.755680	14.279120
14	8.333550	4.946900	12.147450
14	6.422120	3.858590	11.362730
14	8.341450	7.171000	11.400570
14	10.256440	3.856880	11.375850
14	6.431250	3.862680	9.023210
14	4.521620	4.970660	12.153400
14	6.427250	1.655590	12.151410
14	8.348400	7.175400	9.047220
14	6.428310	8.282580	12.161990
14	10.255200	8.294410	12.138240
14	10.256410	3.863510	9.024860
14	10.256770	1.653390	12.155820
14	12.174500	4.965060	12.070440
14	4.520820	2.756420	8.243340
14	6.436650	6.075110	8.251930
14	8.344770	2.754500	8.246640
14	2.613670	3.862630	11.381630
14	4.517280	7.178450	11.386280
14	4.517330	0.557180	11.367050
14	8.341460	0.550690	11.387540



14	10.276000	6.074920	8.255590
14	8.345190	9.382400	8.252220
14	12.169620	7.181300	11.386170
14	12.174990	2.757980	8.255250
14	4.526860	2.757080	5.905770
14	2.609480	3.860760	9.032070
14	4.519020	0.549240	9.025810
14	6.440290	6.071240	5.905770
14	4.521480	7.176870	9.039610
14	8.353720	2.757080	5.905770
14	8.348360	0.548610	9.039630
14	2.603340	1.653290	12.146910
14	10.267150	6.071240	5.905770
14	12.174270	7.181840	9.033550
14	8.353720	9.385400	5.905770
14	14.084420	8.282630	12.153460
14	12.180590	2.757080	5.905770
14	2.613430	1.652360	5.124620
14	4.526860	4.966520	5.124620
14	6.440290	1.652360	5.124620
14	8.353720	4.966520	5.124620
14	6.440290	8.280680	5.124620
14	10.267150	1.652360	5.124620
14	0.688060	0.547930	11.385820
14	12.180590	4.966520	5.124620
14	10.267150	8.280680	5.124620
14	14.088400	6.072230	8.255740
14	12.176260	9.390190	8.248240
14	2.613430	1.652360	2.781160
14	4.526860	4.966520	2.781160
14	6.440290	1.652360	2.781160
14	8.353720	4.966520	2.781160

14	6.440290	8.280680	2.781160
14	10.267150	1.652360	2.781160
14	0.693970	0.547740	9.039400
14	12.180590	4.966520	2.781160
14	14.094020	6.071240	5.905770
14	10.267150	8.280680	2.781160
14	12.180590	9.385400	5.905770
14	2.613430	3.861800	2.000000
14	0.700000	0.547640	2.000000
14	4.526860	0.547640	2.000000
14	6.440290	3.861800	2.000000
14	4.526860	7.175960	2.000000
14	8.353720	0.547640	2.000000
14	10.267150	3.861800	2.000000
14	8.353720	7.175960	2.000000
14	12.180590	7.175960	2.000000
14	14.094020	8.280680	5.124620
14	14.094020	8.280680	2.781160
14	16.007450	9.385400	5.905770
14	16.001610	9.386020	8.253410
6	11.190480	5.806910	16.898280
6	9.825910	5.330700	16.395370
6	9.781850	5.305440	14.871310
1	11.411990	6.822880	16.539770
1	11.997230	5.147060	16.545820
1	9.605920	4.324310	16.784380
1	9.030680	5.993760	16.771120
1	10.543910	4.616520	14.473290
1	9.987760	6.306200	14.465750
1	4.526630	4.957780	13.654980
1	6.409960	1.650170	13.652200
1	6.421720	8.290220	13.664370

1	10.270710	8.333990	13.641420
1	10.265070	1.658630	13.658490
1	2.617470	1.647610	13.649930
1	14.084590	8.278590	13.656990
1	2.614620	3.860930	0.497110
1	0.701400	0.546360	0.497070
1	4.527200	0.545050	0.497040
1	6.442370	3.862450	0.497050
1	4.528010	7.174190	0.497040
1	8.356720	0.545500	0.497070
1	10.268960	3.860550	0.497100
1	8.355700	7.174030	0.497090
1	12.182060	7.173920	0.497100
1	11.224620	5.823410	17.995930

11. HSC6H12SH (2)

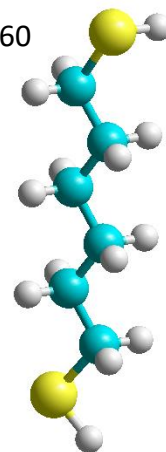
E= -114.5223 eV

box: 15.000000 0 0 0 15.000000 0 0 0 35.000000

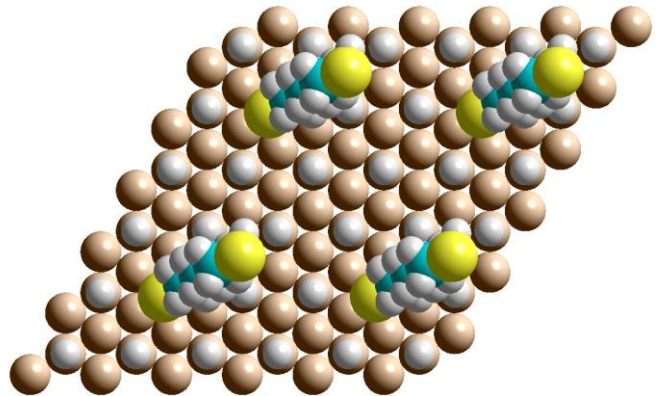
Kpoints: 1 1 1

basis: NGX= 80 NGY= 80 NGZ= 180 NGXF= 160 NGYF= 160 NGZF= 360

16	14.847285	3.798277	16.066160
16	1.534979	10.907950	10.081225
6	0.310345	5.492464	15.577554
6	0.403278	5.718514	14.072060
6	0.720662	7.173314	13.720605
6	0.809941	7.426102	12.215431
6	1.102836	8.888027	11.875648



6	1.185792	9.136509	10.372632
1	14.517588	6.122210	16.012704
1	1.249678	5.769757	16.079987
1	1.180905	5.057090	13.651747
1	14.453325	5.414671	13.601980
1	14.945359	7.830630	14.153423
1	1.671667	7.470012	14.197715
1	1.594869	6.782089	11.780998
1	14.862904	7.119998	11.736939
1	0.316876	9.530345	12.308956
1	2.051054	9.194144	12.350046
1	0.235069	8.869162	9.887890
1	1.988830	8.530199	9.927833
1	0.941817	3.186417	15.564000
1	1.550201	10.856220	8.732436



12. Si(111)-H 3x3 1:9 (SiH)8(Si.)0(SiSC6H12SH)1

E= -577.6538 eV

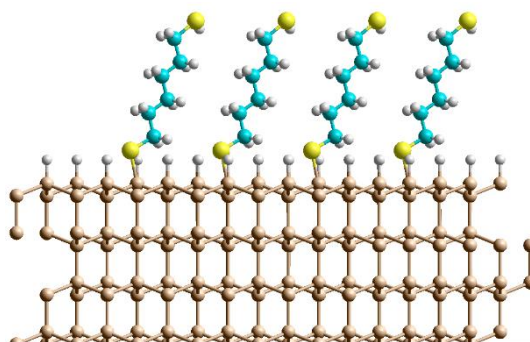
box: 11.480586 0 0 5.740293 9.942479 0 0 0 35.000000

Kpoints: 2 2 1

basis: NGX= 56 NGY= 56 NGZ= 180 NGXF= 112 NGYF= 112 NGZF= 360

16	12.045706	6.930892	22.427365
16	7.915478	4.754461	14.240244
14	2.613431	3.861800	2.000000
14	2.613431	1.652360	2.781155
14	4.526862	4.966520	2.781155
14	0.700000	0.547640	2.000000

14	4.526862	0.547640	2.000000
14	2.613431	1.652360	5.124620
14	6.440293	3.861800	2.000000
14	4.526862	7.175959	2.000000
14	4.526862	4.966520	5.124620
14	6.440293	1.652360	2.781155
14	4.526862	2.757080	5.905775
14	8.353724	4.966520	2.781155
14	6.440293	8.280679	2.781155
14	6.440293	6.071239	5.905775
14	8.353724	0.547640	2.000000
14	6.440293	1.652360	5.124620
14	4.518328	2.752471	8.244051
14	10.267150	3.861800	2.000000
14	8.353724	7.175959	2.000000
14	8.353724	4.966520	5.124620
14	6.440293	8.280679	5.124620
14	6.439532	6.074661	8.251348
14	10.267150	1.652360	2.781155
14	8.353724	2.757080	5.905775
14	2.608734	3.861154	9.027828
14	6.430702	3.859382	9.013553
14	4.523938	0.544769	9.030268
14	12.180590	4.966520	2.781155
14	10.267150	8.280679	2.781155
14	10.267150	6.071239	5.905775
14	8.353724	9.385399	5.905775
14	4.526849	7.178026	9.041316
14	8.354485	7.173702	9.043115
14	10.267150	1.652360	5.124620
14	8.352901	2.757459	8.251789
14	2.613826	3.862020	11.369732



14	6.419641	3.852793	11.348637
14	4.525745	0.551062	11.372631
14	12.180590	7.175959	2.000000
14	12.180590	4.966520	5.124620
14	10.267150	8.280679	5.124620
14	10.265815	6.069701	8.253282
14	8.350606	9.381723	8.250607
14	4.529697	7.175423	11.388602
14	8.350308	7.172539	11.393649
14	12.180590	2.757080	5.905775
14	10.262179	3.864430	9.048606
14	8.354053	0.550105	9.042917
14	2.612949	1.653897	12.142308
14	4.522028	4.964264	12.148095
14	6.435508	1.653954	12.146782
14	8.321678	4.951481	12.142993
14	14.094020	8.280679	2.781155
14	14.094020	6.071239	5.905775
14	12.180590	9.385399	5.905775
14	12.179992	7.176598	9.035085
14	6.440931	8.280884	12.162909
14	10.267746	8.286317	12.140637
14	12.173010	2.756019	8.253095
14	10.260209	3.859787	11.401997
14	8.351735	0.549835	11.390311
14	0.700075	0.544085	11.384289
14	14.094020	8.280679	5.124620
14	14.095091	6.072163	8.251586
14	12.183148	9.387707	8.251783
14	12.181827	7.177610	11.381379
14	10.268213	1.648360	12.162382
14	12.185406	4.966541	12.142975

14	0.700373	0.545676	9.038628
14	16.007450	9.385399	5.905775
14	14.094931	8.280378	12.151763
14	16.006024	9.386850	8.252688
6	9.392666	5.395651	15.119355
6	9.063168	5.477007	16.605338
6	10.248635	5.930471	17.457602
6	9.897556	5.996031	18.944150
6	11.065210	6.431132	19.829767
6	10.679151	6.494091	21.303438
1	10.235082	4.712670	14.937266
1	9.655717	6.384911	14.717378
1	8.719228	4.487857	16.953496
1	8.215204	6.167466	16.750008
1	10.595685	6.921203	17.114889
1	11.096745	5.239225	17.309238
1	9.538013	5.005023	19.274644
1	9.049220	6.689362	19.085875
1	11.427194	7.422477	19.506366
1	11.913612	5.738176	19.706531
1	10.346262	5.505350	21.657536
1	9.840584	7.188641	21.463908
1	12.270545	8.163477	21.921971
1	2.613910	3.862140	0.496800
1	0.699877	0.547448	0.496753
1	4.527758	0.547598	0.496819
1	6.440868	3.861486	0.496801
1	4.526852	7.175133	0.496770
1	8.353582	0.547390	0.496771
1	10.267714	3.862013	0.496807
1	8.354960	7.175736	0.496815
1	12.180765	7.175485	0.496811

1	2.618756	1.656009	13.646519
1	4.518231	4.945445	13.649178
1	6.417938	1.655806	13.647761
1	6.442467	8.290945	13.665346
1	10.279720	8.310389	13.645232
1	10.277949	1.643527	13.665907
1	12.221807	4.968387	13.646435
1	14.088498	8.277552	13.655773

13. Si(111)-H 3x3 1:1 (SiH)O(Si.)O(SiSC6H12SH)9

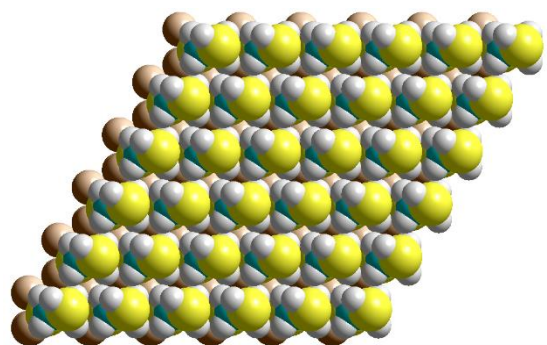
E=-1442.4569 eV

box: 11.480586 0 0 5.740293 9.942480 0 0 0 35.000000

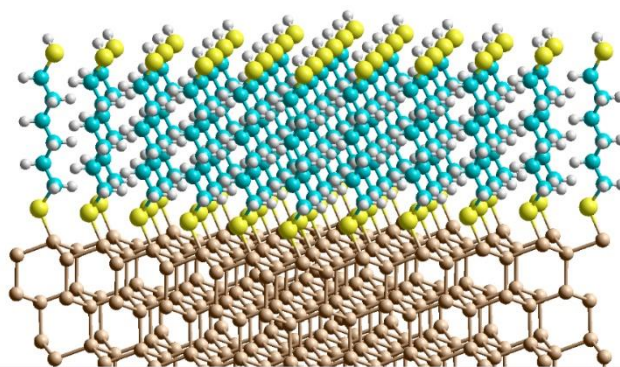
Kpoints: 2 2 1

basis: NGX= 84 NGY= 84 NGZ= 256 NGXF= 126 NGYF= 126 NGZF= 392

16	3.791596	1.422363	14.127922
16	1.213798	1.714808	23.519802
16	7.618458	8.050683	14.127922
16	5.040660	8.343128	23.519802
16	5.705027	4.736523	14.127922
16	3.127229	5.028968	23.519802
16	11.445320	1.422363	14.127922
16	8.867522	1.714808	23.519802
16	15.272182	8.050683	14.127922
16	12.694384	8.343128	23.519802
16	13.358751	4.736523	14.127922
16	10.780953	5.028968	23.519802
16	7.618458	1.422363	14.127922



16	5.040660	1.714808	23.519802
16	11.445320	8.050683	14.127922
16	8.867522	8.343128	23.519802
16	9.531889	4.736523	14.127922
16	6.954091	5.028968	23.519802
14	2.613000	0.548000	2.000000
14	4.527000	1.652000	2.781000
14	4.527000	1.652000	5.125000
14	2.613000	2.757000	5.906000
14	2.598965	2.760735	8.249889
14	2.599045	0.551817	9.032066
14	2.728315	0.537579	11.377204
14	4.642758	1.648473	12.162466
14	6.439862	7.176320	2.000000
14	8.353862	8.280320	2.781000
14	8.353862	8.280320	5.125000
14	6.439862	9.385320	5.906000
14	6.425827	9.389055	8.249889
14	6.425907	7.180137	9.032066
14	6.555177	7.165899	11.377204
14	8.469620	8.276793	12.162466
14	4.526431	3.862160	2.000000
14	6.440431	4.966160	2.781000
14	6.440431	4.966160	5.125000
14	4.526431	6.071160	5.906000
14	4.512396	6.074895	8.249889
14	4.512476	3.865977	9.032066
14	4.641746	3.851739	11.377204
14	6.556189	4.962633	12.162466
14	10.266724	0.548000	2.000000
14	12.180724	1.652000	2.781000
14	12.180724	1.652000	5.125000



14	10.266724	2.757000	5.906000
14	10.252689	2.760735	8.249889
14	10.252769	0.551817	9.032066
14	10.382039	0.537579	11.377204
14	12.296482	1.648473	12.162466
14	14.093586	7.176320	2.000000
14	16.007586	8.280320	2.781000
14	16.007586	8.280320	5.125000
14	14.093586	9.385320	5.906000
14	14.079551	9.389055	8.249889
14	14.079631	7.180137	9.032066
14	14.208901	7.165899	11.377204
14	16.123344	8.276793	12.162466
14	12.180155	3.862160	2.000000
14	14.094155	4.966160	2.781000
14	14.094155	4.966160	5.125000
14	12.180155	6.071160	5.906000
14	12.166120	6.074895	8.249889
14	12.166200	3.865977	9.032066
14	12.295470	3.851739	11.377204
14	14.209913	4.962633	12.162466
14	6.439862	0.548000	2.000000
14	8.353862	1.652000	2.781000
14	8.353862	1.652000	5.125000
14	6.439862	2.757000	5.906000
14	6.425827	2.760735	8.249889
14	6.425907	0.551817	9.032066
14	6.555177	0.537579	11.377204
14	8.469620	1.648473	12.162466
14	10.266724	7.176320	2.000000
14	12.180724	8.280320	2.781000
14	12.180724	8.280320	5.125000

14	10.266724	9.385320	5.906000
14	10.252689	9.389055	8.249889
14	10.252769	7.180137	9.032066
14	10.382039	7.165899	11.377204
14	12.296482	8.276793	12.162466
14	8.353293	3.862160	2.000000
14	10.267293	4.966160	2.781000
14	10.267293	4.966160	5.125000
14	8.353293	6.071160	5.906000
14	8.339258	6.074895	8.249889
14	8.339338	3.865977	9.032066
14	8.468608	3.851739	11.377204
14	10.383051	4.962633	12.162466
6	1.065934	1.575709	15.571918
6	4.065524	1.588832	16.853818
6	1.068331	1.595251	18.139521
6	4.070069	1.591906	19.426843
6	1.068511	1.600538	20.715740
6	4.055968	1.600948	21.987250
6	4.892796	8.204029	15.571918
6	7.892386	8.217152	16.853818
6	4.895193	8.223571	18.139521
6	7.896931	8.220226	19.426843
6	4.895373	8.228858	20.715740
6	7.882830	8.229268	21.987250
6	2.979365	4.889869	15.571918
6	5.978955	4.902992	16.853818
6	2.981762	4.909411	18.139521
6	5.983500	4.906066	19.426843
6	2.981942	4.914698	20.715740
6	5.969399	4.915108	21.987250
6	8.719658	1.575709	15.571918

6	11.719248	1.588832	16.853818
6	8.722055	1.595251	18.139521
6	11.723793	1.591906	19.426843
6	8.722235	1.600538	20.715740
6	11.709692	1.600948	21.987250
6	12.546520	8.204029	15.571918
6	15.546110	8.217152	16.853818
6	12.548917	8.223571	18.139521
6	15.550655	8.220226	19.426843
6	12.549097	8.228858	20.715740
6	15.536554	8.229268	21.987250
6	10.633089	4.889869	15.571918
6	13.632679	4.902992	16.853818
6	10.635486	4.909411	18.139521
6	13.637224	4.906066	19.426843
6	10.635666	4.914698	20.715740
6	13.623123	4.915108	21.987250
6	4.892796	1.575709	15.571918
6	7.892386	1.588832	16.853818
6	4.895193	1.595251	18.139521
6	7.896931	1.591906	19.426843
6	4.895373	1.600538	20.715740
6	7.882830	1.600948	21.987250
6	8.719658	8.204029	15.571918
6	11.719248	8.217152	16.853818
6	8.722055	8.223571	18.139521
6	11.723793	8.220226	19.426843
6	8.722235	8.228858	20.715740
6	11.709692	8.229268	21.987250
6	6.806227	4.889869	15.571918
6	9.805817	4.902992	16.853818
6	6.808624	4.909411	18.139521

6	9.810362	4.906066	19.426843
6	6.808804	4.914698	20.715740
6	9.796261	4.915108	21.987250
1	2.613605	0.547448	0.497115
1	1.742480	0.716350	15.542163
1	1.662061	2.485178	15.445841
1	3.405594	0.713847	16.860485
1	3.396723	2.456439	16.841805
1	1.730918	2.467484	18.138277
1	1.735608	0.726522	18.137929
1	4.066529	2.331426	24.224151
1	3.406715	0.720180	19.426618
1	3.400586	2.459127	19.427548
1	1.720167	2.480675	20.717971
1	1.743611	0.737378	20.721405
1	3.447879	0.690711	22.063114
1	3.374450	2.455762	22.007184
1	6.440467	7.175768	0.497115
1	5.569342	7.344670	15.542163
1	5.488923	9.113498	15.445841
1	7.232456	7.342167	16.860485
1	7.223585	9.084759	16.841805
1	5.557780	9.095804	18.138277
1	5.562470	7.354842	18.137929
1	7.893391	8.959746	24.224151
1	7.233577	7.348500	19.426618
1	7.227448	9.087447	19.427548
1	5.547029	9.108995	20.717971
1	5.570473	7.365698	20.721405
1	7.274741	7.319031	22.063114
1	7.201312	9.084082	22.007184
1	4.527036	3.861608	0.497115

1	3.655911	4.030510	15.542163
1	3.575492	5.799338	15.445841
1	5.319025	4.028007	16.860485
1	5.310154	5.770599	16.841805
1	3.644349	5.781644	18.138277
1	3.649039	4.040682	18.137929
1	5.979960	5.645586	24.224151
1	5.320146	4.034340	19.426618
1	5.314017	5.773287	19.427548
1	3.633598	5.794835	20.717971
1	3.657042	4.051538	20.721405
1	5.361310	4.004871	22.063114
1	5.287881	5.769922	22.007184
1	10.267329	0.547448	0.497115
1	9.396204	0.716350	15.542163
1	9.315785	2.485178	15.445841
1	11.059318	0.713847	16.860485
1	11.050447	2.456439	16.841805
1	9.384642	2.467484	18.138277
1	9.389332	0.726522	18.137929
1	11.720253	2.331426	24.224151
1	11.060439	0.720180	19.426618
1	11.054310	2.459127	19.427548
1	9.373891	2.480675	20.717971
1	9.397335	0.737378	20.721405
1	11.101603	0.690711	22.063114
1	11.028174	2.455762	22.007184
1	14.094191	7.175768	0.497115
1	13.223066	7.344670	15.542163
1	13.142647	9.113498	15.445841
1	14.886180	7.342167	16.860485
1	14.877309	9.084759	16.841805

1	13.211504	9.095804	18.138277
1	13.216194	7.354842	18.137929
1	15.547115	8.959746	24.224151
1	14.887301	7.348500	19.426618
1	14.881172	9.087447	19.427548
1	13.200753	9.108995	20.717971
1	13.224197	7.365698	20.721405
1	14.928465	7.319031	22.063114
1	14.855036	9.084082	22.007184
1	12.180760	3.861608	0.497115
1	11.309635	4.030510	15.542163
1	11.229216	5.799338	15.445841
1	12.972749	4.028007	16.860485
1	12.963878	5.770599	16.841805
1	11.298073	5.781644	18.138277
1	11.302763	4.040682	18.137929
1	13.633684	5.645586	24.224151
1	12.973870	4.034340	19.426618
1	12.967741	5.773287	19.427548
1	11.287322	5.794835	20.717971
1	11.310766	4.051538	20.721405
1	13.015034	4.004871	22.063114
1	12.941605	5.769922	22.007184
1	6.440467	0.547448	0.497115
1	5.569342	0.716350	15.542163
1	5.488923	2.485178	15.445841
1	7.232456	0.713847	16.860485
1	7.223585	2.456439	16.841805
1	5.557780	2.467484	18.138277
1	5.562470	0.726522	18.137929
1	7.893391	2.331426	24.224151
1	7.233577	0.720180	19.426618

1	7.227448	2.459127	19.427548
1	5.547029	2.480675	20.717971
1	5.570473	0.737378	20.721405
1	7.274741	0.690711	22.063114
1	7.201312	2.455762	22.007184
1	10.267329	7.175768	0.497115
1	9.396204	7.344670	15.542163
1	9.315785	9.113498	15.445841
1	11.059318	7.342167	16.860485
1	11.050447	9.084759	16.841805
1	9.384642	9.095804	18.138277
1	9.389332	7.354842	18.137929
1	11.720253	8.959746	24.224151
1	11.060439	7.348500	19.426618
1	11.054310	9.087447	19.427548
1	9.373891	9.108995	20.717971
1	9.397335	7.365698	20.721405
1	11.101603	7.319031	22.063114
1	11.028174	9.084082	22.007184
1	8.353898	3.861608	0.497115
1	7.482773	4.030510	15.542163
1	7.402354	5.799338	15.445841
1	9.145887	4.028007	16.860485
1	9.137016	5.770599	16.841805
1	7.471211	5.781644	18.138277
1	7.475901	4.040682	18.137929
1	9.806822	5.645586	24.224151
1	9.147008	4.034340	19.426618
1	9.140879	5.773287	19.427548
1	7.460460	5.794835	20.717971
1	7.483904	4.051538	20.721405
1	9.188172	4.004871	22.063114

1 9.114743 5.769922 22.007184

14. Si(111)-H 3x3 8:9 (SiH)0(Si.)1(SiSC6H12SH)8

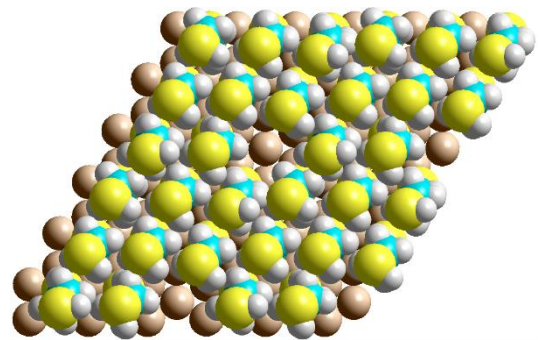
E=-1330.9651 eV

box: 11.480586 0 0 5.740293 9.942479 0 0 0 30.000000

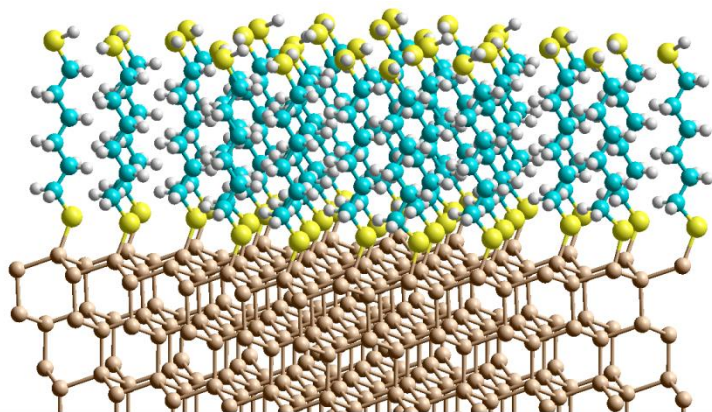
Kpoints: 2 2 1

basis: NGX= 84 NGY= 84 NGZ= 224 NGXF= 126 NGYF= 126 NGZF= 336

16 4.746504 2.421328 14.119885
16 8.502673 9.134341 14.118100
16 6.702214 5.709213 14.132402
16 16.338723 9.035534 14.177937
16 8.709988 2.362304 14.122511
16 4.553005 1.236377 23.524881
16 14.219294 5.514950 14.200309
16 12.403193 9.050488 14.145829
16 10.483034 5.724764 14.145264
16 7.863686 8.291221 23.564224
16 6.176008 4.724409 23.550312
16 15.559566 7.648576 23.443907
16 8.473691 1.337304 23.577505
16 13.509029 4.037111 23.425192
16 11.771373 8.104290 23.574029
16 9.912711 4.749811 23.557360
14 4.514902 1.576505 12.150290
14 2.583173 0.504931 11.356641
14 2.658659 0.567309 9.016272
14 8.321014 8.242381 12.168001



14	12.153536	1.578430	12.133933
14	2.646005	2.778364	8.253225
14	6.482203	9.396822	8.247471
14	6.421593	7.104159	11.384375
14	10.264309	0.471383	11.337730
14	2.613431	2.757080	5.905775
14	6.440293	9.385399	5.905775
14	6.482994	7.189560	9.037531
14	10.300202	0.548705	9.003791
14	6.430765	4.887273	12.163641
14	16.018957	8.232262	12.190888
14	8.365784	1.565792	12.148745
14	4.526862	1.652360	5.124620
14	12.180586	1.652360	5.124620
14	8.353724	8.280679	5.124620
14	16.007448	8.280679	5.124620
14	4.566129	6.086665	8.253308
14	10.303321	2.765802	8.251535
14	14.124315	9.381759	8.246782
14	4.510544	3.791100	11.370033
14	14.086584	7.117183	11.419248
14	6.428386	0.474071	11.383832
14	4.526862	1.652360	2.781155
14	12.180586	1.652360	2.781155
14	10.267155	2.757080	5.905775
14	8.353724	8.280679	2.781155
14	4.526862	6.071239	5.905775
14	16.007448	8.280679	2.781155
14	14.094017	9.385399	5.905775
14	4.569910	3.876714	9.027590
14	14.136194	7.182140	9.059271
14	6.486641	0.559902	9.037529



14	14.078390	4.890986	12.151379
14	12.162578	8.209096	12.177924
14	2.613431	0.547640	2.000000
14	10.267155	0.547640	2.000000
14	8.353724	1.652360	5.124620
14	6.440293	7.175959	2.000000
14	6.440293	4.966519	5.124620
14	14.094017	4.966519	5.124620
14	14.094017	7.175959	2.000000
14	12.180586	8.280679	5.124620
14	12.217541	6.078628	8.263912
14	6.479904	2.767063	8.250639
14	10.311004	9.399137	8.250055
14	12.145586	3.794231	11.425116
14	10.231633	7.131943	11.390841
14	8.353724	1.652360	2.781155
14	6.440293	2.757080	5.905775
14	6.440293	4.966519	2.781155
14	14.094017	4.966519	2.781155
14	12.180586	6.071239	5.905775
14	12.180586	8.280679	2.781155
14	10.267155	9.385399	5.905775
14	12.210670	3.867931	9.058892
14	10.306373	7.193053	9.040545
14	10.233085	4.915918	12.166966
14	6.440293	0.547640	2.000000
14	4.526862	3.861799	2.000000
14	12.180586	3.861799	2.000000
14	10.267155	4.966519	5.124620
14	10.267155	7.175959	2.000000
14	8.393342	6.084153	8.252965
14	8.333735	3.783439	11.375805

14	10.267155	4.966519	2.781155
14	8.353724	6.071239	5.905775
14	8.394402	3.874202	9.032034
14	8.353724	3.861799	2.000000
6	4.385073	1.378778	15.574103
6	4.869575	2.068129	16.843865
6	4.464963	1.345311	18.127658
6	4.918180	2.039678	19.408219
6	8.134990	8.091140	15.563318
6	4.511076	1.327927	20.697266
6	8.415692	8.873163	16.842507
6	5.003523	2.039857	21.946951
6	8.152815	8.096189	18.133973
6	6.393263	4.644921	15.579864
6	15.842016	7.934825	15.542404
6	8.362309	1.294609	15.562060
6	8.373204	8.916563	19.404887
6	6.824525	5.373237	16.849083
6	16.273788	8.573156	16.857441
6	8.967413	1.890774	16.830939
6	8.126418	8.163682	20.714421
6	6.511131	4.613881	18.139631
6	13.696623	4.289831	15.447186
6	15.824915	7.790653	18.092746
6	11.968702	8.025279	15.589629
6	8.463579	1.241209	18.124457
6	8.284705	9.036798	21.955770
6	6.859070	5.368709	19.423301
6	14.105395	4.880490	16.797205
6	16.243634	8.462930	19.398370
6	12.445211	8.714286	16.863074
6	9.065726	1.822694	19.404818

6	6.497889	4.625400	20.711484
6	13.689290	4.083598	18.032758
6	10.148565	4.646027	15.577935
6	15.793585	7.720824	20.655963
6	11.981857	8.031416	18.150595
6	8.519324	1.219697	20.704053
6	6.794262	5.408862	21.985905
6	14.116858	4.777303	19.328431
6	10.567393	5.361112	16.857522
6	16.234180	8.423196	21.934419
6	12.467757	8.703878	19.434007
6	9.159751	1.805250	21.957227
6	13.711050	4.035275	20.602111
6	10.193029	4.617052	18.139086
6	11.963940	8.043668	20.720245
6	14.107280	4.779551	21.873459
6	10.590808	5.338961	19.424934
6	12.465062	8.700630	22.002007
6	10.179932	4.622977	20.711943
6	10.553005	5.383123	21.977304
1	3.299796	1.230906	15.608049
1	4.465095	3.085433	16.871209
1	3.372671	1.229942	18.146122
1	4.512967	3.056442	19.422434
1	7.081503	7.810411	15.484581
1	3.417559	1.237801	20.727902
1	7.807630	9.793284	16.841722
1	4.633824	3.066647	21.986817
1	7.131901	7.706107	18.123841
1	5.316870	4.446074	15.590412
1	4.821161	6.952172	15.385329
1	14.754322	7.807662	15.493480

1	8.753821	0.297788	15.340371
1	7.272305	1.231872	15.637027
1	2.616815	0.548137	0.497299
1	10.270167	0.548381	0.497270
1	6.443818	7.175282	0.497304
1	14.097945	7.175662	0.497255
1	7.730038	9.814254	19.374626
1	6.317377	6.343955	16.878470
1	5.883656	8.687365	16.869509
1	15.882778	9.596706	16.912544
1	10.066677	1.831441	16.775315
1	8.721397	2.956363	16.869922
1	7.126093	7.724611	20.698467
1	5.439744	4.379935	18.153761
1	2.712950	3.335598	15.240093
1	12.613374	4.148678	15.370025
1	4.746385	6.768613	18.055966
1	14.733475	7.663416	18.076033
1	12.430568	7.041010	15.453365
1	10.879710	7.907232	15.581973
1	8.643434	0.163417	18.094454
1	7.371485	1.348804	18.164130
1	6.442553	0.549194	0.497300
1	4.530201	3.861476	0.497315
1	12.183639	3.861133	0.497343
1	10.269051	7.174301	0.497258
1	7.645340	9.930705	21.884200
1	6.327716	6.326901	19.415672
1	3.716694	5.021617	16.803826
1	13.696154	5.900169	16.877214
1	5.853498	8.581840	19.412930
1	15.852048	9.487631	19.419602

1	13.538732	8.767786	16.845426
1	12.100919	9.754817	16.865931
1	10.164689	1.716788	19.377820
1	8.871282	2.898119	19.422179
1	5.427602	4.388652	20.688594
1	2.637050	3.073597	17.993827
1	12.601280	3.938040	18.035957
1	10.665313	3.687290	15.453956
1	9.073420	4.447492	15.566472
1	4.697223	6.692588	20.651999
1	14.700264	7.613779	20.648104
1	12.325639	6.990172	18.146749
1	10.883848	7.981037	18.157579
1	8.645354	0.133326	20.697056
1	7.435608	1.386784	20.745055
1	8.357150	3.861093	0.497343
1	6.317009	6.390877	21.951020
1	3.727056	4.930476	19.318742
1	13.696673	5.796043	19.349926
1	11.647241	5.537425	16.833887
1	10.106303	6.356552	16.875963
1	5.842144	8.402131	22.037509
1	15.940871	9.477985	21.913696
1	13.562792	8.704548	19.434576
1	12.179528	9.761302	19.428526
1	10.248037	1.638187	21.968688
1	9.024526	2.890556	21.987949
1	2.673321	3.031946	20.612044
1	12.625346	3.871735	20.605214
1	10.643922	3.615291	18.127250
1	9.109167	4.453282	18.146061
1	5.254228	7.592317	24.111329

1	12.262668	6.988581	20.719321
1	10.865013	8.043919	20.723816
1	8.830119	0.025307	23.623393
1	3.711986	4.913943	21.966643
1	13.693201	5.797695	21.864494
1	11.675505	5.489868	19.428796
1	10.154927	6.346406	19.423075
1	13.555216	8.633272	22.078574
1	12.228177	9.769083	22.020855
1	3.062610	3.179370	23.640265
1	10.637358	3.625332	20.738380
1	9.095221	4.461895	20.704639
1	12.466677	6.944968	23.639928
1	11.638481	5.470106	22.075425
1	10.176854	6.411571	21.945902
1	10.826798	3.765277	23.708653
1	4.861341	0.406301	15.411936
1	5.959785	2.184600	16.809870
1	4.867422	0.326255	18.111559
1	6.008927	2.161231	19.391983
1	4.894563	0.301784	20.691090
1	6.096394	2.107865	21.956045
1	5.786681	1.348120	24.071138
1	8.740512	7.180514	15.485302
1	9.460426	9.199471	16.832720
1	8.799996	7.209469	18.160488
1	9.400897	9.287285	19.405235
1	8.813369	7.309355	20.782572
1	9.312144	9.393845	22.065076
1	9.036497	7.635759	23.739126
1	6.923132	3.696652	15.430723
1	7.894953	5.602871	16.802350

1 7.025106 3.641949 18.130762
1 7.923985 5.628679 19.427674
1 7.017927 3.656915 20.741906
1 7.865337 5.600599 22.107110
1 7.134854 3.781094 23.696329

15. Si(111)-H 3x3 8:9 (SiH)1(Si.)0(SiSC6H12SH)8

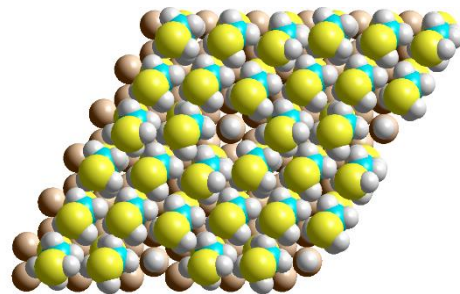
E=-1335.4211 eV

box: 11.480586 0 0 5.740293 9.942479 0 0 0 30.000000

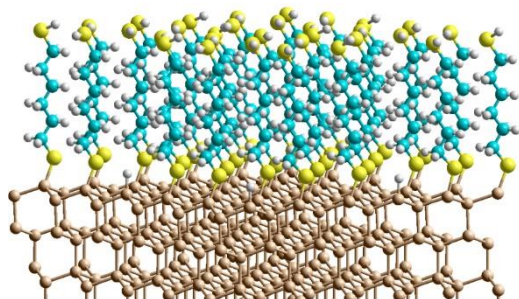
Kpoints: 2 2 1

basis: NGX= 84 NGY= 84 NGZ= 224 NGXF= 126 NGYF= 126 NGZF= 336

16 4.739867 2.420072 14.120621
16 8.521953 9.113287 14.123446
16 6.698574 5.702696 14.132301
16 16.331876 9.014144 14.183532
16 8.687817 2.362825 14.123267
16 4.551953 1.227888 23.525451
16 14.211676 5.508121 14.197657
16 12.403423 9.046046 14.144393
16 10.480098 5.717303 14.143460
16 7.852568 8.282850 23.564591
16 6.165823 4.713086 23.549294
16 15.547790 7.633207 23.444333
16 8.470617 1.327837 23.576262
16 13.503294 4.029579 23.422043
16 11.762240 8.094072 23.570437
16 9.902705 4.741004 23.553984



14	4.512771	1.577216	12.150422
14	2.574922	0.510456	11.370099
14	2.648580	0.569680	9.029302
14	8.317158	8.241972	12.169109
14	12.151258	1.606728	12.168371
14	2.638105	2.777348	8.250944
14	6.477779	9.397840	8.247765
14	6.420291	7.103389	11.385021
14	10.267229	0.478335	11.348461
14	2.613431	2.757080	5.905775
14	6.440293	9.385399	5.905775
14	6.476806	7.191337	9.038470
14	10.299286	0.554631	9.014924
14	6.425289	4.885717	12.161677
14	16.016872	8.231986	12.190889
14	8.359613	1.563812	12.149402
14	4.526862	1.652360	5.124620
14	12.180586	1.652360	5.124620
14	8.353724	8.280679	5.124620
14	16.007448	8.280679	5.124620
14	4.559655	6.089318	8.253226
14	10.295121	2.767699	8.247931
14	14.124981	9.387614	8.249931
14	4.505403	3.790841	11.367073
14	14.085581	7.118947	11.418371
14	6.424786	0.472916	11.381989
14	4.526862	1.652360	2.781155
14	12.180586	1.652360	2.781155
14	10.267155	2.757080	5.905775
14	8.353724	8.280679	2.781155
14	4.526862	6.071239	5.905775
14	16.007448	8.280679	2.781155



14	14.094017	9.385399	5.905775
14	4.561409	3.877377	9.024577
14	14.131098	7.186372	9.059689
14	6.480356	0.560438	9.034849
14	14.074113	4.891907	12.147237
14	12.158708	8.206958	12.175922
14	2.613431	0.547640	2.000000
14	10.267155	0.547640	2.000000
14	8.353724	1.652360	5.124620
14	6.440293	7.175959	2.000000
14	6.440293	4.966519	5.124620
14	14.094017	4.966519	5.124620
14	14.094017	7.175959	2.000000
14	12.180586	8.280679	5.124620
14	12.214697	6.080766	8.262323
14	6.472552	2.768283	8.249247
14	10.300620	9.402930	8.252589
14	12.137213	3.812114	11.404271
14	10.225099	7.133070	11.387162
14	8.353724	1.652360	2.781155
14	6.440293	2.757080	5.905775
14	6.440293	4.966519	2.781155
14	14.094017	4.966519	2.781155
14	12.180586	6.071239	5.905775
14	12.180586	8.280679	2.781155
14	10.267155	9.385399	5.905775
14	12.202713	3.870898	9.051189
14	10.301578	7.194820	9.038842
14	10.222745	4.917691	12.161804
14	6.440293	0.547640	2.000000
14	4.526862	3.861799	2.000000
14	12.180586	3.861799	2.000000

14	10.267155	4.966519	5.124620
14	10.267155	7.175959	2.000000
14	8.387743	6.086637	8.252091
14	8.325826	3.780823	11.372295
14	10.267155	4.966519	2.781155
14	8.353724	6.071239	5.905775
14	8.386842	3.875857	9.028534
14	8.353724	3.861799	2.000000
6	4.380491	1.373873	15.572766
6	4.865176	2.060873	16.843548
6	4.460229	1.335554	18.125786
6	4.913243	2.028167	19.407248
6	8.133743	8.076172	15.566668
6	4.506929	1.316455	20.696746
6	8.411886	8.861806	16.843924
6	4.998616	2.029907	21.945923
6	8.147747	8.086826	18.135970
6	6.385311	4.639310	15.579286
6	15.832051	7.915913	15.546170
6	8.356471	1.287248	15.560712
6	8.365749	8.908068	19.406422
6	6.817977	5.365758	16.849169
6	16.266427	8.557337	16.858798
6	8.963487	1.882638	16.828894
6	8.117792	8.155083	20.715575
6	6.503624	4.605253	18.139010
6	13.687072	4.281071	15.442371
6	15.817318	7.776974	18.094732
6	11.965921	8.019349	15.585832
6	8.459940	1.232225	18.121938
6	8.272279	9.029256	21.956520
6	6.852193	5.359120	19.423096

6	14.097942	4.868106	16.793082
6	16.235817	8.449197	19.399967
6	12.441153	8.706521	16.860589
6	9.063192	1.811510	19.402813
6	6.491835	4.614965	20.710933
6	13.681124	4.070499	18.027681
6	10.142123	4.638569	15.575217
6	15.783834	7.706917	20.656588
6	11.979104	8.020880	18.147090
6	8.515002	1.209322	20.701786
6	6.786046	5.398522	21.985893
6	14.109456	4.763209	19.323547
6	10.561713	5.353320	16.854857
6	16.223456	8.408851	21.935611
6	12.463051	8.693499	19.431187
6	9.156440	1.793607	21.955106
6	13.703758	4.021963	20.598002
6	10.185989	4.609404	18.136225
6	11.958798	8.032985	20.716932
6	14.099752	4.768606	21.868298
6	10.583229	5.330988	19.422337
6	12.457824	8.690520	21.999213
6	10.172118	4.614038	20.708697
6	10.543815	5.374353	21.974299
1	3.295443	1.224172	15.606753
1	4.460855	3.078111	16.872888
1	3.367970	1.220074	18.143418
1	4.507566	3.044737	19.422013
1	7.078387	7.804239	15.482061
1	3.413627	1.225108	20.728267
1	7.803174	9.781570	16.839936
1	4.626187	3.055748	21.984977

1	7.126929	7.696471	18.124994
1	5.308124	4.443551	15.589577
1	4.809125	6.932027	15.390763
1	14.744450	7.791265	15.497952
1	8.755089	0.294651	15.332903
1	7.267533	1.216152	15.641122
1	2.617065	0.547937	0.497309
1	10.269864	0.547916	0.497269
1	6.443797	7.174885	0.497313
1	14.096449	7.176727	0.497324
1	7.721626	9.805160	19.374814
1	6.312677	6.337408	16.879774
1	5.876650	8.669509	16.869189
1	15.877262	9.581751	16.911797
1	10.062601	1.823190	16.772031
1	8.717884	2.948208	16.869084
1	7.118411	7.713745	20.698088
1	5.431884	4.372266	18.152848
1	2.700260	3.325662	15.233265
1	12.603677	4.143766	15.365676
1	4.737957	6.754527	18.058667
1	14.725872	7.650848	18.077728
1	12.426194	7.034251	15.449668
1	10.876781	7.902841	15.575818
1	8.638824	0.154297	18.090502
1	7.367826	1.340988	18.162253
1	6.442618	0.547724	0.497312
1	4.530277	3.861865	0.497318
1	12.183268	3.861915	0.497334
1	10.270646	7.174999	0.497302
1	7.629943	9.920884	21.883687
1	6.320723	6.317109	19.416223

1	3.709519	5.006638	16.799365
1	13.691224	5.888528	16.874246
1	5.845796	8.567125	19.415552
1	15.844951	9.473982	19.421253
1	13.534627	8.761758	16.843364
1	12.094950	9.746425	16.865407
1	10.161981	1.703357	19.376026
1	8.870676	2.887113	19.420756
1	5.421980	4.376427	20.687587
1	2.628235	3.060203	17.987613
1	12.592946	3.925949	18.031101
1	10.656543	3.678411	15.452428
1	9.066509	4.442679	15.563511
1	4.686961	6.678472	20.652356
1	14.690502	7.600935	20.647092
1	12.325104	6.980302	18.141913
1	10.881187	7.967780	18.153958
1	8.639100	0.122854	20.694456
1	7.431611	1.378252	20.742571
1	8.356716	3.861672	0.497358
1	6.307390	6.380019	21.951174
1	3.719763	4.915648	19.313509
1	13.690315	5.782325	19.345126
1	11.641919	5.527788	16.831615
1	10.102167	6.349637	16.873138
1	5.831452	8.388144	22.039930
1	15.929384	9.463455	21.915137
1	13.558103	8.695783	19.432690
1	12.173429	9.750461	19.425308
1	10.244405	1.624887	21.966143
1	9.023059	2.879057	21.985695
1	2.667113	3.019133	20.608808

1	12.618116	3.858056	20.601369
1	10.636538	3.607486	18.124704
1	9.102152	4.445969	18.142837
1	5.240439	7.584089	24.115772
1	12.258465	6.978326	20.716891
1	10.859955	8.032008	20.719361
1	8.820328	0.014147	23.620968
1	3.704412	4.903299	21.961364
1	13.685400	5.786733	21.857599
1	11.667828	5.482428	19.426461
1	10.146866	6.338221	19.420838
1	13.547818	8.623669	22.077413
1	12.220475	9.758837	22.016773
1	3.062033	3.179769	23.643330
1	10.630197	3.616657	20.734700
1	9.087469	4.452610	20.700466
1	12.459428	6.935937	23.638537
1	11.629201	5.462554	22.073209
1	10.166616	6.402470	21.942001
1	10.817899	3.757793	23.707058
1	12.174275	1.666257	13.663516
1	4.857962	0.402427	15.408432
1	5.955445	2.176965	16.809522
1	4.862821	0.316642	18.107436
1	6.003931	2.150315	19.390585
1	4.891331	0.290748	20.691316
1	6.091262	2.101010	21.954380
1	5.791765	1.322367	24.061605
1	8.732996	7.160934	15.497000
1	9.456418	9.188507	16.834706
1	8.795016	7.200330	18.163897
1	9.392993	9.279781	19.408123

1	8.806424	7.302319	20.785387
1	9.298405	9.389824	22.066273
1	9.026455	7.629760	23.738948
1	6.911860	3.689112	15.431186
1	7.888821	5.593386	16.802801
1	7.016811	3.632904	18.129329
1	7.916945	5.619464	19.426828
1	7.013937	3.647608	20.741138
1	7.856786	5.591568	22.108219
1	7.119704	3.764295	23.691933

16. Si(111)-H 3x3 7:9 (SiH)1(Si.)1(SiSC6H12SH)5

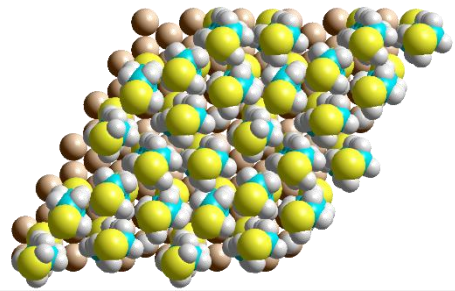
E=-1225.0282 eV

box: 11.480586 0 0 5.740293 9.942479 0 0 0 30.000000

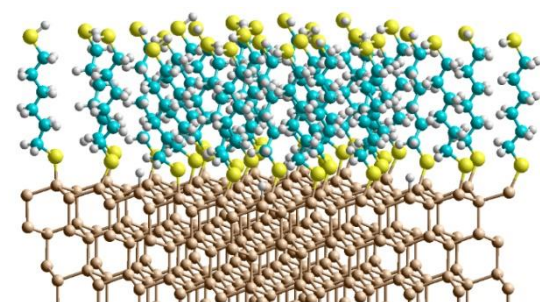
Kpoints: 2 2 1

basis: NGX= 84 NGY= 84 NGZ= 224 NGXF= 126 NGYF= 126 NGZF= 336

16	4.057290	2.019224	14.129678
16	6.663990	5.577719	14.184166
16	16.644321	9.078221	14.118581
16	8.952615	2.454200	14.119613
16	3.326612	0.103792	23.046665
16	14.321503	5.524209	14.288141
16	12.445374	9.206214	14.210051
16	10.272028	6.040366	14.161547
16	5.781713	3.420751	23.275524
16	5.459391	7.926568	23.402187
16	9.453596	1.495775	23.434612



16	12.902685	3.748177	23.345563
16	12.652591	7.672704	23.581469
16	9.182441	5.197700	23.524661
14	4.484260	1.613031	12.073660
14	2.581887	0.531303	11.308046
14	2.622741	0.569245	8.982138
14	8.353036	8.285186	12.095404
14	12.212596	1.686445	12.155804
14	2.624845	2.801053	8.263582
14	6.458017	9.397321	8.229333
14	6.483429	7.136312	11.320240
14	10.334254	0.542961	11.333453
14	2.613431	2.757080	5.905775
14	6.440293	9.385399	5.905775
14	6.480043	7.187043	8.990856
14	10.306196	0.587768	9.003807
14	6.467548	4.945790	12.143210
14	16.125825	8.294830	12.164657
14	8.465720	1.658769	12.170082
14	4.526862	1.652360	5.124620
14	12.180590	1.652360	5.124620
14	8.353724	8.280679	5.124620
14	16.007450	8.280679	5.124620
14	4.550347	6.092464	8.251447
14	10.312808	2.804281	8.253745
14	14.125951	9.418809	8.256081
14	4.519247	3.858937	11.401486
14	14.145212	7.216638	11.461910
14	6.494300	0.587818	11.430568
14	4.526862	1.652360	2.781155
14	12.180590	1.652360	2.781155
14	10.267160	2.757080	5.905775



14	8.353724	8.280679	2.781155
14	4.526862	6.071239	5.905775
14	16.007450	8.280679	2.781155
14	14.094020	9.385399	5.905775
14	4.555387	3.888331	9.046942
14	14.148991	7.225847	9.084580
14	6.491976	0.603423	9.064255
14	14.112866	4.999608	12.206041
14	12.230846	8.329169	12.235164
14	2.613431	0.547640	2.000000
14	10.267160	0.547640	2.000000
14	8.353724	1.652360	5.124620
14	6.440293	7.175959	2.000000
14	6.440293	4.966519	5.124620
14	14.094020	4.966519	5.124620
14	14.094020	7.175959	2.000000
14	12.180590	8.280679	5.124620
14	12.238519	6.113824	8.265008
14	6.480216	2.804776	8.258768
14	10.313156	9.440543	8.250638
14	12.162001	3.921764	11.479732
14	10.303484	7.255975	11.372874
14	8.353724	1.652360	2.781155
14	6.440293	2.757080	5.905775
14	6.440293	4.966519	2.781155
14	14.094020	4.966519	2.781155
14	12.180590	6.071239	5.905775
14	12.180590	8.280679	2.781155
14	10.267160	9.385399	5.905775
14	12.206880	3.920783	9.098886
14	10.334191	7.238202	9.026292
14	10.240216	5.069051	12.219108

14	6.440293	0.547640	2.000000
14	4.526862	3.861799	2.000000
14	12.180590	3.861799	2.000000
14	10.267160	4.966519	5.124620
14	10.267160	7.175959	2.000000
14	8.416471	6.114430	8.247375
14	8.393423	3.867548	11.383149
14	10.267160	4.966519	2.781155
14	8.353724	6.071239	5.905775
14	8.406452	3.910386	9.035012
14	8.353724	3.861799	2.000000
6	3.524967	0.573137	15.115169
6	3.969271	0.936037	16.530476
6	3.407555	0.122534	17.692725
6	4.031061	0.621211	18.997432
6	3.430568	0.062994	20.284932
6	4.161868	0.600533	21.505247
6	6.227321	4.256505	15.357447
6	4.827673	8.007999	15.545989
6	8.749717	1.373466	15.579584
6	6.252392	4.861480	16.752311
6	5.738289	8.424701	16.700913
6	9.594759	1.892124	16.741223
6	6.221814	3.848346	17.894973
6	13.432002	4.394871	15.412390
6	5.190981	7.968543	18.051976
6	12.175013	8.136585	15.671119
6	9.206002	1.267899	18.081190
6	6.101211	4.555998	19.243803
6	14.056128	4.581740	16.792743
6	6.076288	8.306491	19.247665
6	12.796190	8.739630	16.928859

6	10.049029	1.728736	19.272456
6	6.146527	3.640844	20.465222
6	13.285367	3.933733	17.943834
6	9.805221	5.085751	15.645044
6	5.420847	7.913029	20.571848
6	12.382556	8.012954	18.212715
6	9.446285	1.304111	20.614209
6	5.966603	4.416743	21.765746
6	2.463701	4.215646	19.296312
6	9.800827	5.994641	16.872097
6	6.256230	8.254349	21.797134
6	13.059540	8.538252	19.478349
6	10.260685	1.745254	21.822621
6	13.151413	3.731441	20.511160
6	9.584852	5.234009	18.182170
6	12.566874	7.869082	20.764399
6	13.836844	4.099813	21.822391
6	9.590787	6.108397	19.437692
6	13.255910	8.399281	22.019409
6	9.463043	5.295605	20.725994
6	9.611989	6.108715	22.009159
1	2.433891	0.462314	15.022134
1	3.704279	1.991096	16.711110
1	2.312973	0.240316	17.733625
1	3.937849	1.720267	19.022887
1	2.367198	0.343059	20.340041
1	4.199171	1.695476	21.485161
1	5.227722	3.884576	15.115391
1	4.993915	6.966295	15.254149
1	15.248836	8.125461	15.804869
1	9.027109	0.356251	15.288117
1	7.682046	1.390043	15.836252

1	2.619734	0.549511	0.497408
1	10.268277	0.548800	0.497453
1	6.445375	7.177095	0.497572
1	14.094758	7.178335	0.497343
1	5.383933	5.525100	16.844083
1	6.746733	8.016455	16.526681
1	5.852159	9.522172	16.714720
1	10.662251	1.727999	16.521561
1	9.461388	2.974878	16.829053
1	5.379907	3.151864	17.760108
1	2.048978	3.362806	15.049242
1	12.374454	4.684586	15.396201
1	5.002442	6.887742	18.041095
1	15.686072	8.429596	18.202787
1	12.587165	7.142617	15.452876
1	11.089276	8.050063	15.782804
1	9.249661	0.175887	18.009971
1	8.149055	1.506612	18.282536
1	6.442828	0.551064	0.497535
1	4.535555	3.863361	0.497414
1	12.183079	3.859831	0.497363
1	10.272078	7.178196	0.497448
1	5.151663	5.113572	19.255373
1	3.604090	4.193195	16.769164
1	14.150427	5.662560	16.997718
1	7.050943	7.803350	19.140274
1	6.294680	9.386722	19.252058
1	13.888331	8.728208	16.838070
1	12.513079	9.797638	17.022558
1	11.075794	1.341086	19.173639
1	10.140704	2.822861	19.258541
1	5.363762	2.873837	20.382629

1	1.719534	2.845198	17.782477
1	12.255816	4.321607	17.951553
1	10.518476	4.264358	15.770239
1	8.812903	4.662109	15.460966
1	5.197256	6.837246	20.566528
1	15.930491	8.419000	20.654672
1	12.587634	6.932921	18.114459
1	11.293845	8.106881	18.328079
1	9.317280	0.214275	20.639684
1	8.431766	1.721712	20.704436
1	8.356841	3.863210	0.497581
1	5.048607	5.019642	21.720592
1	3.466879	3.760184	19.311219
1	14.111201	5.304441	19.389941
1	10.764173	6.508300	16.940458
1	9.035291	6.779083	16.744878
1	7.226594	7.742992	21.774454
1	6.478046	9.330050	21.830425
1	14.146257	8.396077	19.393657
1	12.903231	9.626647	19.555415
1	11.252195	1.271146	21.840022
1	10.443317	2.826850	21.799483
1	1.525109	2.641430	20.462091
1	12.146437	4.177737	20.493790
1	10.390325	4.492429	18.280992
1	8.653792	4.651887	18.143732
1	5.561215	6.579007	23.383125
1	12.708582	6.777799	20.699222
1	11.483437	8.028512	20.864177
1	9.517892	0.144225	23.454794
1	3.332373	3.604979	21.912960
1	14.024237	5.184536	21.855819

1	10.522353	6.684372	19.469871
1	8.776668	6.849249	19.379283
1	14.342345	8.241263	21.991687
1	13.101409	9.484318	22.118567
1	1.652142	2.412660	23.352296
1	10.233656	4.510976	20.727453
1	8.503959	4.760929	20.737924
1	13.601065	6.720967	23.698620
1	10.631270	6.492231	22.139751
1	8.955128	6.990240	22.010230
1	10.334112	4.488648	23.593298
1	12.255239	1.670302	13.650082
1	4.008940	-0.338616	14.741717
1	5.070000	0.910527	16.552502
1	3.597849	-0.954005	17.555752
1	5.116338	0.423068	18.980349
1	3.462355	-1.037157	20.280631
1	5.202093	0.246196	21.521363
1	4.099837	0.862795	23.856879
1	6.939816	3.429915	15.234403
1	7.134809	5.509603	16.869974
1	7.130419	3.225678	17.866642
1	6.890376	5.321326	19.326601
1	7.100545	3.093165	20.496881
1	6.801582	5.114893	21.922723
1	7.071926	3.005265	23.344531

17. Si(111)-H 3x3 2:3 (SiH)₂(Si)₁(SiSC₆H₁₂SH)₆

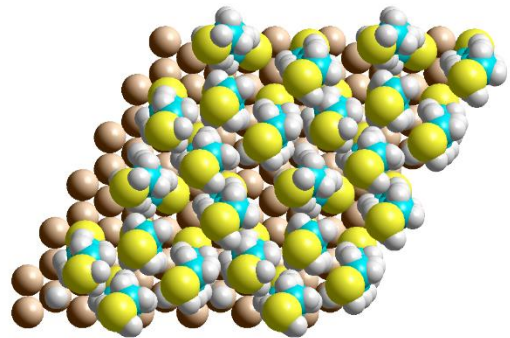
E=-1116.5652 eV

box: 11.480586 0 0 5.740293 9.942479 0 0 0 30.000000

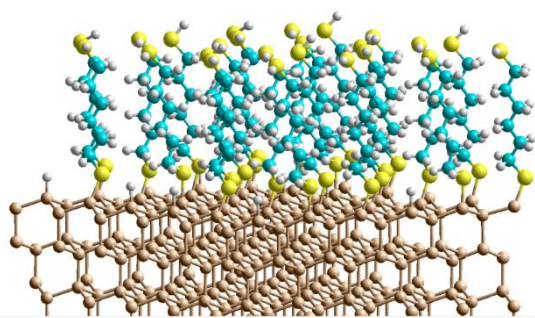
Kpoints: 2 2 1

basis: NGX= 84 NGY= 84 NGZ= 224 NGXF= 126 NGYF= 126 NGZF= 336

16	6.644943	5.570053	14.165135
16	16.549453	8.925170	14.185847
16	8.937825	2.392299	14.137103
16	14.093436	5.116638	14.373254
16	12.556014	8.755525	14.315390
16	10.413424	5.855652	14.151876
16	6.435074	3.214414	23.156031
16	4.557758	6.813349	23.300636
16	8.886835	0.559850	23.337274
16	1.782246	2.398779	23.110122
16	9.717618	9.190315	22.980938
16	10.265814	4.941078	23.474217
14	4.589875	1.626891	12.157610
14	2.662476	0.526852	11.398546
14	2.668540	0.564605	9.042602
14	8.376668	8.255396	12.121536
14	12.224691	1.629442	12.142504
14	2.645658	2.778556	8.259740
14	6.497203	9.398375	8.246860
14	6.498210	7.131660	11.321404
14	10.352218	0.487696	11.326952
14	2.613431	2.757080	5.905775
14	6.440293	9.385399	5.905775
14	6.475873	7.181271	8.992575
14	10.320445	0.558596	9.001156
14	6.523654	4.941668	12.127341
14	16.113216	8.245403	12.180432



14	8.489272	1.619997	12.160325
14	4.526862	1.652360	5.124620
14	12.180590	1.652360	5.124620
14	8.353724	8.280679	5.124620
14	16.007450	8.280679	5.124620
14	4.550210	6.076036	8.256491
14	10.324748	2.775339	8.244634
14	14.132859	9.395562	8.263258
14	4.574428	3.851235	11.424778
14	14.123737	7.164492	11.517767
14	6.519419	0.566102	11.385744
14	4.526862	1.652360	2.781155
14	12.180590	1.652360	2.781155
14	10.267160	2.757080	5.905775
14	8.353724	8.280679	2.781155
14	4.526862	6.071239	5.905775
14	16.007450	8.280679	2.781155
14	14.094020	9.385399	5.905775
14	4.562654	3.875113	9.060547
14	14.153622	7.194802	9.119932
14	6.502878	0.605798	9.031012
14	14.133790	4.913513	12.228227
14	12.198103	8.330616	12.213520
14	2.613431	0.547640	2.000000
14	10.267160	0.547640	2.000000
14	8.353724	1.652360	5.124620
14	6.440293	7.175959	2.000000
14	6.440293	4.966519	5.124620
14	14.094020	4.966519	5.124620
14	14.094020	7.175959	2.000000
14	12.180590	8.280679	5.124620
14	12.245418	6.099844	8.266446



14	6.490694	2.812038	8.251748
14	10.327130	9.424555	8.252229
14	12.223161	3.850315	11.411544
14	10.308751	7.188987	11.393507
14	8.353724	1.652360	2.781155
14	6.440293	2.757080	5.905775
14	6.440293	4.966519	2.781155
14	14.094020	4.966519	2.781155
14	12.180590	6.071239	5.905775
14	12.180590	8.280679	2.781155
14	10.267160	9.385399	5.905775
14	12.221614	3.891552	9.054254
14	10.336909	7.221572	9.037688
14	10.325953	4.982689	12.191424
14	6.440293	0.547640	2.000000
14	4.526862	3.861799	2.000000
14	12.180590	3.861799	2.000000
14	10.267160	4.966519	5.124620
14	10.267160	7.175959	2.000000
14	8.414842	6.103125	8.254121
14	8.435311	3.829517	11.377692
14	10.267160	4.966519	2.781155
14	8.353724	6.071239	5.905775
14	8.425859	3.894317	9.031378
14	8.353724	3.861799	2.000000
6	6.260495	4.188866	15.293406
6	15.985235	7.803742	15.507919
6	8.707872	1.248890	15.543984
6	6.836802	4.584421	16.646872
6	5.335914	8.068348	16.762009
6	9.545065	1.655971	16.754156
6	6.544903	3.605043	17.782726

6	2.590072	3.492353	15.243278
6	4.737063	7.395072	18.000872
6	11.005577	8.862300	15.299405
6	9.129614	0.881167	18.009793
6	6.912892	4.217233	19.133800
6	2.663074	3.879798	16.720596
6	5.493035	7.697875	19.295121
6	11.239439	9.750152	16.531856
6	9.777839	1.380086	19.303560
6	6.648261	3.339021	20.355520
6	2.496494	2.784861	17.775535
6	10.670054	4.773432	15.596009
6	4.797002	7.095504	20.518073
6	10.394639	9.332453	17.746406
6	9.255154	0.652054	20.548243
6	6.909535	4.115628	21.639520
6	2.732905	3.402581	19.162882
6	10.843138	5.643060	16.842232
6	5.453642	7.463219	21.845229
6	5.138635	0.001261	19.068074
6	9.597366	1.357204	21.859267
6	2.330842	2.533819	20.351971
6	10.816944	4.845060	18.148348
6	10.148733	9.372586	20.286726
6	2.578061	3.221810	21.693634
6	10.947588	5.715487	19.398238
6	5.060701	-0.191642	21.616183
6	10.728038	4.930348	20.693448
6	10.823169	5.780876	21.954918
1	5.169406	4.085351	15.338080
1	4.613360	6.770062	15.165477
1	14.916758	8.000077	15.684826

1	8.966616	0.242427	15.204092
1	7.642015	1.269463	15.796245
1	2.618895	0.549602	0.497138
1	10.267641	0.547319	0.497410
1	6.445816	7.181848	0.497240
1	14.099203	7.178679	0.497196
1	6.438039	5.574027	16.918974
1	6.369144	7.724165	16.590864
1	5.411549	9.154202	16.940557
1	10.617181	1.513624	16.537085
1	9.414978	2.727347	16.955686
1	5.475043	3.335054	17.783703
1	3.439908	2.873415	14.928164
1	13.151144	2.943364	14.997333
1	4.688119	6.303654	17.851610
1	15.168248	7.713075	18.121068
1	10.797693	7.835608	15.611501
1	10.162551	9.193278	14.675935
1	9.335794	-0.189116	17.872906
1	8.035227	0.962003	18.122302
1	6.443389	0.549545	0.497231
1	4.535349	3.864158	0.497215
1	12.181710	3.859702	0.497206
1	10.271308	7.175856	0.497221
1	6.348952	5.156713	19.246615
1	3.624180	4.388280	16.898909
1	13.378669	4.647819	16.912790
1	6.530133	7.327464	19.219720
1	5.576337	8.791228	19.420423
1	12.300151	9.668742	16.822701
1	5.329552	0.867379	16.274322
1	10.876724	1.285796	19.241421

1	9.574270	2.457570	19.405592
1	5.601120	2.994742	20.342494
1	3.197223	1.951851	17.597109
1	1.483193	2.348990	17.721318
1	11.539479	4.130151	15.425745
1	9.780432	4.143888	15.690867
1	4.747255	5.998959	20.424359
1	15.227535	7.428778	20.545286
1	10.449449	8.237473	17.839463
1	9.328813	9.567388	17.580884
1	9.640881	-0.375639	20.572576
1	8.159424	0.550339	20.478264
1	8.356513	3.861480	0.497464
1	6.335439	5.048691	21.622492
1	3.795680	3.685568	19.246881
1	13.656422	4.354030	19.222703
1	11.779050	6.222977	16.764665
1	10.018848	6.374537	16.876787
1	6.501774	7.135674	21.893988
1	5.472842	8.555056	21.972695
1	6.220334	-0.195214	19.176193
1	5.026555	1.098087	19.051509
1	10.681619	1.478843	22.005390
1	9.171702	2.371376	21.870858
1	2.883462	1.585011	20.331600
1	12.744570	2.268158	20.271507
1	11.597775	4.069225	18.147310
1	9.859718	4.305256	18.209486
1	5.221282	5.634854	23.415714
1	10.118030	8.277428	20.202357
1	9.095881	9.700599	20.279655
1	9.841831	-0.380533	23.504214

1	3.653291	3.330975	21.902171
1	13.641032	4.240228	21.695656
1	11.930102	6.218937	19.412577
1	10.194779	6.518687	19.342157
1	6.039313	-0.677908	21.733046
1	5.223012	0.892107	21.700673
1	2.397342	1.188348	22.969470
1	11.439767	4.092816	20.757324
1	9.729948	4.469096	20.658985
1	10.381127	9.798712	23.983550
1	11.841029	6.170648	22.107074
1	10.159198	6.655155	21.894502
1	11.129221	3.900055	23.409844
1	12.190788	1.611226	13.634529
1	6.712127	3.265806	14.907377
1	7.924605	4.728603	16.544840
1	7.095134	2.666642	17.620751
1	7.974851	4.518599	19.117361
1	7.265341	2.430734	20.326566
1	7.969877	4.385062	21.743188
1	7.617371	3.366114	23.791800
1	4.637755	1.587170	13.659987